CALIFORNIA INSTITUTE OF TECHNOLOGY

EARTHQUAKE ENGINEERING RESEARCH LABORATORY

DYNAMIC ANALYSES OF LIQUID STORAGE TANKS

BY

MEDHAT AHMED HAROUN

EERL 80-04

A Report on Research Conducted under Grants from the National Science Foundation

PASADENA, CALIFORNIA

FEBRUARY, 1980

This investigation was sponsored by Grant No. PFR77-23687 from the National Science Foundation, Division of Problem-Focused Research Applications, under the supervision of G. W. Housner. Any opinions, findings, and conclusions or recommendations expressed in this publication are those of the author and do not necessarily reflect the views of the National Science Foundation.

50272-101

REPORT DOCUMENTATION PAGE	1. REPORT NO. NSF/RA-800217	2.	3. Recipient's Accession No. PB81 123275
4. Title and Subtitle: Dynamic Analysis of Liquid Storage Tanks			5. Report Date: February 1980 6.
7. Author(s): M. A. Haroun			8. Performing Organization Rept. No. EERL 80-04
9. Performing Organization Name and Address: California Institute of Technology, Earthquake Engineering Research Laboratory, Pasadena, CA 91125			10. Project/Task/Work Unit No. 11. Contract(C) or Grant(G) No. (C) (G) PFR7723687
12. Sponsoring Organization Name and Address: Engineering and Applied Science (EAS), National Science Foundation, 1800 G Street, N.W., Washington, D.C. 20550			13. Type of Report & Period Covered 14.

15. Supplementary Notes

16. Abstract (Limit: 200 words)

The dynamic behavior of cylindrical liquid storage tanks was investigated to improve their ability to resist earthquakes. The study comprised three phases: a theoretical treatment of the liquid-shell system; an investigation of the dynamic characteristics of full-scale tanks; and development of an improved design procedure based on an approximate analysis. Natural vibration frequencies and associated mode shapes were found by using a discretization scheme in which the elastic shell is modeled by finite elements and the fluid region is treated as a continuum by boundary solution techniques. The number of unknowns is substantially less than in those analyses in which both tank wall and fluid are subdivided into finite elements. A method is presented to compute earthquake response of both circular and irregular tanks based on superposition of the free lateral vibrational modes. Numerical examples illustrate the dynamic characteristics of tanks with widely different properties. Ambient and forced vibration tests were conducted on three full-scale water storage tanks to determine their dynamic characteristics. Comparison with previously computed mode shapes and frequencies shows general agreement with experimental results, thereby confirming the reliability of the theoretical analysis. Approximate solutions also were developed to provide practicing engineers with simple, fast, and accurate tools for estimating seismic response of storage tanks.

17. Document Analysis a. Descriptors

Storage tanks
Cylindrical bodies
Dynamic structural analysis
Elastic shells
Earthquake resistant structures
Seismic response
Mathematical models
Vibration tests

b. Identifiers/Open-Ended Terms

Liquid storage tanks
Discretization scheme

Earthquake Hazards Mitigation

c. COSATI Field/Group

18. Availability Statement	19. Security Class (This Report)	21. No. of Pages
NTIS	20. Security Class (This Page)	22. Price

(See ANSI-Z39.18) See Instructions on Reverse

OPTIONAL FORM 272 (4-77)
(Formerly NTIS-35)
Department of Commerce

CALIFORNIA INSTITUTE OF TECHNOLOGY

EARTHQUAKE ENGINEERING RESEARCH LABORATORY

DYNAMIC ANALYSES OF LIQUID STORAGE TANKS

Medhat Ahmed Haroun

EERL 80-04

A Report on Research Conducted under Grants
from the National Science Foundation

Pasadena, California

February, 1980

1.a

ACKNOWLEDGMENTS

This report presents the results of research carried out at the California Institute of Technology during the years 1976-79 and originally appeared as part of the author's Ph.D. thesis (California Institute of Technology, December 1979). The author acknowledges the guidance and encouragement of his advisor Professor G. W. Housner. Valuable suggestions were also given by Professors C. D. Babcock, T.J.R. Hughes and P. C. Jennings and by Dr. A. Abdel-Ghaffar during the various phases of the study.

The cooperation of the Metropolitan Water District of Southern California in making available its facilities for conducting tests is gratefully acknowledged. The assistance of Raul Relles in maintaining the instrumentation system and in conducting the tests is greatly appreciated. Gratitude is also extended to G. Cherepon and A. Rashed who helped in carrying out the tests.

Sincere thanks are given to Gloria Jackson and Sharon Vedrode for their skillful typing of the manuscript, and the help given by Cecilia Lin in drawing the figures is also much appreciated.

The research reported here was supported in part by the National Science Foundation and by the Earthquake Research Affiliates of the California Institute of Technology.

ABSTRACT

Theoretical and experimental investigations of the dynamic behavior of cylindrical liquid storage tanks are conducted to seek possible improvements in the design of such tanks to resist earthquakes. The study is carried out in three phases: 1) a detailed theoretical treatment of the liquid-shell system, 2) an experimental investigation of the dynamic characteristics of full-scale tanks, and 3) a development of an improved design-procedure based on an approximate analysis.

Natural frequencies of vibration and the associated mode shapes are found through the use of a discretization scheme in which the elastic shell is modeled by finite elements and the fluid region is treated as a continuum by boundary solution techniques. In this approach, the number of unknowns is substantially less than in those analyses where both tank wall and fluid are subdivided into finite elements. A method is presented to compute the earthquake response of both perfect circular and irregular tanks; it is based on superposition of the free lateral vibrational modes. Detailed numerical examples are presented to illustrate the applicability and effectiveness of the analysis and to investigate the dynamic characteristics of tanks with widely different properties. Ambient and forced vibration tests are conducted on three full-scale water storage tanks to determine their dynamic characteristics. Comparison with previously computed mode shapes and frequencies shows good agreement with the experimental results, thus confirming the reliability of the theoretical analysis. Approximate solutions are also developed to provide practicing engineers with simple, fast, and sufficiently accurate tools for estimating the seismic response of storage tanks.

TABLE OF CONTENTS

TABLE OF CONTENTS (CONTINUED)

TABLE OF CONTENTS (CONTINUED)

TABLE OF CONTENTS (CONTINUED)

DYNAMIC ANALYSES OF LIQUID STORAGE TANKS

GENERAL INTRODUCTION

The progress of scientific investigations into the dynamic behavior of liquid storage tanks reflects the increasing importance of these structures. Early uses for liquid containers were found in the petroleum industry and in municipal water supply systems. As their numbers and sizes began to grow, their tendency to vibrate under seismic loading became a matter of concern. For instance, the possible failure of large tanks containing flammable liquids in and around densely populated areas presents a critical fire hazard during severe earthquakes. In addition, the consequences of total spills of the contained liquid, as well as structural damage to the tank and its accessories, may pose a considerable economic loss. In recent times, the use of liquid containers in nuclear reactor installations has led to several investigations of their vibrational properties. However, the performance of liquid storage tanks during the 1964 Alaska and the 1971 San Fernando earthquakes revealed a much more complex behavior than was implied by design assumptions. Thus, although the problem has been recognized, the state of knowledge of liquid-tank seismic vibrations is, still, not entirely satisfactory.

The present study develops a method of analyzing the dynamic behavior of ground-supported, circular cylindrical, liquid storage tanks by means of a digital computer. The reliability of the theoretical analysis was confirmed by conducting vibration tests on full-scale tanks.

In addition, approximate solutions are also developed to provide practicing engineers with simple, fast and sufficiently accurate tools for estimating the seismic response of storage tanks.

The following sections present a brief historical review of the literature and outline the methods of analysis employed in the present study.

A. Historical Background

Seismic damage of liquid storage tanks during recent earthquakes demonstrates the need for a reliable technique to assess their seismic safety. The Alaska earthquake of 1964 caused the first large-scale damage to tanks of modern design [1,2] and profoundly influenced the research into their vibrational characteristics. Prior to that time, the development of seismic response theories of liquid storage tanks considered the container to be rigid and focused attention on the dynamic response of the contained liquid.

One of the earliest of these studies, due to L. M. Hoskins and L. S. Jacobsen [3], reported analytical and experimental investigations of the hydrodynamic pressure developed in rectangular tanks when subjected to horizontal motion. Later, Jacobsen [4] and Jacobsen and Ayre [5] investigated the dynamic behavior of rigid cylindrical containers.

In the mid 1950's, G. W. Housner [6,7] formulated an idealization, commonly applied in civil engineering practice, for estimating liquid response in seismically excited rigid, rectangular and cylindrical tanks. He divided the hydrodynamic pressure of the contained liquid into two components; the impulsive pressure caused by the portion of the

liquid accelerating with the tank and the convective pressure caused by the portion of the liquid sloshing in the tank. The convective component was then modeled by a single degree of freedom oscillator. The study presented values for equivalent masses and their locations that would duplicate the forces and moments exerted by the liquid on the tank. The properties of this mechanical analog can be computed from the geometry of the tank and the characteristics of the contained liquid. Housner's model is widely used to predict the maximum seismic response of storage tanks by means of a response spectrum characterizing the design earthquake [8,9,10].

At this point the subject appears to have been laid to rest until the seismic damage in 1964 initiated investigations into the dynamic characteristics of flexible containers. In addition, the evolution of both the digital computer and various associated numerical techniques have significantly enhanced solution capability.

The first use of a digital computer in analyzing this problem was completed in 1969 by N. W. Edwards [11]. The finite element method was used with a refined shell theory to predict the seismic stresses and displacements in a circular cylindrical liquid-filled container whose height to diameter ratio was smaller than one. This investigation treated the coupled interaction between the elastic wall of the tank and the contained liquid. The tank was regarded as anchored to its foundation and restrained against cross-section distortions.

A similar approach was used by H. Hsiung and V. Weingarten [12] to investigate the free vibrations of an axisymmetric thin elastic shell partly filled with liquid. The liquid was discretized into annular

elements of rectangular cross-section. Two simplified cases were treated; one neglecting the mass of the shell and the other neglecting the liquid-free surface effect. In a more recent study, S. Shaaban and W. Nash [13] undertook similar research concerned with the earthquake response of circular cylindrical, elastic tanks using the finite element method. Shortly after [13], T. Balendra and W. Nash [14] offered further generalization of this analysis by including an elastic dome on top of the tank.

A different approach to the solution of the problem of flexible containers was developed by A. S. Veletsos [15]. He presented a simple procedure for evaluating the hydrodynamic forces induced in flexible liquid-filled tanks. The tank was assumed to behave as a single degree of freedom system, to vibrate in a prescribed mode and to remain circular during vibrations. The hydrodynamic pressure distribution, base shears and overturning moments corresponding to several assumed modes of vibrations were presented. He concluded that the seismic effects in flexible tanks may be substantially greater than those induced in similarly excited rigid tanks. Later, Veletsos and Yang [16] presented simplified formulas to obtain the fundamental natural frequencies of the liquid-filled shells by the Rayleigh-Ritz energy method. Special attention was given to the $\cos\theta$-type modes of vibration for which there is a single cosine wave of deflection in the circumferential direction.

Another approach to the free vibration problem of storage tanks was investigated by C. Wu, T. Mouzakis, W. Nash and J. Colonell [17]. They developed an analytical solution of the problem using an iteration procedure but the assumptions employed in their analysis forced the modes

of vibration to be of a shape that cannot be justified in real "tall" tanks. They also computed the natural frequencies and mode shapes of the $\cos n\theta$-type deformations of the tank wall, neglecting the initial hoop stresses due to the hydrostatic pressure, which introduced certain errors.

Until recently, it was believed that, only, the $\cos\theta$-type of modes were important in the analysis of the vibrational behavior of liquid storage tanks under seismic excitations. However, shaking table experiments with aluminum tank models conducted recently by D. Clough [18] and A. Niwa [19] showed that $\cos n\theta$-type modes were significantly excited by earthquake-type of motion. Since a perfect circular cylindrical shell should exhibit only $\cos\theta$-type modes with no $\cos n\theta$-type deformations of the wall, these experimentally observed deformations have been attributed to initial irregularities of the shell radius. Shortly after the foregoing tests were completed, J. Turner and A. Veletsos [20] made an approximate analysis of the effects of initial out-of-roundness on the dynamic response of tanks, in an effort to interpret the unexpected results.

Extensive research on the dynamic behavior of liquid storage tanks has also been carried on in the aerospace industry. With the advent of the space age, attention was focused on the behavior of cylindrical fuel tanks of rockets, the motivation being to investigate the influence of their vibrational characteristics on the flight control system. However, the difference in support conditions between the aerospace tanks and the civil engineering tanks makes it difficult to apply the aerospace analyses to civil engineering problems, and vice-versa. A

comprehensive review of the theoretical and experimental investigations of the dynamic behavior of fuel tanks of space vehicles can be found in [21].

B. Outline of the Present Study

Recent developments in seismic response analyses of liquid storage tanks have not found widespread application in current seismic design. Most of the elaborate analyses developed so far assume ideal geometry and boundary conditions never achieved in the real world. In addition, the lack of experimental confirmation of the theoretical concepts has raised doubts among engineers about their applicability in the design stage. With few exceptions, current design procedures are based on the mechanical model derived by Housner for rigid tanks.

The following study develops a method for analyzing the dynamic behavior of deformable, cylindrical liquid storage tanks. The study was carried out in three phases: 1) a detailed theoretical treatment of the liquid-shell system, 2) an extensive experimental investigation of the dynamic characteristics of full-scale tanks, and 3) a development of an improved design-procedure based on an approximate analysis.

A necessary first step was to compute the natural frequencies of vibration and the associated mode shapes. These were determined by means of a discretization scheme in which the elastic shell is modeled by finite elements and the fluid region is treated as a continuum by boundary solution techniques. In this approach, the number of unknowns is substantially less than in those analyses where both tank wall and fluid are subdivided into finite elements.

DYNAMIC ANALYSES OF LIQUID STORAGE TANKS

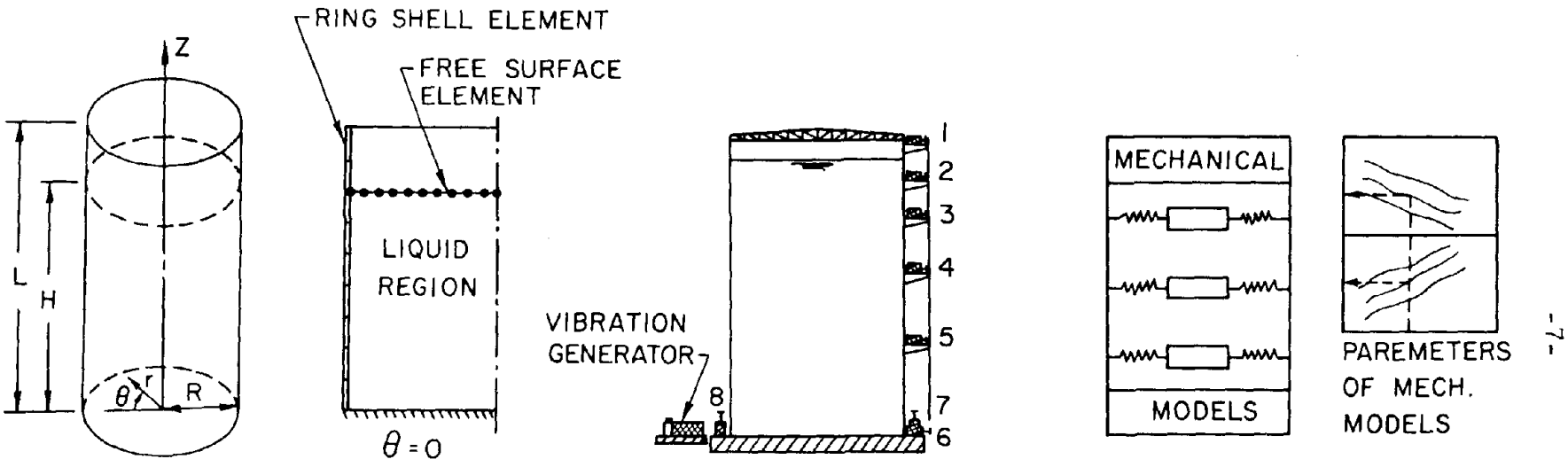

A. Theoretical Study
   (i) Free Vibration Analysis
   (ii) Earthquake Response

B. Vibration Tests of Full-Scale Liquid Storage Tanks

C. Seismic Design
   (i) Simplified Analyses
   (ii) Design Curves

Outline of the Present Study

Having established the basic approach to be used, the analysis was applied to investigate the effect of the initial hoop stress due to the hydrostatic pressure, the effect of the coupling between liquid sloshing and shell vibrations, the effect of the flexibility of the foundation, and the influence of the rigidity of the roof.

The remainder of the first phase of the study was devoted to analyzing the response to earthquake excitation. Special attention was first given to the $\cos\theta$-type modes for which there is a single cosine wave of deflection in the circumferential direction. The importance of the $\cos n\theta$-type modes was then evaluated by examining their influence on the overall seismic response.

The second phase of research involved vibration tests of full-scale tanks. The vibrations of three water storage tanks, with different types of foundations, were measured. Ambient as well as forced vibration measurements were made of the natural frequencies and mode shapes. Measurements were made at selected points along the shell height, at the roof circumference, and around the tank bottom.

The principal aim of the final phase of research was to devise a practical approach which would allow, from the engineering point of view, a simple, fast and satisfactorily accurate estimate of the dynamic response of storage tanks to earthquakes. To achieve this, some simplified analyses were developed. As a natural extension of Housner's model, the effect of the soil deformability on the seismic response of rigid tanks was investigated. To account for the flexibility of relatively tall containers, the tank was assumed to behave as a cantilever beam with bending and shear stiffness. The combined effects of the wall flexibility

and the soil deformability were then investigated. To further simplify the design procedure, a mechanical model which takes into account the flexibility of the tank wall was developed; it is based on the results of the finite element analysis of the liquid-shell system. The parameters of such a model are displayed in charts which facilitate the calculations of the equivalent masses, their centers of gravity, and the periods of vibration. Space limitations necessitate that much of the analysis of the third phase of the study be not included in this report. However, the details of such analysis will be presented in a separate Earthquake Engineering Research Laboratory report entitled "A Procedure for Seismic Design of Liquid Storage Tanks."

The foregoing research advances the understanding of the dynamic behavior of liquid storage tanks, and provides results that should be of practical value.

C. Organization of This Report

This report is divided into two parts covering the first two phases of the study. Each part consists of one or more chapters and each chapter is further divided into sections and subsections. The subject matter is covered in four chapters and each is written in a self-contained manner, and may be read more or less independently of the others. The letter symbols are defined where they are first introduced in the text; they are also summarized in alphabetical order following each chapter. Many references have been included so that the reader may easily obtain a more complete discussion of the various phases of the total subject.

REFERENCES

1. Hanson, R.D., "Behavior of Liquid Storage Tanks," The Great Alaska Earthquake of 1964, Engineering, National Academy of Sciences, Washington, D.C., 1973, pp. 331-339.

2. Rinne, J.E., "Oil Storage Tanks," The Prince William Sound, Alaska, Earthquake of 1964, and Aftershocks, Vol. II, Part A, ESSA, U.S. Coast and Geodetic Survey, Washington: Government Printing Office, 1967, pp. 245-252.

3. Hoskins, L.M., and Jacobsen, L.S., "Water Pressure in a Tank Caused by a Simulated Earthquake," Bulletin Seism. Soc. America, Vol. 24, 1934, pp. 1-32.

4. Jacobsen, L.S., "Impulsive Hydrodynamics of Fluid Inside a Cylindrical Tank and of a Fluid Surrounding a Cylindrical Pier," Bulletin Seism. Soc. America, Vol. 39, 1949, pp. 189-204.

5. Jacobsen, L.S., and Ayre, R.S., "Hydrodynamic Experiments with Rigid Cylindrical Tanks Subjected to Transient Motions," Bulletin Seism. Soc. America, Vol. 41, 1951, pp. 313-346.

6. Housner, G.W., "Dynamic Pressures on Accelerated Fluid Containers," Bulletin Seism. Soc. America, Vol. 47, No. 1, 1957, pp. 15-35.

7. Housner, G.W., "The Dynamic Behavior of Water Tanks," Bulletin Seism. Soc. America, Vol. 53, No. 1, 1963, pp. 381-387.

8. U.S. Atomic Energy Commission, "Nuclear Reactors and Earthquakes," TID-7024, Washington, D.C., 1963, pp. 367-390.

9. Wozniak, R.S., and Mitchell, W.W., "Basis of Seismic Design Provisions for Welded Steel Oil Storage Tanks," Advances in Storage Tank Design, API, 43rd Midyear Meeting, Toronto, Ontario, Canada, 1978.

10. Miles, R.W., "Practical Design of Earthquake Resistant Steel Reservoirs," Proceedings of The Lifeline Earthquake Engineering Specialty Conference, Los Angeles, California, ASCE, 1977.

11. Edwards, N.W., "A Procedure for Dynamic Analysis of Thin Walled Cylindrical Liquid Storage Tanks Subjected to Lateral Ground Motions," Ph.D. Thesis, University of Michigan, Ann Arbor, Michigan, 1969.

12. Hsiung, H.H., and Weingarten, V.I., "Dynamic Analysis of Hydroelastic Systems Using the Finite Element Method," Department of Civil Engineering, University of Southern California, Report USCCE 013, November 1973.

13. Shaaban, S.H., and Nash, W.A., "Finite Element Analysis of a Seismically Excited Cylindrical Storage Tank, Ground Supported, and Partially Filled with Liquid," University of Massachusetts Report to National Science Foundation, August 1975.

14. Balendra, T., and Nash, W.A., "Earthquake Analysis of a Cylindrical Liquid Storage Tank with a Dome by Finite Element Method," Department of Civil Engineering, University of Massachusetts, Amherst, Massachusetts, May 1978.

15. Veletsos, A.S., "Seismic Effects in Flexible Liquid Storage Tanks," Proceedings of the International Association for Earthquake Eng. Fifth World Conference, Rome, Italy, 1974, Vol. 1, pp. 630-639.

16. Veletsos, A.S., and Yang, J.Y., "Earthquake Response of Liquid Storage Tanks," Advances in Civil Engineering through Engineering Mechanics, Proceedings of the Annual EMD Specialty Conference, Raleigh, N.C., ASCE, 1977, pp. 1-24.

17. Wu, C.I., Mouzakis, T., Nash, W.A., and Colonell, J.M., "Natural Frequencies of Cylindrical Liquid Storage Containers," Department of Civil Engineering, University of Massachusetts, June 1975.

18. Clough, D.P., "Experimental Evaluation of Seismic Design Methods for Broad Cylindrical Tanks," University of California Earthquake Engineering Research Center, Report No. UC/EERC 77-10, May 1977.

19. Niwa, A., "Seismic Behavior of Tall Liquid Storage Tanks," University of California Earthquake Engineering Research Center, Report No. UC/EERC 78-04, February 1978.

20. Turner, J.W., "Effect of Out-of-Roundness on the Dynamic Response of Liquid Storage Tanks," M.S. Thesis, Rice University, Houston, Texas, May 1978.

21. Abramson, H.N., ed., "The Dynamic Behavior of Liquids in Moving Containers," NASA SP-106, National Aeronautics and Space Administration, Washington, D.C., 1966.

PART (A)

CHAPTER I

FREE LATERAL VIBRATIONS OF LIQUID STORAGE TANKS

Knowledge of the natural frequencies of vibration and the associated mode shapes is a necessary first step in analyzing the seismic response of deformable, liquid storage tanks. The purpose of this chapter is to establish the basic set of equations which govern the dynamic behavior of the liquid-shell system, and to develop a method of dynamic analysis for free vibrations of ground-supported, circular cylindrical tanks partly filled with liquid.

In the first section, the problem is stated, the coordinate system is introduced, and the possible modes of vibration are discussed. The second section contains the basic equations which govern the liquid motion: the differential equation formulation and the variational formulation. The third section discusses the different expressions for energy in the vibrating shell and the derivation of its equations of motion by means of Hamilton's Principle. In the fourth section, topics which receive attention are: the application of the boundary solution technique to the liquid region, the variational formulation of the overall system, the finite element idealization of the shell, and the evaluation of the several matrices involved in the eigenvalue problem. The fifth section presents detailed numerical examples and explores some of the results which may be deduced about the nature of the dynamic characteristics of the system.

It is worthwhile to mention that the method of analysis presented in this chapter is not only competitively accurate, but it is also computationally effective in the digital computer. In addition, the efficiency of the method facilitates the evaluation of the influence of the various factors which affect the dynamic characteristics, as will be demonstrated in the second chapter.

I-1. Preliminary Considerations

The purpose of this section is to present a brief description of the structural members of a "typical" liquid storage tank and to discuss the advantages of the circular cylindrical tank over other types of containers. This section is also intended to outline the coordinate system used in the analysis, and it contains a discussion of the possible modes of vibration of the liquid-shell system.

I-1-1. Structural Members of a "Typical" Tank

A considerable variety in the configuration of liquid storage tanks can be found in civil engineering applications. However, ground-supported, circular cylindrical tanks are more popular than any other type of containers because they are simple in design, efficient in resisting primary loads, and can be easily constructed.

A "typical" tank consists essentially of a circular cylindrical steel wall that resists the outward liquid pressure, a thin flat bottom plate that rests on the ground and prevents the liquid from leaking out, and a fixed or floating roof that protects the contained liquid from the atmosphere.

The tank wall usually consists of several courses of welded, or riveted, thin steel plates of varying thickness. Since the circular cross-section is not distorted by the hydrostatic pressure of the contained liquid, the wall of the container is designed as a membrane to carry a purely tensile hoop stress. This provides an efficient design because steel is a very economic material especially when used in a condition of tensile stress.

Several roof configurations are employed to cover the contained liquid: a cone, a dome, a plate or a floating roof. A commonly used type is composed of a system of trusses supporting a thin steel plate. The roof-to-shell connection is normally designed as a weak connection so that if the tank is overfilled, the connection will fail before the failure of the shell-to-bottom plate connection. In addition, enough freeboard above the maximum filling height is usually provided to avoid contact between sloshing waves and roof plate.

Different types of foundation may be used to support the tank: a concrete ring wall, a solid concrete slab, or a concrete base supported by piles or caissons. The tank may be anchored to the foundation; in this case, careful attention must be given to the attachment of the anchor bolts to the shell to avoid the possibility of tearing the shell when the tank is subjected to seismic excitations. For unanchored tanks, the bottom plate may be stiffened around the edge to reduce the amount of uplift.

To summarize, circular cylindrical tanks are efficient structures with very thin walls; they are therefore very flexible.

I-1-2. Coordinate System

The liquid-shell system under consideration is shown in Fig. I-1. It is a ground-supported, circular cylindrical, thin-walled liquid container of radius $R^{(*)}$, length L, and thickness h. The tank is partly filled with an inviscid, incompressible liquid to a height H.

Let r, θ, and z denote the radial, circumferential and axial coordinates, respectively, of a point in the region occupied by the tank. The corresponding displacement components of a point on the shell middle surface are denoted by w, v, and u as indicated in Fig. I-1. To describe the location of a point on the free surface during vibration, let ξ measure the superelevation of that point from the quiescent liquid free surface. Lastly, let S_1 denote the quiescent liquid free surface, and S_2 and S_3 denote the wetted surfaces of the shell and the bottom plate, respectively.

In the following analysis, the shell bottom is regarded as anchored to its rigid foundation, and the top of the tank is assumed to be open. The effect of the soil flexibility and the roof rigidity will be discussed later in the second chapter.

I-1-3. Types of Vibrational Modes

The natural, free lateral vibrational modes of a circular cylindrical tank can be classified as the $\cos\theta$-type modes for which there is a single cosine wave of deflection in the circumferential direction, and

---

*The letter symbols are defined where they are first introduced in the text, and they are also summarized in alphabetical order in Appendix I-a.

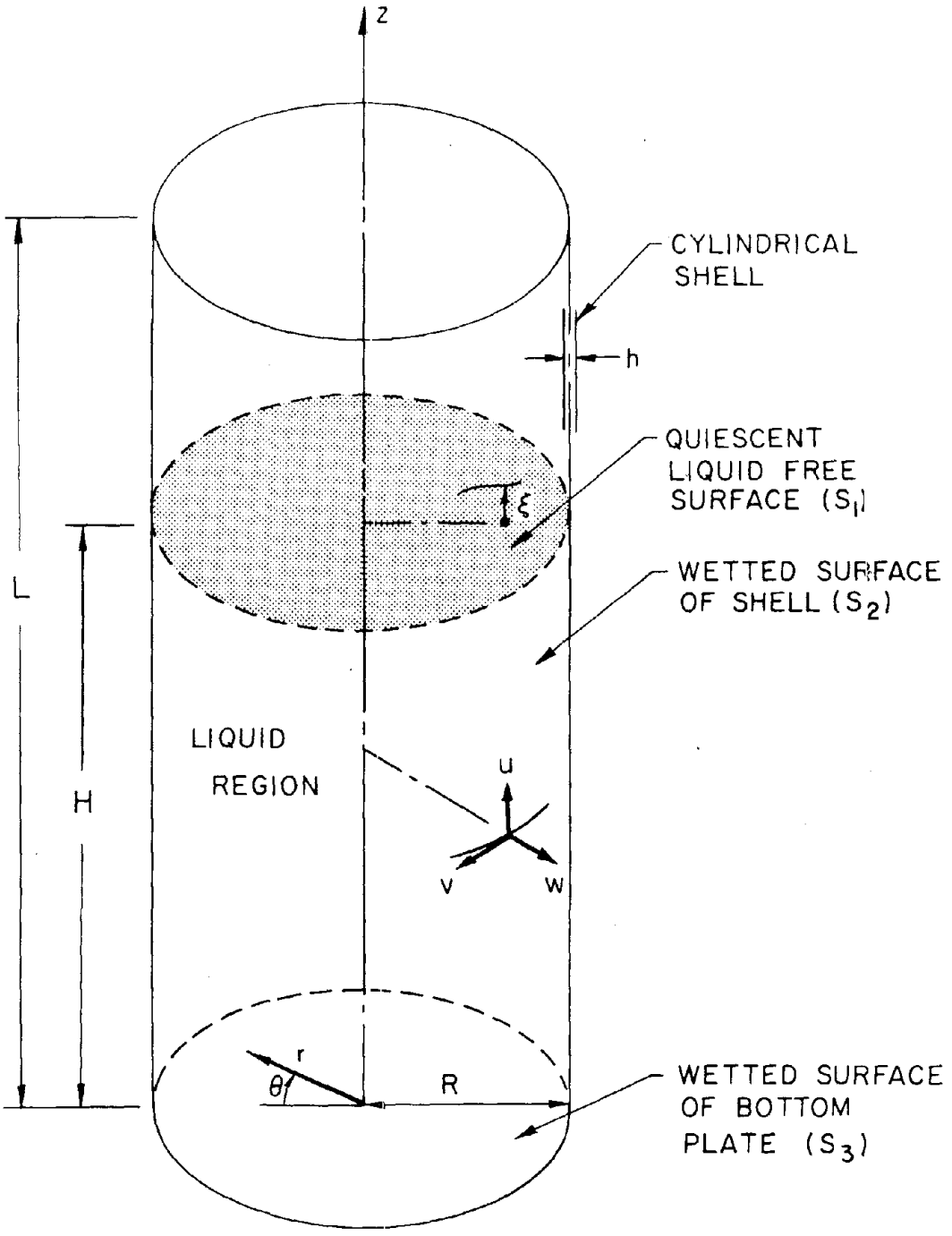

Fig. I-1. Cylindrical Tank and Coordinate System.

as the cosnθ-type modes for which the deflection of the shell involves a number of circumferential waves higher than 1. Figure I-2-a illustrates the circumferential and the vertical nodal patterns of these modes. For a tall tank, the cosθ-type modes can be denoted beam-type modes because the tank behaves like a vertical cantilever beam.

In addition to the shell vibrational modes, there are the low-frequency sloshing modes of the contained liquid. Fig. I-2-b shows the first two free surface modes of a liquid in a rigid circular cylindrical tank.

I-2. Equations Governing Liquid Motion

The following section contains the basic equations which govern the liquid motion inside the tank. The fundamental assumptions involved in the derivation of these equations are briefly presented. The full set of the differential equations and their associated boundary conditions is clearly stated. Finally, the variational equations of the liquid motion are introduced and the equivalence of the two formulations is demonstrated.

I-2-1. Fundamental Assumptions

In a consideration of the different factors affecting the motion of the liquid, the following conventional assumptions are made:

1. The liquid is homogeneous, inviscid and incompressible.
2. The flow field is irrotational.
3. No sources, sinks or cavities are anywhere in the flow field.
4. Only small amplitude oscillations are to be considered.

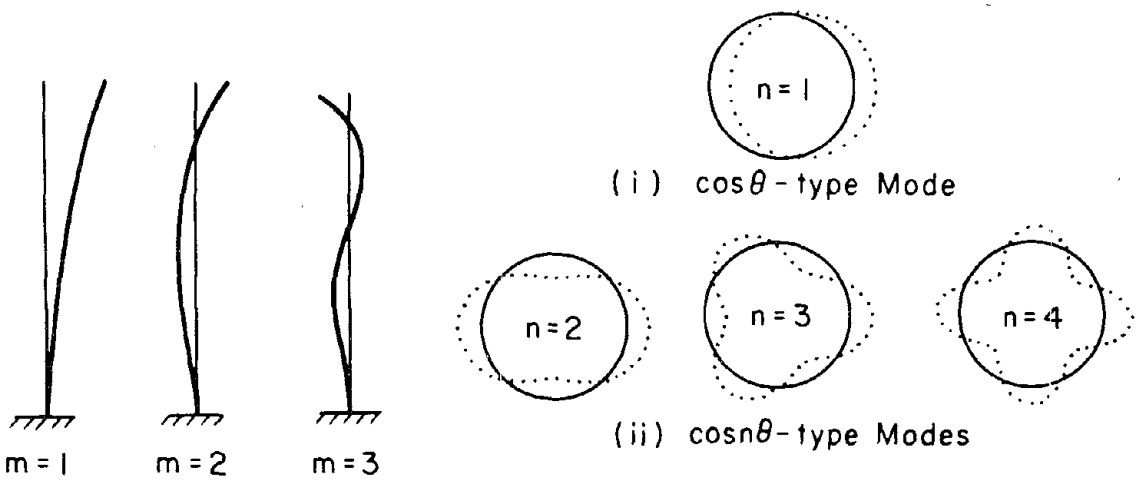

(a) Shell Vibrational Modes

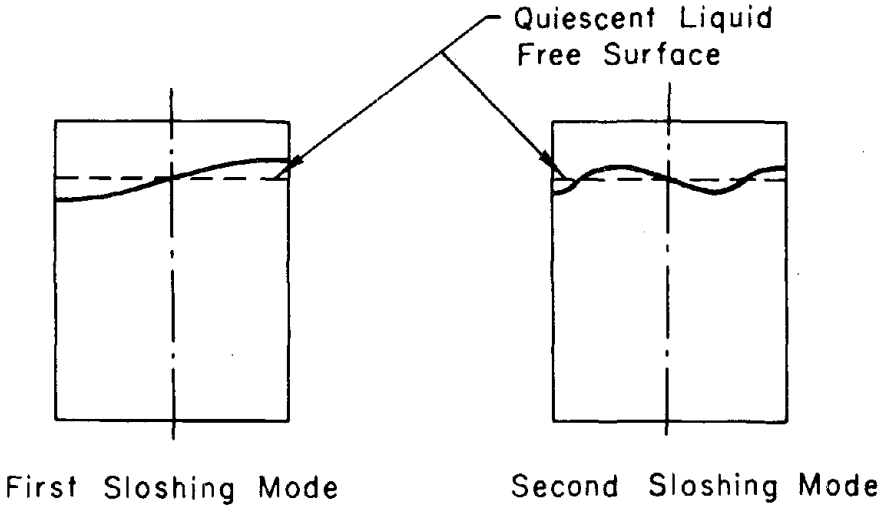

(b) Sloshing Modes in Rigid Tanks

Fig. I-2. Types of Vibrational Modes of the Liquid-Shell System.

I-2-2. Differential Equation Formulation

For the irrotational flow of an incompressible inviscid liquid, the velocity potential, $\phi(r,\theta,z,t)$, satisfies the Laplace equation

$$\nabla^2\phi = 0 \tag{1.1}$$

in the region occupied by the liquid ($0 \le r \le R$, $0 \le \theta \le 2\pi$, $0 \le z \le H$) where

$$\nabla^2 = \frac{\partial^2}{\partial r^2} + \frac{1}{r}\frac{\partial}{\partial r} + \frac{1}{r^2}\frac{\partial^2}{\partial \theta^2} + \frac{\partial^2}{\partial z^2}$$

In addition to being a harmonic function, ϕ must satisfy the proper boundary conditions. Since it is primarily viscous effects which prohibit the liquid from slipping along the solid boundaries, the condition of no tangential slipping at the boundary is relaxed and only the velocities of the liquid and the container normal to their mutual boundaries should be matched. The velocity vector of the liquid is the gradient of the velocity potential, and consequently, the liquid-container boundary conditions can be expressed as follows:

1. At the rigid tank bottom, $z = 0$, the liquid velocity in the vertical direction is zero

$$\frac{\partial\phi}{\partial z}(r,\theta,0,t) = 0 \tag{1.2}$$

2. The liquid adjacent to the wall of the elastic shell, $r = R$, must move radially with it by the same velocity

$$\frac{\partial\phi}{\partial r}(R,\theta,z,t) = \frac{\partial w}{\partial t}(\theta,z,t) \tag{1.3}$$

where $w(\theta,z,t)$ is the shell radial displacement.

At the liquid free surface, $z = H + \xi(r,\theta,t)$, two boundary conditions must be imposed. The first of these conditions is called the kinematic condition which states that a fluid particle on the free surface at some time will always remain on the free surface. The other boundary condition is the dynamic one specifying that the pressure on the free surface is zero. This condition is implemented through the Bernoulli equation for unsteady, irrotational motion

$$\frac{\partial \phi}{\partial t} + \frac{p}{\rho_\ell} + \frac{1}{2} \nabla\phi \cdot \nabla\phi + g \cdot (z-H) = 0 \tag{1.4}$$

where p is the liquid pressure; ρ_ℓ is the liquid density; and g is the gravity acceleration. By considering small-amplitude waves, the free surface boundary conditions become

$$\frac{\partial \phi}{\partial z}(r,\theta,H,t) = \frac{\partial \xi}{\partial t}(r,\theta,t) \tag{1.5}$$

$$\rho_\ell \frac{\partial \phi}{\partial t}(r,\theta,H,t) + \rho_\ell g\, \xi(r,\theta,t) = 0 \tag{1.6}$$

in which the second-order terms are neglected. Equations 1.5 and 1.6 are often combined to yield the following boundary condition which involves only the velocity potential

$$\frac{\partial^2 \phi}{\partial t^2}(r,\theta,H,t) + g \frac{\partial \phi}{\partial z}(r,\theta,H,t) = 0 \tag{1.7}$$

The pressure distribution, $p(r,\theta,z,t)$, can be determined from the Bernoulli equation and is given by

$$p(r,\theta,z,t) = -\rho_\ell \frac{\partial \phi}{\partial t} + \rho_\ell\, g \cdot (H-z) \tag{1.8}$$

where the nonlinear term $\nabla\phi\cdot\nabla\phi$ is neglected as being quadratically small. It should be noted that the pressure p is the sum of the hydrostatic pressure

$$p_s = \rho_\ell g \cdot (H-z) \tag{1.9}$$

and the dynamic pressure

$$p_d = -\rho_\ell \frac{\partial \phi}{\partial t} \tag{1.10}$$

I-2-3. Variational Formulation

There are often two different but equivalent formulations of a problem: a differential formulation and a variational formulation. In the differential formulation, as we have seen, the problem is to integrate a differential equation or a system of differential equations subject to given boundary conditions. In the variational formulation, the problem is to find the unknown function or functions, from a class of admissible functions, by demanding the stationarity of a functional or a system of functionals. The two formulations are equivalent because the functions that satisfy the differential equations and their boundary conditions also extremize the associated functionals. However, the variational formulation often has advantages over the differential formulation from the standpoint of obtaining an approximate solution.

The most generally applicable variational concept is Hamilton's Principle, which may be expressed as follows

$$\delta I = \delta \int_{t_1}^{t_2} (T - U + W)\, dt = 0 \tag{1.11}$$

where T is the kinetic energy, U is the potential energy, W is the work done by external loads and δ is a variational operator taken during the indicated time interval. Hence, this approach necessitates the formulation of the kinetic energy of the liquid, the potential energy of the free surface and the work done by the liquid-shell interface forces.

It has been shown [3] that the appropriate variational functional for the liquid is given by

$$I(\phi) = \int_{t_1}^{t_2} \left\{ \frac{\rho_\ell}{2} \int_V (\nabla\phi \cdot \nabla\phi)\, dv - \frac{\rho_\ell}{2g} \int_{S_1} \left(\frac{\partial\phi}{\partial t}\right)^2 ds - \rho_\ell \int_{S_2} \phi\, \dot{w}\, ds \right\} dt \tag{1.12}$$

where w is the prescribed radial velocity of a point on the middle surface of the shell and V is the original volume occupied by the liquid and bounded by the surface $S = S_1 + S_2 + S_3$; S_1 being the quiescent liquid free surface, and S_2 and S_3 are the wetted surfaces of the elastic shell and the rigid bottom plate, respectively.

By requiring that the first variation of I be identically zero [3], the differential equation (Eq. 1.1) and the associated linear boundary conditions (Eqs. 1.2, 1.3, and 1.7) can be obtained.

A different variational formulation was presented by Luke [4] to obtain the two nonlinear boundary conditions at the free surface. He extended the variational principle used by Bateman [5] by including the free surface displacement among the quantities to be varied and employing the functional

$$I_c(\phi,\xi) = \int_{t_1}^{t_2} L_c(\phi,\xi)\, dt \tag{1.13}$$

where L_c is the complementary Lagrangian functional; ϕ is the liquid velocity potential; and ξ is the free surface displacement measured from the quiescent liquid free surface.

As mentioned earlier, a linearized version of the free surface boundary conditions, Eqs. 1.5 and 1.6, can be deduced by considering small amplitude surface waves. Under this linearization scheme, the complementary Lagrangian functional takes the following form:

$$L_c(\phi,\xi) = -\frac{\rho_\ell}{2}\int_V (\nabla\phi \cdot \nabla\phi)\, dv + \rho_\ell \int_{S_1} (\phi\dot{\xi} - \frac{g\xi^2}{2})\, ds + \rho_\ell \int_{S_2} \phi\, \dot{w}\, ds \tag{1.14}$$

We shall now proceed to show that the requirement for the first variation of the functional $I_c(\phi,\xi)$ to be zero, will provide us with all the Eqs. 1.1 to 1.3, 1.5 and 1.6. Performing the variation, one can obtain

$$\delta I_c = -\rho_\ell \int_{t_1}^{t_2}\int_V (\nabla\phi\cdot\nabla\delta\phi)\, dv\, dt + \rho_\ell \int_{t_1}^{t_2}\int_{S_1} (\phi\delta\dot{\xi} + \dot{\xi}\delta\phi - g\xi\delta\xi)\, ds\, dt + \rho_\ell \int_{t_1}^{t_2}\int_{S_2} \dot{w}\,\delta\phi\, ds\, dt \tag{1.15}$$

Applying Green's theorem to the first term and integrating the second by parts, yields

$$\delta I_c = \rho_\ell \int_{t_1}^{t_2} \int_V \nabla^2\phi \, \delta\phi \, dv \, dt - \rho_\ell \int_{t_1}^{t_2} \int_S \frac{\partial\phi}{\partial\nu} \delta\phi \, ds \, dt$$

$$+ \rho_\ell \int_{t_1}^{t_2} \int_{S_1} (-\dot{\phi}\delta\xi + \dot{\xi}\delta\phi - g\xi\delta\xi) \, ds \, dt + \rho_\ell \int_{S_1} (\phi\delta\xi) \Big|_{t_1}^{t_2} ds$$

$$+ \rho_\ell \int_{t_1}^{t_2} \int_{S_2} \dot{w} \, \delta\phi \, ds \, dt = \rho_\ell \int_{t_1}^{t_2} \int_V \nabla^2\phi \, \delta\phi \, dv \, dt$$

$$- \rho_\ell \int_{t_1}^{t_2} \int_{S_1} \left(\frac{\partial\phi}{\partial\nu} - \dot{\xi}\right) \delta\phi \, ds \, dt - \rho_\ell \int_{t_1}^{t_2} \int_{S_1} (\dot{\phi} + g\xi) \, \delta\xi \, ds \, dt$$

$$- \rho_\ell \int_{t_1}^{t_2} \int_{S_2} \left(\frac{\partial\phi}{\partial\nu} - \dot{w}\right) \delta\phi \, ds \, dt - \rho_\ell \int_{t_1}^{t_2} \int_{S_3} \frac{\partial\phi}{\partial\nu} \delta\phi \, ds \, dt \qquad (1.16)$$

where $\frac{\partial\phi}{\partial\nu}$ is the derivative of the potential function ϕ in the direction of the outward normal vector $\underset{\sim}{\nu}$. Note that the variation and differentiation operators are commutative and the order of integration with respect to space coordinates and time is interchangeable. Also, by definition, $\delta\xi\ (r,\theta,t)$ is zero at $t = t_1$ and $t = t_2$.

The integral in Eq. 1.16 must vanish for any arbitrary values of $\delta\phi$ and $\delta\xi$. These variations can be set equal to zero along S and S_1, respectively, with $\delta\phi$ different from zero throughout the domain V. Therefore, one must have

$$\nabla^2\phi = 0 \qquad \text{in V} \qquad (1.17)$$

Furthermore, because of the arbitrary nature of the variations $\delta\phi$ and $\delta\xi$, one can write

$$\frac{\partial\phi}{\partial\nu} - \dot{\xi} = 0 \text{ along } S_1 \qquad \text{i.e. } \frac{\partial\phi}{\partial z}(r,\theta,H,t) = \frac{\partial\xi}{\partial t}(r,\theta,t) \tag{1.18}$$

$$\dot{\phi} + g\xi = 0 \text{ along } S_1 \qquad \text{i.e. } \frac{\partial\phi}{\partial t}(r,\theta,H,t) + g\xi(r,\theta,t) = 0 \tag{1.19}$$

$$\frac{\partial\phi}{\partial\nu} - \dot{w} = 0 \text{ along } S_2 \qquad \text{i.e. } \frac{\partial\phi}{\partial r}(R,\theta,z,t) = \frac{\partial w}{\partial t}(\theta,z,t) \tag{1.20}$$

$$\frac{\partial\phi}{\partial\nu} = 0 \text{ along } S_3 \qquad \text{i.e. } \frac{\partial\phi}{\partial z}(r,\theta,0,t) = 0 \tag{1.21}$$

Thus, the first variation of the functional I_c has furnished the fundamental differential equation (Eq. 1.17) and the appropriate boundary conditions (Eqs. 1.18 to 1.21).

The functional $I_c(\phi,\xi)$ will be adopted in the following analyses; it is particularly effective in analyzing the dynamic behavior of the liquid-shell-surface wave system, as will be explained later.

I-3. Equations Governing Shell Motion

Shells have all characteristics of plates along with an additional one - curvature. However, a large number of different sets of equations have been derived to describe the motion of a given shell; this is in contrast with the thin plate theory, wherein a single fourth order differential equation of motion is universally agreed upon.

The main purpose of this section is to present a straightforward formulation of the potential and kinetic energies of a circular cylindrical shell, and to derive its equations of motion by means of Hamilton's Principle.

I-3-1. Potential Energy of the Shell

The present formulation of the potential energy is based upon a first approximation theory for thin shells due to V. V. Novozhilov [7]. For simplicity and convenience, the theory will be developed in Appendix I-b for the special case of circular cylindrical shells following an analogous procedure as outlined by Novozhilov for arbitrary shells.

The potential energy stored in the flexible shell is in the form of a strain energy due to the effect of both stretching and bending. The force and moment resultants acting upon an infinitesimal shell element are depicted in Figs. I-3-a and I-3-b, respectively. The strain energy expression can be written as

$$U(t) = \frac{1}{2} \int_0^L \int_0^{2\pi} \left(N_z \varepsilon_z + N_\theta \varepsilon_\theta + \tilde{N}\, \varepsilon_{z\theta} + M_z K_z + M_\theta K_\theta + \tilde{M}\, K_{z\theta} \right) R \, d\theta \, dz \tag{1.22}$$

In equation 1.22, N_z and N_θ are the membrane force resultants; and M_z and M_θ are the bending moment resultants. The quantities $\tilde{N}$ and $\tilde{M}$ are referred to as the effective membrane shear force resultant and the effective twisting moment resultant, respectively; they are related to $N_{z\theta}$, $N_{\theta z}$, $M_{z\theta}$ and $M_{\theta z}$ by

$$\tilde{N} = N_{z\theta} - \frac{M_{\theta z}}{R} = N_{\theta z} \tag{1.23-a}$$

$$\tilde{M} = \frac{1}{2} \left(M_{z\theta} + M_{\theta z} \right) \tag{1.23-b}$$

Now, the shell material is assumed to be homogeneous, isotropic and linearly elastic. Hence, the force and moment resultants can be expressed in terms of the normal and shear strains in the middle

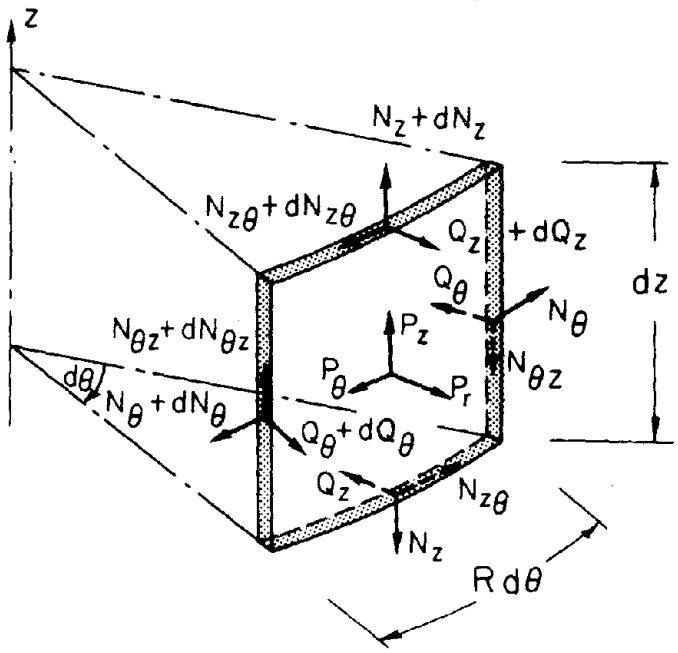

(a) FORCE RESULTANTS

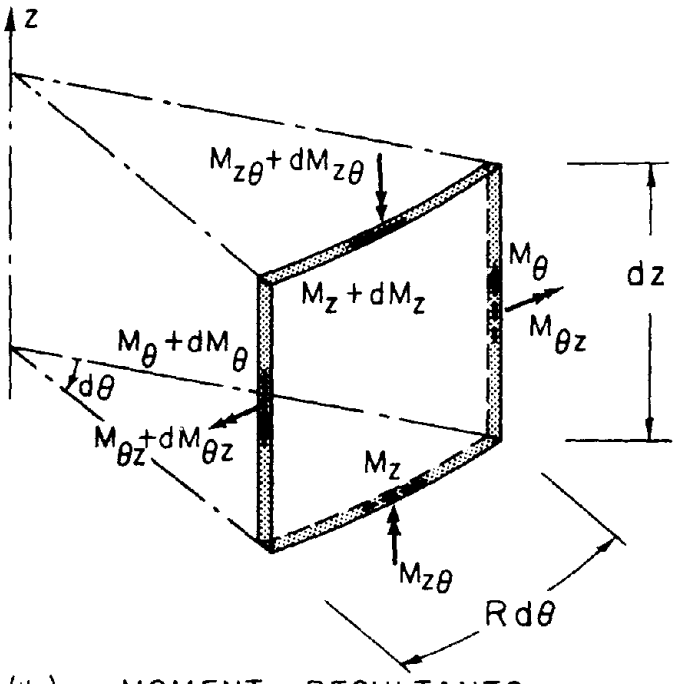

(b) MOMENT RESULTANTS

Fig. I-3. Notation and Positive Directions of Force and Moment Resultants.

surface ε_z, ε_θ and $\varepsilon_{z\theta}$; in terms of the midsurface changes in curvature K_z and K_θ; and in terms of the midsurface twist $K_{z\theta}$ as follows:

$$N_z = k_1 (\varepsilon_z + \nu \varepsilon_\theta) \tag{1.24-a}$$

$$N_\theta = k_1 (\varepsilon_\theta + \nu \varepsilon_z) \tag{1.24-b}$$

$$\tilde{N} = k_1 (\tfrac{1-\nu}{2}) \varepsilon_{z\theta} \tag{1.24-c}$$

$$M_z = k_2 (K_z + \nu K_\theta) \tag{1.24-d}$$

$$M_\theta = k_2 (K_\theta + \nu K_z) \tag{1.24-e}$$

$$\tilde{M} = k_2 (\tfrac{1-\nu}{2}) K_{z\theta} \tag{1.24-f}$$

where k_1 is the extensional rigidity and k_2 is the bending rigidity; they are given by

$$k_1 = \frac{Eh}{1-\nu^2} \tag{1.25-a}$$

$$k_2 = \frac{Eh^3}{12(1-\nu^2)} \tag{1.25-b}$$

where E is the modulus of elasticity of the shell material; ν is Poisson's ratio; and h is the shell thickness.

Equations 1.24-a to f can be written, more conveniently, in the following matrix form:

$$\{\sigma\} = [D]\{\varepsilon\} \tag{1.26}$$

where

$$\{\sigma\} = \begin{Bmatrix} N_z \\ N_\theta \\ \tilde{N} \\ M_z \\ M_\theta \\ \tilde{M} \end{Bmatrix} \quad (1.27\text{-a}) \quad ; \quad \{\varepsilon\} = \begin{Bmatrix} \varepsilon_z \\ \varepsilon_\theta \\ \varepsilon_{z\theta} \\ K_z \\ K_\theta \\ K_{z\theta} \end{Bmatrix} \quad (1.27\text{-b}) \quad ;$$

and

$$[D] = k_1 \begin{bmatrix} 1 & \nu & 0 & 0 & 0 & 0 \\ \nu & 1 & 0 & 0 & 0 & 0 \\ 0 & 0 & \frac{1-\nu}{2} & 0 & 0 & 0 \\ 0 & 0 & 0 & \frac{h^2}{12} & \frac{\nu h^2}{12} & 0 \\ 0 & 0 & 0 & \frac{\nu h^2}{12} & \frac{h^2}{12} & 0 \\ 0 & 0 & 0 & 0 & 0 & \frac{(1-\nu)h^2}{24} \end{bmatrix} \tag{1.27-c}$$

The normal and shear strains in the middle surface are related to the components of the displacement by

$$\varepsilon_z = \frac{\partial u}{\partial z} \tag{1.28-a}$$

$$\varepsilon_\theta = \frac{1}{R}\left(\frac{\partial v}{\partial \theta} + w\right) \tag{1.28-b}$$

$$\varepsilon_{z\theta} = \frac{\partial v}{\partial z} + \frac{1}{R}\frac{\partial u}{\partial \theta} \tag{1.28-c}$$

Also, the changes in the midsurface curvatures K_z and K_θ and the midsurface twist $K_{z\theta}$ are given by

$$K_z = -\frac{\partial^2 w}{\partial z^2} \tag{1.29-a}$$

$$K_\theta = -\frac{1}{R^2}\left(\frac{\partial^2 w}{\partial \theta^2} - \frac{\partial v}{\partial \theta}\right) \tag{1.29-b}$$

$$K_{z\theta} = -\frac{2}{R}\frac{\partial^2 w}{\partial z \partial \theta} + \frac{2}{R}\frac{\partial v}{\partial z} \tag{1.29-c}$$

Now, the generalized strain vector $\{\varepsilon\}$ can be expressed in terms of the displacement vector $\{d\}$ as follows:

$$\{\varepsilon\} = [P]\{d\} \tag{1.30}$$

where $\{d\} = \begin{Bmatrix} u \\ v \\ w \end{Bmatrix}$ (1.31) ; and $[P]$ is a differential operator matrix defined by

$$[P] = \begin{bmatrix} \frac{\partial}{\partial z} & 0 & 0 \\ 0 & \frac{1}{R}\frac{\partial}{\partial \theta} & \frac{1}{R} \\ \frac{1}{R}\frac{\partial}{\partial \theta} & \frac{\partial}{\partial z} & 0 \\ 0 & 0 & -\frac{\partial^2}{\partial z^2} \\ 0 & \frac{1}{R^2}\frac{\partial}{\partial \theta} & -\frac{1}{R^2}\frac{\partial^2}{\partial \theta^2} \\ 0 & \frac{2}{R}\frac{\partial}{\partial z} & -\frac{2}{R}\frac{\partial^2}{\partial z \partial \theta} \end{bmatrix} \tag{1.32}$$

With the aid of equations 1.22, 1.26, and 1.30, the potential energy expression can be written as

$$U(t) = \frac{1}{2}\int_0^L \int_0^{2\pi} (\{\varepsilon\}^T\{\sigma\})\, R\, d\theta\, dz$$

$$= \frac{1}{2}\int_0^L \int_0^{2\pi} (\{\varepsilon\}^T[D]\{\varepsilon\})\, R\, d\theta\, dz \tag{1.33}$$

or, in terms of the displacement vector, as

$$U(t) = \frac{R}{2}\int_0^L \int_0^{2\pi} \left\{([P]\{d\})^T[D]([P]\{d\})\right\}\, d\theta\, dz \tag{1.34}$$

It is worthwhile to indicate that Eqs. 1.24-a to f are as simple as possible, but they still fulfill the requirements which are sufficient for the validity of the fundamental theorems of the theory of elasticity in the theory of shells [8].

I-3-2. Kinetic Energy of the Shell

The kinetic energy of the shell, neglecting rotary inertia, can be written as

$$T(t) = \frac{1}{2} \int_0^L \int_0^{2\pi} \left\{ m(z) \left[\left(\frac{\partial u(\theta,z,t)}{\partial t} \right)^2 + \left(\frac{\partial v(\theta,z,t)}{\partial t} \right)^2 + \left(\frac{\partial w(\theta,z,t)}{\partial t} \right)^2 \right] \right\} R \, d\theta \, dz \qquad (1.35)$$

where m(z) is the mass of the shell per unit area. Eq. 1.35 can be written, more conveniently, as follows

$$T(t) = \frac{1}{2} \int_0^L \int_0^{2\pi} \left(m(z) \{\dot{d}\}^T \{\dot{d}\} \right) R \, d\theta \, dz \qquad (1.36)$$

where {d} is the displacement vector, defined by Eq. 1.31, and $\dot{(\ )}$ means differentiation with respect to the time, t.

I-3-3. Derivation of the Equations of Motion of the Shell

The differential equations of motion of the elastic shell and their associated boundary conditions will be derived by means of Hamilton's Principle. The use of this variational principle has

the advantage of furnishing, automatically, the correct number of boundary conditions and their correct expressions. It employs the different expressions of energy of the vibrating shell which have been derived in the preceding sections. In addition, an expression of the work done by the liquid-shell interface forces, through an arbitrary virtual displacement δw, is required; it can be given by

$$\delta W = \int_0^H \int_0^{2\pi} \left(p(R,\theta,z,t)\, \delta w\right) R\, d\theta\, dz \tag{1.37}$$

where $p(R,\theta,z,t)$ is the prescribed liquid pressure per unit area of the middle surface of the shell; and H is the liquid height.

Many investigators have considered various simplifying assumptions so that it may be possible to obtain closed form solutions to the resulting set of differential equations. Since the method of solution to be used in this analysis is a numerical one, such considerations need not be made.

The variation of the kinetic energy, T(t), has the form

$$\delta T(t) = \int_0^L \int_0^{2\pi} \left\{ m(z) \left[\frac{\partial u}{\partial t}\, \delta\left(\frac{\partial u}{\partial t}\right) + \frac{\partial v}{\partial t}\, \delta\left(\frac{\partial v}{\partial t}\right) + \frac{\partial w}{\partial t}\, \delta\left(\frac{\partial w}{\partial t}\right) \right] \right\} R\, d\theta\, dz$$

$$= \int_0^L \int_0^{2\pi} \left\{ m(z) \left[\frac{\partial u}{\partial t} \frac{\partial}{\partial t} (\delta u) + \frac{\partial v}{\partial t} \frac{\partial}{\partial t} (\delta v) + \frac{\partial w}{\partial t} \frac{\partial}{\partial t} (\delta w) \right] \right\} R\, d\theta\, dz;$$

therefore,

$$\int_{t_1}^{t_2} \delta T(t)dt = \int_{t_1}^{t_2}\int_{0}^{L}\int_{0}^{2\pi}\left\{m(z)\left[\frac{\partial u}{\partial t}\frac{\partial}{\partial t}(\delta u) + \frac{\partial v}{\partial t}\frac{\partial}{\partial t}(\delta v) + \frac{\partial w}{\partial t}\frac{\partial}{\partial t}(\delta w)\right]\right\}R\, d\theta dz dt$$

$$= \int_{0}^{L}\int_{0}^{2\pi}\left\{m(z)\left[\left(\frac{\partial u}{\partial t}\,\delta u\right)\Big|_{t_1}^{t_2} + \left(\frac{\partial v}{\partial t}\,\delta v\right)\Big|_{t_1}^{t_2} + \left(\frac{\partial w}{\partial t}\,\delta w\right)\Big|_{t_1}^{t_2}\right]\right\}R\, d\theta dz$$

$$- \int_{t_1}^{t_2}\int_{0}^{L}\int_{0}^{2\pi}\left\{m(z)\left[\frac{\partial^2 u}{\partial t^2}\,\delta u + \frac{\partial^2 v}{\partial t^2}\,\delta v + \frac{\partial^2 w}{\partial t^2}\,\delta w\right]\right\}R\, d\theta dz dt$$

$$= -\int_{t_1}^{t_2}\int_{0}^{L}\int_{0}^{2\pi}\left\{m(z)\left[\frac{\partial^2 u}{\partial t^2}\,\delta u + \frac{\partial^2 v}{\partial t^2}\,\delta v + \frac{\partial^2 w}{\partial t^2}\,\delta w\right]\right\}R\, d\theta dz dt \qquad (1.38)$$

Note that, by definition, $\delta u(\theta,z,t)$, $\delta v(\theta,z,t)$, and $\delta w(\theta,z,t)$ are zero at $t = t_1$ and $t = t_2$.

The strain energy expression, Eq. 1.33, can be written, in terms of u, v, and w, as follows

$$U(t) = \frac{Eh}{2(1-\nu^2)}\int_{0}^{L}\int_{0}^{2\pi}\left\{\left(\left[\frac{\partial u}{\partial z} + \frac{1}{R}\left(\frac{\partial v}{\partial \theta} + w\right)\right]^2 - \frac{2(1-\nu)}{R}\left[\frac{\partial u}{\partial z}\left(\frac{\partial v}{\partial \theta} + w\right)\right] + \right.\right.$$

$$\left.\frac{(1-\nu)}{2}\left[\frac{1}{R}\frac{\partial u}{\partial \theta} + \frac{\partial v}{\partial z}\right]^2\right) + \frac{h^2}{12}\left(\left[\frac{\partial^2 w}{\partial z^2} + \frac{1}{R^2}\left(\frac{\partial^2 w}{\partial \theta^2} - \frac{\partial v}{\partial \theta}\right)\right]^2 -\right.$$

$$\left.\left.\frac{2(1-\nu)}{R^2}\left[\frac{\partial^2 w}{\partial z^2}\left(\frac{\partial^2 w}{\partial \theta^2} - \frac{\partial v}{\partial \theta}\right)\right] + \frac{2(1-\nu)}{R^2}\left[\frac{\partial^2 w}{\partial z \partial \theta} - \frac{\partial v}{\partial z}\right]^2\right)\right\} R\, d\theta\, dz \qquad (1.39)$$

and therefore, the variation of the strain energy can be expressed as

$$\delta U(t) = \frac{Eh}{(1-\nu^2)} \int_0^L \int_0^{2\pi} \left\{ \left[\frac{\partial u}{\partial z} + \frac{1}{R}\left(\frac{\partial v}{\partial \theta} + w\right) \right] \left[\delta\left(\frac{\partial u}{\partial z}\right) + \frac{1}{R}\delta\left(\frac{\partial v}{\partial \theta}\right) + \frac{1}{R}\delta w \right] - \frac{(1-\nu)}{R} \cdot \right.$$

$$\left[\frac{\partial u}{\partial z}\,\delta\left(\frac{\partial v}{\partial \theta}\right) + \frac{\partial u}{\partial z}\,\delta w + \left(\frac{\partial v}{\partial \theta} + w\right)\delta\left(\frac{\partial u}{\partial z}\right) \right] + \frac{1-\nu}{2} \left[\frac{1}{R}\frac{\partial u}{\partial \theta} + \frac{\partial v}{\partial z} \right] \left[\frac{1}{R}\,\delta\left(\frac{\partial u}{\partial \theta}\right) + \delta\left(\frac{\partial v}{\partial z}\right) \right]$$

$$+ \frac{h^2}{12} \left[\frac{\partial^2 w}{\partial z^2} + \frac{1}{R^2}\left(\frac{\partial^2 w}{\partial \theta^2} - \frac{\partial v}{\partial \theta}\right) \right] \left[\delta\left(\frac{\partial^2 w}{\partial z^2}\right) + \frac{1}{R^2}\delta\left(\frac{\partial^2 w}{\partial \theta^2}\right) - \frac{1}{R^2}\delta\left(\frac{\partial v}{\partial \theta}\right) \right] - \frac{(1-\nu)h^2}{12R^2} \cdot$$

$$\left[\frac{\partial^2 w}{\partial z^2}\,\delta\left(\frac{\partial^2 w}{\partial \theta^2}\right) - \frac{\partial^2 w}{\partial z^2}\,\delta\left(\frac{\partial v}{\partial \theta}\right) + \left(\frac{\partial^2 w}{\partial \theta^2} - \frac{\partial v}{\partial \theta}\right)\delta\left(\frac{\partial^2 w}{\partial z^2}\right) \right] + \frac{2(1-\nu)h^2}{12R^2} \left[\frac{\partial^2 w}{\partial z \partial \theta} - \frac{\partial v}{\partial z} \right] \cdot$$

$$\left. \left[\delta\left(\frac{\partial^2 w}{\partial z \partial \theta}\right) - \delta\left(\frac{\partial v}{\partial z}\right) \right] \right\} R\, d\theta\, dz,$$

then integrating by parts, if it is necessary, yields

$$\delta U(t) = \frac{Eh}{(1-\nu^2)} \int_0^L \int_0^{2\pi} \left\{ - \left[\frac{\partial^2 u}{\partial z^2} + \frac{(1-\nu)}{2R^2}\frac{\partial^2 u}{\partial \theta^2} + \frac{(1+\nu)}{2R}\frac{\partial^2 v}{\partial z \partial \theta} + \frac{\nu}{R}\frac{\partial w}{\partial z} \right] \delta u \right.$$

$$- \left[\frac{(1+\nu)}{2R}\frac{\partial^2 u}{\partial z \partial \theta} + \frac{(1-\nu)}{2}\frac{\partial^2 v}{\partial z^2} + \frac{1}{R^2}\frac{\partial^2 v}{\partial \theta^2} + \frac{h^2}{12R^2}\left(\frac{1}{R^2}\frac{\partial^2 v}{\partial \theta^2} + 2(1-\nu)\frac{\partial^2 v}{\partial z^2} \right) + \frac{1}{R^2}\frac{\partial w}{\partial \theta} \right.$$

$$\left. - \frac{h^2}{12R^2}\left(\frac{1}{R^2}\frac{\partial^3 w}{\partial \theta^3} + (2-\nu)\frac{\partial^3 w}{\partial z^2 \partial \theta} \right) \right] \delta v + \left[\frac{\nu}{R}\frac{\partial u}{\partial z} + \frac{1}{R^2}\frac{\partial v}{\partial \theta} - \frac{h^2}{12R^2}\left(\frac{1}{R^2}\frac{\partial^3 v}{\partial \theta^3} \right.\right.$$

$$+ (2-\nu) \frac{\partial^3 v}{\partial z^2 \partial \theta}\Bigg) + \frac{w}{R^2} + \frac{h^2}{12}\left(\frac{\partial^4 w}{\partial z^4} + \frac{2}{R^2}\frac{\partial^4 w}{\partial z^2 \partial \theta^2} + \frac{1}{R^4}\frac{\partial^4 w}{\partial \theta^4}\right)\Bigg] \delta w \Bigg\} R \, d\theta \, dz$$

$$+ \frac{Eh}{(1-\nu^2)} \int_0^{2\pi} \left\{ \left[\frac{\partial u}{\partial z} + \frac{\nu}{R}\left(\frac{\partial v}{\partial \theta} + w\right)\right] \cdot \delta u \Big|_0^L + \frac{1-\nu}{2}\left[\frac{1}{R}\frac{\partial u}{\partial \theta} + \frac{\partial v}{\partial z}\right.\right.$$

$$\left. - \frac{h^2}{3R^2}\left(\frac{\partial^2 w}{\partial z \partial \theta} - \frac{\partial v}{\partial z}\right)\right] \cdot \delta v \Big|_0^L + \frac{h^2}{12}\left[\frac{\partial^2 w}{\partial z^2} + \frac{\nu}{R^2}\left(\frac{\partial^2 w}{\partial \theta^2} - \frac{\partial v}{\partial \theta}\right)\right] \cdot \delta\left(\frac{\partial w}{\partial z}\right)\Big|_0^L$$

$$\left. - \frac{h^2}{12}\left[\frac{\partial^3 w}{\partial z^3} + \frac{\nu}{R^2}\left(\frac{\partial^3 w}{\partial z \partial \theta^2} - \frac{\partial^2 v}{\partial z \partial \theta}\right)\right] \cdot \delta w \Big|_0^L \right\} R \, d\theta \qquad (1.40)$$

Introducing Eqs. 1.38 and 1.40 into Eq. 1.11, and assuming that the tank is empty for the time being, gives

$$\frac{Eh}{(1-\nu^2)} \int_{t_1}^{t_2} \int_0^L \int_0^{2\pi} \left\{ \left[\frac{\partial^2 u}{\partial z^2} + \frac{1-\nu}{2R^2}\frac{\partial^2 u}{\partial \theta^2} - \frac{m(1-\nu^2)}{Eh}\frac{\partial^2 u}{\partial t^2} + \frac{(1+\nu)}{2R}\frac{\partial^2 v}{\partial z \partial \theta} + \frac{\nu}{R}\frac{\partial w}{\partial z}\right] \cdot \delta u \right.$$

$$+ \left[\frac{(1+\nu)}{2R}\frac{\partial^2 u}{\partial z \partial \theta} + \frac{1-\nu}{2}\frac{\partial^2 v}{\partial z^2} + \frac{1}{R^2}\frac{\partial^2 v}{\partial \theta^2} - \frac{m(1-\nu^2)}{Eh}\frac{\partial^2 v}{\partial t^2} + \frac{h^2}{12R^2}\left(\frac{1}{R^2}\frac{\partial^2 v}{\partial \theta^2} + \right.\right.$$

$$\left. 2\,(1-\nu)\frac{\partial^2 v}{\partial z^2}\right) + \frac{1}{R^2}\frac{\partial w}{\partial \theta} - \frac{h^2}{12R^2}\left(\frac{1}{R^2}\frac{\partial^3 w}{\partial \theta^3} + (2-\nu)\frac{\partial^3 w}{\partial z^2 \partial \theta}\right)\Bigg] \cdot \delta v -$$

$$\left[\frac{\nu}{R}\frac{\partial u}{\partial z} + \frac{1}{R^2}\frac{\partial v}{\partial \theta} - \frac{h^2}{12R^2}\left(\frac{1}{R^2}\frac{\partial^3 v}{\partial \theta^3} + (2-\nu)\frac{\partial^3 v}{\partial z^2 \partial \theta}\right) + \frac{w}{R^2} + \frac{m(1-\nu^2)}{Eh}\frac{\partial^2 w}{\partial t^2}\right.$$

$$+\frac{h^2}{12}\left(\frac{\partial^4 w}{\partial z^4}+\frac{2}{R^2}\frac{\partial^4 w}{\partial z^2\partial\theta^2}+\frac{1}{R^4}\frac{\partial^4 w}{\partial\theta^4}\right)\Bigg]\cdot\delta w\Bigg\}\,R\,d\theta\,dz\,dt$$

$$+\frac{Eh}{(1-\nu^2)}\int_{t_1}^{t_2}\int_0^{2\pi}\Bigg\{-\left[\frac{\partial u}{\partial z}+\frac{\nu}{R}\left(\frac{\partial v}{\partial\theta}+w\right)\right]\cdot\delta u\Bigg|_0^L-\frac{(1-\nu)}{2}\left[\frac{1}{R}\frac{\partial u}{\partial\theta}+\frac{\partial v}{\partial z}-\frac{h^2}{3R^2}\cdot\right.$$

$$\left.\left(\frac{\partial^2 w}{\partial z\partial\theta}-\frac{\partial v}{\partial z}\right)\right]\cdot\delta v\Bigg|_0^L-\frac{h^2}{12}\left[\frac{\partial^2 w}{\partial z^2}+\frac{\nu}{R^2}\left(\frac{\partial^2 w}{\partial\theta^2}-\frac{\partial v}{\partial\theta}\right)\right]\cdot\delta\left(\frac{\partial w}{\partial z}\right)\Bigg|_0^L+\frac{h^2}{12}\left[\frac{\partial^3 w}{\partial z^3}+\frac{\nu}{R^2}\cdot\right.$$

$$\left.\left(\frac{\partial^3 w}{\partial z\partial\theta^2}-\frac{\partial^2 v}{\partial z\partial\theta}\right)\right]\cdot\delta w\Bigg|_0^L\Bigg\}\,R\,d\theta\,dt=0 \qquad (1.41)$$

The integral must vanish for any arbitrary values of δu, δv, δw, and $\delta\left(\frac{\partial w}{\partial z}\right)$, so these variations can be set equal to zero at $z = 0$ and $z = L$, and different from zero throughout the domain $0<z<L$. Therefore, one must have

$$\frac{\partial^2 u}{\partial z^2}+\frac{(1-\nu)}{2R^2}\frac{\partial^2 u}{\partial\theta^2}-\frac{m(1-\nu^2)}{Eh}\frac{\partial^2 u}{\partial t^2}+\frac{(1+\nu)}{2R}\frac{\partial^2 v}{\partial z\partial\theta}+\frac{\nu}{R}\frac{\partial w}{\partial z}=0 \qquad (1.42)$$

$$\frac{1+\nu}{2R}\frac{\partial^2 u}{\partial z\partial\theta}+\frac{1-\nu}{2}\frac{\partial^2 v}{\partial z^2}+\frac{1}{R^2}\frac{\partial^2 v}{\partial\theta^2}-\frac{m(1-\nu^2)}{Eh}\frac{\partial^2 v}{\partial t^2}+\frac{h^2}{12R^2}\left(\frac{1}{R^2}\frac{\partial^2 v}{\partial\theta^2}+2(1-\nu)\frac{\partial^2 v}{\partial z^2}\right)$$

$$+\frac{1}{R^2}\frac{\partial w}{\partial\theta}-\frac{h^2}{12R^2}\left(\frac{1}{R^2}\frac{\partial^3 w}{\partial\theta^3}+(2-\nu)\frac{\partial^3 w}{\partial z^2\partial\theta}\right)=0 \qquad (1.43)$$

$$\frac{\nu}{R}\frac{\partial u}{\partial z} + \frac{1}{R^2}\frac{\partial v}{\partial \theta} - \frac{h^2}{12R^2}\left(\frac{1}{R^2}\frac{\partial^3 v}{\partial \theta^3} + (2-\nu)\frac{\partial^3 v}{\partial z^2 \partial \theta}\right) + \frac{w}{R^2} + \frac{m(1-\nu^2)}{Eh}\frac{\partial^2 w}{\partial t^2} +$$

$$\frac{h^2}{12}\left(\frac{\partial^4 w}{\partial z^4} + \frac{2}{R^2}\frac{\partial^4 w}{\partial z^2 \partial \theta^2} + \frac{1}{R^4}\frac{\partial^4 w}{\partial \theta^4}\right) = 0 \qquad (1.44)$$

Eqs. 1.42, 1.43, and 1.44 are the basic differential equations of motion of the shell and can be expressed in the following matrix form

$$[L]\{d\} = \{0\} \qquad (1.45)$$

where $\{d\}$ is the displacement vector defined in Eq. 1.31; and $[L]$ is a linear differential operator which can be written as

$$[L] = \begin{bmatrix} \frac{\partial^2}{\partial z^2} + \frac{(1-\nu)}{2R^2}\frac{\partial^2}{\partial \theta^2} - \frac{\rho_s(1-\nu^2)}{E}\frac{\partial^2}{\partial t^2} & \frac{(1+\nu)}{2R}\frac{\partial^2}{\partial z \partial \theta} & \frac{\nu}{R}\frac{\partial}{\partial z} \\ \frac{1+\nu}{2R}\frac{\partial^2}{\partial z \partial \theta} & \frac{(1-\nu)}{2}\frac{\partial^2}{\partial z^2} + \frac{1}{R^2}\frac{\partial^2}{\partial \theta^2} - \frac{\rho_s(1-\nu^2)}{E}\frac{\partial^2}{\partial t^2} + \alpha\left[2(1-\nu)\frac{\partial^2}{\partial z^2} + \frac{1}{R^2}\frac{\partial^2}{\partial \theta^2}\right] & \frac{1}{R^2}\frac{\partial}{\partial \theta} - \alpha\left[(2-\nu)\frac{\partial^3}{\partial z^2 \partial \theta} + \frac{1}{R^2}\frac{\partial^3}{\partial \theta^3}\right] \\ \frac{\nu}{R}\frac{\partial}{\partial z} & \frac{1}{R^2}\frac{\partial}{\partial \theta} - \alpha\left[(2-\nu)\frac{\partial^3}{\partial z^2 \partial \theta} + \frac{1}{R^2}\frac{\partial^3}{\partial \theta^3}\right] & \frac{1}{R^2} + \alpha R^2 \Delta^4 + \frac{\rho_s(1-\nu^2)}{E}\frac{\partial^2}{\partial t^2} \end{bmatrix} \qquad (1.46)$$

where

$$\alpha = \frac{h^2}{12R^2} \; ; \quad \Delta^4 = \Delta^2 \Delta^2 \; ; \; \Delta^2 = \frac{\partial^2}{\partial z^2} + \frac{1}{R^2}\frac{\partial^2}{\partial \theta^2} \; ; \text{ and } \rho_s = \frac{m}{h} \tag{1.47}$$

Furthermore, because of the arbitrary nature of the variation, in considering Eq. 1.41, one can write

$$\left\{ \frac{Eh}{(1-\nu^2)} \left[\frac{\partial u}{\partial z} + \frac{\nu}{R}\left(\frac{\partial v}{\partial \theta} + w \right) \right] \right\} \cdot \delta u \Big|_0^L = 0 \quad , \tag{1.48}$$

$$\left\{ \frac{Eh}{2(1+\nu)} \left[\frac{1}{R}\frac{\partial u}{\partial \theta} + \frac{\partial v}{\partial z} - \frac{h^2}{3R^2}\left(\frac{\partial^2 w}{\partial z \partial \theta} - \frac{\partial v}{\partial z} \right) \right] \cdot \delta v \right|_0^L = 0 \quad , \tag{1.49}$$

$$\left\{ \frac{Eh^3}{12(1-\nu^2)} \left[\frac{\partial^2 w}{\partial z^2} + \frac{\nu}{R^2}\left(\frac{\partial^2 w}{\partial \theta^2} - \frac{\partial v}{\partial \theta} \right) \right] \right\} \cdot \delta\left(\frac{\partial w}{\partial z} \right) \Big|_0^L = 0 \quad , \tag{1.50}$$

$$\text{and } \left\{ \frac{Eh^3}{12(1-\nu^2)} \left[\frac{\partial^3 w}{\partial z^3} + \frac{\nu}{R^2}\left(\frac{\partial^3 w}{\partial z \partial \theta^2} - \frac{\partial^2 v}{\partial z \partial \theta} \right) \right] \right\} \cdot \delta w \Big|_0^L = 0 \tag{1.51}$$

In order to clarify the four terms in parentheses in the preceding equations, reference can be made to Eqs. 1.23, 1.24, 1.25, 1.28, and 1.29. It will be recognized that these terms represent the resultants N_z, $\left(N_{z\theta} + \frac{M_{z\theta}}{R} \right)$, M_z, and $\left(Q_z + \frac{1}{R}\frac{\partial M_{z\theta}}{\partial \theta} \right)$, respectively. Hence, Eqs. 1.48, 1.49, 1.50, and 1.51 take into account the possibility that either

$$N_z = 0 \quad \text{or} \quad u = 0 \quad \text{at} \quad z = 0, \; z = L \tag{1.52}$$

$$N_{z\theta} + \frac{M_{z\theta}}{R} = 0 \quad \text{or} \quad v = 0 \quad \text{at} \quad z = 0, \; z = L \tag{1.53}$$

$$M_z = 0 \quad \text{or} \quad \frac{\partial w}{\partial z} = 0 \quad \text{at} \quad z = 0, \; z = L \tag{1.54}$$

$$Q_z + \frac{1}{R}\frac{M_{z\theta}}{\partial\theta} = 0 \quad \text{or} \quad w = 0 \quad \text{at} \quad z = 0, \; z = L \tag{1.55}$$

Equations 1.52, 1.53, 1.54, and 1.55 represent both the natural and geometrical boundary conditions associated with the equations of motion of the shell.

For a partly filled liquid container, the equations of motion take the following form

$$[L]\{d\} = \frac{(1-\nu^2)}{Eh}\{F\} \tag{1.56}$$

where $\{F\} = \{0\}$ $(H<z<L)$ and $\{F\} = \begin{Bmatrix} 0 \\ 0 \\ p \end{Bmatrix}$ $(0<z<H)$; p being the liquid pressure.

I-4. A Numerical Approach to the Lateral Free Vibration - The Finite Element and the Boundary Solution Methods

The finite element method is now recognized as an effective discretization procedure which is applicable to a variety of engineering problems. It provides a convenient and reliable idealization of the system and is particularly effective in digital-computer analyses. However, for some specific simple problems, the so-called boundary solution technique [10] may be even more economical and

simpler to use. We shall briefly discuss the similarities and differences of these two procedures.

In the standard procedure of the finite element method, the unknown function is approximated by trial functions which do not satisfy the continuum equations exactly either in the domain or, in general, on the boundaries. The unknown nodal values are determined by an approximate satisfaction of both the differential equations and the boundary conditions in an integrated mean sense. The boundary solution technique consists in essence of choosing a set of trial functions which satisfies, a priori, the differential equations throughout the domain. Now, only the boundary conditions have to be satisfied in an average integral sense. Since the boundary solution technique involves only the boundary, a much reduced number of unknowns can be used as compared with the standard finite element procedure. At this point, we must remark that the boundary solution technique is limited to relatively simple homogeneous and linear problems in which suitable trial functions can be identified.

Since each procedure has certain merits and limitations of its own, it may be advantageous to solve one part of the region using the boundary solution technique and the other part by the finite element method. In the following section, such a combination has been used successfully. The liquid region is treated as a continuum by boundary solution technique and the elastic shell is modelled by finite elements. In this approach, the number of unknowns is sub-

stantially less than in those analyses where both tank wall and liquid are subdivided into finite elements [3, 12, 13].

I-4-1. Application of the Boundary Solution Technique to the Liquid Region

It has been shown that the functional $I_c(\phi,\xi)$ defined by Eqs. 1.13 and 1.14, together with the variational statement $\delta I_c = 0$, provide the necessary differential equation to be satisfied throughout the liquid domain as well as the appropriate boundary conditions. Henceforth, we shall be concerned with the variational formulation, demanding stationarity of

$$I_c(\phi,\xi) = \int_{t_1}^{t_2} \left\{ -\frac{\rho_\ell}{2} \int_V (\nabla\phi \cdot \nabla\phi)\, dv + \rho_\ell \int_{S_1} \left(\phi\dot{\xi} - \frac{g\xi^2}{2}\right) ds + \rho_\ell \int_{S_2} \phi\dot{w}\, ds \right\} dt \tag{1.57}$$

Once a set of trial functions, $\overset{*}{N}_i(r,\theta,z)$, which are solutions of the Laplace equation, have been identified, then one can assume that

$$\phi(r,\theta,z,t) = \sum_{i=1}^{I} \overset{*}{N}_i(r,\theta,z) \cdot A_i(t) \tag{1.58}$$

where I is the number of trial functions to be used in the expansion of the potential function ϕ.

Since the velocity potential function defined by Eq. 1.58 satisfies the Laplace equation, $\nabla^2\phi = 0$, identically throughout the liquid

domain, one can replace the volume integral in Eq. 1.57 by a surface integral using Green's theorem:

$$\int_V (\nabla\phi\cdot\nabla\phi)\, dv = \int_S \phi \frac{\partial\phi}{\partial\nu}\, ds - \int_V \phi\, \nabla^2\phi\, dv = \int_S \phi \frac{\partial\phi}{\partial\nu}\, ds \qquad (1.59)$$

where $\frac{\partial\phi}{\partial\nu}$ is the derivative of the potential function ϕ in the direction of the outward normal vector $\underset{\sim}{\nu}$.

Now, we seek the stationarity of the functional

$$\tilde{I}_c(\phi,\xi) = \int_{t_1}^{t_2} \left\{ -\frac{\rho_\ell}{2} \int_S \phi \frac{\partial\phi}{\partial\nu}\, ds + \rho_\ell \int_{S_1} (\phi\dot{\xi} - \frac{g\xi^2}{2})\, ds + \rho_\ell \int_{S_2} \phi\dot{w}\, ds \right\} dt \qquad (1.60)$$

The functional $\tilde{I}_c(\phi,\xi)$ defined in the preceding equation involves only the boundaries of the liquid region, and therefore a finite element discretization of the liquid region itself is not needed.

I-4-2. Variational Formulation of the Equations of Motion of the Liquid-Shell System

As was seen, the extremization of the complementary functional $I_c(\phi,\xi)$, assuming that the shell velocity is prescribed, leads to the differential equation of motion of the liquid and the appropriate boundary conditions. Similarly, it was demonstrated that the set of equations which govern the shell motion can be obtained by means of Hamilton's Principle, assuming that the liquid pressure is prescribed.

A combination of the preceding variational formulations can be made to provide a variational formulation of the motion of the liquid-shell system; the variational functional can be written as

$$J(u,v,w,\phi,\xi) = \int_{t_1}^{t_2} \left\{ T(\dot{u},\dot{v},\dot{w}) - U(u,v,w) - \frac{\rho_\ell}{2} \int_V (\nabla\phi \cdot \nabla\phi)\, dv \right.$$

$$\left. + \rho_\ell \int_{S_1} (\dot{\xi}\phi - \frac{g\xi^2}{2})\, ds + \rho_\ell \int_{S_2} \dot{w}\, \phi\, ds \right\} dt \qquad (1.61)$$

where u, v, and w are the displacement components of the shell in the axial, circumferential, and radial directions, respectively; T and U are the kinetic and strain energies of the shell; ρ_ℓ is the liquid density; ϕ is the liquid velocity potential; ξ is the free surface displacement; and g is the gravity acceleration.

When it is noted that the volume integral in Eq. 1.61 can be replaced by a surface integral, refer to sec. I-4-1, the functional J takes the form

$$J(u,v,w,\phi,\xi) = \int_{t_1}^{t_2} \left\{ T(\dot{u},\dot{v},\dot{w}) - U(u,v,w) - \frac{\rho_\ell}{2} \int_S \phi\, \frac{\partial\phi}{\partial\nu}\, ds \right.$$

$$\left. + \rho_\ell \int_{S_1} \left(\dot{\xi}\phi - \frac{g\xi^2}{2}\right) ds + \rho_\ell \int_{S_2} \dot{w}\, \phi\, ds \right\} dt \qquad (1.62)$$

In this chapter, only the impulsive pressure of the liquid will be considered; this is equivalent to assuming a zero gravity acceleration. Given this new situation, the functional J can be written as

$$J(u,v,w,\phi,\xi) = \int_{t_1}^{t_2} \left\{ T(\dot{u},\dot{v},\dot{w}) - U(u,v,w) - \frac{\rho_\ell}{2} \int_S \phi \frac{\partial \phi}{\partial \nu} ds \right.$$

$$\left. + \rho_\ell \int_{S_1} \dot{\xi} \phi \, ds + \rho_\ell \int_{S_2} \dot{w} \phi \, ds \right\} dt \qquad (1.63)$$

Now, it can be recognized that the shell vibrational motion is independent of the free surface motion, and consequently, it is possible to omit the term in Eq. 1.63 involving the free surface velocity. Hence, the functional J is given by

$$J(u,v,w,\phi) = \int_{t_1}^{t_2} \left\{ T(\dot{u},\dot{v},\dot{w}) - U(u,v,w) - \frac{\rho_\ell}{2} \int_S \phi \frac{\partial \phi}{\partial \nu} ds + \rho_\ell \int_{S_2} \dot{w} \phi \, ds \right\} dt \qquad (1.64)$$

The effect of the coupling between liquid sloshing and shell vibrations will be discussed later in chapter II.

I-4-3. Expansion of the Velocity Potential Function

The solution $\phi(r,\theta,z,t)$ of the Laplace equation, $\nabla^2\phi = 0$, can be obtained by the method of separation of variables. Thus a solution is sought in the form

$$\phi(r,\theta,z,t) = \hat{R}(r) \cdot \hat{\Theta}(\theta) \cdot \hat{Z}(z) \cdot \hat{T}(t) \qquad (1.65)$$

Appendix I-c gives a detailed derivation of all possible solutions of the Laplace equation which can be stated as follows:

$$\phi(r,\theta,z,t) = \hat{T}_n(t)\cos(n\theta)\begin{cases} J_n(kr)\cosh(kz) \\ J_n(kr)\sinh(kz) \\ r^n z \\ r^n \\ I_n(kr)\cos(kz) \\ I_n(kr)\sin(kz) \end{cases}, \quad (n\geq 1) \qquad (1.66)$$

where J_n and I_n are the Bessel functions and the modified Bessel functions, respectively, of the first kind of order n; k is a separation constant; and n is the circumferential wave number. It should be noted that the terms containing the Bessel functions and the modified Bessel functions of the second kind, Y_n and K_n, as well as the terms zr^{-n} and r^{-n} have been discarded, since they are singular at r = 0.

In a solution by the separation of variables, the terms given by Eq. 1.66 should be superimposed to satisfy the boundary conditions. Therefore, it is desirable to retain only those terms which have vanishing derivative with respect to z at z = 0. Hence, the terms $J_n(kr)\cosh(kz)$, $I_n(kr)\cos(kz)$, and r^n are retained. The separation constant is chosen to satisfy that the liquid pressure at the free surface is zero, or equivalently, the time derivative of the velocity potential function at z = H is zero for all time. Hence, the trial functions $\overset{*}{N}_i$ are given by

$$\overset{*}{N}_i(r,\theta,z) = \sum_{n=1}^{\infty} I_n(\alpha_i r)\cos(\alpha_i z)\cos(n\theta) \qquad (1.67)$$

where $\alpha_i = \frac{(2i-1)\pi}{2H}$ (1.68)

The velocity potential function, $\phi(r,\theta,z,t)$, can then be expressed as

$$\phi(r,\theta,z,t) = \sum_{i=1}^{I} A_i(t) \overset{*}{N}_i(r,\theta,z) \quad , \tag{1.69}$$

or in a matrix form as

$$\phi(r,\theta,z,t) = \left\{A(t)\right\}^T \cdot \left\{\overset{*}{N}(r,\theta,z)\right\} \tag{1.70}$$

I-4-4. Idealization of the Shell

The first step in the finite-element idealization of the shell is to divide it into an appropriate number of ring-shaped elements. These elements are interconnected only at a finite number of nodal points as shown in Fig. I-4-a. (it is probably more descriptive to speak of the "edges" of the element rather than the "nodes"; however, these terms will be used interchangeably). The element size is arbitrary; they may all be of the same size or may all be different.

The equations of motion of the shell admit the representation of the displacement components u, v, and w in the following form

$$u(\theta,z,t) = \sum_{n=1}^{\infty} u_n(z,t) \cos(n\theta) \tag{1.71-a}$$

$$v(\theta,z,t) = \sum_{n=1}^{\infty} v_n(z,t) \sin(n\theta) \tag{1.71-b}$$

$$w(\theta,z,t) = \sum_{n=1}^{\infty} w_n(z,t) \cos(n\theta) \tag{1.71-c}$$

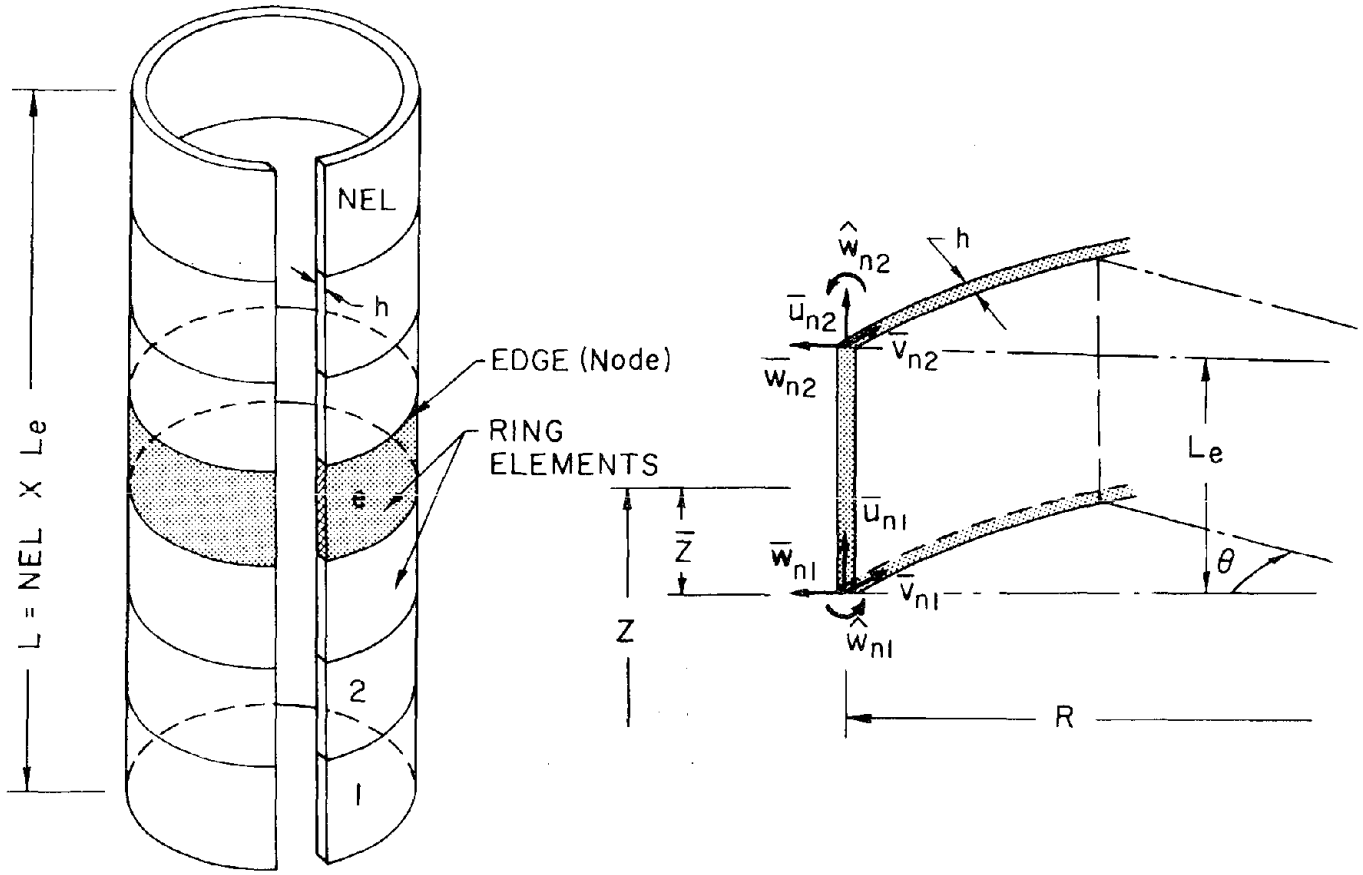

(a) Finite-element Idealization of the Shell

(b) Shell Element

Fig. I-4. Finite-element Definition Diagram.

Now, the displacement functions $u_n(z,t)$, $v_n(z,t)$, and $w_n(z,t)$ can be expressed in terms of the nodal displacements of the finite elements by means of an appropriate set of interpolation functions. The shape functions associated with the axial and tangential displacements are taken to be linear between the nodal points. However, those associated with the radial displacement are cubic Hermitian polynomials to assure slope continuity at the nodes.

Consider a typical shell element of length L_e with a local axial coordinate $\bar{z}$ as shown in Fig. I-4-b. The displacements $u_{ne}(\bar{z},t)$, $v_{ne}(\bar{z},t)$ and $w_{ne}(\bar{z},t)$ can be written in terms of the nodal displacements as follows

$$u_{ne}(\bar{z},t) = \sum_{i=1}^{2} S_i(\bar{z})\, \bar{u}_{ni}(t) \qquad (1.72\text{-a})$$

$$v_{ne}(\bar{z},t) = \sum_{i=1}^{2} S_i(\bar{z})\, \bar{v}_{ni}(t) \qquad (1.72\text{-b})$$

$$w_{ne}(\bar{z},t) = \sum_{i=1}^{2} \left(N_i(\bar{z})\, \bar{w}_{ni}(t) + \hat{N}_i(\bar{z})\, \hat{w}_{ni}(t)\right) \qquad (1.72\text{-c})$$

where e is the subscript indicating "element" and $\bar{u}_{ni}(t)$, $\bar{v}_{ni}(t)$, $\bar{w}_{ni}(t)$, and $\hat{w}_{ni}(t)$ are the generalized nodal displacements of the element. The shape functions are given by

$$
\begin{aligned}
S_1(\bar{z}) &= 1 - \frac{\bar{z}}{L_e} \\
S_2(\bar{z}) &= \frac{\bar{z}}{L_e} \\
N_1(\bar{z}) &= 1 - 3\frac{\bar{z}^2}{L_e^2} + 2\frac{\bar{z}^3}{L_e^3} \\
N_2(\bar{z}) &= 3\frac{\bar{z}^2}{L_e^2} - 2\frac{\bar{z}^3}{L_e^3} \\
\hat{N}_1(\bar{z}) &= \bar{z} - 2\frac{\bar{z}^2}{L_e} + \frac{\bar{z}^3}{L_e^2} \\
\hat{N}_2(\bar{z}) &= -\frac{\bar{z}^2}{L_e} + \frac{\bar{z}^3}{L_e^2}
\end{aligned}
\tag{1.73}
$$

Since the displacements of each circumferential wave number n are uncoupled, it is appropriate to omit the subscript n for brevity.

Eqs. 1.72-a to c can be written in a matrix form as

$$\{d(\bar{z},t)\}_e = [Q(\bar{z})]\{\bar{d}(t)\}_e \tag{1.74}$$

and

$$w_e(\bar{z},t) = \{\bar{N}(\bar{z})\}^T\{\bar{d}(t)\}_e = \{\bar{\bar{N}}(\bar{z})\}^T\{\bar{\bar{d}}(t)\}_e \tag{1.75}$$

where

$$\{d(\bar{z},t)\}_e = \begin{Bmatrix} u_e(\bar{z},t) \\ v_e(\bar{z},t) \\ w_e(\bar{z},t) \end{Bmatrix} \qquad (1.76);$$

$$[Q(\bar{z})] = \begin{bmatrix} S_1(\bar{z}) & 0 & 0 & 0 & S_2(\bar{z}) & 0 & 0 & 0 \\ 0 & S_1(\bar{z}) & 0 & 0 & 0 & S_2(\bar{z}) & 0 & 0 \\ 0 & 0 & N_1(\bar{z}) & \hat{N}_1(\bar{z}) & 0 & 0 & N_2(\bar{z}) & \hat{N}_2(\bar{z}) \end{bmatrix} \qquad (1.77);$$

$$\{\bar{d}(t)\}_e = \begin{Bmatrix} \bar{u}_1(t) \\ \bar{v}_1(t) \\ \bar{w}_1(t) \\ \hat{w}_1(t) \\ \bar{u}_2(t) \\ \bar{v}_2(t) \\ \bar{w}_2(t) \\ \hat{w}_2(t) \end{Bmatrix}_e \qquad (1.78);$$

$$\{\bar{N}(\bar{z})\}^T = \{0 \quad 0 \quad N_1(\bar{z}) \quad \hat{N}_1(\bar{z}) \quad 0 \quad 0 \quad N_2(\bar{z}) \quad \hat{N}_2(\bar{z})\} \qquad (1.79);$$

$$\{\bar{\bar{N}}(\bar{z})\}^T = \{N_1(\bar{z}) \quad \hat{N}_1(\bar{z}) \quad N_2(\bar{z}) \quad \hat{N}_2(\bar{z})\} \qquad (1.80); \text{ and}$$

$$\{\bar{\bar{d}}(t)\}_e = \begin{Bmatrix} \bar{w}_1(t) \\ \hat{w}_1(t) \\ \bar{w}_2(t) \\ \hat{w}_2(t) \end{Bmatrix}_e \tag{1.81}$$

$$\text{Finally, let } \{q\} = \sum_{e=1}^{NEL} \{\bar{d}(t)\}_e \tag{1.82}$$

where $\{q\}$ is the assemblage nodal displacement vector; and NEL is the number of shell elements along the shell length.

I-4-5. Evaluation of the Shell Stiffness Matrix

The elastic properties of the shell are found by evaluating the properties of the individual finite elements and superposing them appropriately. Therefore, the problem of defining the stiffness properties of the shell is reduced basically to evaluating the stiffness of a typical element.

The strain energy of the shell due to stretching and bending (Eq. 1.33) can be written as

$$U(t) = \frac{R}{2} \int_0^L \int_0^{2\pi} (\{\varepsilon\}^T [D]\{\varepsilon\})\, d\theta\, dz \tag{1.83}$$

where $\{\varepsilon\} = [P]\{d\}$ (1.84); and [P] is a differential operator matrix defined by Eq. 1.32.

For each circumferential wave number n, the displacement vector $\{d\}$ of any point (R,θ,z) on the middle surface of the shell can be expressed in terms of the vector $\{d_n\}$ as follows

$$\{d\} = [\Theta_n]\{d_n\} \tag{1.85}$$

where

$$[\Theta_n] = \begin{bmatrix} \cos(n\theta) & 0 & 0 \\ 0 & \sin(n\theta) & 0 \\ 0 & 0 & \cos(n\theta) \end{bmatrix} \tag{1.86};$$

$$\{d_n(z,t)\} = \begin{Bmatrix} u_n(z,t) \\ v_n(z,t) \\ w_n(z,t) \end{Bmatrix} \tag{1.87};$$

u_n and w_n being the axial and radial displacement at $\theta = 0$; and v_n is the maximum tangential displacement.

Substitute Eq. 1.85 into Eq. 1.84, then one can write

$$\{\varepsilon\} = [P]\{d\} = [P][\Theta_n]\{d_n\} = [\hat{\Theta}_n][\hat{P}_n(z)]\{d_n\} \tag{1.88}$$

where

$$[\hat{\Theta}_n] = \begin{bmatrix} \cos(n\theta) & 0 & 0 & 0 & 0 & 0 \\ 0 & \cos(n\theta) & 0 & 0 & 0 & 0 \\ 0 & 0 & \sin(n\theta) & 0 & 0 & 0 \\ 0 & 0 & 0 & \cos(n\theta) & 0 & 0 \\ 0 & 0 & 0 & 0 & \cos(n\theta) & 0 \\ 0 & 0 & 0 & 0 & 0 & \sin(n\theta) \end{bmatrix} \quad (1.89) ;$$

$$\text{and } [\hat{P}_n(z)] = \begin{bmatrix} \frac{\partial}{\partial z} & 0 & 0 \\ 0 & \frac{n}{R} & \frac{1}{R} \\ -\frac{n}{R} & \frac{\partial}{\partial z} & 0 \\ 0 & 0 & -\frac{\partial^2}{\partial z^2} \\ 0 & \frac{n}{R^2} & \frac{n^2}{R^2} \\ 0 & \frac{2}{R}\frac{\partial}{\partial z} & \frac{2n}{R}\frac{\partial}{\partial z} \end{bmatrix} \quad (1.90)$$

With the aid of Eq. 1.88, the strain energy expression (Eq. 1.83) can be written as

$$U(t) = \frac{R}{2} \int_0^L \left\{ ([\hat{P}_n]\{d_n\})^T \left(\int_0^{2\pi} [\hat{\Theta}_n]^T [D] [\hat{\Theta}_n] \, d\theta \right) ([\hat{P}_n]\{d_n\}) \right\} dz$$

$$= \frac{\pi R}{2} \int_0^L \left\{ ([\hat{P}_n]\{d_n\})^T [D] ([\hat{P}_n]\{d_n\}) \right\} dz \qquad (1.91)$$

Again, the displacements of each circumferential wave number n are uncoupled, and therefore, it is appropriate to omit the subscript n for brevity.

Now, the strain energy (Eq. 1.91) may be expressed, with the aid of the displacement model (Eq. 1.74), as

$$U(t) = \frac{\pi R}{2} \sum_{e=1}^{NEL} \int_0^{L_e} \left(([\hat{P}][Q]\{\bar{d}\}_e)^T [D]_e ([\hat{P}][Q]\{\bar{d}\}_e) \right) d\bar{z} \qquad (1.92)$$

where NEL is the total number of shell elements along the shell length; and $[D]_e$ is the element constitutive matrix; it is assumed constant over the entire element.

Eq. 1.92 may be expressed conveniently in terms of the element stiffness matrix as

$$U(t) = \frac{1}{2} \sum_{e=1}^{NEL} \{\bar{d}\}_e^T [K_s]_e \{\bar{d}\}_e \qquad (1.93)$$

where

$$[K_s]_e = \pi R \int_0^{L_e} [B]^T [D]_e [B] \, d\bar{z} \qquad (1.94)$$;

and

$$[B] = [\hat{P}][Q] \qquad (1.95)$$

$$
= \begin{bmatrix}
-\frac{1}{L_e} & 0 & 0 & 0 & \frac{1}{L_e} & 0 & 0 & 0 \\
0 & \frac{n}{R}\left(1-\frac{\bar{z}}{L_e}\right) & \frac{1}{R}\left(1-\frac{3\bar{z}^2}{L_e^2}+\frac{2\bar{z}^3}{L_e^3}\right) & \frac{1}{R}\left(\bar{z}-\frac{2\bar{z}^2}{L_e}+\frac{\bar{z}^3}{L_e^2}\right) & 0 & \frac{n\bar{z}}{RL_e} & \frac{1}{R}\left(\frac{3\bar{z}^2}{L_e^2}-\frac{2\bar{z}^3}{L_e^3}\right) & \frac{1}{R}\left(-\frac{\bar{z}^2}{L_e}+\frac{\bar{z}^3}{L_e^2}\right) \\
-\frac{n}{R}\left(1-\frac{\bar{z}}{L_e}\right) & -\frac{1}{L_e} & 0 & 0 & -\frac{n\bar{z}}{RL_e} & \frac{1}{L_e} & 0 & 0 \\
0 & 0 & \frac{6}{L_e^2}\left(1-\frac{2\bar{z}}{L_e}\right) & \frac{2}{L_e}\left(2-\frac{3\bar{z}}{L_e}\right) & 0 & 0 & -\frac{6}{L_e^2}\left(1-\frac{2\bar{z}}{L_e}\right) & \frac{2}{L_e}\left(1-\frac{3\bar{z}}{L_e}\right) \\
0 & \frac{n}{R^2}\left(1-\frac{\bar{z}}{L_e}\right) & \frac{n^2}{R^2}\left(1-\frac{3\bar{z}^2}{L_e^2}+\frac{2\bar{z}^3}{L_e^3}\right) & \frac{n^2}{R^2}\left(\bar{z}-\frac{2\bar{z}^2}{L_e}+\frac{\bar{z}^3}{L_e^2}\right) & 0 & \frac{n\bar{z}}{R^2L_e} & \frac{n^2}{R^2}\left(\frac{3\bar{z}^2}{L_e^2}-\frac{2\bar{z}^3}{L_e^3}\right) & \frac{n^2}{R^2}\left(-\frac{\bar{z}^2}{L_e}+\frac{\bar{z}^3}{L_e^2}\right) \\
0 & -\frac{2}{RL_e} & -\frac{12n}{RL_e^2}\left(\bar{z}-\frac{\bar{z}^2}{L_e}\right) & \frac{2n}{R}\left(1-\frac{4\bar{z}}{L_e}+\frac{3\bar{z}^2}{L_e^2}\right) & 0 & \frac{2}{RL_e} & \frac{12n}{RL_e^2}\left(\bar{z}-\frac{\bar{z}^2}{L_e}\right) & -\frac{2n}{R}\left(\frac{2\bar{z}}{L_e}-\frac{3\bar{z}^2}{L_e^2}\right)
\end{bmatrix}
$$

(1.96)

The integration involved in the evaluation of $[K_s]_e$ can be accomplished by using the Gaussian integration method along the element length. A Four-points integration rule is required to exactly compute the elements of the stiffness matrix; it can be stated as follows

$$\int_0^{L_e} G(\bar{z})d\bar{z} = \sum_{i=1}^{4} G(\bar{z}_i)\, W_i \tag{1.97}$$

where $\bar{z}_i = \frac{L_e}{2}(1 + \eta_i)$; $\eta_1 = \mp 0.339981$; $\eta_2 = \mp 0.861136$;

$W_1 = W_4 = 0.326\, L_e$; and $W_2 = W_3 = 0.174\, L_e$.

The process of constructing the equations for the assemblage from the equations for the individual elements is routine. Nodal compatibility is used as the basis for this process. Since the displacements are matched at the nodes, the stiffnesses are added at these locations. The assemblage stiffness matrix and the nodal displacement vector can be written as

$$[K_s] = \sum_{e=1}^{NEL} [K_s]_e \quad \text{and} \quad \{q\} = \sum_{e=1}^{NEL} \{\bar{d}\}_e \tag{1.98}$$

Now, the strain energy expression becomes

$$U(t) = \frac{1}{2} \{q\}^T [K_s] \{q\} \tag{1.99}$$

Finally, when it is noted that the strain energy stored in the shell during deformations must always be positive, it is evident that

$$\frac{1}{2} \{q\}^T [K_s] \{q\} > 0$$

Matrices which satisfy this condition, where $\{q\}$ is any arbitrary nonzero vector, are said to be positive definite; positive definite matrices are nonsingular and can be inverted. The stiffness matrix $[K_s]$ is also symmetric and banded.

I-4-6. Evaluation of the Shell Mass Matrix

The kinetic energy of the elastic shell (Eq. 1.36) can be written as

$$T(t) = \frac{1}{2} \int_0^L \int_0^{2\pi} \left(m(z) \{\dot{d}\}^T \{\dot{d}\} \right) R \, d\theta \, dz \qquad (1.100)$$

Substituting Eq. 1.85 into Eq. 1.100, one can obtain

$$T(t) = \frac{R}{2} \int_0^L \left\{ m(z) \{\dot{d}_n\}^T \left(\int_0^{2\pi} [\Theta_n]^T [\Theta_n] \, d\theta \right) \{\dot{d}_n\} \right\} dz$$

$$= \frac{\pi R}{2} \int_0^L \left(m(z) \{\dot{d}_n\}^T \{\dot{d}_n\} \right) dz \qquad (1.101)$$

When the interpolation displacement model is used, Eq. 1.74 can be inserted into the expression of the translational kinetic energy to obtain

$$T(t) = \frac{\pi R}{2} \sum_{e=1}^{NEL} \left\{ m_e \int_0^{L_e} ([Q]\{\dot{\bar{d}}\}_e)^T([Q]\{\dot{\bar{d}}\}_e)\, d\bar{z} \right\} \tag{1.102}$$

where the subscript n is omitted for brevity and m_e denotes the mass of the shell element per unit area; it is assumed uniform over the entire element.

Equation 1.102 can also be written as

$$T(t) = \frac{1}{2} \sum_{e=1}^{NEL} \{\dot{\bar{d}}\}_e^T [M_s]_e \{\dot{\bar{d}}\}_e \tag{1.103}$$

where $[M_s]_e$ is the consistent mass matrix of the element which can be defined by

$$[M_s]_e = \pi R m_e \int_0^{L_e} [Q]^T[Q]\, d\bar{z} \tag{1.104}$$

When the integration involved in the evaluation of $[M_s]_e$ is carried out, the resulting consistent mass matrix is

$$\left[M_s\right]_e = \pi R m_e \begin{bmatrix} \frac{L_e}{3} & 0 & 0 & 0 & \frac{L_e}{6} & 0 & 0 & 0 \\ 0 & \frac{L_e}{3} & 0 & 0 & 0 & \frac{L_e}{6} & 0 & 0 \\ 0 & 0 & \frac{13L_e}{35} & \frac{11L_e^2}{210} & 0 & 0 & \frac{9L_e}{70} & -\frac{13L_e^2}{420} \\ 0 & 0 & \frac{11L_e^2}{210} & \frac{L_e^3}{105} & 0 & 0 & \frac{13L_e^2}{420} & -\frac{L_e^3}{140} \\ \frac{L_e}{6} & 0 & 0 & 0 & \frac{L_e}{3} & 0 & 0 & 0 \\ 0 & \frac{L_e}{6} & 0 & 0 & 0 & \frac{L_e}{3} & 0 & 0 \\ 0 & 0 & \frac{9L_e}{70} & \frac{13L_e^2}{420} & 0 & 0 & \frac{13L_e}{35} & -\frac{11L_e^2}{210} \\ 0 & 0 & -\frac{13L_e^2}{420} & -\frac{L_e^3}{140} & 0 & 0 & -\frac{11L_e^2}{210} & \frac{L_e^3}{105} \end{bmatrix} \quad (1.105)$$

The mass matrix of the complete assemblage can be developed by exactly the same type of superposition procedure as that described for the development of the assemblage stiffness matrix. The assemblage consistent mass matrix is

$$\left[M_s\right] = \sum_{e=1}^{NEL} \left[M_s\right]_e \quad (1.106),$$

and therefore, the translational kinetic energy can be written as

$$T(t) = \frac{1}{2} \{\dot{q}\}^T [M_s] \{\dot{q}\} \tag{1.107}$$

I-4-7. The Matrix Equations of Motion

As a consequence of neglecting the free surface oscillation modes, the motion of the tank wall can be analyzed by introducing an additional mass matrix in the matrix equations of motion of the shell; it represents the effect of the liquid dynamic pressure during vibration.

To establish the matrix equations of motion of the liquid-shell system, one can make use of the variational functional (Eq. 1.64) which can be written as

$$J(u,v,w,\phi) = \int_{t_1}^{t_2} \left\{ T(\dot{u},\dot{v},\dot{w}) - U(u,v,w) - \frac{\rho_\ell}{2} \int_S \phi \frac{\partial \phi}{\partial \nu} ds + \rho_\ell \int_{S_2} \dot{w} \phi \, ds \right\} dt \tag{1.108}$$

The scalar energy quantities, U(t) and T(t), are already obtained in terms of the assemblage nodal displacement vector, {q}, and are given by Eqs. 1.99 and 1.107, respectively.

Now, inserting the expression for the potential function (Eq. 1.70) into the third term of the functional J, and noting that the trial functions, given by Eqs. 1.67 and 1.68, satisfy the conditions that $\phi = 0$ along S_1 and $\frac{\partial \phi}{\partial z} = 0$ along S_3, one can write

$$\frac{\rho_\ell}{2} \int_S \phi \frac{\partial \phi}{\partial \nu} \, ds = \frac{\rho_\ell}{2} \int_{S_2} \phi \frac{\partial \phi}{\partial \nu} \, ds \tag{1.109}$$

$$= \frac{\rho_\ell}{2} \int_0^H \int_0^{2\pi} \left(\phi(R,\theta,z,t) \cdot \frac{\partial \phi}{\partial r}(R,\theta,z,t) \right) R \, d\theta \, dz$$

$$= \frac{R\rho_\ell}{2} \{A(t)\}^T \left(\int_0^H \int_0^{2\pi} \{\overset{*}{N}(R,\theta,z)\} \left\{\frac{\partial \overset{*}{N}}{\partial r}(R,\theta,z)\right\}^T d\theta \, dz \right) \{A(t)\} \tag{1.110}$$

where $\overset{*}{N}_i(r,\theta,z) = \sum_{n=1}^{\infty} I_n(\alpha_i r) \cos(\alpha_i z) \cos(n\theta)$; and

$$\alpha_i = \frac{(2i-1)\pi}{2H} \quad , \quad i = 1,2,\ldots,I.$$

Performing the integration involved in Eq. 1.110, one can obtain, for the n^{th} circumferential wave, the following

$$\frac{\rho_\ell}{2} \int_S \phi \frac{\partial \phi}{\partial \nu} \, ds = \frac{\pi R \rho_\ell}{2} \{A\}^T [C] \{A\} \tag{1.111}$$

where $[C]$ is a diagonal matrix whose elements are given by

$$C_{ii} = \frac{\alpha_i H}{2} I_n(\alpha_i R) \cdot I_n'(\alpha_i R) \quad , \quad i = 1,2,\ldots,I. \tag{1.112}$$

With the aid of the radial displacement expression (Eq. 1.71-c), the last term of the variational functional (Eq. 1.108) becomes

$$\rho_\ell \int_{S_2} \dot{w}\, \phi\, ds = \rho_\ell \int_0^H \int_0^{2\pi} \left(\dot{w}(\theta,z,t) \cdot \phi(R,\theta,z,t) \right) R\, d\theta\, dz$$

$$= R\rho_\ell \int_0^H \left[\dot{w}_n(z,t) \left(\int_0^{2\pi} \cos(n\theta) \cdot \phi(R,\theta,z,t) d\theta \right) \right] dz \qquad (1.113)$$

and upon using the potential function expression (Eq. 1.70) in Eq. 1.113, it can be obtained

$$\rho_\ell \int_{S_2} \dot{w}\, \phi\, ds = \pi R \rho_\ell \int_0^H \left(\dot{w}_n(z,t) \cdot \left\{ \overset{*}{N}(z) \right\}^T \cdot \left\{ A(t) \right\} \right) dz \qquad (1.114)$$

where

$$\overset{*}{N}_i(z) = I_n(\alpha_i R) \cos(\alpha_i z) \qquad (1.115)$$

Now, inserting the shell displacement model (Eq. 1.75) into Eq. 1.114 to get

$$\rho_\ell \int_{S_2} \dot{w}\, \phi\, ds = \pi R \rho_\ell \sum_{e=1}^{NEH} \left(\int_0^{L_e} \left\{ \dot{\bar{d}}(t) \right\}_e^T \left\{ \bar{N}(\bar{z}) \right\} \left\{ \overset{*}{N}(\bar{z}) \right\}_e^T \left\{ A(t) \right\} d\bar{z} \right)$$

$$= \pi R \rho_\ell \sum_{e=1}^{NEH} \left(\left\{ \dot{\bar{d}}(t) \right\}_e^T \left[\hat{C} \right]_e \left\{ A(t) \right\} \right) \qquad (1.116)$$

where NEH is the number of shell elements in contact with the liquid along the shell length; and $[\hat{C}]_e$ is a matrix of order 8 x I which can be expressed as follows:

$$[\hat{C}]_e = \begin{bmatrix} 0 & 0 & 0 & .. & .. & 0 \\ 0 & 0 & 0 & .. & .. & 0 \\ \hat{C}_{31} & \hat{C}_{32} & \hat{C}_{33} & .. & .. & \hat{C}_{3I} \\ \hat{C}_{41} & \hat{C}_{42} & \hat{C}_{43} & .. & .. & \hat{C}_{4I} \\ 0 & 0 & 0 & .. & .. & 0 \\ 0 & 0 & 0 & .. & .. & 0 \\ \hat{C}_{71} & \hat{C}_{72} & \hat{C}_{73} & .. & .. & \hat{C}_{7I} \\ \hat{C}_{81} & \hat{C}_{82} & \hat{C}_{83} & .. & .. & \hat{C}_{8I} \end{bmatrix} \tag{1.117}$$

where

$$\hat{C}_{3i} = I_n(\alpha_i R)L_e\left(-\left(\frac{1}{\beta_i}+\frac{6}{\beta_i^3}\right)\sin[\beta_i(e-1)] + \frac{12}{\beta_i^4}\cos[\beta_i(e-1)] - \frac{6}{\beta_i^3}\right.$$
$$\left.\sin[\beta_i e] - \frac{12}{\beta_i^4}\cos[\beta_i e]\right);$$

$$\hat{C}_{4i} = I_n(\alpha_i R)L_e^2\left(-\frac{4}{\beta_i^3}\sin[\beta_i(e-1)] - \left(\frac{1}{\beta_i^2}-\frac{6}{\beta_i^4}\right)\cos[\beta_i(e-1)] - \frac{2}{\beta_i^3}\right.$$
$$\left.\sin[\beta_i e] - \frac{6}{\beta_i^4}\cos[\beta_i e]\right);$$

$$\hat{C}_{7i} = I_n(\alpha_i R)L_e\left(\frac{6}{\beta_i^3}\sin[\beta_i(e-1)] - \frac{12}{\beta_i^4}\cos[\beta_i(e-1)] + \left(\frac{1}{\beta_i}+\frac{6}{\beta_i^3}\right)\right.$$
$$\left.\sin[\beta_i e] + \frac{12}{\beta_i^4}\cos[\beta_i e]\right);$$

$$\hat{C}_{8i} = I_n(\alpha_i R)L_e^2\left(-\frac{2}{\beta_i^3}\sin[\beta_i(e-1)] + \frac{6}{\beta_i^4}\cos[\beta_i(e-1)] - \frac{4}{\beta_i^3}\sin[\beta_i e]\right.$$
$$\left.+\left(\frac{1}{\beta_i^2}-\frac{6}{\beta_i^4}\right)\cos[\beta_i e]\right);$$

$\beta_i = \alpha_i L_e$; and e is the number of the element (refer to Fig. I-4-a).

Using Eq. 1.82 , one can write Eq. 1.116 in terms of the assemblage nodal displacement vector as follows

$$\rho_\ell \int_{S_2} \dot{w}\, \phi \, ds = \pi R \rho_\ell \left\{\dot{q}\right\}^T [\hat{C}] \left\{A\right\} \tag{1.118}$$

where

$$[\hat{C}] = \sum_{e=1}^{NEH} [\hat{C}]_e \tag{1.119}$$

It is more convenient to redefine the matrices $[C]$ and $[\hat{C}]$ as

$$[C] = \pi R \rho_\ell [C] \quad ; \quad [\hat{C}] = \pi R \rho_\ell [\hat{C}] \tag{1.120}$$

Hence, Eqs. 1.111 and 1.118 can be written as

$$\frac{\rho_\ell}{2} \int_S \phi \frac{\partial \phi}{\partial \nu} \, ds = 1/2 \left\{A\right\}^T [C] \left\{A\right\} \tag{1.121}$$

and

$$\rho_\ell \int_{S_2} \dot{w}\, \phi \, ds = \left\{\dot{q}\right\}^T [\hat{C}] \left\{A\right\} \tag{1.122}$$

Now, inserting Eqs. 1.99, 1.107, 1.121, and 1.122 into the variational functional (Eq. 1.108), one can obtain for the assemblage

$$\delta \int_{t_1}^{t_2} \Big(1/2 \left\{\dot{q}\right\}^T [M_s] \left\{\dot{q}\right\} - 1/2 \left\{q\right\}^T [K_s] \left\{q\right\} - 1/2 \left\{A\right\}^T [C] \left\{A\right\} + \left\{\dot{q}\right\}^T [\hat{C}] \left\{A\right\} \Big) dt = 0$$

Applying the variational operator yields

$$\int_{t_1}^{t_2} \Big(\{\delta\dot{q}\}^T[M_s]\{\dot{q}\} - \{\delta q\}^T[K_s]\{q\} - \{\delta A\}^T[C]\{A\} + \{\delta\dot{q}\}^T[\hat{C}]\{A\} + \{\delta A\}^T[\hat{C}]^T\{\dot{q}\} \Big) dt = 0 \tag{1.123}$$

Integrating the first and fourth terms in Eq. 1.123 by parts with respect to time, and noting that the displacement vector must satisfy the conditions $\{q(t_1)\} = \{q(t_2)\} = \{0\}$, then one can write

$$\int_{t_1}^{t_2} \Big\{ \{\delta q\}^T \cdot \Big[[M_s]\{\ddot{q}\} + [K_s]\{q\} + [\hat{C}]\{\dot{A}\}\Big] + \{\delta A\}^T \cdot \Big[[C]\{A\} - [\hat{C}]^T\{\dot{q}\}\Big] \Big\} dt = 0 \tag{1.124}$$

Since the variations of both the nodal displacement, $\{\delta q\}$, and the coefficients, $\{\delta A\}$, are arbitrary, the expressions in brackets must vanish. Therefore, the matrix equations of motion for the liquid-shell system can be obtained in the form

$$[M_s]\{\ddot{q}\} + [K_s]\{q\} + [\hat{C}]\{\dot{A}\} = \{0\} \tag{1.125}$$

and

$$[C]\{A\} - [\hat{C}]^T\{\dot{q}\} = \{0\} \tag{1.126}$$

Since the matrix $[C]$ is not singular, then one can write Eq. 1.126 as

$$\{A\} = [C]^{-1}[\hat{C}]^T\{\dot{q}\} \tag{1.127}$$

Now, differentiating Eq. 1.127 with respect to time

$$\{\dot{A}\} = [C]^{-1}[\hat{C}]^T\{\ddot{q}\} \tag{1.128}$$

and substituting Eq. 1.128 into Eq. 1.125 to get

$$[M_s]\{\ddot{q}\} + [K_s]\{q\} + [\hat{C}][C]^{-1}[\hat{C}]^T\{\ddot{q}\} = \{0\} \tag{1.129}$$

Now, define an added mass matrix [DM] as follows

$$[DM] = [\hat{C}][C]^{-1}[\hat{C}]^T \tag{1.130}$$

The matrix [DM] is symmetric and is a partially complete matrix (i.e., not banded); the elements are well distributed over the matrix. The general form for such a matrix and for the banded consistent mass matrix is shown schematically in Fig. I-5; only the hatched blocks are non-zero elements.

Finally, the governing matrix equation of the lateral vibration of the liquid-filled shell is given by

$$\left([M_s] + [DM]\right)\{\ddot{q}\} + [K_s]\{q\} = \{0\} \tag{1.131}$$

I-4-8. An Alternative Approach to the Formulation of the Added Mass Matrix

In the preceding section, the matrix equations of motion of the liquid-shell system were derived by means of the variational functional (Eq. 1.64). Another way of treating the problem is to derive the added mass matrix directly from the appropriate expression for the work done by the liquid-shell interface forces, and then, to derive the governing matrix equation of motion of the shell by means of Hamilton's Principle. This approach is simpler and easier to follow; it will be explained in this section.

It has been shown that the potential function $\phi(r,\theta,z,t)$ which

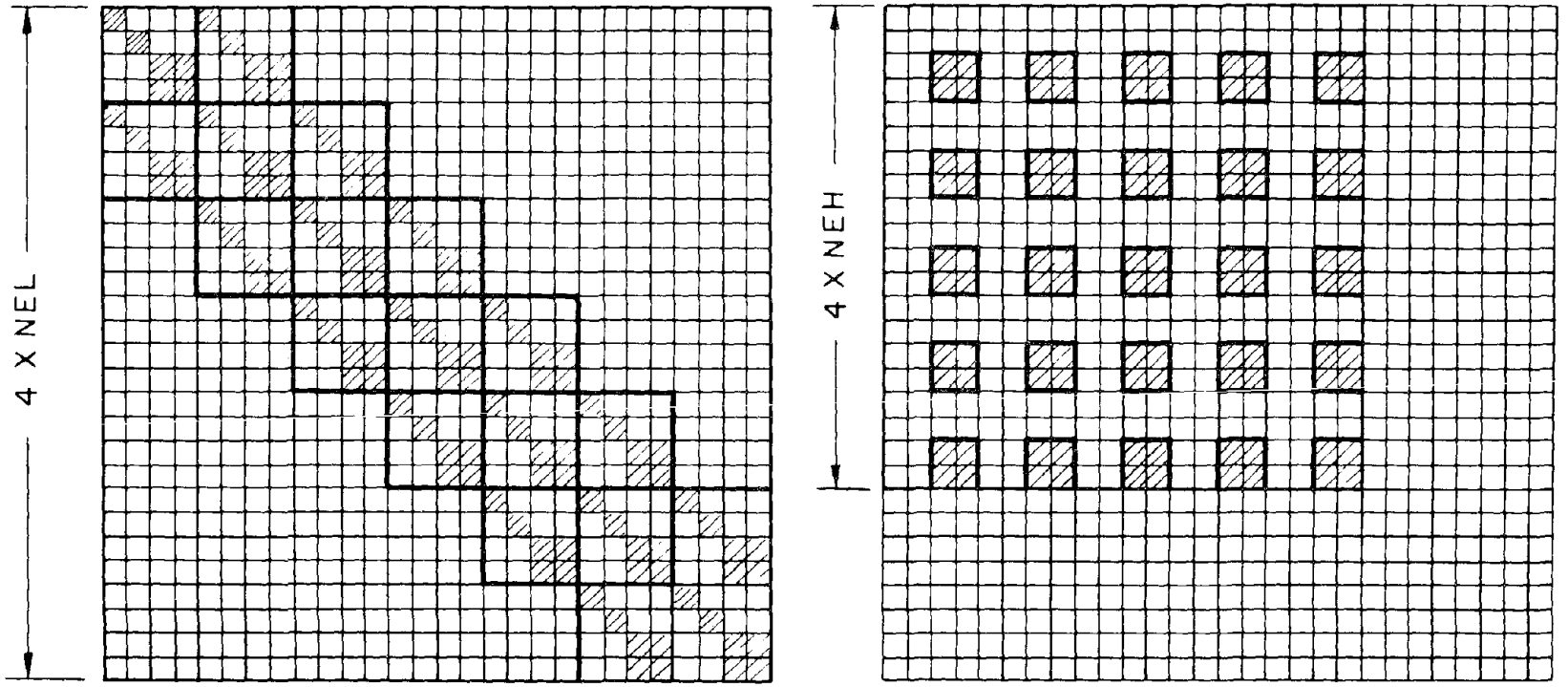

General Form of The "Banded" Consistent Mass Matrix $[M_s]$

General Form of The "Full" Added Mass Matrix $[DM]$

Fig. I-5. Schematics of the Form of the Consistent and the Added Mass Matrices.

satisfies the appropriate boundary conditions at the liquid free surface, and at the rigid bottom plate, can be expressed as

$$\phi(r,\theta,z,t) = \sum_{n=1}^{\infty} \sum_{i=1}^{\infty} \left(A_{ni}\, I_n(\alpha_i r)\, \cos(\alpha_i z)\, \cos(n\theta) \right) \tag{1.132}$$

The remaining boundary condition at the liquid-shell interface (Eq. 1.3) can be written as

$$\sum_{n=1}^{\infty} \left\{ \sum_{i=1}^{\infty} \left[A_{ni}\, \alpha_i\, I_n'(\alpha_i R)\, \cos(\alpha_i z) \right] - \dot{w}_n(z,t) \right\} \cos(n\theta) = 0 \tag{1.133}$$

and consequently,

$$\sum_{i=1}^{\infty} \left[A_{ni}\, \alpha_i\, I_n'(\alpha_i R)\, \cos(\alpha_i z) \right] = \dot{w}_n(z,t) \tag{1.134}$$

The functions $A_{ni}(t)$ can be determined in terms of $\dot{w}_n(z,t)$ by employing the orthogonality relations of the cosine functions, namely,

$$\int_0^H \cos(\alpha_i z)\, \cos(\alpha_j z)\, dz = \begin{cases} 0 & i \neq j \\ \dfrac{H}{2} & i = j \end{cases} \tag{1.135}$$

After the appropriate algebraic manipulations of Eq. 1.134, the following expressions for $A_{ni}(t)$ result

$$A_{ni} = \frac{2 \int_0^H \dot{w}_n(z,t)\, \cos(\alpha_i z)\, dz}{\alpha_i\, H\, I_n'(\alpha_i R)}, \qquad i = 1,2,\ldots. \tag{1.136}$$

and therefore, the dynamic pressure, for the n^{th} circumferential

distribution, can be given by

$$P_d\ (R,\theta,z,t) \;=\; -\rho_\ell\ \frac{\partial \phi}{\partial t}\ (R,\theta,z,t)$$

$$= \; -\frac{2\rho_\ell}{H} \sum_{i=1}^{\infty} \frac{\int_0^H \ddot{w}_n(\eta,t)\ \cos(\alpha_i \eta)\ d\eta}{\alpha_i\ I_n'(\alpha_i R)}\ I_n(\alpha_i R)\cdot\cos(\alpha_i z)\ \cdot\ \cos(n\theta) \tag{1.137}$$

The work done by the liquid pressure through an arbitrary virtual displacement, $\delta w_n\ \cos(n\theta)$, can then be written as

$$\delta W \;=\; \int_0^H \int_0^{2\pi} \Big(p_d(R,\theta,z,t)\cdot\delta w_n\cdot\cos(n\theta)\Big) R\ d\theta\ dz$$

$$= \; -\frac{2\pi R\rho_\ell}{H} \sum_{i=1}^{\infty} \left\{ \frac{I_n(\alpha_i R)}{\alpha_i\ I_n'(\alpha_i R)} \cdot \left(\int_0^H \delta w\ \cos(\alpha_i z)\ dz\right)\left(\int_0^H \ddot{w}\ \cos(\alpha_i z)\ dz\right)\right\} \tag{1.138}$$

and by defining b_{ni} as

$$b_{ni} \;=\; \frac{2\pi R\rho_\ell\ I_n(\alpha_i R)}{H\ \alpha_i\ I_n'(\alpha_i R)} \tag{1.139},$$

one can write

$$\delta W \;=\; -\sum_{i=1}^{\infty} \left\{ b_{ni} \left(\int_0^H \delta w\ \cos(\alpha_i z)\ dz\right)\left(\int_0^H \ddot{w}\ \cos(\alpha_i z)\ dz\right)\right\} \tag{1.140}$$

The work expression (Eq. 1.140) gives rise to the definition of the added mass matrix [DM]. In order to compute its elements, one has to express the integrals in Eq. 1.140 in terms of the nodal displacement vector. With the aid of the displacement model (Eq. 1.75), one can write

$$\int_0^H \ddot{w}(z,t)\cos(\alpha_i z)\,dz = \sum_{e=1}^{NEH}\int_0^{L_e} \{\bar{N}(\bar{z})\}^T \{\ddot{\bar{d}}(t)\}_e \cos[\alpha_i(\bar{z}+(e-1)L_e)]\,d\bar{z} \tag{1.141}$$

Now, define the vectors $\{f^{(i)}\}_e$ as the integrals

$$\left\{f^{(i)}\right\}_e^T = \int_0^{L_e}\left\{\bar{N}(\bar{z})\right\}^T \cos\left[\alpha_i(\bar{z}+(e-1)L_e)\right] d\bar{z}$$

$$= \left[0\ ,\ 0\ ,\ f_3^{(i)}\ ,\ f_4^{(i)}\ ,\ 0\ ,\ 0\ ,\ f_7^{(i)}\ ,\ f_8^{(i)}\right]_e \tag{1.142}$$

where

$$f_3^{(i)} = L_e\left(-\left(\frac{1}{\beta_i}+\frac{6}{\beta_i^3}\right)\sin[\beta_i(e-1)] + \frac{12}{\beta_i^4}\cos[\beta_i(e-1)] - \frac{6}{\beta_i^3}\sin[\beta_i e]\right.$$

$$\left. - \frac{12}{\beta_i^4}\cos[\beta_i e]\right);$$

$$f_4^{(i)} = L_e^2\left(-\frac{4}{\beta_i^3}\sin[\beta_i(e-1)] - \left(\frac{1}{\beta_i^2}-\frac{6}{\beta_i^4}\right)\cos[\beta_i(e-1)] - \frac{2}{\beta_i^3}\sin[\beta_i e]\right.$$

$$\left. - \frac{6}{\beta_i^4}\cos[\beta_i e]\right);$$

$$f_7^{(i)} = L_e\left(\frac{6}{\beta_i^3}\sin[\beta_i(e-1)] - \frac{12}{\beta_i^4}\cos[\beta_i(e-1)] + \left(\frac{1}{\beta_i}+\frac{6}{\beta_i^3}\right)\sin[\beta_i e]\right.$$

$$\left. + \frac{12}{\beta_i^4}\cos[\beta_i e]\right);$$

$$f_8^{(i)} = L_e^2\left(-\frac{2}{\beta_i^3}\sin[\beta_i(e-1)] + \frac{6}{\beta_i^4}\cos[\beta_i(e-1)] - \frac{4}{\beta_i^3}\sin[\beta_i e]\right.$$

$$\left. + \left(\frac{1}{\beta_i^2}-\frac{6}{\beta_i^4}\right)\cos[\beta_i e]\right);$$

and $\beta_i = \alpha_i L_e$, $i = 1,2,....$

The next step is to define the vectors $\{F^{(i)}\}$ as

$$\{F^{(i)}\} = \sum_{e=1}^{NEH} \{f^{(i)}\}_e \tag{1.143}$$

and therefore, Eq. 1.141 can be written as

$$\int_0^H \ddot{w}(z,t) \cos(\alpha_i z)\, dz = \{F^{(i)}\}^T \{\ddot{q}(t)\} \tag{1.144}$$

Eq. 1.140 can then be expressed as

$$\begin{aligned} \delta W &= - \sum_{i=1}^{\infty} b_{ni} \{\delta q\}^T \{F^{(i)}\}\{F^{(i)}\}^T \{\ddot{q}\} \\ &= - \{\delta q\}^T \left(\sum_{i=1}^{\infty} b_{ni} \{F^{(i)}\}\{F^{(i)}\}^T \right) \{\ddot{q}\} \end{aligned} \tag{1.145}$$

Equation 1.145 leads to the definition of the added mass matrix [DM] as

$$[DM] = \sum_{i=1}^{\infty} b_{ni} \{F^{(i)}\} \{F^{(i)}\}^T \tag{1.146}$$

It is important to note that the series in Eq. 1.146 converges very rapidly and only the first few terms are needed for adequate representation of the infinite series. Eq. 1.145 may be expressed conveniently in terms of the added mass matrix as

$$\delta W = - \{\delta q\}^T [DM] \{\ddot{q}\} \tag{1.147}$$

Now, inserting Eq. 1.99, 1.107, and 1.147 into Hamilton's Principle

(Eq. 1.11) to obtain

$$\int_{t_1}^{t_2} \left(\{\delta\dot{q}\}^T [M_s] \{\dot{q}\} - \{\delta q\}^T [K_s] \{q\} - \{\delta q\}^T [DM] \{\ddot{q}\} \right) dt = 0 \qquad (1.148)$$

Integration of the first term by parts with respect to time gives

$$\int_{t_1}^{t_2} \left(\{\delta\dot{q}\}^T [M_s] \{\dot{q}\} \right) dt = \left(\{\delta q\}^T [M_s] \{\dot{q}\} \right) \Big|_{t_1}^{t_2} - \int_{t_1}^{t_2} \{\delta q\}^T [M_s] \{\ddot{q}\} \, dt \qquad (1.149)$$

Noting that, $\{\delta q(t_1)\} = \{\delta q(t_2)\} = \{0\}$, the first term on the right hand side of Eq. 1.149 vanishes. Substituting the remaining term into Eq. 1.148 gives

$$\int_{t_1}^{t_2} \{\delta q\}^T \left[\left([M_s] + [DM] \right) \{\ddot{q}\} + [K_s] \{q\} \right] dt = 0 \qquad (1.150)$$

Since the variations of the nodal displacement, $\{\delta q\}$, are arbitrary, the expression in brackets must vanish. Therefore, the governing matrix equation of the lateral vibration of the liquid-filled shell is given by

$$\left([M_s] + [DM] \right) \{\ddot{q}\} + [K_s] \{q\} = \{0\} \qquad (1.151)$$

It is worthwhile to indicate that the elements of the added mass matrix, derived in this section, are identical to those derived in the preceding section, if the infinite series in Eq. 1.146 is truncated after the I^{th} term.

I-4-9. The Eigenvalue Problem

The matrix equation for the free lateral undamped vibrations of the tank wall is given by

$$[M]\{\ddot{q}\} + [K]\{q\} = \{0\} \tag{1.152}$$

where $[M] = [M_s] + [DM]$; and $[K] = [K_s]$.

By writing the solutions of Eq. 1.152 in the familiar form

$$\{q(t)\} = \{\overset{*}{q}\}\, e^{i\omega t} \quad ; \quad i = \sqrt{-1} \tag{1.153}$$

and substituting Eq. 1.153 into Eq. 1.152 (leaving out the common factor $e^{i\omega t}$), the following equation is obtained

$$\left(-\omega^2 [M] + [K]\right)\{\overset{*}{q}\} = \{0\} \tag{1.154}$$

where $\{\overset{*}{q}\}$ is the vector of the displacement amplitudes of vibrations (which does not change with time), and ω is the natural circular frequency.

A nontrivial solution of Eq. 1.154 is possible only if the determinant of the coefficients vanishes, i.e.,

$$\left\| [K] - \omega^2 [M] \right\| = 0 \tag{1.155}$$

Expanding the determinant will give an algebraic equation of the N^{th} degree in the frequency parameter ω^2 for a system having NEL elements, where $N = 4 \times NEL$.

Because of the positive definitiveness of [M] and [K], the eigenvalues $\omega_1^2, \omega_2^2, \ldots, \omega_N^2$ are real and positive quantities; Eq. 1.154

provides nonzero solution vectors $\{\overset{*}{q}\}$(eigenvectors) for each eigenvalue ω^2.

I-5. Computer Implementation and Numerical Examples

A digital computer program has been written to compute the natural frequencies and mode shapes of vibration of the coupled liquid-shell system by the method outlined in the preceding section. The shell node displacements (eigenvectors) are a direct result of the solution, and these are then used to solve for the shell force and moment resultants, and for the hydrodynamic pressure acting on the wall of the tank. No attempt will be made in this report to explain the mechanics of the computer program; however, a brief description of the general structure of the program, and of the necessary input data is presented.

Several examples of liquid storage tanks with widely different properties are also presented to demonstrate the applicability of the analysis developed herein, and to cover the dynamic characteristics of these tanks. The analysis was first applied to various special cases, due to other investigators, which served as a check on the formulation of the problem, on the convergence of the solution, and on the validity of the entire idealization process. The program was then used to compute the dynamic characteristics of real, full-scale tanks which have been tested experimentally in the second phase of this study; a comparison between the computed and the measured characteristics will be presented in Chapter IV.

Numerical results are also included in this section to demonstrate the variation of the dynamic characteristics with the geometric

dimensions of the tank such as the shell radius, length, and thickness, and the liquid depth. Additional information about the variation of these characteristics with the end conditions of the tank (due to soil flexibility and roof rigidity) will be discussed in Chapter II.

I-5-1. Computer Implementation

The FORTRAN program was written in accordance with the method developed in section I-4, and was implemented on the Caltech digital computer (IBM 370/158 system).

The "FREE VIBRATION (1)" program consists of several subroutines to develop the element stiffness matrix (Eq. 1.94), the element mass matrix (Eq. 1.105), and the added mass matrix (Eq. 1.146); to assemble the shell stiffness and mass matrices; and to extract the eigenvalues (natural frequencies), and the eigenvectors (natural modes). The computation of the eigenvalues ω^2_{mn} and the eigenvectors $\{\overset{*}{q}\}_{mn}$ for the lateral vibrations is worked out through a double precision subroutine which is available from the Caltech computer program library.

Only the fixed-free boundary conditions for the shell are treated in this program; however, the effect of the soil flexibility and the roof rigidity will be discussed in the following chapter, and accordingly, a generalization of this program will be made.

Data input to the program follows the scheme outlined in Fig. I-6. The program output consists of a listing of all the natural frequencies of the discrete system and of only the first few vertical modes for each circumferential wave number required; it also displays these vertical modes in charts.

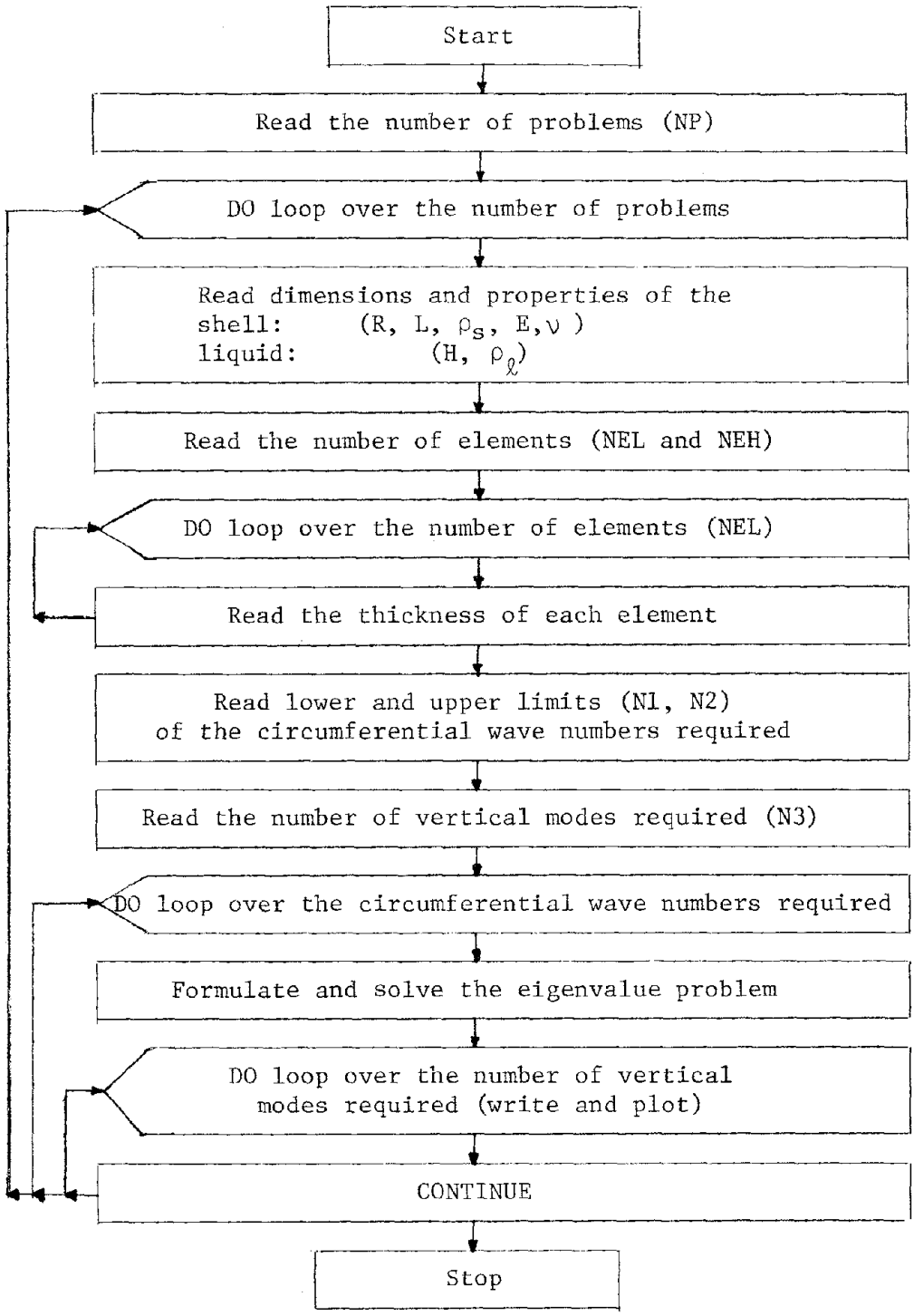

Fig. I-6. Input Data.

I-5-2. Illustrative Numerical Examples

In the following examples, the free lateral vibrations of liquid storage tanks are analyzed to check the accuracy of the computer program and to explore some of the results which may be deduced about the nature of the dynamic characteristics.

Example 1 Empty Storage Tanks

The computer program was first utilized to check the formulation of the shell stiffness and mass matrices by computing the natural frequencies and modes of vibration of an empty tank which has the following dimensions:

$$R = 60 \text{ ft}, \; L = 40 \text{ ft}, \text{ and } h = 1 \text{ inch}.$$

The tank wall is made of steel whose properties are:

$$E = 30 \times 10^6 \text{ lb/in}^2, \; \rho_s = 0.733 \times 10^{-3} \text{ lb. sec}^2/\text{in}^4, \text{ and } \nu = 0.3.$$

The number of elements (NEL) was taken to be 12 elements; therefore, the number of expected modes is (4 x NEL) (i.e. 48 modes are expected), and the length of each element (L_e) is 3.33 ft.

The computed natural frequencies are presented in Table I-1-a along with those calculated by other investigators for comparison. The first two vertical mode shapes (relative nodal values) of the axial, circumferential and radial displacements (u, v, and w) are shown in Fig. I-7. The fundamental mode of vibration of the radial displacement w was also computed using 10 elements; it is displayed in Table I-1-b along with the results of Ref. [17].

In addition, the fundamental natural frequency ω_{11} was computed by the approximate method suggested in [16]; it is given by

Table I-1

a. Natural Frequencies of the cosθ-type Modes (f_{m1} cps)

n = 1

Vertical Mode No. (m)	Present Analysis	Finite Element		Ritz Method	Analytical
		Ref. [14]	Ref. [15]	Ref. [16]	Ref. [17]
1	34.04	34.08	34.03	34.66	34.04
2	43.86	43.91	43.85	44.02	43.81
3	44.54	44.64	44.57	44.64	44.44
4	45.02	45.19	45.07	45.25	44.83
5	45.68	45.92	45.77	-	45.40

b. Fundamental Vertical Mode Shape

(Radial Displacement w)

z/L	Present Analysis	Ref. [17]	z/L	Present Analysis	Ref. [17]
0.1	0.2245	0.2242	0.6	0.7946	0.7949
0.2	0.3765	0.3773	0.7	0.8699	0.8702
0.3	0.4920	0.4920	0.8	0.9294	0.9298
0.4	0.6035	0.6036	0.9	0.9716	0.9720
0.5	0.7052	0.7054	1.0	1.0000	1.0000

Table I-2

Natural Frequencies of the cosnθ-type Modes (f_{m3}, f_{m4} cps)

Vertical Mode No. (m)	n = 3		n = 4	
	Present Analysis	Ref. [17]	Present Analysis	Ref. [17]
1	255.8	250	213.6	209
2	1272.4	1240	829.7	797

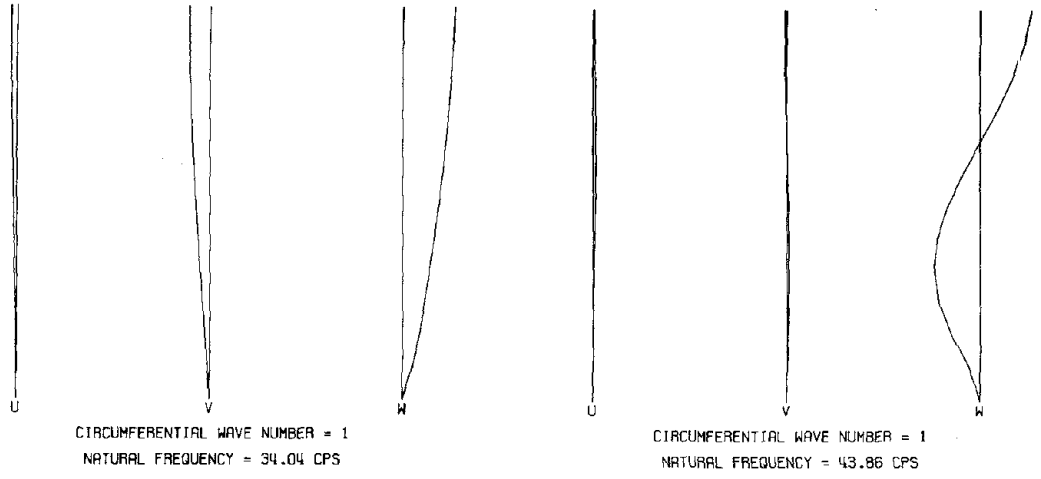

(m = 1) (m = 2)

Fig. I-7. Vertical Mode Shapes of the cosθ-type Modes of an Empty Tank.

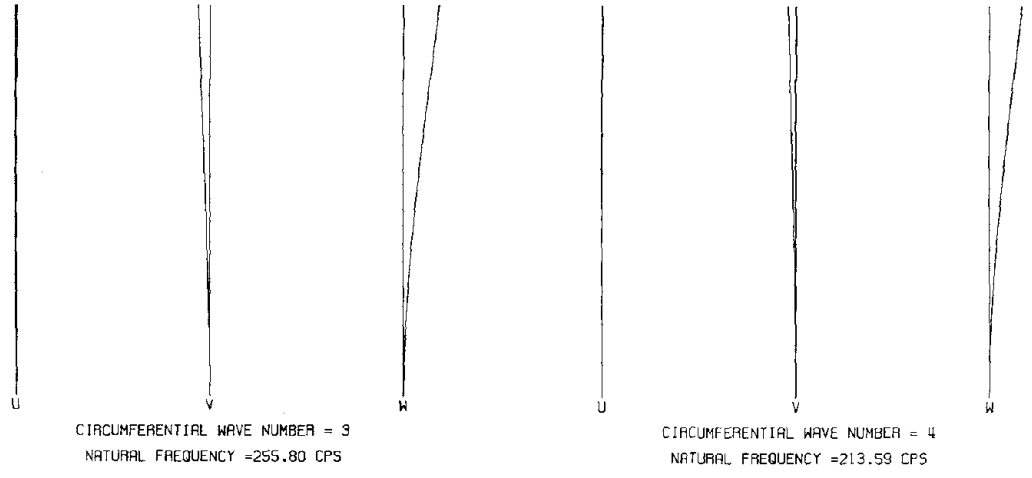

(m = 1) (m = 1)

Fig. I-8. Vertical Mode Shapes of the cosnθ-type Modes of an Empty Tank.

$$\frac{1}{\omega_{11}^2} = \frac{1}{\omega_b^2} + \frac{1}{\omega_s^2} + \frac{1}{\omega_r^2} \qquad (1.156)$$

where $\omega_b = \frac{2.486\ R}{L^2}\sqrt{\frac{E}{\rho_s}}$ is the fundamental natural frequency of the tank acting as a cantilever flexural beam;

$\omega_s = \frac{\pi}{4\sqrt{1+\nu}}\frac{1}{H}\sqrt{\frac{E}{\rho_s}}$ is the fundamental natural frequency of the tank acting as a cantilever shear beam; and

$\omega_r = \frac{1}{R\sqrt{1-\nu^2}}\sqrt{\frac{E}{\rho_s}}$ is the fundamental natural frequency of ovalling motion of a ring of unit width which has the cross sectional dimensions of the tank.

Upon using Eq. 1.156, the fundamental natural frequency ω_{11} is given by

$$\omega_{11} = 205 \text{ rad/sec}$$

$$\text{i.e., } f_{11} = \frac{\omega_{11}}{2\pi} = 32.63 \text{ cps}$$

It is easy, now, to compare the results obtained by the method of analysis under study and the results obtained by other investigators; Table I-1-a and b indicates a very close agreement between these solutions.

It is also of interest to check the natural frequencies of the cosnθ-type modes with those computed in [17]. The tank consists of a cylindrical shell of radius R = 3 inches, of length L = 12 inches, and of thickness h = 0.010 inches, and having the properties:

$E = 29.6 \times 10^6$ lb/in^2, $\rho_s = 0.733 \times 10^{-3}$ lb·sec^2/in^4; and $\nu = 0.29$. The natural frequencies for the circumferential wave numbers (n = 3 and n = 4) are presented in Table I-2 and the fundamental natural modes are displayed in Fig. I-8.

Example 2 Completely Filled Tanks

Let us consider the same first tank of the previous example, but now with a full depth of water $\left(\rho_\ell = 0.94 \times 10^{-4} \text{ lb. sec}^2/\text{in}^4\right)$. Table I-3-a presents the computed natural frequencies of the cosθ-type modes, while Fig. I-9-a shows the fundamental vertical mode of vibration.

Again, to illustrate the effectiveness of the analysis under consideration, a comparison between the obtained results and those of Refs. [12, 13] has been made. It is clear, from Table I-3-a, that the computed frequencies are in good agreement with those calculated in Refs. [12, 13].

The influence of the aspect ratio (length to radius ratio) on the dynamic characteristics was investigated by computing the natural frequencies and modes of vibration of a "tall" tank; its dimensions are:

$$R = 24 \text{ ft}, \; L = 72 \text{ ft}, \text{ and } h = 1 \text{ inch}.$$

The frequencies are given in Table I-3-b and the fundamental mode is shown in Fig. I-9-b. Inspection of Figs. I-9-a and b shows that the mode shapes of "broad" and "tall" tanks are indeed quite different. The hydrodynamic pressure distribution for these two cases and for similar rigid tanks [16] is also shown in Fig. I-10 for comparison.

The natural frequencies of the same "tall" tank were also computed for different values of the shell thickness; they are presented in

Table I-3

a. Natural Frequencies of a Full "Broad" Tank (f_{ml} cps)

n = 1

m	Present Analysis	Ref. [12]	Ref. [13]
1	6.18	6.13	6.20
2	11.28	11.15	11.41
3	15.10	15.11	15.54
4	17.79	18.16	18.72

b. Natural Frequencies of a Full "Tall" Tank (f_{ml} cps)

n = 1

m	h = 1.0 in	h = 0.43 in	h = 0.288 in	$\bar{h}$ = 0.43 in*
1	5.31	3.56	2.93	3.82
2	15.64	10.45	8.59	10.38
3	23.24	15.55	12.79	15.11
4	29.85	20.08	16.54	18.62
5	34.85	23.61	19.48	21.77

*Variable thickness (average $\bar{h}$) - Refer to Chapter IV.

c. Convergence of the Natural Frequencies (f_{ml} cps)

n = 1

m	I = 5	I = 10**	I = 20
1	5.34	5.31	5.31
2	15.70	15.64	15.63
3	23.45	23.24	23.20
4	30.05	29.85	29.77
5	36.20	34.85	34.75

**Standard

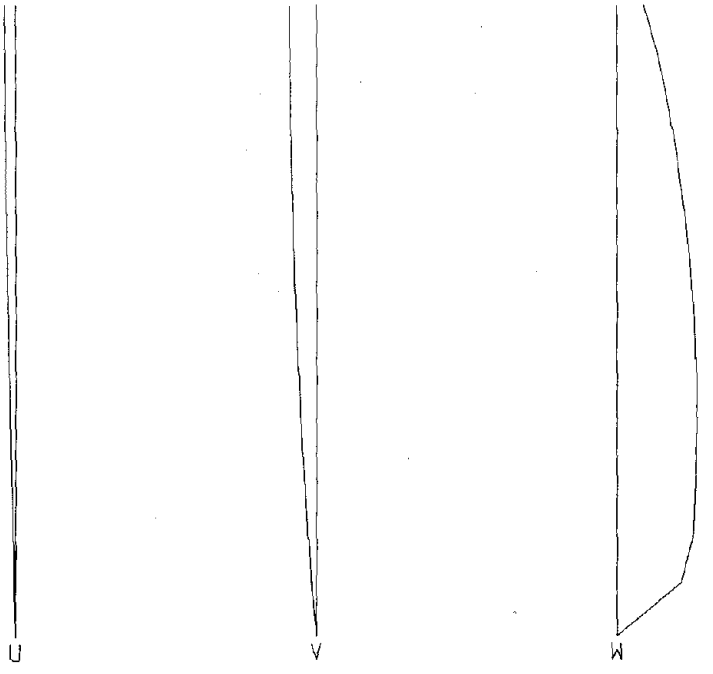

a. "Broad" Tank
(L/R = 0.67)

CIRCUMFERENTIAL WAVE NUMBER = 1
NATURAL FREQUENCY = 6.18 CPS

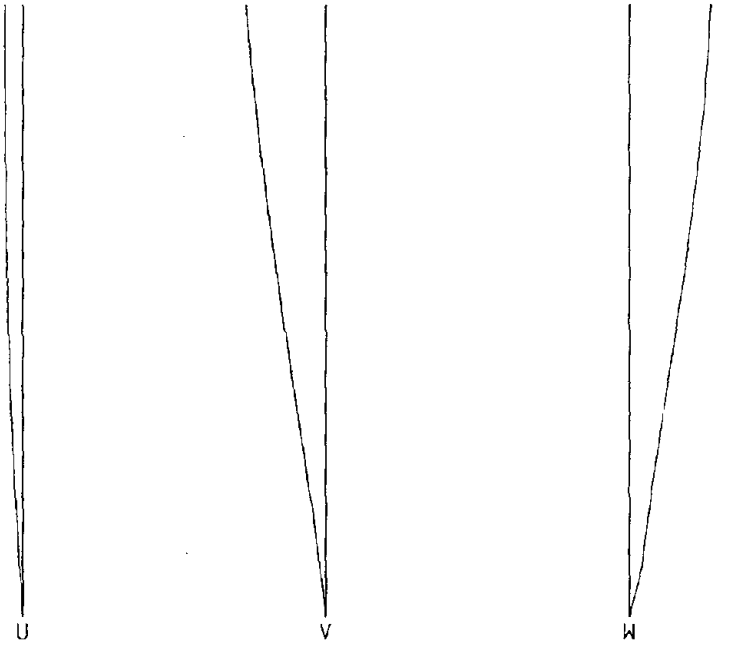

b. "Tall" Tank
(L/R = 3.00)

CIRCUMFERENTIAL WAVE NUMBER = 1
NATURAL FREQUENCY = 5.31 CPS

Fig. I-9. Fundamental Natural Modes of Full Tanks

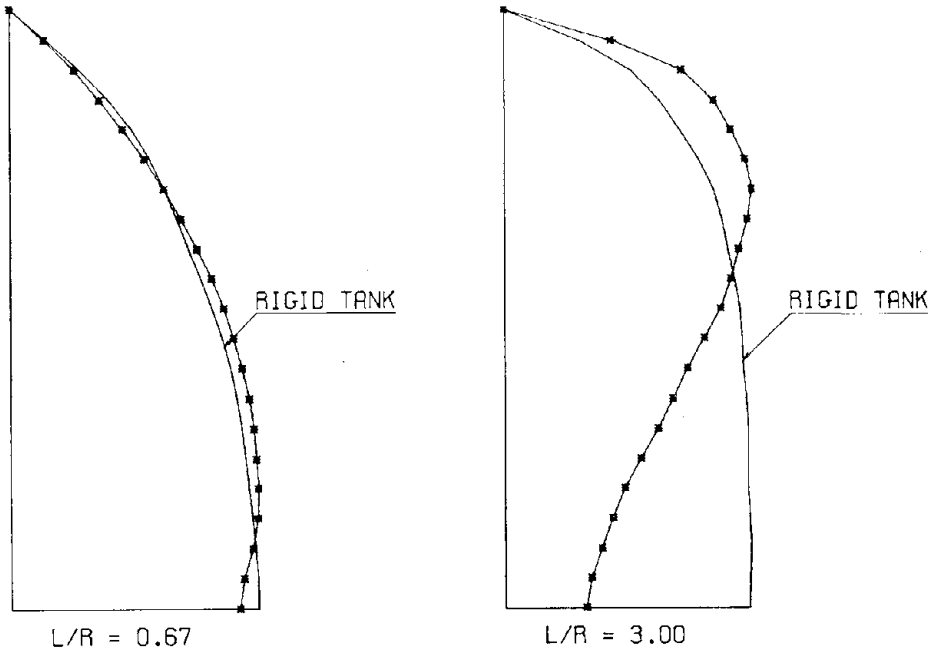

Fig. I-10. Hydrodynamic Pressure Distribution on Full Flexible and Rigid Tanks.

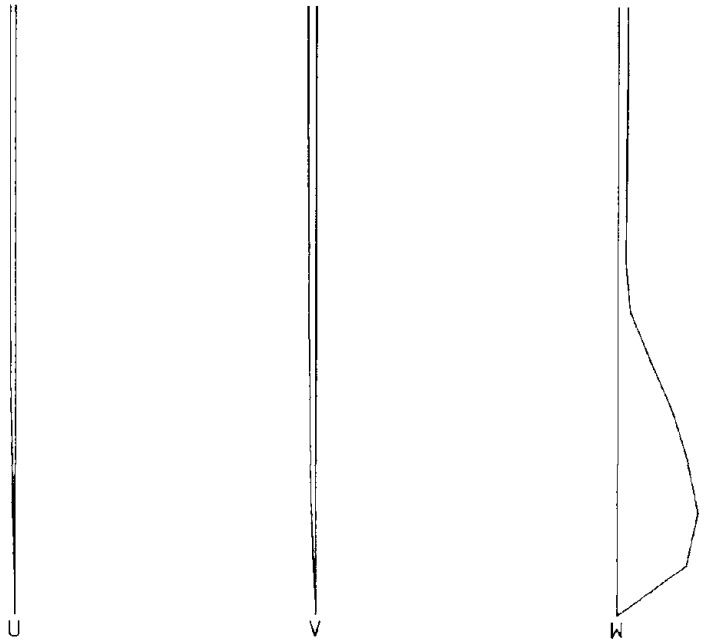

Fig. I-11. Fundamental Vertical Mode of a Half-Full "Broad" Tank.

Table I-3-b. It is observed that the thicker the shell, the higher the natural frequencies, as is expected.

The convergence of the solution is also illustrated in Table I-3-c by computing the natural frequencies using 5, 10 (standard), and 20 terms in the series expansion of the velocity potential ϕ (Eqs. 1.132 and 1.146).

Lastly, the fundamental natural frequency is checked by the method suggested in [16]. For the "tall" tank under consideration, and for a shell thickness of 0.288 inch, it gives

$$\omega_{11} = 18.28 \text{ rad/sec, i.e., } f_{11} = 2.91 \text{ cps}$$

which is in close agreement with the computed frequency shown in Table I-3-b.

Example 3 Partly Filled Tanks

Again, let us consider the same tanks discussed in the previous example but, now, partly filled with water. For the half-full "broad" tank, the computed natural frequencies and those found in Refs. [12, 13] are shown in Table I-4, and the fundamental mode shape is plotted in Fig. I-11. The vertical mode shapes of the "tall" tank under consideration were also computed for a 75% and a 50% of the full depth of water; they are displayed in Fig. I-12. The associated hydrodynamic pressure distributions are also shown in Fig. I-13.

Finally, calculations of the natural frequencies for different values of liquid depths were carried out to investigate the influence of liquid heights on the dynamic characteristics. These frequencies are presented in Table I-5-a and b, and are also shown in Fig. I-14-a and b.

Table I-4

Natural Frequencies of a Half-Full "Broad" Tank (f_{mi} cps)

n = 1

m	Present Analysis	Ref. [12]	Ref. [13]
1	9.88	10.15	9.91
2	17.05	17.85	17.74

Table I-5

Natural Frequencies of Partly-Filled Tanks (f_{ml} cps)

n = 1

a. A "Broad" Tank

% liquid in tank	m = 1	m = 2	m = 3	m = 4
100 (Full)	6.18	11.28	15.10	17.79
80	7.24	12.96	17.07	20.18
60	8.79	15.37	20.05	24.28
50	9.88	17.05	22.48	28.22
30	13.82	24.00	34.27	36.55
0	34.04	43.86	44.54	45.02

b. A "Tall" Tank

% liquid in tank	m = 1	m = 2	m = 3	m = 4
100 (Full)	5.31	15.64	23.24	29.85
80	7.05	18.76	26.99	34.22
60	9.64	22.45	30.57	37.02
50	11.42	24.03	30.87	38.88
30	16.46	25.61	38.80	51.07
0 (Empty)	19.26	56.42	86.38	97.02

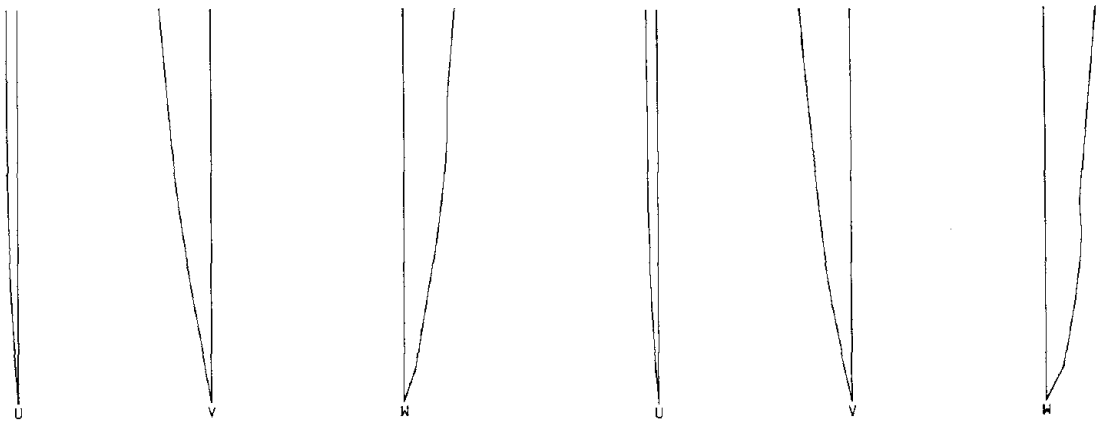

Fig. I-12. Fundamental Modes of a Partly-Filled "Tall" Tank.

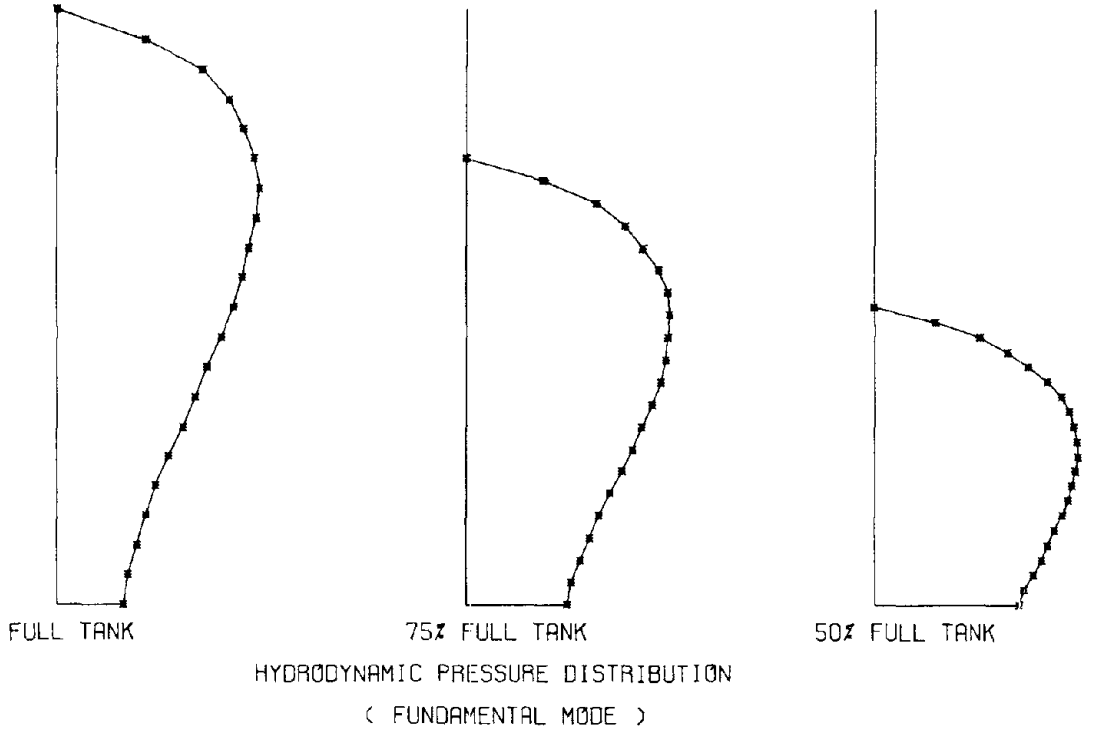

Fig. I-13. Hydrodynamic Pressure Distribution on a Partly-Filled "Tall" Tank

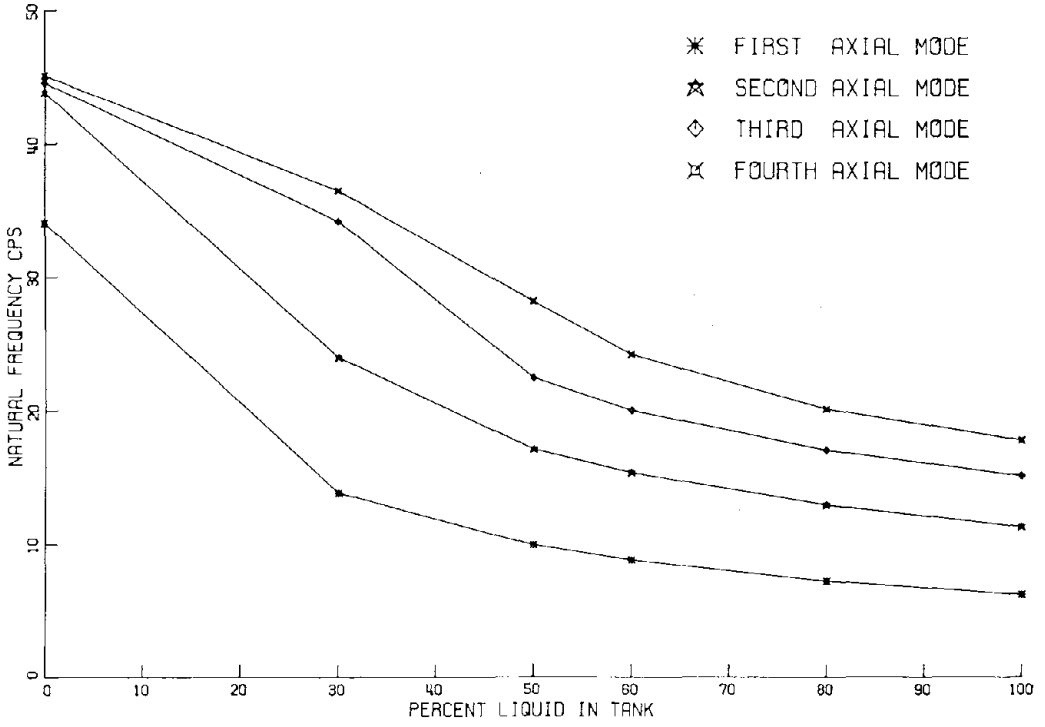

a. A "Broad" Tank

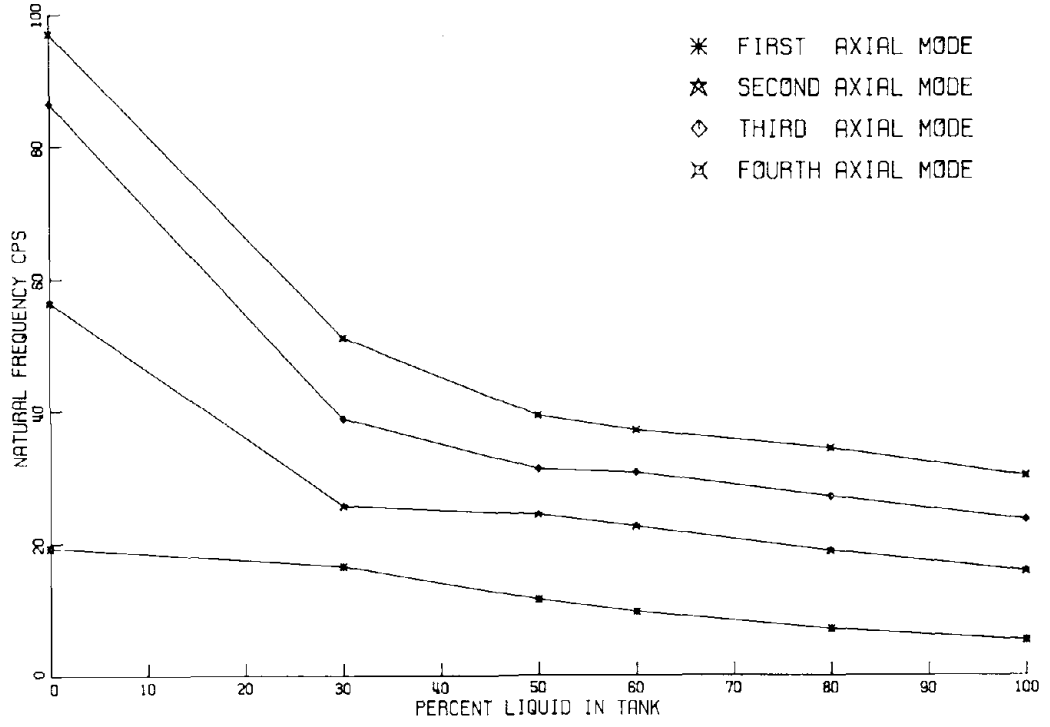

b. A "Tall" Tank

Fig. I-14. Natural Frequencies of Partly-Filled Tanks

They clearly demonstrate the significant contribution of the added-mass of the liquid.

It is important to note that, in all the previous numerical examples, attention was given to the $\cos\theta$-type modes only; these modes are unaffected by the hydrostatic pressure of the liquid. In contrast, the $\cos n\theta$-type modes may be significantly influenced by the initial hoop tension due to the hydrostatic pressure and this will be discussed in the following chapter.

I-6. Appendices

Appendix I-a

List of Symbols

The letter symbols are defined where they are first introduced in the text, and they are also summarized herein in alphabetical order:

$A_i(t)$ and $A_{ni}(t)$	Time dependent coefficients of the velocity potential, Eq. 1.58 and Eq. 1.132, respectively.
$\{A\}$	Vector of the coefficients A_i, Eq. 1.70.
$[B]$	Square matrix defined by Eq. 1.96.
b_{ni}	Coefficients defined by Eq. 1.139.
$[C]$	Diagonal matrix defined by Eqs. 1.112 and 1.120.
$[\hat{C}]_e$	A matrix of order 8 x I defined by Eq. 1.117.
$[\hat{C}]$	A matrix defined by Eqs. 1.119 and 1.120.
$[DM]$	Added mass matrix defined by Eq. 1.130.
$[D]$	Constitutive matrix defined by Eq. 1.27-c.
$[D]_e$	Constitutive matrix of the element "e", Eq. 1.92.
$\{d(\theta,z,t)\}$	Shell displacement vector, Eq. 1.31.
$\{d(\bar{z},t)\}_e$ and $\{d_n\}$	Vectors of the maximum displacement components of the n^{th} circumferential mode, Eqs. 1.76 and 1.87, respectively.
$\{\bar{d}\}_e$	Generalized displacement vector of the element "e", of order 8 x 1, Eq. 1.78.
$\{\bar{\bar{d}}\}_e$	Vector of the generalized displacements (radial and slope only) of the element "e", of order 4 x 1, Eq. 1.81.

E	Young's Modulus of the shell material.
e	Indicate element, and occasionally used as the number of the element "e".
$\{F\}$	Force vector, Eq. 1.56.
$\{f^{(i)}\}_e$ and $\{F^{(i)}\}$	Vectors defined by Eqs. 1.142 and 1.143, respectively.
f_{mn}	Natural frequencies, cps.
$G(\ )$	Function used in Eq. 1.97.
g	Acceleration of gravity.
H	Liquid depth.
h	Shell thickness.
I	Number of terms in the series expansion of the velocity potential, Eq. 1.58.
$I_n(\ )$	Modified Bessel functions of the first kind of order n, Eq. 1.66.
$\acute{I}_n(\ )$	Derivative of $I_n(\ )$ with respect to the radial coordinate, Eq. 1.112.
I, I_c, and $\tilde{I}_c$	Variational functionals, Eqs. 1.12, 1.13 and 1.60, respectively.
i	$\sqrt{-1}$, Eq. 1.153.
J	Variational functional, Eq. 1.61.
$J_n(\ )$	Bessel functions of the first kind of order n, Eq. 1.66.
$[K_s]_e$ and $[K_s]$	Element stiffness matrix and the assemblage stiffness matrix, Eqs. 1.94 and 1.98, respectively.
$[K]$	Stiffness matrix, Eq. 1.152.

$K_n(\ )$	Modified Bessel functions of the second kind of order n.
K_z and K_θ	Midsurface changes in curvature.
$K_{z\theta}$	Midsurface twist.
k	Separation constant, Eq. 1.66.
k_1	Extensional rigidity, Eq. 1.25-a.
k_2	Bending rigidity, Eq. 1.25-b.
L	Shell length.
L_e	Element length.
L_c	Complementary Lagrangian functional, Eq. 1.14.
[L]	Linear differential operator matrix, Eq. 1.46.
$[M_s]_e$ and $[M_s]$	Element mass matrix and the assemblage mass matrix, Eqs. 1.104 and 1.106, respectively.
[M]	Mass matrix, Eq. 1.152.
M_z and M_θ	Bending moment resultants.
$M_{z\theta}$ and $M_{\theta z}$	Twisting moment resultants.
$\tilde{M}$	Effective twisting moment resultant, Eq. 1.23-b.
m	Number of vertical mode.
m(z)	Mass of the shell per unit area.
m_e	Element mass per unit area.
N	Constant = 4 x NEL.
NEL	Number of shell elements along the shell length.
NEH	Number of shell elements in contact with the liquid.
N_z and N_θ	Membrane force resultants.
$N_{z\theta}$ and $N_{\theta z}$	Membrane shear force resultants.
$\tilde{N}$	Effective membrane shear force resultant, Eq. 1.23-a.

N_i and $\hat{N}_i$	Interpolation functions, Eq. 1.73.
$\overset{*}{N}_i(r,\theta,z)$	Trial functions defined by Eq. 1.67.
$\overset{*}{N}_i(z)$	Trial functions defined by Eq. 1.115.
$\{\bar{N}\}$ and $\{\bar{\bar{N}}\}$	Vectors of the interpolation functions, Eqs. 1.79 and 1.80, respectively.
$\{\overset{*}{N}(r,\theta,z)\}$	Vector of the trial functions $\overset{*}{N}_i(r,\theta,z)$, Eq. 1.70.
$\{\overset{*}{N}(z)\}$	Vector of the trial functions $\overset{*}{N}_i(z)$.
n	Number of circumferential waves.
[P]	Differential operator matrix, Eq. 1.32.
$[\hat{P}_n]$	Differential operator matrix for the n^{th} circumferential wave number, Eq. 1.90.
p, p_s, and p_d	Liquid pressure, hydrostatic pressure, and dynamic pressure, respectively.
[Q]	Matrix of interpolation functions, of order 3 x 8, Eq. 1.77.
{q}	The assemblage nodal displacement vector, Eq. 1.82.
$\{\overset{*}{q}\}$	Time independent nodal displacement vector, Eq. 1.153.
R	Tank radius.
$\hat{R}(r)$	Separation-of-variables function, Eq. 1.65.
r	Radial coordinate of the cylindrical coordinate system.
S,S_1,S_2, and S_3	Liquid surface, quiescent free surface, wetted surfaces of the shell and the bottom plate, respectively.
S_i	Interpolation functions, Eq. 1.73.

$T(t)$	Kinetic energy.
$\hat{T}(t)$	Separation-of-variables function, Eq. 1.65.
$T_n(t)$	Functions of time, Eq. 1.66.
t	Time.
t_1 and t_2	Limits of the time interval under consideration, Eq. 1.11.
$U(t)$	Potential energy or strain energy.
V	Liquid volume
$W(t)$	Work done by external loads.
u,v, and w	Shell displacements in the axial, tangential, and radial directions, respectively.
$u_n(z,t), v_n(z,t)$, and $w_n(z,t)$	Displacement functions for the n^{th} circumferential wave, Eq. 1.71.
$u_{ne}(\bar{z},t), v_{ne}(\bar{z},t)$, and $w_{ne}(\bar{z},t)$	Displacement functions for the n^{th} circumferential wave in the local axial coordinate of the element "e", Eq. 1.72.
$\bar{u}_{ni}, \bar{v}_{ni}, \bar{w}_{ni}$ and $\hat{w}_{ni}$	Generalized nodal displacements of an element, Eq. 1.72
W_1, W_2, W_3, and W_4	Weights of the Gaussian integration rule, Eq. 1.97.
$Y_n(\ )$	Bessel functions of the second kind of order n.
$\hat{Z}(z)$	Separation-of-variables function, Eq. 1.65.
z	Axial coordinate of the cylindrical coordinate system.
$\bar{z}$	Local axial coordinate.
α	Constant defined by Eq. 1.47.

α_i	Coefficients defined by Eq. 1.68.
β_i	Coefficients $= \alpha_i L_e$.
δ	Variational operator.
ε_z and ε_θ	Normal strains in the middle surface.
$\varepsilon_{z\theta}$	Shear strain in the middle surface.
$\{\varepsilon\}$	Generalized strain vector, Eq. 1.27-b.
ξ	Free surface displacement.
η_1, η_2, η_3, and η_4	Integration points, Eq. 1.97.
$[\Theta_n]$	Diagonal matrix defined by Eq. 1.86.
$[\hat{\Theta}_n]$	Diagonal matrix defined by Eq. 1.89.
$\hat{\Theta}(\theta)$	Separation-of-variables function, Eq. 1.65.
θ	Circumferential coordinate of the cylindrical coordinate system.
ν	Poisson's ratio.
$\underset{\sim}{\nu}$	Outward normal vector.
ρ_ℓ and ρ_s	Mass density of the liquid and the shell material, respectively.
$\{\sigma\}$	Generalized force resultant vector, Eq. 1.27-a.
ϕ	Liquid velocity potential function.
ω_b, ω_s, and ω_r	Natural frequencies, Eq. 1.156.
ω, ω_m, and ω_{mn}	Circular natural frequencies.
Δ^2 and Δ^4	Differential operators defined by Eq. 1.47.
∇^2	Laplacian operator.
∇	Gradient operator.
$(\dot{})$	Differentiation with respect to time.

Appendix I-b

A Linear Shell Theory

The present investigation is based upon a first-approximation theory for thin shells due to V.V. Novozhilov [7]. For simplicity and convenience, the theory will be developed herein for the special case of circular cylindrical shells following an analogous procedure as outlined by Novozhilov for arbitrary shells.

I-b-1. Fundamental Assumptions

In the classical theory of small displacements of thin shells, the following assumptions were made by Love:

a. The thickness of the shell is small compared to the radius of curvature.

b. The deflections of the shell are small in comparison to the shell thickness.

c. The transverse normal stress is small compared with other normal stress components and is negligible.

d. Normals to the undeformed middle surface remain straight and normal to the deformed middle surface and suffer no extention. This assumption is known as Kirchhoff's hypothesis.

These four assumptions give rise to what Love called his "first approximation" shell theory and are universally accepted by others in the derivation of thin shell theories.

I-b-2. Coordinate System and Notations

Consider a right, circular cylindrical shell of radius R, length L,

and thickness h. Let r, θ, and z denote the radial, circumferential and axial coordinates, respectively, of a point on the shell middle surface. The corresponding displacement components are denoted by w, v, and u, as indicated in Fig. I-b-i. To describe the location of an arbitrary point in the space occupied by the shell, let x measure the distance of the point along r from the corresponding point on the middle surface $\left(-\frac{h}{2} \leq x \leq \frac{h}{2}\right)$.

In addition to the letter symbols being summarized in appendix I-a, the following symbols are also used in the following derivation of the linear shell theory:

e_z, e_θ, and e_x	Normal strains at an arbitrary point in the space occupied by the shell, Eq. I-b-1.
F_z, F_θ, and F_r	Axial, circumferential and radial forces per unit area of the shell midsurface, respectively.
I_1, I_2, and I_3	Functions defined by Eq. I-b-22.
P_z, P_θ, and P_r	Axial, circumferential and radial forces per unit area of the shell midsurface including inertia forces, respectively.
Q_z and Q_θ	Transverse shearing forces.
Q_0, Q_1, and Q_2	Functions defined by Eq. I-b-19.
U, V, and W	Displacement components at an arbitrary point.
x	Shell coordinate (refer to Fig. I-b-i).
$\gamma_{z\theta}$, $\gamma_{\theta x}$, and γ_{xz}	Shear strains, Eq. I-b-1.
$\bar{\varepsilon}_z$, $\bar{\varepsilon}_\theta$, and $\bar{\varepsilon}_{z\theta}$	Dimensionless quantities defined by Eq. I-b-21.
σ_z, σ_θ, and σ_x	Normal stresses, Eq. I-b-9.
$\sigma_{z\theta}$, $\sigma_{\theta x}$, and σ_{xz}	Shear stresses, Eq. I-b-9.

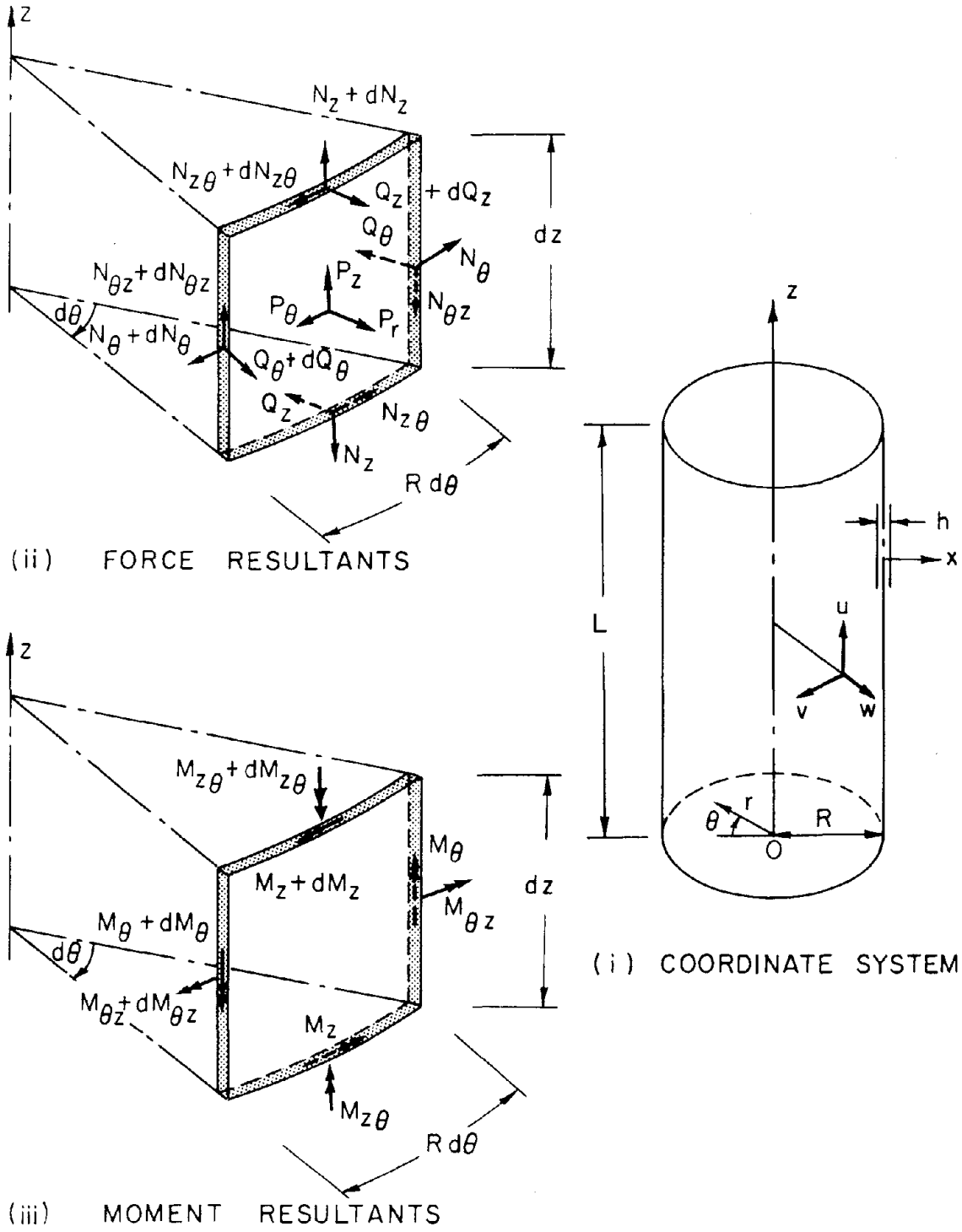
z
$N_z + dN_z$
$N_{z\theta} + dN_{z\theta}$
$Q_z + dQ_z$
Q_θ
N_θ
$N_{\theta z} + dN_{\theta z}$
P_z
P_θ
P_r
$N_{\theta z}$
$d\theta$
$N_\theta + dN_\theta$
$Q_\theta + dQ_\theta$
Q_z
$N_{z\theta}$
N_z
dz
R dθ
(ii) FORCE RESULTANTS
z
$M_{z\theta} + dM_{z\theta}$
M_θ
$M_z + dM_z$
$M_{\theta z}$
$M_\theta + dM_\theta$
$d\theta$
$M_{\theta z} + dM_{\theta z}$
M_z
$M_{z\theta}$
dz
R dθ
(iii) MOMENT RESULTANTS
z
h
x
L
u
v
w
r
θ
R
O
(i) COORDINATE SYSTEM

Fig. I-b.

Ψ_z and Ψ_θ Rotations of the normal to the middle surface during deformation about the θ and z axes, respectively.

I-b-3. Strain-Displacement Relations

The well-known strain-displacement equations of the three-dimensional theory of elasticity can be expressed in the coordinates (z,θ,x) as follows:

$$\left.\begin{aligned} e_z &= \frac{\partial U}{\partial z}, \\ e_\theta &= \frac{1}{R\left(1+\frac{x}{R}\right)}\left(\frac{\partial V}{\partial \theta} + W\right), \\ e_x &= \frac{\partial W}{\partial x} \\ \gamma_{z\theta} &= \gamma_{\theta z} = \frac{1}{R\left(1+\frac{x}{R}\right)}\frac{\partial U}{\partial \theta} + \frac{\partial V}{\partial z}, \\ \gamma_{zx} &= \gamma_{xz} = \frac{\partial W}{\partial z} + \frac{\partial U}{\partial x}, \\ \text{and} \quad \gamma_{\theta x} &= \gamma_{x\theta} = \frac{1}{R\left(1+\frac{x}{R}\right)}\left(\frac{\partial W}{\partial \theta} - V\right) + \frac{\partial V}{\partial x} \end{aligned}\right\} \quad \text{(I-b-1)}$$

where e_z, e_θ, and e_x are the normal strains;

$\gamma_{z\theta}$, γ_{zx}, and $\gamma_{\theta x}$ are the shear strains;

and U, V, and W are the displacement components at an arbitrary point.

As a consequence of Kirchoff's hypothesis

$$e_x = 0, \ \gamma_{zx} = 0 \text{ and } \gamma_{\theta x} = 0 \qquad \text{(I-b-2)}$$

Now, in order to satisfy this hypothesis, the class of

displacements is restricted to the following linear relationships:

$$\begin{aligned} U(z,\theta,x) &= u(z,\theta) + x\ \Psi_z(z,\theta) \\ V(z,\theta,x) &= v(z,\theta) + x\ \Psi_\theta(z,\theta) \\ W(z,\theta,x) &= w(z,\theta) \end{aligned} \qquad \text{(I-b-3)}$$

where u, v, and w are the displacement components at the middle surface in the z, θ, and normal directions, respectively; and Ψ_z and Ψ_θ are the rotations of the normal to the middle surface during deformation about the θ and z axes, respectively; i.e.,

$$\begin{aligned} \Psi_z &= \frac{\partial U(z,\theta,x)}{\partial x} \\ \Psi_\theta &= \frac{\partial V(z,\theta,x)}{\partial x} \end{aligned} \qquad \text{(I-b-4)}$$

The first of Eqs. I-b-2 is satisfied by restricting W to be independent of x; i.e., W is completely defined by the middle surface component w. Substituting Eqs. I-b-3 into Eqs. I-b-1, the last two of Eqs. I-b-2 are satisfied provided that

$$\Psi_z = -\frac{\partial w}{\partial z} \quad \text{and} \quad \Psi_\theta = \frac{1}{R}\left(v - \frac{\partial w}{\partial \theta}\right) \qquad \text{(I-b-5)}$$

Substitution of Eqs. I-b-3 and I-b-5 into Eqs. I-b-1 yields

$$\left.\begin{aligned} e_z &= \frac{\partial u}{\partial z} - x\frac{\partial^2 w}{\partial z^2} \\ e_\theta &= \frac{1}{\left(1 + \frac{x}{R}\right)}\left[\frac{1}{R}\left(\frac{\partial v}{\partial \theta} + w\right) - \frac{x}{R^2}\left(\frac{\partial^2 w}{\partial \theta^2} - \frac{\partial v}{\partial \theta}\right)\right] \\ \gamma_{z\theta} &= \frac{1}{\left(1 + \frac{x}{R}\right)}\left[\left(\frac{\partial v}{\partial z} + \frac{1}{R}\frac{\partial u}{\partial \theta}\right) + \frac{2x}{R}\left(1 + \frac{x}{2R}\right)\left(\frac{\partial v}{\partial z} - \frac{\partial^2 w}{\partial \theta \partial z}\right)\right] \end{aligned}\right\} \text{(I-b-6)}$$

Eqs. I-b-6 may be expressed conveniently in terms of the normal and shear strains in the middle surface ε_z, ε_θ and $\varepsilon_{z\theta}$, in terms of the midsurface changes in curvature K_z and K_θ, and in terms of the midsurface twist $K_{z\theta}$ as follows:

$$\left.\begin{aligned} e_z &= \varepsilon_z + x\, K_z \\ e_\theta &= \frac{1}{\left(1 + \frac{x}{R}\right)}\left(\varepsilon_\theta + x\, K_\theta\right) \\ \gamma_{z\theta} &= \frac{1}{\left(1 + \frac{x}{R}\right)}\left(\varepsilon_{z\theta} + x\left(1 + \frac{x}{2R}\right)K_{z\theta}\right) \end{aligned}\right\} \qquad \text{(I-b-7)}$$

where

$$\left.\begin{aligned} \varepsilon_z &= \frac{\partial u}{\partial z} \\ \varepsilon_\theta &= \frac{1}{R}\left(\frac{\partial v}{\partial \theta} + w\right) \\ \varepsilon_{z\theta} &= \frac{1}{R}\frac{\partial u}{\partial \theta} + \frac{\partial v}{\partial z} \\ K_z &= -\frac{\partial^2 w}{\partial z^2} \\ K_\theta &= -\frac{1}{R^2}\left(\frac{\partial^2 w}{\partial \theta^2} - \frac{\partial v}{\partial \theta}\right) \\ K_{z\theta} &= -\frac{2}{R}\left(\frac{\partial^2 w}{\partial z\, \partial \theta} - \frac{\partial v}{\partial z}\right) \end{aligned}\right\} \qquad \text{(I-b-8)}$$

I-b-4. Force and Moment Resultants

As was shown in the preceding section, the strain variation through the thickness is completely defined with respect to x. Thus, if the relationships between stresses and strains are defined, the

resulting stresses can be integrated over the shell thickness. The resultants of the integrals will be termed "force resultants" and "moment resultants".

Now, the shell material will be assumed homogeneous, isotropic and linearly elastic. Hence, the stress strain relationships can be expressed as

$$\left.\begin{aligned} e_z &= \frac{1}{E}\left[\sigma_z - \nu\,(\sigma_\theta + \sigma_x)\right] \\ e_\theta &= \frac{1}{E}\left[\sigma_\theta - \nu\,(\sigma_z + \sigma_x)\right] \\ e_x &= \frac{1}{E}\left[\sigma_x - \nu\,(\sigma_z + \sigma_\theta)\right] \\ \gamma_{z\theta} &= \frac{2(1+\nu)}{E}\,\sigma_{z\theta} \\ \gamma_{zx} &= \frac{2(1+\nu)}{E}\,\sigma_{zx} \\ \gamma_{\theta x} &= \frac{2(1+\nu)}{E}\,\sigma_{\theta x} \end{aligned}\right\} \qquad \text{(I-b-9)}$$

where E is Young's modulus; and ν is Poisson's ratio. The Kirchhoff's hypothesis yields $e_x = \gamma_{zx} = \gamma_{\theta x} = 0$, whence, by Eqs. I-b-9, $\sigma_{zx} = \sigma_{\theta x} = 0$ and $\sigma_x = \nu\,(\sigma_z + \sigma_\theta)$. But Love's third assumption is that σ_x is negligibly small, which is one unavoidable contradiction. Another contradiction is that σ_{zx} and $\sigma_{\theta x}$ are clearly not zero, since their integrals must supply the transverse shearing forces needed for equilibrium; but they are usually small in comparison with σ_z, σ_θ, and $\sigma_{z\theta}$.

Retaining the assumption that σ_x is negligibly small reduces the problem to one of plane stress; i.e., Eqs. I-b-9 are reduced to

$$\left.\begin{aligned} e_z &= \frac{1}{E}(\sigma_z - \nu\,\sigma_\theta) \\ e_\theta &= \frac{1}{E}(\sigma_\theta - \nu\,\sigma_z) \\ \gamma_{z\theta} &= \frac{2(1+\nu)}{E}\,\sigma_{z\theta} \end{aligned}\right\} \qquad \text{(I-b-10)}$$

which, when inverted, give

$$\left.\begin{aligned} \sigma_z &= \frac{E}{1-\nu^2}(e_z + \nu e_\theta) \\ \sigma_\theta &= \frac{E}{1-\nu^2}(e_\theta + \nu e_z) \\ \sigma_{z\theta} &= \frac{E}{2(1+\nu)}\gamma_{z\theta} \end{aligned}\right\} \qquad \text{(I-b-11)}$$

Now, consider the face of a shell element that is perpendicular to the z-axis. By integrating the stresses σ_z, $\sigma_{z\theta}$ and σ_{zx} over the shell thickness, the force resultants, per unit length of the middle surface, acting on this face can be expressed as

$$\begin{Bmatrix} N_z \\ N_{z\theta} \\ Q_z \end{Bmatrix} = \int_{-\frac{h}{2}}^{\frac{h}{2}} \begin{Bmatrix} \sigma_z \\ \sigma_{z\theta} \\ \sigma_{zx} \end{Bmatrix} \left(1 + \frac{x}{R}\right) dx \qquad \text{(I-b-12)}$$

and, similarly, the force resultants on the face perpendicular to the θ-axis will be

$$\begin{Bmatrix} N_\theta \\ N_{\theta z} \\ Q_\theta \end{Bmatrix} = \int_{-\frac{h}{2}}^{\frac{h}{2}} \begin{Bmatrix} \sigma_\theta \\ \sigma_{\theta z} \\ \sigma_{\theta x} \end{Bmatrix} dx \qquad \text{(I-b-13)}$$

Analogously, the moment resultants are given by

$$\begin{Bmatrix} M_z \\ M_{z\theta} \end{Bmatrix} = \int_{-\frac{h}{2}}^{\frac{h}{2}} \begin{Bmatrix} \sigma_z \\ \sigma_{z\theta} \end{Bmatrix} \left(1 + \frac{x}{R}\right) x \, dx$$

$$\begin{Bmatrix} M_\theta \\ M_{\theta z} \end{Bmatrix} = \int_{-\frac{h}{2}}^{\frac{h}{2}} \begin{Bmatrix} \sigma_\theta \\ \sigma_{\theta z} \end{Bmatrix} x \, dx \qquad \text{(I-b-14)}$$

and, consequently, have dimensions of moment per unit length of the middle surface.

The force and moment resultants acting upon an infinitesimal shell element are depicted in Figs. I-b-ii and I-b-iii, respectively. It is worthy to note that although $\sigma_{z\theta} = \sigma_{\theta z}$ from the symmetry of the stress tensor, it is clear from Eqs. I-b-12, I-b-13, and I-b-14 that $N_{z\theta} \neq N_{\theta z}$ and $M_{z\theta} \neq M_{\theta z}$.

I-b-5. Force-Strain and Moment-Curvature Relationships

From the theory of elasticity the well-known expression for the strain energy stored in a body during elastic deformation is

$$U = \frac{1}{2} \int_V (\sigma_z e_z + \sigma_\theta e_\theta + \sigma_x e_x + \sigma_{z\theta}\gamma_{z\theta} + \sigma_{zx}\gamma_{zx} + \sigma_{\theta x}\gamma_{\theta x})\, dv \qquad \text{(I-b-15)}$$

where dv is the volume of an infinitesimal element and is given by

$$dv = R\left(1 + \frac{x}{R}\right) d\theta\, dz\, dx$$

Applying the Kirchhoff's hypothesis reduces Eq. I-b-15 to

$$U = \frac{1}{2} \int_V \left(\sigma_z e_z + \sigma_\theta e_\theta + \sigma_{z\theta}\gamma_{z\theta}\right) dv \qquad \text{(I-b-16)}$$

Substituting Eqs. I-b-11 into Eq. I-b-16 yields

$$U = \frac{E}{2(1 - \nu^2)} \int_V \left[e_z^2 + e_\theta^2 + 2\nu\, e_\theta e_z + \frac{(1 - \nu)}{2}\gamma_{z\theta}^2\right] dv \qquad \text{(I-b-17)}$$

Substituting further the expressions for the total strains in terms of the middle surface strains and changes in curvature given by Eqs. I-b-7, Eq. I-b-17 becomes

$$U = \frac{E}{2(1 - \nu^2)} \int_V \left[\left(1 + \frac{x}{R}\right)\left(\varepsilon_z + x\, K_z\right)^2 + \left(1 + \frac{x}{R}\right)^{-1}\left(\varepsilon_\theta + x\, K_\theta\right)^2 + 2\nu\,(\varepsilon_z + x\, K_z)\,(\varepsilon_\theta + x\, K_\theta) + \frac{(1 - \nu)}{2}\left(1 + \frac{x}{R}\right)^{-1}\left(\varepsilon_{z\theta} + x\left(1 + \frac{x}{2R}\right) K_{z\theta}\right)^2\right] R\, d\theta\, dz\, dx \qquad \text{(I-b-18)}$$

Replacing $\left(1 + \frac{x}{R}\right)^{-1}$ in Eq. I-b-18 by its series expansion given by $\sum_{j=0}^{\infty}\left(-\frac{x}{R}\right)^j$, and neglecting terms raised to powers of x greater than

two in the integrand, one obtains

$$U = \frac{E}{2(1 - \nu^2)} \int_V (Q_0 + x\, Q_1 + x^2\, Q_2)\, R\, d\theta\, dz\, dx \qquad \text{(I-b-19)}$$

where

$$Q_0 = (\varepsilon_z + \varepsilon_\theta)^2 - 2(1 - \nu)\left(\varepsilon_z \varepsilon_\theta - \frac{\varepsilon_{z\theta}^2}{4}\right)$$

$$Q_2 = (K_z + K_\theta)^2 - 2(1 - \nu)\left(K_z K_\theta - \frac{K_{z\theta}^2}{4}\right) + \frac{2}{R}(\varepsilon_z K_z - \varepsilon_\theta K_\theta)$$

$$- \frac{(1 - \nu)}{2} \frac{\varepsilon_{z\theta} K_{z\theta}}{R} + \frac{\varepsilon_\theta^2}{R^2} + \frac{(1 - \nu)}{2} \frac{\varepsilon_{z\theta}^2}{R^2}$$

Note that the value of Q_1 is of no interest, since

$$\int_{-\frac{h}{2}}^{\frac{h}{2}} Q_1\, x\, dx = Q_1 \int_{-\frac{h}{2}}^{\frac{h}{2}} x\, dx = 0$$

Carrying out the integration of Eq. I-b-19 over the thickness, gives

$$U = \frac{Eh}{2(1 - \nu^2)} \int_z \int_\theta \left(Q_0 + \frac{h^2}{12} Q_2\right) R\, d\theta\, dz \qquad \text{(I-b-20)}$$

Now, Eq. I-b-20 will be examined carefully to determine which terms are to be retained. First, the curvature changes and twist are replaced by dimensionless quantities defined by

$$\bar{\varepsilon}_z = \frac{h}{2} K_z\,, \quad \bar{\varepsilon}_\theta = \frac{h}{2} K_\theta \text{ and } \bar{\varepsilon}_{z\theta} = h\, K_{z\theta} \qquad \text{(I-b-21)}$$

where $\bar{\varepsilon}_z$, $\bar{\varepsilon}_\theta$ and $\bar{\varepsilon}_{z\theta}$ can be physically interpreted as the strains in the extreme fibers of the shell resulting from K_z, K_θ and $K_{z\theta}$, respectively.

Substituting Eqs. I-b-21 into Eq. I-b-20, one obtains

$$U = \frac{Eh}{2(1-\nu^2)} \iint_z \int_\theta (I_1 + I_2 + I_3)\, R\, d\theta\, dz \qquad \text{(I-b-22)}$$

where $I_1 = (\varepsilon_z + \varepsilon_\theta)^2 - 2(1-\nu)\left(\varepsilon_z\varepsilon_\theta - \frac{\varepsilon_{z\theta}^2}{4}\right) + \frac{1}{3}\left[(\bar{\varepsilon}_z + \bar{\varepsilon}_\theta)^2 - 2(1-\nu)\left(\bar{\varepsilon}_z\,\bar{\varepsilon}_\theta - \frac{\bar{\varepsilon}_{z\theta}^2}{16}\right)\right]$

$$I_2 = \frac{h}{R}\left[\frac{1}{3}(\varepsilon_z\bar{\varepsilon}_z - \varepsilon_\theta\,\bar{\varepsilon}_\theta) - \frac{(1-\nu)}{24}\varepsilon_{z\theta}\bar{\varepsilon}_{z\theta}\right]$$

$$I_3 = \frac{h^2}{R^2}\left[\frac{1}{12}\varepsilon_\theta^2 + \frac{(1-\nu)}{24}\varepsilon_{z\theta}^2\right]$$

It is now clear that I_2 and I_3 are of the orders $\left(\frac{h}{R}\right)$ and $\left(\frac{h}{R}\right)^2$, respectively, with respect to unity; hence, I_2 and I_3 will be neglected in comparison with I_1, giving

$$U = \frac{Eh}{2(1-\nu^2)} \iint_z \int_\theta \left\{ \left[(\varepsilon_z + \varepsilon_\theta)^2 - 2(1-\nu)\left(\varepsilon_z\varepsilon_\theta - \frac{\varepsilon_{z\theta}^2}{4}\right)\right] + \frac{h^2}{12}\left[(K_z + K_\theta)^2 - 2(1-\nu)\left(K_zK_\theta - \frac{K_{z\theta}^2}{4}\right)\right]\right\} R\, d\theta\, dz \qquad \text{(I-b-23)}$$

Taking the variation of Eq. I-b-23 yields

$$\delta U = \frac{Eh}{(1-\nu^2)} \iint_{z\,\theta} \Big\{ \Big[(\varepsilon_z + \nu\varepsilon_\theta)\,\delta\varepsilon_z + (\varepsilon_\theta + \nu\,\varepsilon_z)\delta\varepsilon_\theta + \frac{(1-\nu)}{2}\,\varepsilon_{z\theta}\,\delta\varepsilon_{z\theta}\Big] + \frac{h^2}{12}\Big[(K_z + \nu\,K_\theta)\,\delta K_z + (K_\theta + \nu\,K_z)\,\delta K_\theta + \frac{(1-\nu)}{2} K_{z\theta}\,\delta K_{z\theta}\Big]\Big\}\, R\,d\theta\,dz \tag{I-b-24}$$

Returning to the strain energy functional given by Eq. I-b-16 and taking its variation gives:

$$\delta U = \int_V (\sigma_z\,\delta e_z + \sigma_\theta\,\delta e_\theta + \sigma_{z\theta}\,\delta\gamma_{z\theta})\,dv\ ,$$

and upon using Eqs. I-b-7, it can be written as

$$\delta U = \iiint_{z\,\theta\,x} \Big[\sigma_z\Big(1+\frac{x}{R}\Big)(\delta\varepsilon_z + x\,\delta K_z) + \sigma_\theta(\delta\varepsilon_\theta + x\,\delta K_\theta) + \sigma_{z\theta}\delta\varepsilon_{z\theta} + x\,\sigma_{z\theta}\Big(1+\frac{x}{2R}\Big)\delta K_{z\theta}\Big] R\,d\theta\,dz\,dx \tag{I-b-25}$$

Making use of the definitions of the force and the moment resultants (Eqs. I-b-12, I-b-13, and I-b-14), Eq. I-b-25 can be rewritten as

$$\delta U = \iint_{z\,\theta} (N_z\delta\varepsilon_z + N_\theta\,\delta\varepsilon_\theta + \tilde{N}\,\delta\varepsilon_{z\theta} + M_z\,\delta K_z + M_\theta\,\delta K_\theta + \tilde{M}\,\delta K_{z\theta})\,R\,d\theta\,dz \tag{I-b-26}$$

where

$$\tilde{N} = N_{\theta z} = N_{z\theta} - \frac{M_{\theta z}}{R}$$

$$\tilde{M} = \frac{1}{2}(M_{z\theta} + M_{\theta z})$$

Comparing Eqs. I-b-26 and I-b-24 leads to the following relationships

$$
\begin{aligned}
N_z &= \frac{Eh}{(1-\nu^2)}(\varepsilon_z + \nu\,\varepsilon_\theta) \\
N_\theta &= \frac{Eh}{(1-\nu^2)}(\varepsilon_\theta + \nu\,\varepsilon_z) \\
\tilde{N} &= \frac{Eh}{2(1+\nu)}\varepsilon_{z\theta} \\
M_z &= \frac{Eh^3}{12(1-\nu^2)}(K_z + \nu\,K_\theta) \\
M_\theta &= \frac{Eh^3}{12(1-\nu^2)}(K_\theta + \nu\,K_z) \\
\tilde{M} &= \frac{Eh^3}{24(1+\nu)}K_{z\theta}
\end{aligned}
\qquad \text{(I-b-27)}
$$

To obtain relationships for $N_{z\theta}$, $M_{z\theta}$ and $M_{\theta z}$ instead of those for $\tilde{N}$ and $\tilde{M}$, some further manipulation is necessary. However, the evaluation of these resultants is needed only for the determination of the transverse shearing forces which are of no practical interest in thin shells.

I-b-6. Equations of motion

The force and moment resultants acting upon an infinitesimal shell element have to satisfy six conditions of equilibrium. The equations of equilibrium are well-known and generally acceptable and can be stated as follows:

$$\left.\begin{aligned}
&\frac{\partial N_z}{\partial z} + \frac{1}{R}\frac{\partial N_{\theta z}}{\partial \theta} + P_z = 0 \\
&\frac{\partial N_{z\theta}}{\partial z} + \frac{1}{R}\frac{\partial N_\theta}{\partial \theta} + \frac{1}{R}Q_\theta + P_\theta = 0 \\
&\frac{\partial Q_z}{\partial z} + \frac{1}{R}\frac{\partial Q_\theta}{\partial \theta} - \frac{1}{R}N_\theta + P_r = 0 \\
&\frac{\partial M_z}{\partial z} + \frac{1}{R}\frac{\partial M_{\theta z}}{\partial \theta} - Q_z = 0 \\
&\frac{\partial M_{z\theta}}{\partial z} + \frac{1}{R}\frac{\partial M_\theta}{\partial \theta} - Q_\theta = 0 \\
&N_{z\theta} - N_{\theta z} - \frac{1}{R}M_{\theta z} = 0
\end{aligned}\right\} \qquad \text{(I-b-28)}$$

It should be noted that the sixth equilibrium equation is identically satisfied. Eliminating Q_z and Q_θ from the remaining five equations of equilibrium gives

$$\left.\begin{aligned}
&\frac{\partial N_z}{\partial z} + \frac{1}{R}\frac{\partial \tilde{N}}{\partial \theta} + P_z = 0 \\
&\frac{\partial \tilde{N}}{\partial z} + \frac{2}{R}\frac{\partial \tilde{M}}{\partial z} + \frac{1}{R}\frac{\partial N_\theta}{\partial \theta} + \frac{1}{R^2}\frac{\partial M_\theta}{\partial \theta} + P_\theta = 0 \\
&\frac{\partial^2 M_z}{\partial z^2} + \frac{2}{R}\frac{\partial^2 \tilde{M}}{\partial z \partial \theta} + \frac{1}{R^2}\frac{\partial^2 M_\theta}{\partial \theta^2} - \frac{1}{R}N_\theta + P_r = 0
\end{aligned}\right\} \qquad \text{(I-b-29)}$$

The force and moment resultant expressions (Eqs. I-b-27) are then substituted into the equilibrium equations, giving them in terms of the generalized strains. Finally, the strain-displacement equations

(Eqs. I-b-8) are substituted, yielding three differential equations of motion having u, v, and w as dependent variables and z, θ, and t (time) as independent variables.

This set of differential equations is of the eighth order. Time enters the equations of motion through inertial terms by replacing P_z, P_θ, and P_r by $F_z - \rho_s h \frac{\partial^2 u}{\partial t^2}$, $F_\theta - \rho_s h \frac{\partial^2 v}{\partial t^2}$, and $F_r - \rho_s h \frac{\partial^2 w}{\partial t^2}$

where ρ_s is the mass density per unit volume; and F_z, F_θ, and F_r represent the applied forces per unit area of the middle surface in the z, θ, and normal directions, respectively. The equations of motion can be written in a matrix form as

$$[L]\{d\} = \frac{1-\nu^2}{Eh}\{F\} \qquad \text{(I-b-30)}$$

where

$\{d\} = \begin{Bmatrix} u \\ v \\ w \end{Bmatrix}$ is the displacement vector,

$F = \begin{Bmatrix} -F_z \\ -F_\theta \\ F_r \end{Bmatrix}$ is the applied force vector,

and $[L]$ is a linear differential operator given by Eq. I-b-31 in which

$$\alpha = \frac{h^2}{12R^2}, \quad \Delta^4 = \Delta^2\Delta^2 \text{ and } \Delta^2 = \frac{\partial^2}{\partial z^2} + \frac{1}{R^2}\frac{\partial^2}{\partial \theta^2}.$$

$$[L] = \begin{bmatrix} \frac{\partial^2}{\partial z^2} + \frac{(1-\nu)}{2R^2}\frac{\partial^2}{\partial \theta^2} - \frac{\rho_s(1-\nu^2)}{E}\frac{\partial^2}{\partial t^2} & \frac{(1+\nu)}{2R}\frac{\partial^2}{\partial z \partial \theta} & \frac{\nu}{R}\frac{\partial}{\partial z} \\ \frac{(1+\nu)}{2}\frac{\partial^2}{\partial z \partial \theta} & \frac{1-\nu}{2}\frac{\partial^2}{\partial z^2} + \frac{1}{R^2}\frac{\partial^2}{\partial \theta^2} - \frac{\rho_s(1-\nu^2)}{E}\frac{\partial^2}{\partial t^2} & \frac{1}{R^2}\frac{\partial}{\partial \theta} \\ & + \alpha\left[2(1-\nu)\frac{\partial^2}{\partial z^2} + \frac{1}{R^2}\frac{\partial^2}{\partial \theta^2}\right] & + \alpha\left[-(2-\nu)\frac{\partial^3}{\partial^2 z \partial \theta} - \frac{1}{R^2}\frac{\partial^3}{\partial \theta^3}\right] \\ \frac{\nu}{R}\frac{\partial}{\partial z} & \frac{1}{R^2}\frac{\partial}{\partial \theta} & \frac{1}{R^2} + \alpha R^2 \Delta^4 + \frac{\rho_s(1-\nu^2)}{E}\frac{\partial^2}{\partial t^2} \\ & + \left[-(2-\nu)\frac{\partial^3}{\partial z^2 \partial \theta} - \frac{1}{R^2}\frac{\partial^3}{\partial \theta^3}\right] & \end{bmatrix} \quad \text{(I-b-31)}$$

Appendix I-c

Solutions of The Laplace Equation

The solution $\phi(r,\theta,z,t)$ of the Laplace equation, $\nabla^2\phi = 0$, can be obtained by the method of separation of variables. Thus, the solution is sought in the form

$$\phi(r,\theta,z,t) = \hat{R}(r)\cdot\hat{\Theta}(\theta)\cdot\hat{Z}(z)\cdot\hat{T}(t) \qquad \text{(I-c-1)}$$

Substituting Eq. I-c-1 into the governing differential equation gives

$$\frac{r}{\hat{R}}\frac{d}{dr}\left(r\frac{d\hat{R}}{dr}\right) + \frac{1}{\hat{\Theta}}\frac{d^2\hat{\Theta}}{d\theta^2} + \frac{r^2}{\hat{Z}}\frac{d^2\hat{Z}}{dz^2} = 0 \qquad \text{(I-c-2)}$$

Following the usual argument of separation of variables, it is observed that the second term in Eq. I-c-2 contains all the θ dependence and is a function of θ only; it must therefore equal a constant. This constant will be chosen to be $-n^2$, where n is an integer. The significance of the minus sign is that trigonometric rather than exponential θ dependence will result, and the significance of n's being integers is that $\phi(\theta) = \phi(\theta + 2\pi)$, as is required. The solution for $\hat{\Theta}(\theta)$ is then

$$\hat{\Theta}_n(\theta) = A_{1n}\sin(n\theta) + A_{2n}\cos(n\theta) \qquad \text{(I-c-3)}$$

The remaining differential equation, after dividing by r^2, is

$$\frac{1}{r\hat{R}}\frac{d}{dr}\left(r\frac{d\hat{R}}{dr}\right) - \frac{n^2}{r^2} + \frac{1}{\hat{Z}}\frac{d^2\hat{Z}}{dz^2} = 0 \qquad \text{(I-c-4)}$$

Again, the separation-of-variables argument requires that the last term in Eq. I-c-4 be equal to a constant; it may be positive, zero,

or negative. If the separation constant is chosen to be positive, say k^2, then

$$\frac{d^2\hat{Z}}{dz^2} - k^2 \hat{Z} = 0 \qquad \text{(I-c-5)}$$

and

$$r \frac{d}{dr}\left(r \frac{d\hat{R}}{dr}\right) + (k^2r^2 - n^2) \hat{R} = 0 \qquad \text{(I-c-6)}$$

The solution $\hat{Z}(z)$ is

$$\hat{Z}(z) = B_1 \cosh(kz) + B_2 \sinh(kz) \qquad \text{(I-c-7)}$$

In addition, Eq. I-c-6 is Bessel's equation of order n whose solution is given by

$$\hat{R}(r) = C_{1n} J_n(kr) + C_{2n} Y_n(kr) \qquad \text{(I-c-8)}$$

where $J_n(kr)$ and $Y_n(kr)$ are the Bessel functions of the first kind and of the second kind, respectively. Since $Y_n(kr)$ is singular for $r = 0$, the coefficients C_{2n} must be zero, i.e., the radial dependence of the velocity potential will be proportional to $J_n(kr)$.

The separation constant may be also negative $(-k^2)$; in this case, the differential equations become

$$\frac{d^2\hat{Z}}{dz^2} + k^2 \hat{Z} = 0 \qquad \text{(I-c-9)}$$

and

$$r \frac{d}{dr}\left(r \frac{d\hat{R}}{dr}\right) - (k^2r^2 + n^2) \hat{R} = 0 \qquad \text{(I-c-10)}$$

Therefore, the solutions $\hat{Z}(z)$ and $\hat{R}(r)$ are given by

$$\hat{Z}(z) = B_1 \cos(kz) + B_2 \sin(kz) \qquad \text{(I-c-11)}$$

$$\hat{R}(r) = C_{1n} I_n(kr) + C_{2n} K_n(kr) \qquad \text{(I-c-12)}$$

where $I_n(kr)$ and $K_n(kr)$ are the modified Bessel functions of the first kind and of the second kind, respectively. Again, the functions $K_n(kr)$ will be discarded because they are singular at $r = 0$.

If the separation constant is chosen to be zero, then the solutions $\hat{Z}(z)$ and $\hat{R}(r)$ become

$$\hat{Z}(z) = B_1 z + B_2 \qquad \text{(I-c-13)}$$

$$\hat{R}(r) = C_{1n} r^n + C_{2n} r^{-n} \qquad \text{(I-c-14)}$$

where C_{2n} must be equal to zero to avoid the singularity at $r = 0$.

To summarize, any solution of the Laplace equation, which is non-singular at $r = 0$, can be given by

$$\phi(r,\theta,z,t) = \hat{T}_n(t) \times \begin{matrix}\cos(n\theta) \\ \sin(n\theta)\end{matrix} \times \begin{cases} J_n(kr)\cosh(kz) \\ J_n(kr)\sinh(kz) \\ r^n z \\ r^n \qquad (n \geq 1) \\ I_n(kr)\cos(kz) \\ I_n(kr)\sin(kz) \end{cases} \qquad \text{(I-c-15)}$$

REFERENCES OF CHAPTER I

1. Currie, I.G., Fundamental Mechanics of Fluids, McGraw-Hill Book Company, 1974.

2. Lamb, H., Hydrodynamics, Cambridge University Press, 1932.

3. Hsiung, H.H., and Weingarten, V.I., "Dynamic Analysis of Hydroelastic Systems Using the Finite Element Method," Department of Civil Engineering, University of Southern California, Report USCCE 013, November 1973.

4. Luke, J.C., "A Variational Principle for a Liquid With Free Surface," J. Fluid Mech., Vol. 27, 1967, pp. 395-397.

5. Bateman, H., Partial Differential Equations, Cambridge University Press, 1944.

6. Leissa, A.W., ed., "Vibration of Shells," NASA SP-288, National Aeronautics and Space Administration, Washington, D.C., 1973.

7. Novozhilov, V.V., Thin Shell Theory, P. Noordhoff LTD., Groningen, The Netherlands, 1964.

8. Gol'denveizer, A.L., Theory of Elastic Thin Shells, Pergamon Press (New York), 1961.

9. Washizu, K., Variational Methods in Elasticity and Plasticity, Pergamon Press, 1975.

10. Zienkiewicz, O.C., The Finite Element Method, McGraw-Hill Book Company, Third Edition, 1977.

11. Huebner, K.H., The Finite Element Method for Engineers, John Wiley & Sons, 1975.

12. Shaaban, S.H., and Nash, W.A., "Finite Element Analysis of a Seismically Excited Cylindrical Storage Tank, Ground Supported, and Partially Filled with Liquid," University of Massachusetts Report to National Science Foundation, August 1975.

13. Balendra, T., and Nash, W.A., "Earthquake Analysis of a Cylindrical Liquid Storage Tank with a Dome by Finite Element Method, "Department of Civil Engineering, University of Massachusetts, Amherst, Massachusetts, May 1978.

14. Shaaban, S.H., and Nash, W.A., "Response of an Empty Cylindrical Ground Supported Liquid Storage Tank to Base Excitation," University of Massachusetts Report to National Science Foundation, August 1975.

15. Edwards, N.W., "A Procedure for Dynamic Analysis of Thin Walled Cylindrical Liquid Storage Tanks Subjected to Lateral Ground Motions," Ph.D. Thesis, University of Michigan, Ann Arbor, Michigan, 1969.

16. Yang, J.Y., "Dynamic Behavior of Fluid-Tank Systems," Ph.D. Thesis, Rice University, Houston, Texas, 1976.

17. Wu, C.I., Mouzakis, T., Nash, W.A., and Colonell, J.M., "Natural Frequencies of Cylindrical Liquid Storage Containers," Department of Civil Engineering, University of Massachusetts, June 1975.

CHAPTER II

COMPLICATING EFFECTS IN THE FREE LATERAL VIBRATION PROBLEM OF LIQUID STORAGE TANKS

A method of analyzing the free lateral vibration of liquid storage tanks has been developed in the preceding chapter; it is based on both the finite element procedure and the boundary solution technique. This method provides a starting point for the consideration of complicating effects upon liquid storage tanks such as the effect of the initial hoop stress due to the hydrostatic pressure, the effect of the coupling between liquid sloshing and shell vibration, the effect of the soil flexibility, and the effect of the roof rigidity.

The first topic, presented in Sec. II-1, is concerned with the initial hoop stress and its influence upon the $\cos n\theta$-type modes of vibration of the tank wall. Most analyses developed so far have considered only the $\cos\theta$-type modes, and assumed that the only stresses present in the shell are those arising from the vibratory motion. This is a valid assumption because this type of mode is insensitive to the existence of the initial hoop stress. However, those analyses which have been made to compute the frequencies and shapes of the $\cos n\theta$-type modes have also neglected the stiffening effect of the initial hoop tension; this may introduce a considerable error, especially in the values of the natural frequencies. In the following analysis, the nonlinear strain-displacement relationships are employed to formulate the added stiffness matrix. The free vibration eigenproblem is then treated in the same manner as in Chapter I.

The second section is devoted to examining the effect of the coupling between liquid sloshing and shell vibration. Although many studies have dealt with the vibration of the liquid-shell system (as shown in Chapter I), little can be found in the literature about the coupling effect. A common assumption has been to neglect this coupling, partly due to the algebraic complexity associated with its consideration, and partly due to the fact that the significant liquid sloshing modes and the shell vibrational modes have well-separated frequency ranges.

The problem of the dynamic interaction between liquid storage tanks and the soil during earthquakes has, so far, not been studied. Because the foundation could influence the seismic response in an important way, an investigation of the soil-tank interaction was made. The significance of such interaction for the response of both rigid and flexible tanks is discussed briefly in the third section, and a quantitative study regarding the interaction of these tanks with the foundation will be presented in a separate report.

The influence of the roof rigidity on the modes of vibration has been also investigated. A simple roof model has been considered in this study which offers a direct insight into a complicated interaction problem. It shows that the roof has an important effect on the $\cos n\theta$-type modes of vibration; this result has been confirmed experimentally.

It is evident that each of the previously discussed factors affects, more or less, the dynamic behavior of tanks; it was therefore important to develop methods capable of dealing with such complications.

II-1. The Effect of the Initial Hoop Stress

In the preceding chapter it was assumed that the only stresses present in the shell are those arising from the vibratory motion. However, tank walls are subjected to hydrostatic pressures which cause hoop tensions. The presence of such stresses affects the vibrational characteristics of the shell, especially the cosnθ-type modes.

To incorporate these effects, it is necessary to modify the strain energy expression of the shell, and to generalize accordingly the equations of motion. Upon using the finite element model, the matrix equation of motion can be easily derived, and it takes the familiar form with an added stiffness matrix due to the presence of the initial stress field.

II-1-1. Modification of the Potential Energy of the Shell

Consider a circular cylindrical shell acted upon by a static initial stress field σ_z^i, σ_θ^i, and $\sigma_{z\theta}^i$ which is in equilibrium. The initial stresses in the shell result from the hydrostatic pressure. During vibrations, the shell stresses consist of the initial stresses plus the additional vibratory stresses σ_z, σ_θ and $\sigma_{z\theta}$. In the subsequent analysis, the bending stresses produced by the initial loading are neglected, i.e., only the initial membrane stresses are considered; this is equivalent to assuming that the bottom of the tank wall has a free end condition instead of a built-in condition.

Since the initial stress state is in equilibrium, the potential energy of the system in this state may be taken as the reference level. Thus, the internal strain energy of the shell can be written as

$$U(t) = \frac{1}{2}\int_0^L\int_0^{2\pi}\int_{-\frac{h}{2}}^{\frac{h}{2}}\left(\sigma_z e_z + \sigma_\theta e_\theta + \sigma_{z\theta}\,\gamma_{z\theta}\right)R\left(1+\frac{x}{R}\right)dx\,d\theta\,dz$$

$$+\int_0^H\int_0^{2\pi}\int_{-\frac{h}{2}}^{\frac{h}{2}}\left(\sigma_\theta^i\, e_\theta\right)R\left(1+\frac{x}{R}\right)dx\,d\theta\,dz \qquad (2.1)$$

in which the initial stresses σ_z^i and $\sigma_{z\theta}^i$ are taken to be zero. The vibratory strains e_z, e_θ, and $\gamma_{z\theta}$, and the vibratory stresses σ_z, σ_θ, and $\sigma_{z\theta}$, are related by Hooke's law as indicated by Eq. I-b-11. The stain-displacement relationships are then substituted into Eq. 2.1. However, because the initial hoop stress may be large, it is necessary to use the second-order, nonlinear strain-displacement equation in the second integral of Eq. 2.1 while using only the linear relationships in the first integral [1]. This maintains the proper homogeneity in the orders of magnitude of the terms in the integrands.

The strain energy expression (Eq. 2.1) can be written conveniently as

$$U(t) = U_1(t) + U_2(t) \qquad (2.2)$$

where $U_1(t)$ is defined by Eq. 1.33, and $U_2(t)$ is given by

$$U_2(t) = \int_0^H \int_0^{2\pi} \left(N_\theta^i \varepsilon_\theta\right) R \, d\theta \, dz \tag{2.3}$$

where N_θ^i is the initial membrane force resultant in the circumferential direction, and ε_θ is the midsurface strain which can be expressed as

$$\varepsilon_\theta = \frac{1}{R}\left(\frac{\partial v}{\partial \theta} + w\right) + \frac{1}{2}\left\{\left(\frac{1}{R}\frac{\partial u}{\partial \theta}\right)^2 + \left[\frac{1}{R}\left(\frac{\partial v}{\partial \theta} + w\right)\right]^2 + \left[\frac{1}{R}\left(v - \frac{\partial w}{\partial \theta}\right)\right]^2\right\} \tag{2.4}$$

The nonlinear terms in Eq. 2.4 are given by Washizu [2]. However, it should be mentioned that the linear terms of the strain-displacement relationships developed by Washizu are identical to those of Novozhilov theory [3] which has been used in the preceding chapter.

The initial force resultant N_θ^i and the liquid hydrostatic pressure p_s (Eq. 1.9) are in equilibrium, and therefore, satisfy Eq. (I-b-29); i.e.,

$$N_\theta^i = \rho_\ell \, g \, R.(H-z), \quad \text{and} \quad \frac{\partial N_\theta^i}{\partial \theta} = 0 \tag{2.5}$$

II-1-2. Derivation of the Modified Equations of Motion of the Shell

The modified equations of motion of the shell can be derived following the same procedure outlined in section I-3-3. Applying Hamilton's Principle, taking the necessary variations with respect to the displacement components u, v, and w, and employing Eq. 2.5, lead to the desired equations of motion. In this case, the differential operator matrix is generalized from Eq. 1.56 to the form

$$[L^*]\{d\} = \frac{1-\nu^2}{Eh}\{F\} \qquad (0 < z < H) \tag{2.6}$$

where $[L^*] = [L] + [L^i]$; $[L]$ is the differential operator defined by Eq. 1.46, and $[L^i]$ is a differential operator containing the additional terms which account for the initial hoop stress; it is given by

$$\left[L^i\right] = \frac{1-\nu^2}{Eh} \begin{bmatrix} N_\theta^i \frac{\partial^2}{\partial\theta^2} & 0 & 0 \\ 0 & N_\theta^i\left(\frac{\partial^2}{\partial\theta^2} - 1\right) & 2\, N_\theta^i \frac{\partial}{\partial\theta} \\ 0 & 2\, N_\theta^i \frac{\partial}{\partial\theta} & N_\theta^i\left(1 - \frac{\partial^2}{\partial\theta^2}\right) \end{bmatrix} \tag{2.7}$$

It should be noted that the force vector {F} in Eq. 2.6 does not include the hydrostatic pressure.

II-1-3. Evaluation of the Added Stiffness Matrix

The potential energy of the shell has been modified to account for the initial hoop stress, and the additional strain energy $U_2(t)$ is given by Eq. 2.3. Since N_θ^i is not a function of θ, the strain energy expression $U_2(t)$ can be rewritten as

$$U_2(t) = R \int_0^H \left\{ N_\theta^i \left(\int_0^{2\pi} \varepsilon_\theta \, d\theta \right) \right\} dz \tag{2.8}$$

The strain-displacement relation (Eq. 2.4) is then inserted into the strain energy expression (Eq. 2.8). However, the linear terms of Eq. 2.4 do not contribute to $U_2(t)$ since

$$\int_0^{2\pi} \cos(n\theta) d\theta = 0 \qquad (n \geq 1)$$

Furthermore, the nonlinear terms can be expressed more conveniently in the following matrix form:

$$\varepsilon_{\theta}^{n\ell} = \frac{1}{2}\left(\left[\bar{P}\right]\{d\}\right)^{T}\left(\left[\bar{P}\right]\{d\}\right) \tag{2.9}$$

where $\{d\}$ is the displacement vector (Eq. 1.31); $\left[\bar{P}\right]$ is a differential operator matrix given by

$$\left[\bar{P}\right] = \frac{1}{R}\begin{bmatrix} \frac{\partial}{\partial\theta} & 0 & 0 \\ 0 & \frac{\partial}{\partial\theta} & 1 \\ 0 & 1 & -\frac{\partial}{\partial\theta} \end{bmatrix} \tag{2.10};$$

and the superscript $n\ell$ indicates "nonlinear".

With the aid of Eqs. 1.85 and 2.10, Eq. 2.9 can be expressed as

$$\varepsilon_{\theta}^{n\ell} = \frac{1}{2}\left(\left[\bar{P}\right]\left[\Theta_n\right]\{d_n\}\right)^{T}\left(\left[\bar{P}\right]\left[\Theta_n\right]\{d_n\}\right)$$

$$= \frac{1}{2}\{d_n\}^{T}\left[\bar{P}_n\right]^{T}\left[\bar{P}_n\right]\{d_n\} \tag{2.11}$$

where

$$\left[\bar{P}_n\right] = \left[\bar{P}\right]\left[\Theta_n\right] = \frac{1}{R}\begin{bmatrix} -n\sin(n\theta) & 0 & 0 \\ 0 & n\cos(n\theta) & \cos(n\theta) \\ 0 & \sin(n\theta) & n\sin(n\theta) \end{bmatrix} \tag{2.12}$$

Now, inserting Eq. 2.11 into the strain energy expression (Eq. 2.8), one obtains

$$U_2(t) = \frac{R}{2}\int_0^H \left\{ N_{\theta}^{i}\ \{d_n\}^{T}\left(\int_0^{2\pi}\left[\bar{P}_n\right]^{T}\left[\bar{P}_n\right]d\theta\right)\{d_n\}\right\} dz$$

$$= \frac{\pi}{2R}\int_0^H \left(N_{\theta}^{i}\ \{d_n\}^{T}\left[C_n\right]\{d_n\}\right) dz \tag{2.13}$$

where

$$\left[C_n\right] = \begin{bmatrix} n^2 & 0 & 0 \\ 0 & n^2+1 & 2n \\ 0 & 2n & n^2+1 \end{bmatrix} \tag{2.14}$$

Again, omitting the subscript n, and using the displacement model (Eq. 1.74), one can write

$$U_2(t) = \frac{1}{2} \sum_{e=1}^{NEH} \left\{\bar{d}\right\}_e^T \left[K_s^i\right]_e \left\{\bar{d}\right\}_e \tag{2.15}$$

where NEH is the number of shell elements in contact with liquid; $\left\{\bar{d}\right\}_e$ is the generalized nodal displacement vector (Eq. 1.78) of the element "e"; and $\left[K_s^i\right]_e$ is the element added stiffness matrix which is given by

$$\left[K_s^i\right]_e = \frac{\pi}{R} \int_0^{L_e} \left\{ N_\theta^i(\bar{z}) \left(\left[Q(\bar{z})\right]^T [C] \left[Q(\bar{z})\right] \right) \right\} d\bar{z} \tag{2.16}$$

The integration involved in the evaluation of $\left[K_s^i\right]_e$ is carried out approximately by assuming uniform hydrostatic pressure along each element; the resulting added stiffness matrix is given by

$$\left[K_s^i\right]_e = \frac{\pi \bar{N}_e}{R} \begin{bmatrix}
\frac{n^2 L_e}{3} & 0 & 0 & 0 & \frac{n^2 L_e}{6} & 0 & 0 & 0 \\
0 & \frac{(n^2+1)L_e}{3} & \frac{7nL_e}{10} & \frac{nL_e^2}{10} & 0 & \frac{(n^2+1)L_e}{6} & \frac{3nL_e}{10} & \frac{-nL_e^2}{15} \\
0 & \frac{7nL_e}{10} & \frac{78(n^2+1)L_e}{210} & \frac{11(n^2+1)L_e^2}{210} & 0 & \frac{3nL_e}{10} & \frac{54(n^2+1)L_e}{420} & \frac{-13(n^2+1)L_e^2}{420} \\
0 & \frac{nL_e^2}{10} & \frac{11(n^2+1)L_e^2}{210} & \frac{2(n^2+1)L_e^3}{210} & 0 & \frac{nL_e^2}{15} & \frac{13(n^2+1)L_e^2}{420} & \frac{-3(n^2+1)L_e^3}{420} \\
\frac{n^2 L_e}{6} & 0 & 0 & 0 & \frac{n^2 L_e}{3} & 0 & 0 & 0 \\
0 & \frac{(n^2+1)L_e}{6} & \frac{3nL_e}{10} & \frac{nL_e^2}{15} & 0 & \frac{(n^2+1)L_e}{3} & \frac{7nL_e}{10} & \frac{-nL_e^2}{10} \\
0 & \frac{3nL_e}{10} & \frac{54(n^2+1)L_e}{420} & \frac{13(n^2+1)L_e^2}{420} & 0 & \frac{7nL_e}{10} & \frac{78(n^2+1)L_e}{210} & \frac{-11(n^2+1)L_e^2}{210} \\
0 & \frac{-nL_e^2}{15} & \frac{-13(n^2+1)L_e^2}{420} & \frac{-3(n^2+1)L_e^3}{420} & 0 & \frac{-nL_e^2}{10} & \frac{-11(n^2+1)L_e^2}{210} & \frac{2(n^2+1)L_e^3}{210}
\end{bmatrix} \tag{2.17}$$

where $\bar{N}_e$ is the membrane force resultant N_θ^i evaluated at the centroid of the element "e".

Finally, let $$\left[K_s^i\right] = \sum_{e=1}^{NEH} \left[K_s^i\right]_e \tag{2.18}$$

where $\left[K_s^i\right]$ is the assemblage added stiffness matrix of the shell.

II-1-4. The Matrix Equations of Motion

The matrix equations of motion of the liquid-shell system take the familiar form

$$[M]\{\ddot{q}\} + [K]\{q\} = 0 \tag{2.19}$$

where $\{q\}$ is the assemblage nodal displacement vector (Eq. 1.82), $[M] = [M_s] + [DM]$; $[M_s]$ and $[DM]$ are the shell mass matrix (Eq. 1.106) and the added mass matrix (Eq. 1.146), respectively, and $[K] = [K_s] + [K_s^i]$; $[K_s]$ and $[K_s^i]$ are the shell stiffness matrix (Eq. 1.98) and the added stiffness matrix (Eq. 2.18), respectively.

The free vibration, eigenvalue problem can then be written as (refer to Sec. I-4-9)

$$\left(-\omega^2[M] + [K]\right)\{\overset{*}{q}\} = \{0\} \tag{2.20}$$

where $\{\overset{*}{q}\}$ is the vector of the displacement amplitudes of vibration (time independent), and ω is the natural circular frequency.

II-1-5. Illustrative Numerical Examples

The computer program "FREE VIBRATION (1)" is generalized by including a subroutine to compute the element added stiffness matrix (Eq. 2.17). The program is then employed to investigate the effect of the initial hoop tension on the $\cos\theta$-type modes of a broad tank (R = 60 ft, L = 40 ft,

and h = 1 inch) and a tall tank (R = 24 ft, L = 72 ft, and h = 0.43 inch). As expected, the influence of such a stress field on modes of this type is insignificant as indicated in Table II-1.

The analysis is also applied to compute the natural frequencies and mode shapes of the cosnθ-type deformations of these two tanks. The computed frequencies are presented in Table II-2, and the mode shapes are shown in Fig. II-1. The natural frequencies are also calculated without including the stiffening effect of the initial hoop tension; they are also shown in Table II-2 for comparison. Inspection of Fig. II-2-a shows that the stiffening effect due to the hydrostatic pressure has a significant influence upon the frequencies of vibration of tall tanks. On the other hand, Fig. II-2-b shows that such effect is, for practical purposes, negligible in broad tanks. It is also of interest to note that the influence of the initial stress upon the cosnθ-type modes becomes more significant as the circumferential wave number n increases.

To illustrate the effectiveness of the analysis under consideration, a comparison between the computed dynamic characteristics and those found experimentally in [4] is made. The physical model employed in [4] is partly filled with water, and has the following dimensions and properties:

$$R = 4 \text{ inches}, \quad L = 12.5 \text{ inches}, \quad H = 11 \text{ inches},$$

$$h = 0.0050 \text{ inch}, \quad E = 0.735 \times 10^{6} \text{ lb/in}^{2},$$

$$\rho_s = 0.133 \times 10^{-3} \text{ lb.sec}^{2}/\text{in}^{4}, \text{ and } \nu = 0.3.$$

As seen from Table II-3 and from Fig. II-3, the computed characteristics

are in good agreement with the experimental results. This confirms the accuracy of the analysis, and the significant role played by the initial hoop tension during the vibration of tall tanks.

TABLE II-1

NATURAL FREQUENCIES OF THE COSθ-TYPE MODES (f_{m1} cps)

Tank	Initial Stress Excluded		Initial Stress Included	
	m = 1	m = 2	m = 1	m = 2
Broad	6.1841	11.276	6.1853	11.279
Tall	3.5586	10.450	3.5593	10.452

TABLE II-2

NATURAL FREQUENCIES OF THE COSnθ-TYPE MODES (f_{mn} cps)

Tank	Initial Stress	m \ n	2	3	4	5	6
Broad	Excluded	1	5.19	4.14	3.31	2.69	2.21
	Included		5.19	4.15	3.35	2.76	2.36
	Excluded	2	10.6	9.98	9.22	8.32	7.43
	Included		10.6	9.99	9.25	8.37	7.52
Tall	Excluded	1	1.65	0.95	0.65	0.55	0.60
	Included		1.69	1.21	1.31	1.62	1.98
	Excluded	2	6.66	4.52	3.28	2.52	2.05
	Included		6.68	4.64	3.68	3.44	3.68

TABLE II-3

NATURAL FREQUENCIES OF THE COSnθ-TYPE MODES (f_{1n} cps)
(Comparison of Theoretical and Experimental Values)

	n = 3	n = 4	n = 5	n = 6	n = 7	n = 8
Initial Stress Excluded	11.85	8.06	6.57	6.77	8.28	10.60
Initial Stress Included	13.42	12.63	14.82	18.15	22.01	26.46
Model Test [4]	-	-	14.50	18.10	21.60	25.90

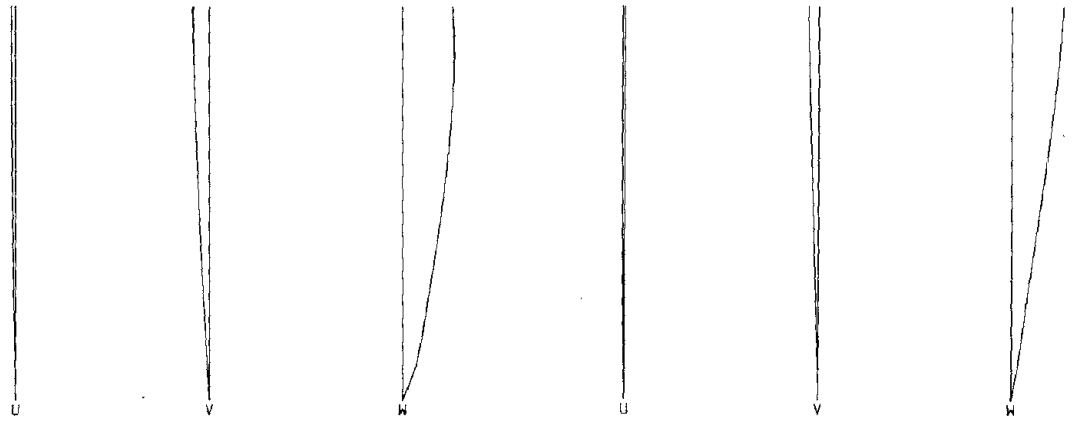

(a) Broad Tank

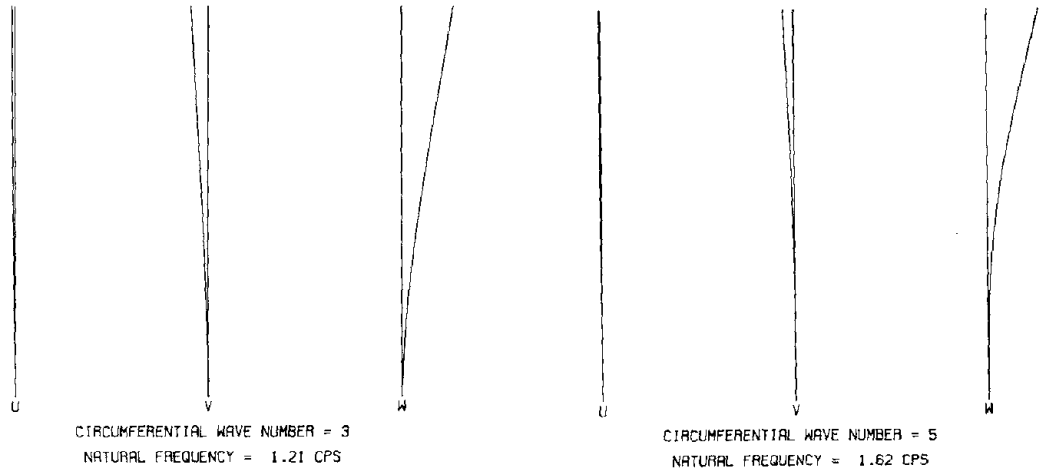

(b) Tall Tank

Fig. II-1. Vertical Mode Shapes of the Cosnθ-type Modes of Full Tanks

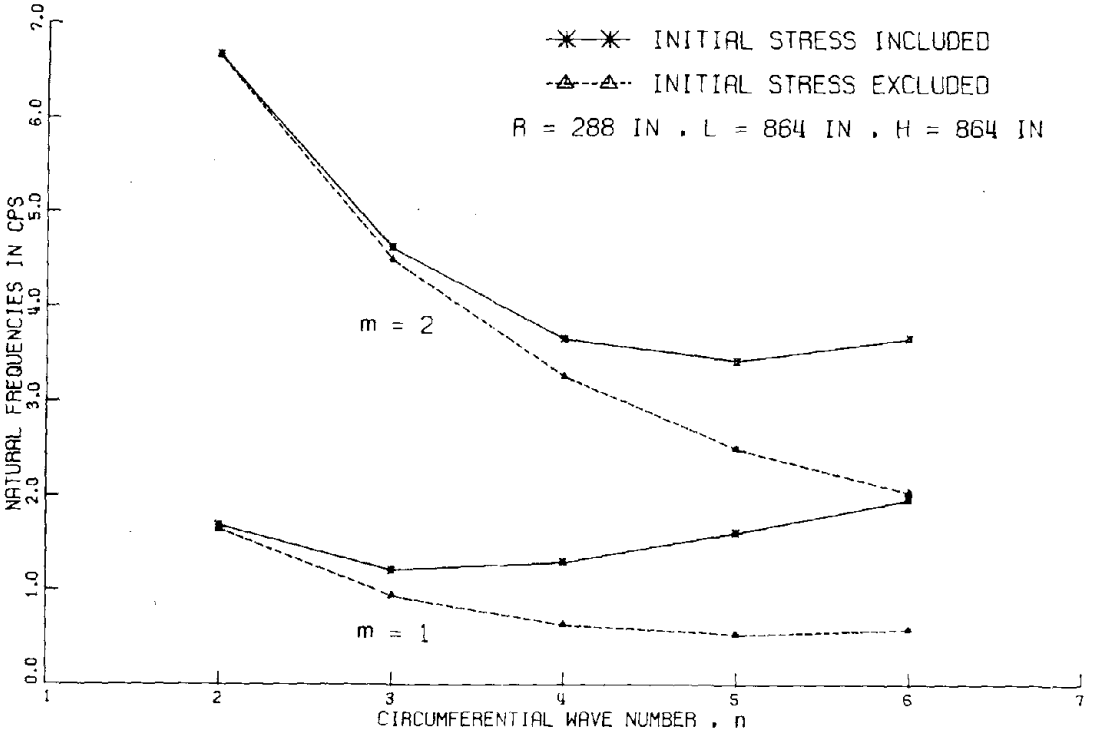

(a) Tall Tank

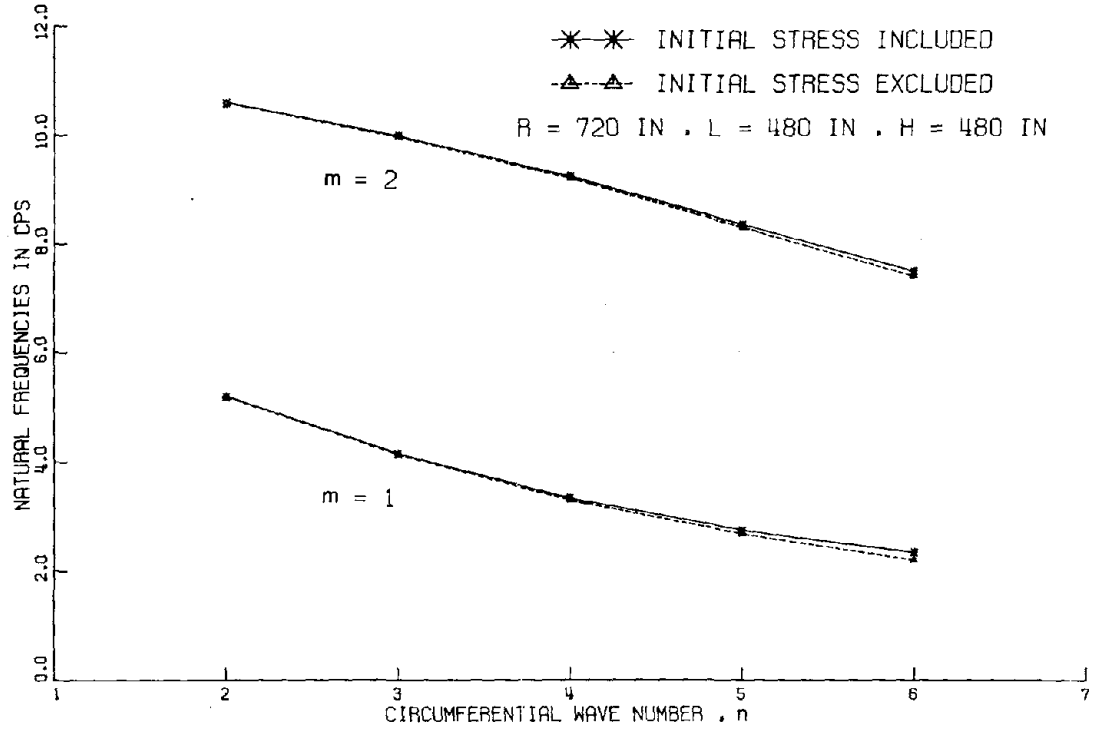

(b) Broad Tank

Fig. II-2. Effect of the Initial Hoop Tension Upon the Natural Frequencies of the Cosnθ-type Modes.

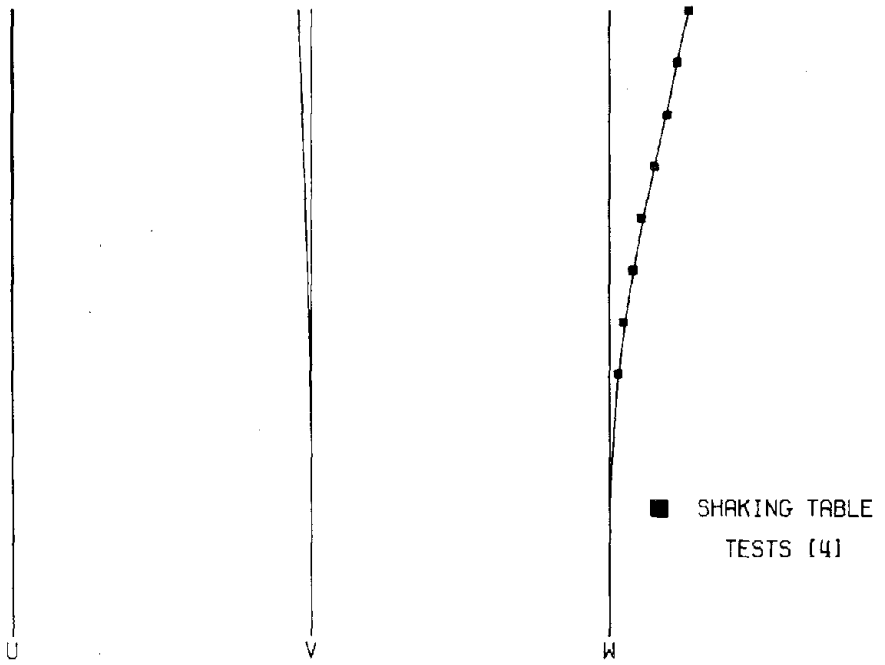

CIRCUMFERENTIAL WAVE NUMBER = 6

NATURAL FREQUENCY = 18.15 CPS

(a) Mode Shape

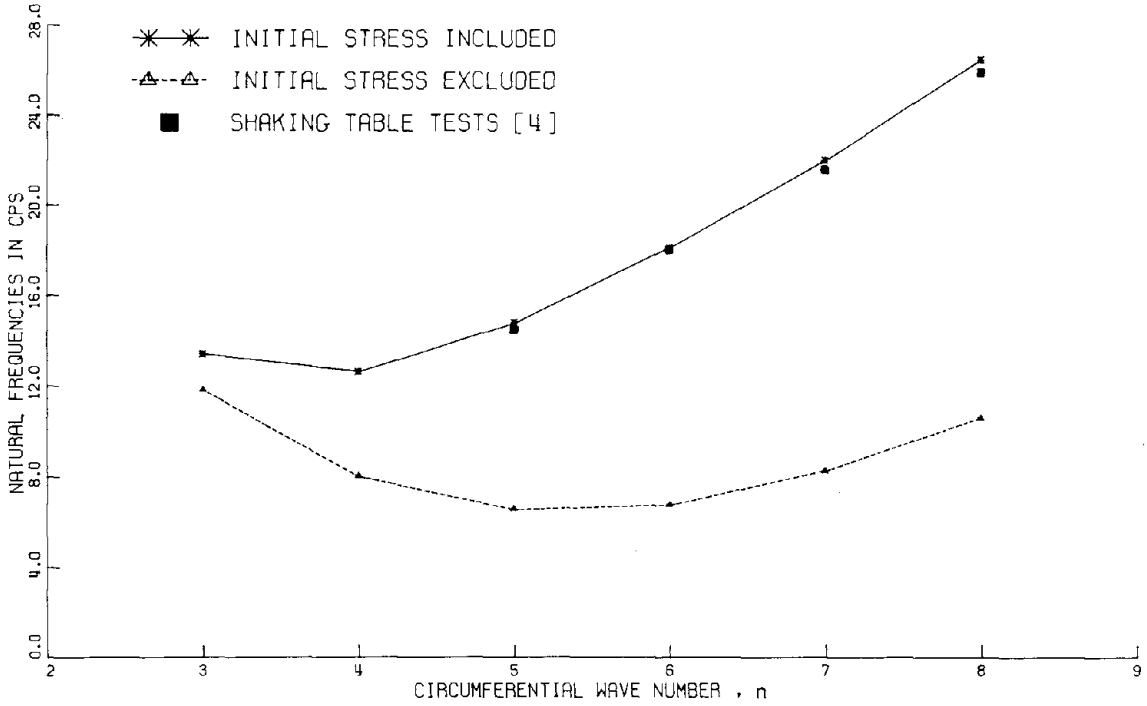

(b) Natural Frequencies

Fig. II-3. Comparison Between Calculated and Measured Characteristics of the Cosnθ-type Modes.

II-2. The Effect of the Coupling between Liquid Sloshing and Shell Vibration

Although the behavior of the coupled liquid-shell system has been regarded as important and considerable theoretical work has been done on this problem [5,6,7,8,9], the dynamic interaction between sloshing waves and shell vibrations has not been yet investigated. The coupling is usually neglected on the ground that the significant sloshing modes are of much lower natural frequencies than those of the vibrating shell.

In the following section, emphasis is placed on the question of whether or not the coupling effect can be significant; in other words, is it necessary to consider the liquid-shell-surface wave system, or only the two uncoupled cases: (i) the liquid-shell system (refer to chapter I) plus (ii) the free surface gravity waves in a similar rigid tank?

II-2-1. Basic Approach

Two different finite element formulations can be employed to analyze the free vibration of the coupled liquid-shell-surface wave system.

In the approach adopted in this investigation, a finite element discretization of the liquid region itself is not necessary. Instead, a series representation of the liquid velocity potential is obtained by proper specification of the velocities at and normal to the liquid boundaries. The elastic shell is modelled by a series of ring-shaped finite elements and the quiescent liquid free surface is represented by concentric annular rings which may be regarded as "free surface elements"

restrained in the normal direction by springs. The formulation of the system matrices is straightforward and leads directly to the matrix equations of motion. This approach is equivalent to employing the functional $J(u,v,w,\phi,\xi)$ defined by Eq. 1.61, and utilizing the boundary solution technique as explained in chapter I.

The second approach to the finite element solution of the problem is based on the variational functional $I(\phi)$ (Eq. 1.12) to establish the liquid matrix equations of motion. The liquid region is discretized into annular elements of rectangular cross-section. The resulting matrix equations of motion of the liquid are then combined with the matrix equations of motion of the elastic shell. However, it was pointed out by previous investigators [5,6,7] that the extraction of the eigenvalues and eigenvectors of the free vibration problem is extremely difficult because these large size matrices are "nonsymmetric". Consequently, they neglected the free surface gravity waves and considered only the liquid-shell system. A careful study of these matrices revealed that their size can be drastically reduced if partitioned to eliminate all the liquid degrees of freedom except those of the free surface. Appropriate algebraic manipulations of this system of matrices lead to the same "symmetric" matrix equations of motion derived by the first approach.

In the following subsections, the basic equations that govern the system behavior are introduced, the matrices involved in the analysis are developed, and the overall free vibration eigenproblem is formulated.

II-2-2. The Governing Equations

It has been shown that the solutions (Eq. 1.66) of the Laplace equation (Eq. 1.1) which are nonsingular at r = 0, and have vanishing derivative with respect to z at z = 0, can be written as

$$\phi(r,\theta,z,t) = \hat{T}_n(t) \cos(n\theta) \begin{cases} J_n(kr)\cosh(kz) \\ r^n \qquad\qquad , (n \geq 1) \\ I_n(kr)\cos(kz) \end{cases} \quad (2.21)$$

The solutions given by Eq. 2.21 should be superimposed to satisfy the boundary conditions at the liquid-shell interface, and at the liquid free surface.

Without affecting the generality of the solution, the potential function $\phi(r,\theta,z,t)$ can be expressed as

$$\phi(r,\theta,z,t) = \sum_{n=1}^{\infty} \left\{ A_{0n}(t)\left(\frac{r}{R}\right)^n + \sum_{i=1}^{\infty} \left[A_{in}(t)\, I_n\left(\frac{\lambda_i r}{H}\right)\cos\left(\frac{\lambda_i z}{H}\right)\right] \right.$$

$$\left. + \sum_{j=1}^{\infty} \left[B_{jn}(t)\, J_n\left(\frac{\varepsilon_{jn} r}{R}\right)\cosh\left(\frac{\varepsilon_{jn} z}{R}\right)\right] \right\} \cos(n\theta) \quad (2.22)$$

where $\lambda_i = i\pi$ $(i = 1,2,\ldots)$; and ε_{jn} are the zeros of the first derivative of Bessel functions J_n, i.e., $'J_n(\varepsilon_{jn}) = 0$ $(j = 1,2,\ldots)$.

The arbitrary functions $A_{0n}(t)$, $A_{in}(t)$, and $B_{jn}(t)$ can be determined by satisfying the boundary conditions (Eqs. 1.3 and 1.5) at r = R and z = H, respectively.

Thus, along the wetted elastic wall of the tank, we have

$$\sum_{n=1}^{\infty} \left\{ \frac{n}{R} A_{0n}(t) + \sum_{i=1}^{\infty} \left[\left(\frac{\lambda_i}{H} \right) A_{in}(t) \acute{I}_n \left(\frac{\lambda_i R}{H} \right) \cos \left(\frac{\lambda_i z}{H} \right) \right] \right\} \cos(n\theta)$$

$$= \sum_{n=1}^{\infty} \dot{w}_n(z,t) \cos(n\theta) \qquad (2.23)$$

in which the shell radial velocity has been expanded in a Fourier series in the circumferential direction. For each circumferential wave number n, Eq. 2.23 uncouples and can be written as

$$\frac{n}{R} A_{0n}(t) + \sum_{i=1}^{\infty} \left[\left(\frac{\lambda_i}{H} \right) A_{in}(t) \acute{I}_n \left(\frac{\lambda_i R}{H} \right) \cos \left(\frac{\lambda_i z}{H} \right) \right] = \dot{w}_n(z,t) \qquad (2.24)$$

Multiply Eq. 2.24 by $\cos\left(\frac{\lambda_s z}{H}\right)$ where s = 0,1,2,..., integrate from 0 to H, and note that

$$\int_0^H \left[\cos \left(\frac{\lambda_i z}{H} \right) \cos \left(\frac{\lambda_s z}{H} \right) \right] dz = \begin{cases} 0 & i \neq s \\ H & i = s = 0 \\ \frac{H}{2} & i = s \ (s \geq 1) \end{cases},$$

then the functions $A_{0n}(t)$ and $A_{in}(t)$ can be expressed in terms of $\dot{w}_n$ as follows:

$$A_{0n}(t) = \frac{R}{nH} \int_0^H \dot{w}_n(z,t) \, dz$$

$$A_{in}(t) = \frac{2}{\lambda_i \acute{I}_n \left(\frac{\lambda_i R}{H} \right)} \int_0^H \dot{w}_n(z,t) \cos \left(\frac{\lambda_i z}{H} \right) dz ; (i = 1,2,..) \qquad (2.25)$$

The linearized free surface condition (Eq. 1.5) implies that

$$\sum_{n=1}^{\infty} \left\{ \sum_{j=1}^{\infty} \left[\left(\frac{\varepsilon_{jn}}{R} \right) B_{jn}(t) \ J_n \left(\frac{\varepsilon_{jn} r}{R} \right) \ \sinh \left(\frac{\varepsilon_{jn} H}{R} \right) \right] \right\} \cos(n\theta) = \dot{\xi}(r,\theta,t) \qquad (2.26)$$

If we write $\dot{\xi}(r,\theta,t) = \sum_{n=1}^{\infty} \dot{\xi}_n(r,t) \cos(n\theta)$, then, for each circumferential wave number n, Eq. 2.26 can be written as

$$\sum_{j=1}^{\infty} \left[\left(\frac{\varepsilon_{jn}}{R} \right) B_{jn}(t) \sinh \left(\frac{\varepsilon_{jn} H}{R} \right) J_n \left(\frac{\varepsilon_{jn} r}{R} \right) \right] = \dot{\xi}_n (r,t) \qquad (2.27)$$

The functions $B_{jn}(t)$ can be determined in terms of $\dot{\xi}_n$ by employing the orthogonality relations of Bessel functions, namely,

$$\int_0^R r \, J_n\left(\frac{\varepsilon_{jn} r}{R} \right) J_n \left(\frac{\varepsilon_{sn} r}{R} \right) dr = \begin{cases} 0 & j \neq s \\ \frac{R^2}{2} \left(1 - \frac{n^2}{\varepsilon_{jn}^2} \right) J_n^2(\varepsilon_{jn}) & j \neq s \end{cases} \qquad (2.28)$$

provided $J_n'(\varepsilon_{jn}) = J_n'(\varepsilon_{sn}) = 0$

After the appropriate algebraic manipulations of Eq. 2.27, the following expressions for $B_{jn}(t)$ result

$$B_{jn}(t) = \frac{2 \int_0^R r \, \dot{\xi}_n(r,t) \, J_n\left(\frac{\varepsilon_{jn} r}{R} \right) dr}{\varepsilon_{jn} R \sinh \left(\frac{\varepsilon_{jn} H}{R} \right) \left(1 - \frac{n^2}{\varepsilon_{jn}^2} \right) J_n^2(\varepsilon_{jn})} , \quad (j = 1,2,\ldots) \qquad (2.29)$$

The potential function $\phi(r,\theta,z,t)$, defined by Eqs. 2.22, 2.25, and 2.29, satisfies the Laplace equation (Eq. 1.1) and the boundary conditions (Eqs. 1.2, 1.3, and 1.5). The remaining boundary condition (Eq. 1.6) can be stated as follows:

$$\rho_\ell \sum_{n=1}^{\infty} \left\{ \dot{A}_{0n}(t)\left(\frac{r}{R}\right)^n + \sum_{i=1}^{\infty} \left[\dot{A}_{in}(t)\cos(\lambda_i) I_n\left(\frac{\lambda_i r}{H}\right)\right] + \sum_{j=1}^{\infty} \left[\dot{B}_{jn}(t) \cosh\left(\frac{\varepsilon_{jn} H}{R}\right) J_n\left(\frac{\varepsilon_{jn} r}{R}\right)\right] + g\, \xi_n(r,t) \right\} \cos(n\theta) = 0 \qquad (2.30)$$

$$(0 \le r \le R,\ 0 \le \theta \le 2\pi)$$

To analyze the overall problem, one has to consider the equations of motion of the circular cylindrical shell. These, including the effect of the initial hoop stress, can be written as (Eqs. 2.6 and 1.45)

$$[L^*]\{d\} = \frac{1-\nu^2}{Eh}\{F\} \quad (0 < z < H,\ 0 \le \theta \le 2\pi)$$

and (2.31)

$$[L]\{d\} = \{0\} \qquad (H < z < L,\ 0 \le \theta \le 2\pi)$$

where $\{d\}$ is the displacement vector; $[L^*]$ and $[L]$ are differential operators defined by Eqs. 2.7 and 1.46, respectively; and $\{F\}$ is the force vector given by

$$\{F\} = \begin{Bmatrix} 0 \\ 0 \\ p_d \end{Bmatrix} \qquad (2.32)$$

With the aid of the potential function expression (Eq. 2.22), the hydrodynamic pressure p_d, acting on the inner surface of the shell, can be given by

$$p_d(R,\theta,z,t) = -\rho_\ell \frac{\partial \phi}{\partial t}(R,\theta,z,t)$$

$$= -\rho_\ell \sum_{n=1}^{\infty} \left\{ \dot{A}_{0n}(t) + \sum_{i=1}^{\infty} \left[\dot{A}_{in}(t) I_n\left(\frac{\lambda_i R}{H}\right) \cos\left(\frac{\lambda_i z}{H}\right)\right] + \sum_{j=1}^{\infty} \left[\dot{B}_{jn}(t)\, J_n(\varepsilon_{jn}) \cosh\left(\frac{\varepsilon_{jn} z}{R}\right)\right] \right\} \cos(n\theta) \qquad (2.33)$$

$$(0 \le z \le H,\ 0 \le \theta \le 2\pi)$$

The solution to the vibration problem of the liquid-shell-surface wave system can now be obtained by satisfying the conditions of dynamic equilibrium (Eqs. 2.30 and 2.31) as well as the equations 2.25, 2.29 and 2.33.

II-2-3. The Governing Integral Equations

The governing integral equations of the coupled system will be derived by employing the principle of virtual displacements. This concept provides an integral expression which is equivalent to the equations of dynamic equilibrium, and is particularly convenient to formulate the finite element matrices.

Consider a system in dynamic equilibrium under the action of a set of forces, including inertia forces defined in accordance with d'Alembert's Principle. By introducing virtual displacements compatible with the system constraints, the total work done by these forces should be zero.

Introducing the virtual displacements δu, δv, δw and $\delta \xi$, then it follows from Eqs. 2.30 and 2.31 that

$$\int_0^H \int_0^{2\pi} \left\{ \frac{Eh}{1-\nu^2} \{\delta d\}^T [L^*] \{d\} \right\} R \, d\theta \, dz + \int_H^L \int_0^{2\pi} \left\{ \frac{Eh}{1-\nu^2} \{\delta d\}^T [L] \{d\} \right\} R \, d\theta \, dz$$

$$+ \int_0^H \int_0^{2\pi} \left\{ \rho_\ell \sum_{n=1}^{\infty} \left[\dot{A}_{0n}(t) + \sum_{i=1}^{\infty} \dot{A}_{in}(t) \, I_n\left(\frac{\lambda_i R}{H}\right) \cos\left(\frac{\lambda_i z}{H}\right) + \sum_{j=1}^{\infty} \dot{B}_{jn}(t) \right. \right.$$

$$J_n\left(\varepsilon_{jn}\right) \cosh\left(\frac{\varepsilon_{jn} z}{R}\right)\Big] \cos(n\theta)\Big\} \delta w \, R \, d\theta \, dz + \int_0^R \int_0^{2\pi} \Big\{ \rho_\ell \sum_{n=1}^{\infty} \Big[\dot{A}_{0n}(t) \cdot$$

$$\left(\frac{r}{R}\right)^n + \sum_{i=1}^{\infty} \dot{A}_{in}(t) \cos\left(\lambda_i\right) I_n\left(\frac{\lambda_i r}{H}\right) + \sum_{j=1}^{\infty} \dot{B}_{jn}(t) \cosh\left(\frac{\varepsilon_{jn} H}{R}\right) J_n\left(\frac{\varepsilon_{jn} r}{R}\right)$$

$$+ \; g \, \xi_n(r,t) \Big] \cos(n\theta)\Big\} \delta\xi \, r \, d\theta \, dr = 0 \qquad (2.34)$$

For each circumferential wave number $n \geq 1$, take $\delta u = \delta u_n(z) \cos(n\theta)$; $\delta v = \delta v_n(z) \sin(n\theta)$; $\delta w = \delta w_n(z) \cos(n\theta)$; and $\delta\xi = \delta\xi_n(r) \cos(n\theta)$. (2.35)

Inserting Eqs. 2.25, 2.29 and 2.35 into Eq. 2.34, one can obtain the following integral relation that govern the motion of the liquid-shell-surface wave system:

$$\int_0^H \left(\frac{\pi R E h}{1-\nu^2} \left\{\delta d_n\right\}^T [L_n^*] \left\{d_n\right\} \right) dz + \int_H^L \left(\frac{\pi R E h}{1-\nu^2} \left\{\delta d_n\right\}^T [L_n] \left\{d_n\right\} \right) dz$$

$$+ a_{0n} \left(\int_0^H \delta w_n(z) \, dz \right) \left(\int_0^H \ddot{w}_n(z,t) \, dz \right) + \sum_{i=1}^{\infty} \Big[a_{in} \left(\int_0^H \delta w_n(z) \cos\left(\frac{\lambda_i z}{H}\right) dz \right) \cdot$$

$$\left(\int_0^H \ddot{w}_n(z,t) \cos\left(\frac{\lambda_i z}{H}\right) dz \right) \Big] + \sum_{j=1}^{\infty} \Big[b_{jn} \left(\int_0^H \delta w_n(z) \cosh\left(\frac{\varepsilon_{jn} z}{R}\right) dz \right) \cdot$$

$$\left(\int_0^R r \, \ddot{\xi}_n(r,t) \, J_n\left(\frac{\varepsilon_{jn} r}{R}\right) dr \right) \Big] + \hat{a}_{0n} \left(\int_0^R r^{n+1} \, \delta\xi_n(r) \, dr \right) \left(\int_0^H \ddot{w}_n(z,t) \, dz \right)$$

$$+ \sum_{i=1}^{\infty} \left[\hat{a}_{in} \left(\int_0^R r \, \delta\xi_n(r) \, I_n\left(\frac{\lambda_i r}{H}\right) dr \right) \left(\int_0^H \ddot{w}_n(z,t) \cos\left(\frac{\lambda_i z}{H}\right) dz \right) \right]$$

$$+ \sum_{j=1}^{\infty} \left[\hat{b}_{jn} \left(\int_0^R r\, \delta\xi_n(r)\, J_n\left(\frac{\varepsilon_{jn} r}{R}\right) dr \right) \left(\int_0^R r\, \ddot{\xi}_n(r,t)\, J_n\left(\frac{\varepsilon_{jn} r}{R}\right) dr \right) \right]$$

$$+ \pi\rho_\ell g \left(\int_0^R r\, \delta\xi_n(r)\, \xi_n(r,t)\, dr \right) = 0 \qquad (2.36)$$

where

$$a_{0n} = \frac{\pi\, \rho_\ell\, R^2}{n\, H} \quad ; \quad a_{in} = \frac{2\pi\, R\, \rho_\ell\, I_n\left(\frac{\lambda_i R}{H}\right)}{\lambda_i\, \acute{I}_n\left(\frac{\lambda_i R}{H}\right)} \quad ;$$

$$b_{jn} = \frac{2\pi\,\rho_\ell}{\varepsilon_{jn} \sinh\left(\frac{\varepsilon_{jn} H}{R}\right)\left(1 - \frac{n^2}{\varepsilon_{jn}^2}\right) J_n\left(\varepsilon_{jn}\right)} \quad ;$$

$$\hat{a}_{0n} = \frac{\pi\,\rho_\ell}{n\, H\, R^{n-1}} \quad ; \quad \hat{a}_{in} = \frac{2\pi\,\rho_\ell \cos\left(\lambda_i\right)}{\lambda_i\, \acute{I}_n\left(\frac{\lambda_i R}{H}\right)} \quad ; \quad \text{and}$$

$$\hat{b}_{jn} = \frac{2\pi\,\rho_\ell}{\varepsilon_{jn}\, R \tanh\left(\frac{\varepsilon_{jn} H}{R}\right)\left(1 - \frac{n^2}{\varepsilon_{jn}^2}\right) J_n^2\left(\varepsilon_{jn}\right)}$$

$$(i = 1,2,\ldots;\ \text{and}\ j = 1,2,\ldots)$$

II-2-4. Derivation of the Matrix Equations of Motion

To establish the matrix equations of motion of the liquid-shell-surface wave system, one can make use of Eq. 2.36; its first two terms must be first integrated by parts with respect to the z coordinate to eliminate the higher order derivatives. The substitution of the shell displacement model (Eq. 1.74) into the integrated terms can lead directly to the shell mass and stiffness matrices obtained in the preceding

analysis.

To formulate the overall problem, one must represent the free surface displacement in terms of a finite number of nodal displacements. Thus, one has to divide the quiescent liquid free surface into concentric annular elements as indicated in Fig. II-4-a. A typical "free surface element" of length R_e with a local radial coordinate $\bar{r}$ is also shown in Fig. II-4-b. The free surface displacement $\xi_{ne}(\bar{r},t)$ can be written in terms of the nodal displacements as follows:

$$\xi_{ne}(\bar{r},t) = \sum_{i=1}^{2} S_i(\bar{r})\, \bar{\xi}_{ni}(t) = \{S(\bar{r})\}^T \{\bar{\xi}(t)\}_e \tag{2.37}$$

where e is the subscript indicating "element" and $\bar{\xi}_{ni}(t)$ are the nodal displacements of the element. The shape functions are given by

$$\begin{aligned} S_1(\bar{r}) &= 1 - \frac{\bar{r}}{R_e} \\ S_2(\bar{r}) &= \frac{\bar{r}}{R_e} \end{aligned} \tag{2.38}$$

With the aid of the shell radial displacement model (Eq. 1.75), and the free surface displacement model (Eq. 2.37), the remaining matrices, involved in the matrix equations of motion, can be evaluated. Thus, Eq. 2.36 can be written as

$$\{\delta q\}^T [M_s]\{\ddot{q}\} + \{\delta q\}^T \left([K_s] + [K_s^i] \right)\{q\} + \{\delta q\}^T [M_{11}]\{\ddot{q}\}$$

$$+ \{\delta q\}^T [M_{12}]\{\ddot{\tilde{q}}\} + \{\delta \tilde{q}\}^T [M_{21}]\{\ddot{q}\} + \{\delta \tilde{q}\}^T [M_{22}]\{\ddot{\tilde{q}}\} + \{\delta \tilde{q}\}^T [K_\ell]\{\tilde{q}\} = 0 \tag{2.39}$$

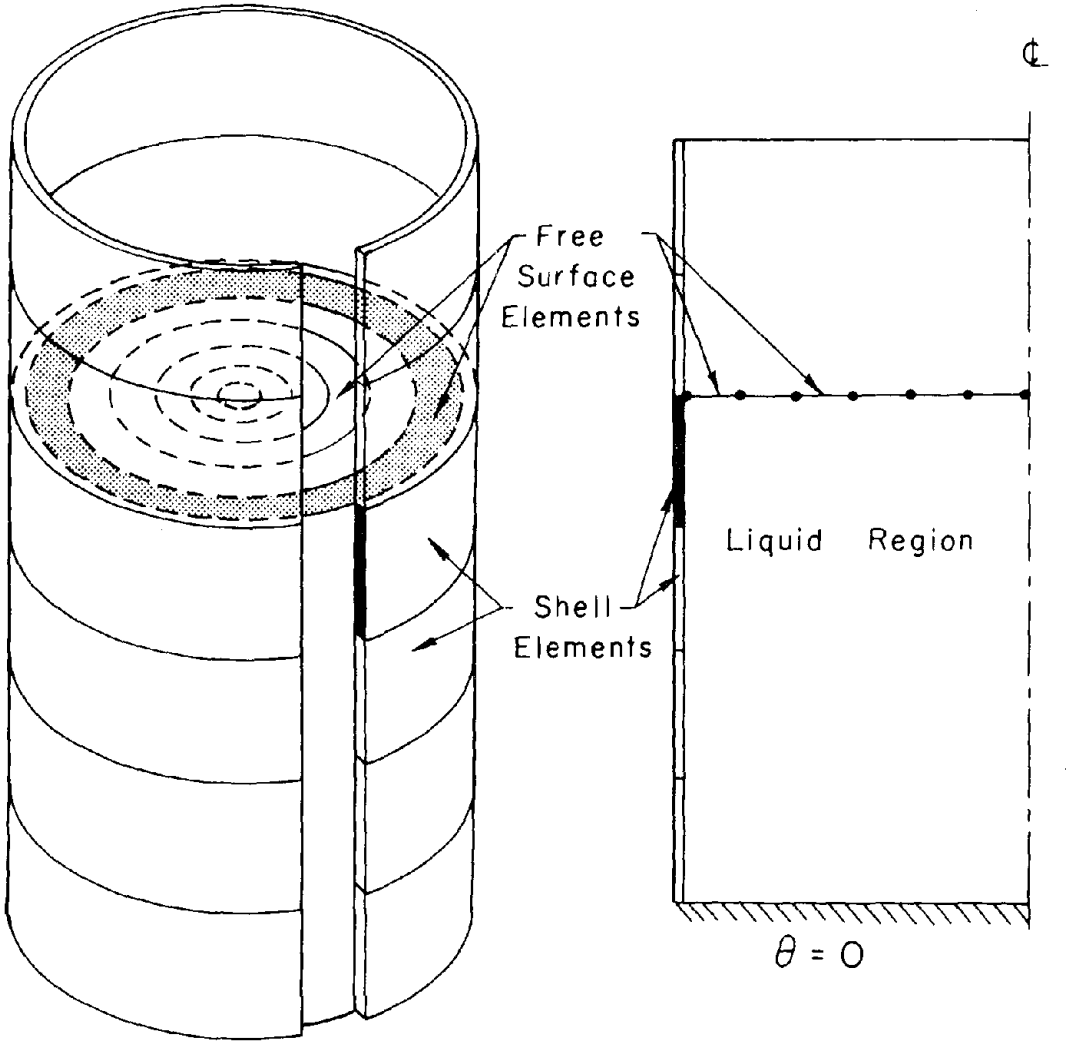

(a) Finite Element Idealization of the Shell and the Free Surface

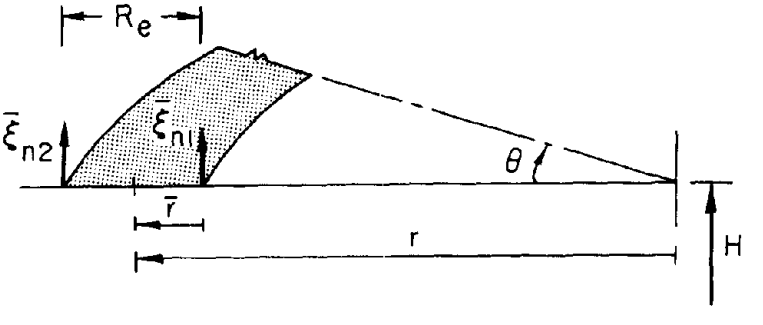

(b) Free Surface "Element"

Fig. II-4. Finite Element Definition Diagram.

where $\{q\}$ and $\{\tilde{q}\}$ are the assemblage nodal displacement vectors of the shell and the free surface, respectively. The shell mass matrix $[M_s]$ and the shell stiffness matrices $[K_s]$ and $[K_s^i]$ were developed in detail in the preceding sections; they are given by Eqs. 1.106, 1.98, and 2.18, respectively. A complete derivation of the remaining matrices is given in Appendix II-b.

Now, the nodal displacements, that is, the unknowns for the entire assemblage, may be written in the following partitioned form

$$\{x\} = \left\{\begin{array}{c} \{q\} \\ \hline \{\tilde{q}\} \end{array}\right\} \tag{2.40}$$

where the subvector $\{q\}$ is of the order (4 x NEL) x 1, and the subvector $\{\tilde{q}\}$ is of the order NER x 1; NER is the number of "free surface elements". The order of the vector $\{x\}$ is, therefore, (4 x NEL + NER) x 1.

With the aid of Eq. 2.40, one can write Eq. 2.39 more conveniently as

$$\{\delta x\}^T \left([M]\{\ddot{x}\} + [K]\{x\} \right) = 0 \tag{2.41}$$

where the overall mass and stiffness matrices are written in the following partitioned forms:

$$[M] = \left[\begin{array}{c|c} [M_s] + [M_{11}] & [M_{12}] \\ \hline [M_{21}] & [M_{22}] \end{array}\right] \tag{2.42};$$

and

$$[K] = \left[\begin{array}{c|c} [K_s] + [K_s^i] & [0] \\ \hline [0] & [K_\ell] \end{array}\right] \tag{2.43}$$

It should be noted that both the mass and stiffness matrices in Eq. 2.41 are symmetric and positive definite; the proof of symmetry of

the mass matrix [M] is given in Appendix II-c. Furthermore, the stiffness matrix [K] is banded, while the mass matrix [M] is partially complete (not banded).

Since the virtual nodal displacement vector $\{\delta x\}$ is arbitrary, the expression in parentheses in Eq. 2.41 must vanish. Therefore, the matrix equation of motion for the assemblage can be obtained in the form

$$[M]\{\ddot{x}\} + [K]\{x\} = \{0\} \tag{2.44}$$

II-2-5. The Overall Eigenvalue Problem

By writing the solutions of Eq. 2.44 in the familiar form

$$\{x(t)\} = \{\overset{*}{x}\}\, e^{i\omega t} \quad ; \quad i = \sqrt{-1} \tag{2.45},$$

and substituting Eq. 2.45 into Eq. 2.44 (leaving out the common factor $e^{i\omega t}$), the following equation is obtained

$$\left(-\omega^2 [M] + [K]\right)\{\overset{*}{x}\} = \{0\} \tag{2.46}$$

where $\{\overset{*}{x}\}$ is the vector of the displacement amplitudes of vibration of the overall system (which does not change with time), and ω is the natural circular frequency. The eigenvector $\{\overset{*}{x}\}$ can be written in the following partitioned form

$$\{\overset{*}{x}\} = \begin{Bmatrix} \{\overset{*}{q}\} \\ \hline \{\overset{*}{\tilde{q}}\} \end{Bmatrix} \tag{2.47}$$

where the subvectors $\{\overset{*}{q}\}$ and $\{\overset{*}{\tilde{q}}\}$ are the generalized nodal displacement vector (independent of time) of the shell and the free surface, respectively.

A nontrivial solution of Eq. 2.46 is possible only if the

determinant of the coefficients vanishes, i.e.,

$$\left\| [K] - \omega^2 [M] \right\| = 0 \qquad (2.48)$$

Expanding the determinant will give an algebraic equation of the N^{th} degree in the frequency parameter ω^2 for a system having NEL shell elements and NER free surface elements, where N = 4 x NEL + NER.

Because of the positive definitiveness of [M] and [K], the eigenvalues $\omega_1^2, \omega_2^2, \ldots, \omega_N^2$ are real and positive quantities; Eq. 2.46 provides nonzero solution vectors $\{x^*\}$ (eigenvectors) for each eigenvalue ω^2.

II-2-6. Computer Implementation and Numerical Examples

A digital computer program has been written to compute the natural frequencies and mode shapes of vibration of the coupled liquid-shell-surface wave system by the method outlined in the preceding subsections.

The program is employed to investigate the coupling between the free surface sloshing modes and the cosθ-type modes of a tall tank (R = 24 ft, L = 72 ft, and h = 0.43 inch). The quiescent liquid free surface is divided into 12 elements (NER = 12), and the elastic shell is modeled by 12 elements (NEL = 12); therefore, the number of expected modes is 60. The tank is assumed to be full of water (NEH = 12).

The computed natural frequencies of the coupled system are presented in Table II-4 along with those calculated for the two uncoupled systems; the sloshing frequencies in a rigid tank are obtained by [10]

$$\omega_{jn}^2 = \frac{g\varepsilon_{jn}}{R} \tanh\left(\frac{\varepsilon_{jn}H}{R}\right) \qquad (2.49)$$

and the frequencies of the cosθ-type modes are obtained by the analysis presented in Chapter I (Table I-3-b). It is evident that the lowest

TABLE II-4

NATURAL FREQUENCIES (cps)

(n = 1)

Mode Number	The Coupled System	Sloshing in a Rigid Tank	Liquid-Shell System
1	0.2497	0.2500	-
2	0.4254	0.4255	-
3	0.5384	0.5384	-
4	0.6307	0.6304	-
13	3.5566	-	3.5586
14	10.433	-	10.450
15	15.515	-	15.551
16	20.006	-	20.075

TABLE II-5

MODE SHAPES

Fundamental Sloshing Mode (ξ)		Fundamental Shell Mode (w)	
Coupled System	Rigid Tank	Coupled System	Liquid-Shell System
0.0000	0.0000	0.0000	0.0000
0.1315	0.1314	0.1646	0.1651
0.2600	0.2604	0.2415	0.2420
0.3848	0.3849	0.3301	0.3308
0.5021	0.5026	0.4244	0.4255
0.6113	0.6116	0.5199	0.5209
0.7093	0.7098	0.6140	0.6156
0.7955	0.7957	0.7037	0.7048
0.8674	0.8679	0.7866	0.7886
0.9249	0.9251	0.8608	0.8624
0.9663	0.9665	0.9238	0.9253
0.9918	0.9916	0.9727	0.9752
1.0000	1.0000	1.0000	1.0000

natural frequencies of the coupled system are in good agreement with the sloshing frequencies in a similar rigid tank. Furthermore, the 13^{th}, 14^{th},...etc. ascending frequencies are, for practical purposes, the same as those computed for the liquid-shell system. Therefore, it may be concluded that the coupling effect is negligible. This is further substantiated by the mode shapes. Fig. II-5 displays the modes of the coupled system corresponding to the lowest two natural frequencies; it is clear that these modes have predominantly free surface motion. With the maximum wave amplitude normalized to unity, the maximum wall displacements for these modes are on the order of 10^{-3} or less. Therefore, the wall participation is essentially negligible, and these modes are characterized as free surface modes. Table II-5 presents a comparison between the free surface displacements associated with the fundamental mode of the liquid-shell system.

As is seen, the vibrational modes of the coupled system can be separated into two groups. In one group, the motion of the free surface is predominant (identical to that in a rigid tank), and in the other group, the displacement of the shell is important and can be evaluated by considering the liquid-shell system only. Therefore, it is sufficient to consider only the two uncoupled systems:

(i) the liquid-shell system,

and (ii) the free surface gravity waves in a similar rigid tank.

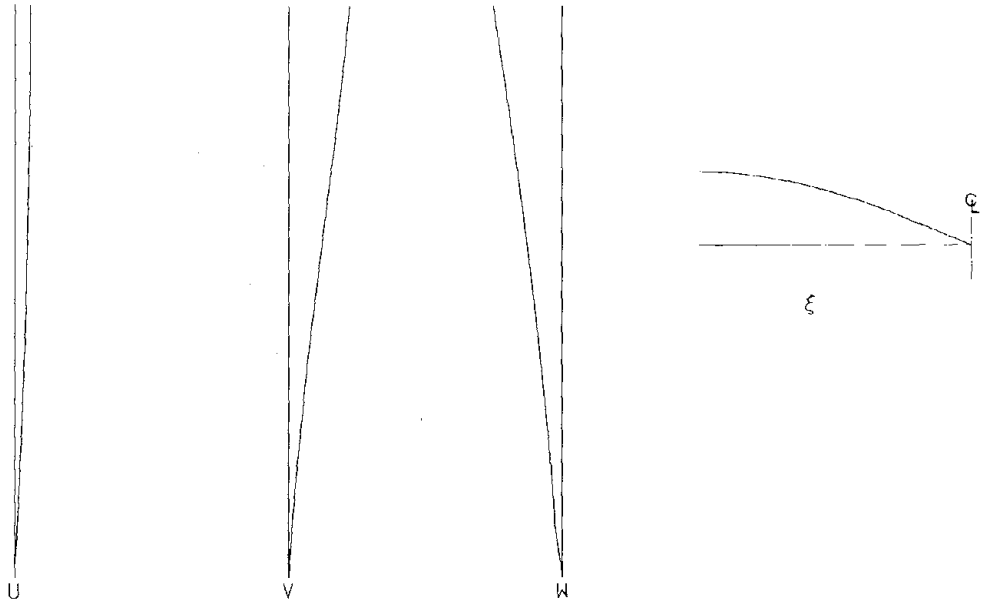

CIRCUMFERENTIAL WAVE NUMBER = 1
NATURAL FREQUENCY = 0.25 CPS

(a) Fundamental Mode

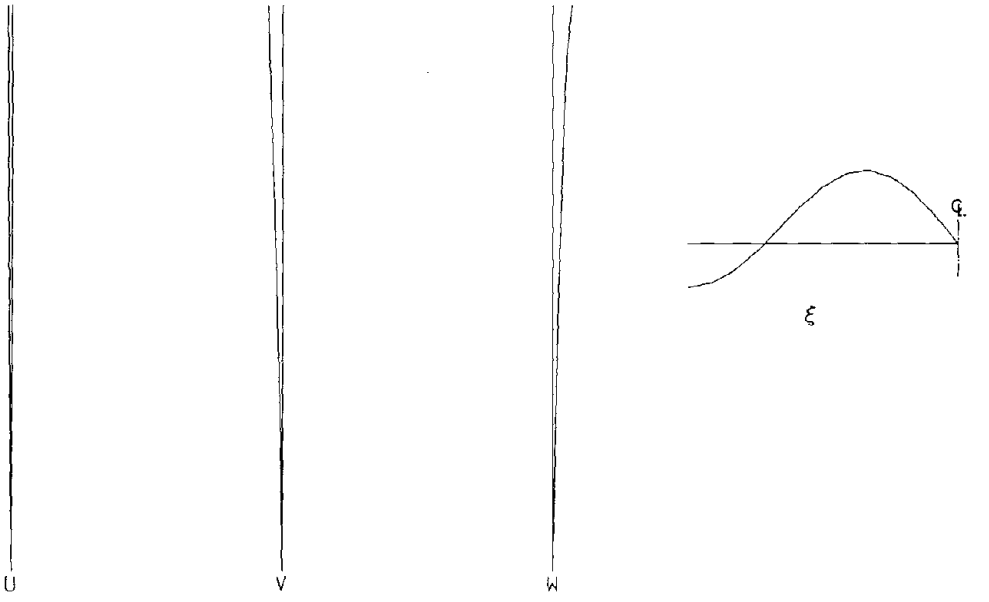

CIRCUMFERENTIAL WAVE NUMBER = 1
NATURAL FREQUENCY = 0.43 CPS

(b) Second Mode

Fig. II-5. Mode Shapes of the Coupled Liquid-Shell-Surface Wave System (shell displacements are magnified 500 time).

II-3. The Effect of the Deformability of the Foundation

It has long been recognized that the dynamic interaction between structures and the supporting soil might influence their seismic response in an important way. During the shaking of an earthquake, seismic waves are transmitted through the soil and excite the structure which in turn modifies the input motion by its movement relative to the ground. Although many studies have dealt extensively with this problem, no attempt has been made, so far, to extend such analysis to the soil-tank system.

A common approach in civil engineering practice is to regard the tank as anchored to its foundation and to consider the foundation soil to be rigid. The mechanical model derived by Housner [11] for rigid tanks can then be employed to estimate the maximum seismic response by means of a response spectrum characterizing the design earthquake.

As a natural extension of Housner's model, the effect of the soil deformability on the seismic response of rigid tanks was investigated. A mechanical model was first derived to duplicate the lateral force and moment exerted on the base of a rigid tank undergoing both translation and rotation. This model was then combined with another simplified model representing the flexibility of, and the damping in, the foundation soil. The analysis, which will be presented in a future report, reveals that rocking motion of rigid "tall" tanks accounts for a significant part of the overall seismic response of such tanks.

Since Housner's investigation, much work involving the dynamic response of deformable containers has been made; again, all of these investigations have considered the foundation soil to be rigid. A

complete analysis of the soil-tank system by the finite element method is beyond the scope of this study; however, a simplified model of the soil can be employed with a finite element model of the shell to exhibit the fundamental characteristics of the dynamic behavior of the overall system and to assess the significance of the interaction on the response of deformable tanks.

Since the cosnθ-type deformations have no lateral force or moment, only the influence upon the cosθ-type modes should be investigated. Furthermore, rocking motion is most pronounced for tanks having aspect ratios (height to radius ratio) ≥ 1. Thus, the soil-tank interaction problem is governed by a beam-type behavior rather than by a shell-type response. Consequently, the system was modeled by a vertical cantilever beam (including bending and shear deformations) supported by a spring-dashpot model. The details of the analysis will be presented, as previously mentioned, in a separate Earthquake Engineering Research Laboratory report (EERL) in the near future.

Although the models discussed in this section represent a highly simplified version of the actual interaction problem, they offer a simple and direct insight into a very complicated problem; and so, they are of a practical value.

II-4. The Effect of the Rigidity of the Roof

Thus far only open top circular cylindrical containers have been analyzed. However, tanks are usually covered either by a fixed roof or by a floating roof to protect the contained liquid from the atmosphere. It is the purpose of this section to investigate the influence of the fixed-type roof on the dynamic characteristics of tanks.

A complete analysis of the problem requires consideration of the equations of motion of the roof simultaneously with the equations of motion of the shell, and enforcing the conditions of continuity of the generalized forces and displacements at the junction. Such analysis has been carried out in Ref. [7] where the dynamic problem of a tank covered by a dome has been treated.

In this section, a simple roof model, commonly used in civil engineering tanks, is considered. It consists essentially of a thin steel plate supported by steel trusses. The plate has a considerable stiffness in its own plane; therefore, it restrains the tangential and radial displacements of the shell at their mutual boundaries. It affects the $\cos\theta$-type modes by restricting the motion of the tank top to be a rigid body translation; i.e.,

$$w(0,L,t) = -v(\tfrac{\pi}{2},L,t) \quad ; \quad (n = 1) \tag{2.50}$$

In addition, it restrains the $\cos n\theta$-type modes against cross-sectional deformations at the tank top; i.e.,

$$w(\theta,L,t) = v(\theta,L,t) = 0 \quad ; \quad (n \geq 2) \tag{2.51}$$

Furthermore, by virtue of its thinness, the plate has very little stiffness in the z-direction transverse to its plane; consequently, it will

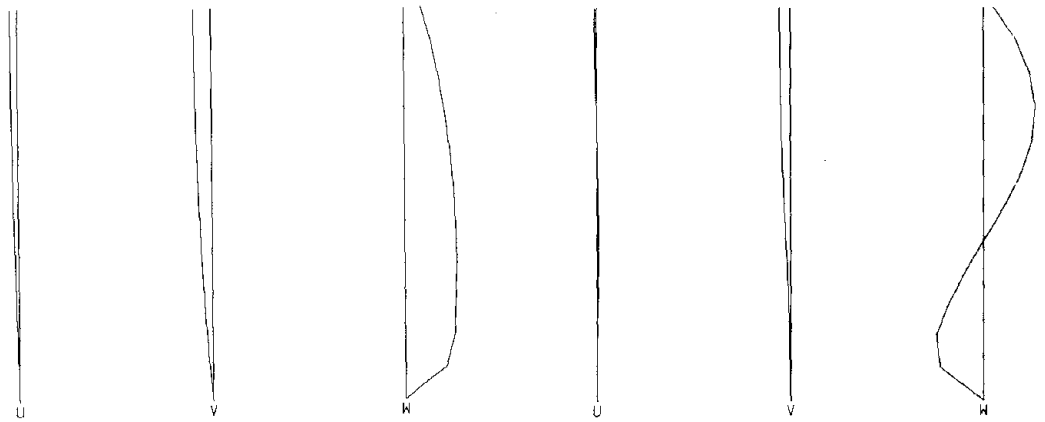

(m = 1) (m = 2)

(a) Broad Tank

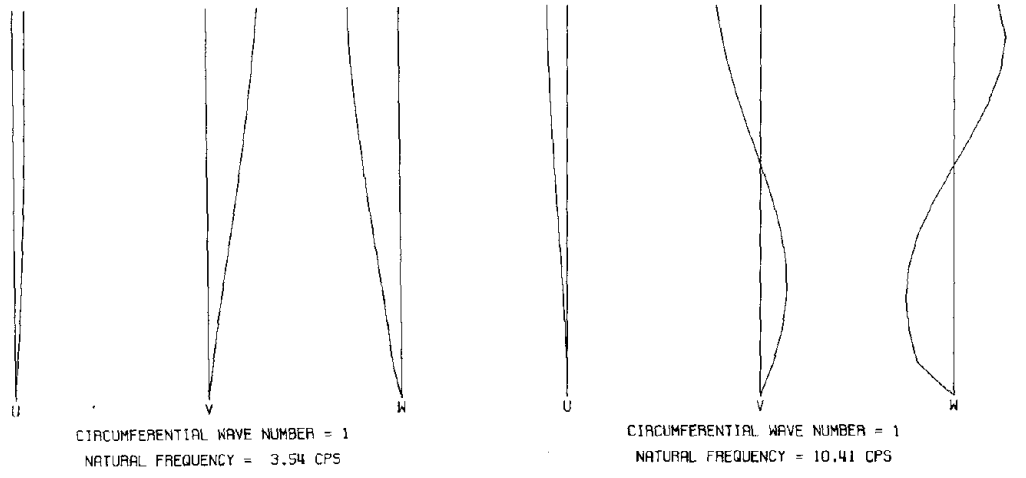

(m = 1) (m = 2)

(b) Tall Tank

Fig. II-6. Effect of the Roof on the Cosθ-type Modes.

TABLE II-6

NATURAL FREQUENCIES OF THE COSθ-TYPE MODES (cps)

Tank	Without Roof		With Roof	
	m = 1	m = 2	m = 1	m = 2
Broad	6.1853	11.279	6.1791	11.260
Tall	3.5593	10.452	3.5387	10.405

TABLE II-7

NATURAL FREQUENCIES OF THE COSnθ-TYPE MODES (cps)

Tank	Roof	n					
		2	3	4	5	6	7
Broad	Without	5.19	4.15	3.35	2.76	2.36	-
	With	6.95	6.62	6.05	-	-	-
Tall	Without	1.69	1.21	1.31	1.62	1.98	-
	With	4.42	3.16	2.70	2.78	3.16	3.65

TABLE II-8

NATURAL FREQUENCIES OF THE COSnθ-TYPE MODES (cps)

	n							
	2	3	4	5	6	7	8	9
No Roof - Initial Stress Excluded	2.33	1.40	0.95	0.70	0.58	0.55	0.59	0.69
Roof - Initial Stress Excluded	4.34	3.03	2.22	1.71	1.39	1.21	1.14	1.16
Roof - Initial Stress Included	4.35	3.14	2.52	2.33	2.55	2.76	3.07	3.39
Full-Scale Vibration Test	4.35	3.12	2.51	2.31	2.61	2.82	3.06	3.37

generate negligible moment M_z and membrane force N_z at the shell top as the shell vibrates. Although the foregoing boundary conditions are highly simplified, the computed frequencies and mode shapes of real full-scale tanks are in good agreement with those measured by vibration tests (refer to Fig. II-9).

The effect of the roof rigidity on the cosθ-type modes is generally negligible as shown in Fig. II-6 and as indicated in Table II-6. The slight reduction in the values of the natural frequencies is due to the additional mass of the roof.

Table II-7 presents the natural frequencies of the cosnθ-type modes with and without roof; it clearly illustrates the significant effect of the roof on these modes which can be also seen in Figs. II-7 and II-8

Finally, the applicability of the analysis is demonstrated by comparing the computed natural frequencies of tank no. 3 (refer to Chapter IV) with those obtained by field tests. Table II-8 and Fig. II-9 clearly emphasize the significant role played by the roof and the initial stress field in estimating the natural frequencies of the cosnθ-type modes. It is also evident that the roof effect is more pronounced for small n, while the initial stress influence is more significant for large n.

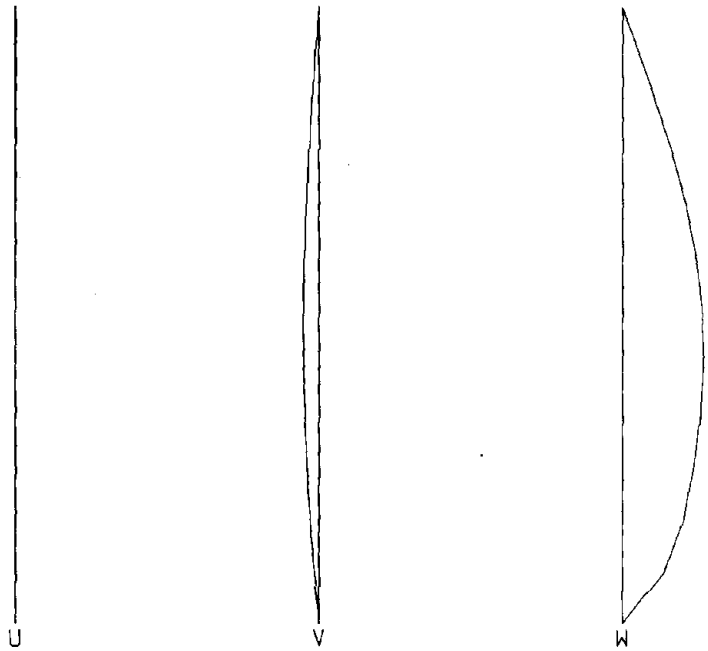

(a) Broad Tank

CIRCUMFERENTIAL WAVE NUMBER = 3
NATURAL FREQUENCY = 6.62 CPS

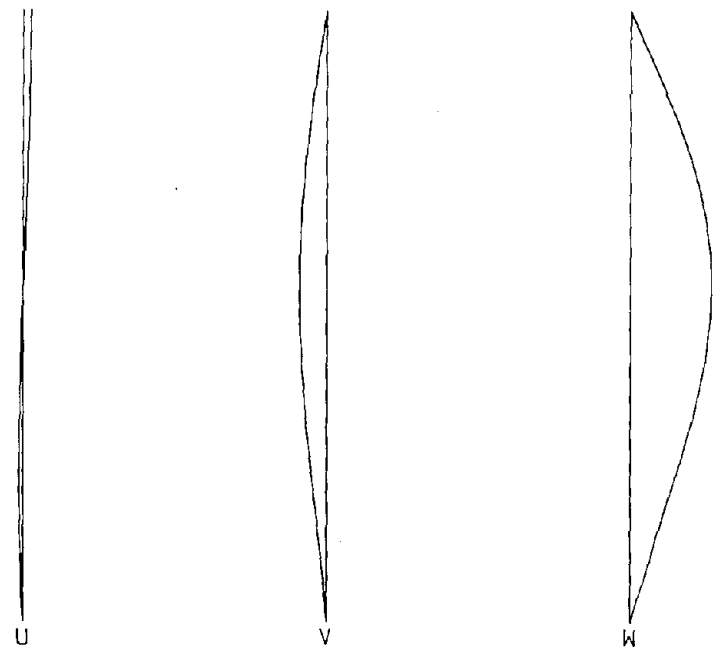

(b) Tall Tank

CIRCUMFERENTIAL WAVE NUMBER = 3
NATURAL FREQUENCY = 3.16 CPS

Fig. II-7. Effect of the Roof on the Cosnθ-type Modes.

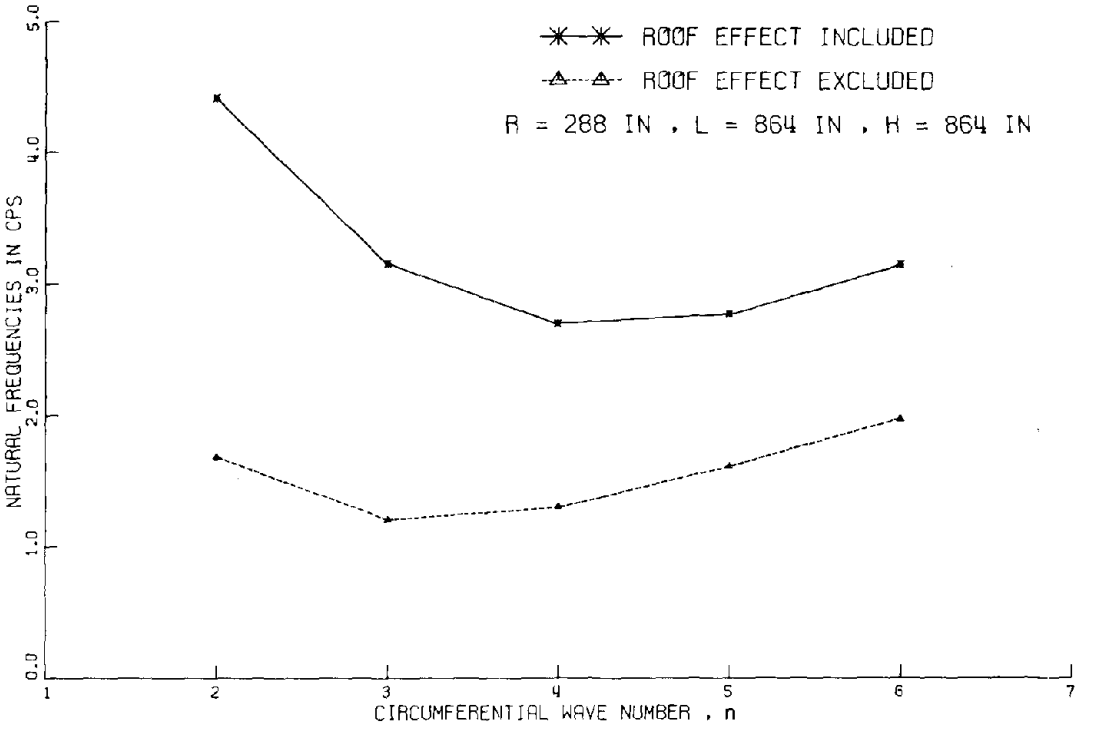

Fig. II-8. Effect of the Roof Rigidity Upon the Natural Frequencies of the Cosnθ-type Modes of a Tall Tank.

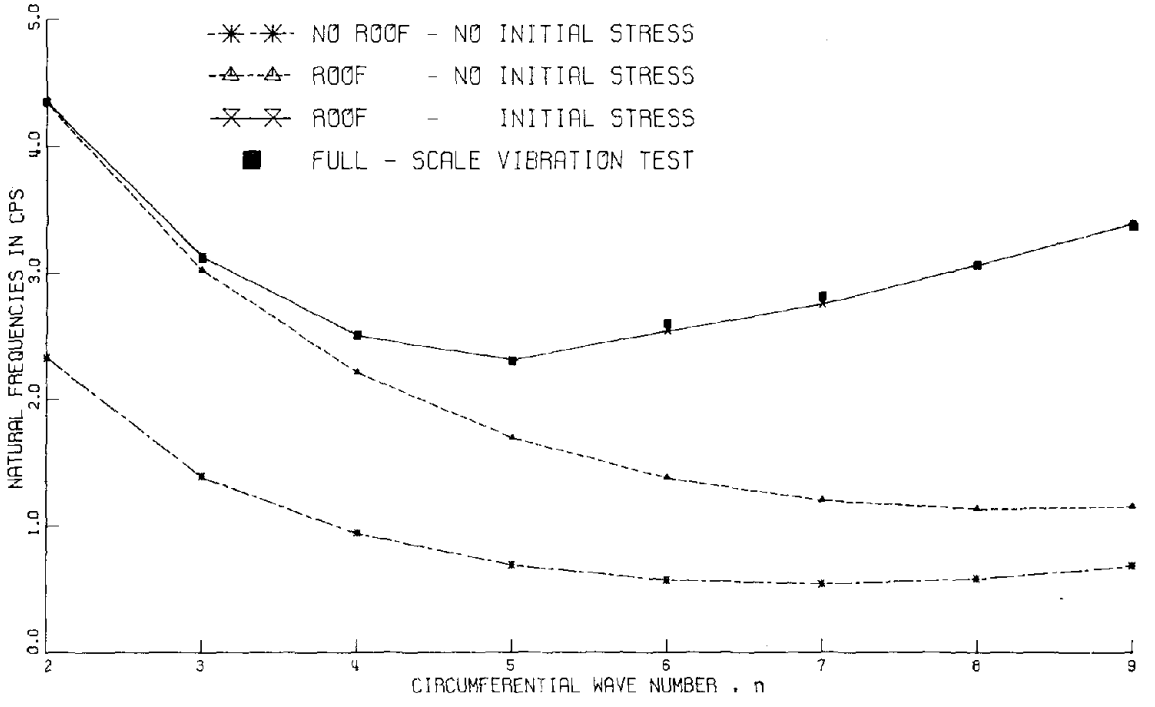

Fig. II-9. Comparison Between Calculated and Measured Natural Frequencies of the Cosnθ-type Modes.

II-5. Appendices

Appendix II-a

List of Symbols

The letter symbols are defined where they are first introduced in the text, and they are also summarized herein in alphabetical order:

$A_{0n}(t)$ and $A_{in}(t)$	Time dependent coefficients of the velocity potential, Eq. 2.22.
a_{0n}, a_{in}, $\hat{a}_{0n}$, and $\hat{a}_{in}$	Coefficients in Eq. 2.36.
$B_{jn}(t)$	Time dependent coefficients of the velocity potential, Eq. 2.22.
b_{jn} and $\hat{b}_{jn}$	Coefficients in Eq. 2.36.
$[C_n]$	Square matrix defined by Eq. 2.14.
[DM]	Added mass matrix defined by Eq. 1.130.
$\{d(\theta,z,t)\}$	Shell displacement vector, Eq. 1.31.
$\{d(\bar{z},t)\}_e$ and $\{d_n\}$	Vectors of the maximum displacement components of the n^{th} circumferential mode, Eqs. 1.76 and 1.87, respectively.
$\{\bar{d}\}_e$	Generalized displacement vector of the element "e", of order 8 x 1, Eq. 1.78.
E	Young's modulus of the shell material.
e	Indicate element, and occasionally used as the number of the element "e".
e_z and e_θ	Vibratory strains, Eq. 2.1.
$\{F\}$	Force vector, Eq. 2.6.

$\{F_0\}$, $\{\bar{F}_0\}$, $\{F_i\}$, and $\{\bar{F}_i\}$	Vectors defined in Appendix II-b.
$\{f_0\}_e$, $\{\bar{f}_0\}_e$, $\{f_i\}_e$, and $\{\bar{f}_i\}_e$	Vectors defined in Appendix II-b.
f_{mn}	Natural frequencies, cps.
g	Acceleration of gravity.
H	Liquid depth.
h	Shell thickness.
$I_n(\ )$	Modified Bessel functions of the first kind of order n, Eq. 2.21.
$\acute{I}_n(\ )$	Derivative of $I_n(\ )$ with respect to the radial coordinate, Eq. 2.23.
I	Variational functional, Eq. 1.12.
i	$\sqrt{-1}$, Eq. 2.45.
J	Variational functional, Eq. 1.61.
$J_n(\ )$	Bessel functions of the first kind of order n, Eq. 2.21.
$[K_s^i]_e$ and $[K_s^i]$	Element stiffness matrix and the assemblage stiffness matrix due to the initial hoop stress, Eqs. 2.17 and 2.18, respectively.
$[K_s]$	Assemblage stiffness matrix of the shell, Eq. 1.98.
$[K_\ell]_e$ and $[K_\ell]$	Element stiffness matrix and the assemblage stiffness matrix of the liquid free surface, Appendix II-b-1 and Eq. 2.39, respectively.

$[K]$	Stiffness matrix, Eqs. 2.19 and 2.43.
k	Separation constant, Eq. 2.21.
L	Shell length.
L_e	Length of shell element.
$[L^*]$, $[L^i]$, and $[L]$	Linear differential operators, Eqs. 2.6, 2.7 and 1.46, respectively.
$[M_s]$	Assemblage mass matrix, Eq. 1.106.
$[M_{11}]$, $[M_{12}]$, $[M_{21}]$, and $[M_{22}]$	Mass Matrices, Eq. 2.39.
$[M]$	Mass Matrix, Eqs. 2.19 and 2.42.
m	Number of vertical mode.
N	Constant = 4 x NEL + NER
NEL	Number of shell elements along the shell length.
NEH	Number of shell elements in contact with the liquid.
NER	Number of "free surface elements".
N_θ^i	Initial hoop force resultant, Eq. 2.3.
$\bar{N}_e$	Initial hoop force resultant evaluated at the centroid of the element "e", Eq. 2.17.
$\{\bar{N}\}$	Vector of the interpolation functions, Eq. 1.79.
n	Circumferential wave number.
$[\bar{P}]$	Differential operator matrix, Eq. 2.10.

$[\bar{P}_n]$	Differential operator matrix for the n^{th} circumferential wave, Eq. 2.12.
p_s and p_d	Liquid hydrostatic and hydrodynamic pressures, respectively.
$[Q]$	Matrix of interpolation functions, of order 3 x 8, Eq. 1.77.
$\{q\}$	The assemblage nodal displacement vector of the shell, Eq. 2.19.
$\{\tilde{q}\}$	The assemblage nodal displacement vector of the free surface, Eq. 2.39.
$\{\overset{*}{q}\}$ and $\{\overset{*}{\tilde{q}}\}$	Time independent nodal displacement vectors of the shell and the free surface, respectively.
R	Tank radius.
R_e	Length of the free surface element "e".
r	Radial coordinate of the cylindrical coordinate system.
$\bar{r}$	Local radial coordinate.
S_i	Interpolation functions, Eq. 2.38.
$\{S\}$	Vector of the interpolation functions, Eq. 2.37.
$\hat{T}_n(t)$	Functions of time, Eq. 2.21.
t	Time.
$U(t)$, $U_1(t)$, and $U_2(t)$	Strain energies, Eqs. 2.1, 1.33 and 2.3, respectively.

u, v, and w	Shell displacements in the axial, tangential, and radial directions, respectively.
$u_n(z,t)$, $v_n(z,t)$ and $w_n(z,t)$	Displacement functions for the n^{th} circumferential wave.
$\{x\}$	The assemblage nodal displacement vector of the overall system, Eq. 2.40.
$\{\overset{*}{x}\}$	Time independent nodal displacement vector of the overall system, Eq. 2.45.
x	Shell coordinate (refer to Fig. I-b-i).
y	Dummy variable, Appendix II-b-3.
z	Axial coordinate of the cylindrical coordinate system.
$\bar{z}$	Local axial coordinate.
α_0 and α_i	Coefficients defined in Appendix II-c.
β_i and $\bar{\beta}_i$	Coefficients defined in Appendix II-b and II-c.
$\gamma_{z\theta}$	Vibratory shear strain, Eq. 2.1.
δ	Variational operator.
ε_θ	Normal strain in the middle surface in the θ-direction, Eq. 2.4.
$\varepsilon_\theta^{n\ell}$	Nonlinear components of ε_θ, Eq. 2.9.
ε_{jn}	Roots of $J_n'(\varepsilon_{jn}) = 0$.
ξ	Free surface displacement.
$\xi_n(r,t)$	Free surface displacement function for the n^{th} circumferential wave.

$\bar{\xi}_{ni}$	Nodal displacement of the free surface, Eq. 2.37.
$\{\bar{\xi}\}_e$	Nodal displacement vector of the free surface element "e", Eq. 2.37.
$[\Theta_n]$	Diagonal matrix defined by Eq. 1.86.
θ	Circumferential coordinate of the cylindrical coordinate system.
λ_i	Constants = $i\pi$; i = 1,2,...
ν	Poisson's ratio.
ρ_ℓ	Mass density of the liquid.
σ_z^i, σ_θ^i, and $\sigma_{z\theta}^i$	Initial stress field, Eq. 2.1.
σ_z, σ_θ, and $\sigma_{z\theta}$	Vibratory stress field, Eq. 2.1.
ϕ	Liquid velocity potential function.
ω, ω_j and ω_{mn}	Circular natural frequencies.
∇^2	Laplacian operator.
$(\dot{})$	Differentiation with respect to time.

Appendix II-b

Formulation of the Matrices of Eq. 2.39

Full development of the matrices involved in Eq. 2.39 is given in the following sections

II-b-1. The Free Surface "Stiffness" Matrix $[K_\ell]$

With the aid of the free surface displacement model (Eq. 2.37), the last term in Eq. 2.36 can be written as

$$\pi\rho_\ell g\int_0^R r\,\delta\xi(r)\xi(r,t)dr = \pi\rho_\ell g\sum_{e=1}^{NER}\int_0^{R_e}\left\{\left(\bar{r}+(e-1)R_e\right)\{\delta\bar{\xi}\}_e^T\{S(\bar{r})\}\{S(\bar{r})\}^T\{\bar{\xi}\}_e\right\}d\bar{r}$$

$$= \sum_{e=1}^{NER}\{\delta\bar{\xi}\}_e^T\left(\pi\rho_\ell g\int_0^{R_e}\left(\bar{r}+(e-1)R_e\right)\{S(\bar{r})\}\{S(\bar{r})\}^T d\bar{r}\right)\{\bar{\xi}\}_e$$

$$= \sum_{e=1}^{NER}\{\delta\bar{\xi}\}_e^T\,[K_\ell]_e\,\{\bar{\xi}\}_e \quad , \quad \text{where}$$

$$[K_\ell]_e = \pi\rho_\ell g R_e^2\begin{bmatrix}\frac{e}{3}-\frac{1}{4} & \frac{e}{6}-\frac{1}{12}\\ \frac{e}{6}-\frac{1}{12} & \frac{e}{3}-\frac{1}{12}\end{bmatrix}\quad ;\quad e = 1,2,\ldots, NER$$

Because the displacements are matched at the nodes, the stiffnesses are added at these locations; therefore, the assemblage stiffness matrix and the nodal displacement vector can be written as follows:

$$[K_\ell] = \sum_{e=1}^{NER}[K_\ell]_e \text{ and } \{\tilde{q}\} = \sum_{e=1}^{NER}\{\bar{\xi}\}_e$$

Thus,

$$\pi\rho_\ell g \int_0^R r\ \delta\xi(r)\ \xi(r,t)\ dr = \{\delta\tilde{q}\}^T[K_\ell]\{\tilde{q}(t)\} \qquad \text{(II-b-1)}$$

II-b-2. The "Added Mass" Matrix $[M_{11}]$

In order to compute the elements of the mass matrix $[M_{11}]$, the following integrals

$$\int_0^H \ddot{w}(z,t)dz \quad \text{and} \quad \int_0^H \ddot{w}(z,t)\cos\left(\frac{\lambda_i z}{H}\right) dz$$

must be first determined in terms of the nodal displacements. With the aid of Eq. 1.75, one can write

$$\int_0^H \ddot{w}(z,t)\ dz = \sum_{e=1}^{NEH} \int_0^{L_e} \{\bar{N}(\bar{z})\}^T \{\ddot{\bar{d}}(t)\}_e\ d\bar{z} \qquad \text{(II-b-2)},$$

$$\text{and} \int_0^H \ddot{w}(z,t)\cos\left(\frac{\lambda_i z}{H}\right) dz = \sum_{e=1}^{NEH} \int_0^{L_e} \{\bar{N}(\bar{z})\}^T \{\ddot{\bar{d}}(t)\}_e \cos\left[\frac{\lambda_i\left(\bar{z}+(e-1)L_e\right)}{H}\right] d\bar{z} \qquad \text{(II-b-3)}$$

where NEH is the number of shell elements in contact with the liquid.

Now, define the vectors $\{f_0\}_e$ and $\{f_i\}_e$ as the integrals

$$\{f_0\}_e^T = \int_0^{L_e} \{\bar{N}(\bar{z})\}^T\ d\bar{z} = \left[0,\ 0,\ \frac{L_e}{2},\ \frac{L_e^2}{12},\ 0,\ 0,\ \frac{L_e}{2},\ \frac{-L_e^2}{12}\right] \qquad \text{(II-b-4)},$$

and

$$\{f_i\}_e^T = \int_0^{L_e} \{\bar{N}(\bar{z})\}^T \cos\left[\frac{\lambda_i\left(\bar{z} + (e-1)\ L_e\right)}{H}\right]\ d\bar{z} = \left[0,\ 0,\ f_{i3},\ f_{i4},\ 0,\ 0,\ f_{i7},\ f_{i8}\right]_e \qquad \text{(II-b-5)}$$

where

$$f_{i3} = L_e \left[-\left(\frac{1}{\beta_i} + \frac{6}{\beta_i^3}\right) \sin \beta_i(e-1) + \frac{12}{\beta_i^4} \cos \beta_i(e-1) - \frac{6}{\beta_i^3} \sin \beta_i e - \frac{12}{\beta_i^4} \cos \beta_i e \right];$$

$$f_{i4} = L_e^2 \left[-\frac{4}{\beta_i^3} \sin \beta_i(e-1) - \left(\frac{1}{\beta_i^2} - \frac{6}{\beta_i^4}\right) \cos \beta_i(e-1) - \frac{2}{\beta_i^3} \sin \beta_i e - \frac{6}{\beta_i^4} \cos \beta_i e \right];$$

$$f_{i7} = L_e \left[\frac{6}{\beta_i^3} \sin \beta_i(e-1) - \frac{12}{\beta_i^4} \cos \beta_i(e-1) + \left(\frac{1}{\beta_i} + \frac{6}{\beta_i^3}\right) \sin \beta_i e + \frac{12}{\beta_i^4} \cos \beta_i e \right];$$

$$f_{i8} = L_e^2 \left[-\frac{2}{\beta_i^3} \sin \beta_i(e-1) + \frac{6}{\beta_i^4} \cos \beta_i(e-1) - \frac{4}{\beta_i^3} \sin \beta_i e + \left(\frac{1}{\beta_i^2} - \frac{6}{\beta_i^4}\right) \cos \beta_i e \right];$$

$$\beta_i = \frac{i\pi L_e}{H} \quad (i = 1,2,\ldots) \quad ; \quad \text{and} \quad e = 1,2,\ldots, \text{NEH}.$$

The next step is to define the vectors $\{F_0\}$ and $\{F_i\}$ as

$$\{F_0\} = \sum_{e=1}^{NEH} \{f_0\}_e \quad \text{and} \quad \{F_i\} = \sum_{e=1}^{NEH} \{f_i\}_e \qquad \text{(II-b-6)}$$

Therefore, Eqs. II-b-2 and II-b-3 can be rewritten as

$$\int_0^H \ddot{w}(z,t)dz = \{F_0\}^T\{\ddot{q}(t)\} \quad \text{and} \quad \int_0^H \ddot{w}(z,t)\cos\left(\frac{\lambda_i z}{H}\right)dz = \{F_i\}^T\{\ddot{q}(t)\};$$

$$(i = 1, 2, \ldots) \qquad \text{(II-b-7)}$$

The third and fourth terms in Eq. 2.36 can then be expressed as follows (omitting the subscript n)

$$a_0\left(\int_0^H \delta w(z)dz\right)\left(\int_0^H \ddot{w}(z,t)dz\right) + \sum_{i=1}^{\infty} a_i\left(\int_0^H \delta w(z)\cos\left(\frac{\lambda_i z}{H}\right)dz\right)\left(\int_0^H \ddot{w}(z,t)\cos\left(\frac{\lambda_i z}{H}\right)dz\right)$$

$$= a_0\{\delta q\}^T\{F_0\}\{F_0\}^T\{\ddot{q}(t)\} + \sum_{i=1}^{\infty} a_i\{\delta q\}^T\{F_i\}\{F_i\}^T\{\ddot{q}(t)\}$$

$$= \{\delta q\}^T\left(a_0\{F_0\}\{F_0\}^T + \sum_{i=1}^{\infty} a_i\{F_i\}\{F_i\}^T\right)\{\ddot{q}(t)\} \qquad \text{(II-b-8)}$$

Eq. II-b-8 leads to the definition of the mass matrix $[M_{11}]$ as

$$[M_{11}] = a_0\{F_0\}\{F_0\}^T + \sum_{i=1}^{\infty} a_i\{F_i\}\{F_i\}^T \qquad \text{(II-b-9)}$$

It is important to note that the series in Eq. II-b-9 converges very rapidly and only the first few terms are needed for adequate representation of the infinite series.

II-b-3. The Mass Matrix $[M_{22}]$

The eighth term in Eq. 2.36 gives rise to the definition of the mass matrix $[M_{22}]$. To calculate the elements of this matrix, consider first the following integrals

$$I_j = \int_0^R r\, \ddot{\xi}(r,t)\, J_n\left(\frac{\epsilon_{jn} r}{R}\right) dr \; ; \; (j = 1,2,\ldots) \qquad \text{(II-b-10)}$$

With the aid of Eq. 2.37, one can write

$$I_j = \sum_{e=1}^{NER} \int_0^{R_e} \left(\bar{r} + (e-1)R_e\right)\{S(\bar{r})\}^T \{\ddot{\bar{\xi}}(t)\}_e\, J_n\left[\frac{\epsilon_{jn}\left(\bar{r} + (e-1)\, R_e\right)}{R}\right] d\bar{r} \qquad \text{(II-b-11)}$$

where NER is the number of the free surface elements. Now, define the vectors $\{f_j\}_e$ as the integrals

$$\{f_j\}_e^T = \int_0^{R_e} \{s(\bar{r})\}^T \left(\bar{r} + (e-1)\, R_e\right) J_n\left[\frac{\epsilon_{jn}\left(\bar{r} + (e-1)R_e\right)}{R}\right] d\bar{r}$$

$$= [f_{j1},\, f_{j2}]_e \quad ; \quad e = 1,2,\ldots, NER \qquad \text{(II-b-12)}$$

where

$$f_{j1} = R_e^2 \int_0^1 \left((e-1) + (2-e)y - y^2\right) J_n\left(\beta_{jn}(e-1+y)\right) dy \; ;$$

$$f_{j2} = R_e^2 \int_0^1 \left((e-1)y + y^2\right)\, J_n\left(\beta_{jn}(e-1+y)\right) dy \quad ;$$

$$\beta_{jn} = \frac{\epsilon_{jn}\, R_e}{R} \quad (j = 1,2,\ldots); \text{ and } y \text{ is a dummy variable.}$$

$$\text{Let } \{F_j\} = \sum_{e=1}^{NER} \{f_j\}_e \qquad \text{(II-b-13)},$$

therefore, Eq. II-b-11 can be written as

$$I_j = \{F_j\}^T \{\ddot{\tilde{q}}\} \qquad \text{(II-b-14)}$$

Now, inserting Eq. II-b-14 into the eighth term of Eq. 2.36, one can obtain

$$\sum_{j=1}^{\infty} \hat{b}_j \left(\int_0^R r\, \delta\xi_r(r)\, J_n\left(\frac{\varepsilon_{jn} r}{R}\right) dr \right) \left(\int_0^R r\, \ddot{\xi}(r,t)\, J_n\left(\frac{\varepsilon_{jn} r}{R}\right) dr \right)$$

$$= \sum_{j=1}^{\infty} \hat{b}_j \{\delta\tilde{q}\}^T \{F_j\}\{F_j\}^T \{\ddot{\tilde{q}}(t)\} = \{\delta\tilde{q}\}^T [M_{22}] \{\ddot{\tilde{q}}(t)\} \qquad \text{(II-b-15)}$$

where $$[M_{22}] = \sum_{j=1}^{\infty} \hat{b}_j \{F_j\}\{F_j\}^T \qquad \text{(II-b-16)}$$

Again, it should be noted that only the first few terms of the series are needed for adequate representation of the mass matrix $[M_{22}]$.

II-b-4. The Coupling Mass Matrix $[M_{12}]$

In order to determine the mass matrix $[M_{12}]$, two integrals have to be evaluated. One of these integrals is already obtained in terms of the free surface nodal displacements and can be expressed as

$$\int_0^R r\, \ddot{\xi}(r,t)\, J_n\left(\frac{\varepsilon_{jn} r}{R}\right) dr = \{F_j\}^T \{\ddot{\tilde{q}}\} \qquad \text{(II-b-17)}$$

where $\{F_j\}$ is defined by Eq. II-b-13.

Using the shell displacement model (Eq. 1.75), the second integral can be written as

$$\int_0^H \delta w(z)\,\cosh\left(\frac{\varepsilon_{jn} z}{R}\right) dz = \sum_{e=1}^{NEH} \int_0^{L_e} \{\delta\bar{d}\}_e^T \{\bar{N}(\bar{z})\} \cosh\left[\frac{\varepsilon_{jn}\left(\bar{z} + (e-1)L_e\right)}{R}\right] d\bar{z} \qquad \text{(II-b-18)}$$

Now, define the vectors $\{\bar{f}_j\}_e$ as the integrals

$$\{\bar{f}_j\}_e^T = \int_0^{L_e} \{\bar{N}(\bar{z})\}^T \cosh\left[\frac{\varepsilon_{jn}\left(\bar{z} + (e-1)L_e\right)}{R}\right] d\bar{z}$$

$$= \left[0,0,\bar{f}_{j3},\bar{f}_{j4},0,0,\bar{f}_{j7},\bar{f}_{j8}\right]_e \quad ; \quad e = 1,2,\ldots, NEH \qquad \text{(II-b-19)}$$

where

$$\bar{f}_{j3} = L_e\left(\left(\frac{6}{\beta_j^3} - \frac{1}{\beta_j}\right)\sinh \beta_j(e-1) + \frac{12}{\beta_j^4}\cosh \beta_j(e-1) + \right.$$

$$\left. \frac{6}{\beta_j^3}\sinh \beta_j e - \frac{12}{\beta_j^4}\cosh \beta_j e\right) ;$$

$$\bar{f}_{j4} = L_e^2\left(\frac{4}{\beta_j^3}\sinh \beta_j(e-1) + \left(\frac{6}{\beta_j^4} + \frac{1}{\beta_j^2}\right)\cosh \beta_j(e-1) + \right.$$

$$\left. \frac{2}{\beta_j^3}\sinh \beta_j e - \frac{6}{\beta_j^4}\cosh \beta_j e\right) ;$$

$$\bar{f}_{j7} = L_e\left(\frac{-6}{\beta_j^3}\sinh\beta_j(e-1) - \frac{12}{\beta_j^4}\cosh\beta_j(e-1) + \left(\frac{1}{\beta_j} - \frac{6}{\beta_j^3}\right)\sinh\beta_j e + \frac{12}{\beta_j^4}\cosh\beta_j e\right) ;$$

$$\bar{f}_{j8} = L_e^2\left(\frac{2}{\beta_j^3}\sinh\beta_j(e-1) + \frac{6}{\beta_j^4}\cosh\beta_j(e-1) + \frac{4}{\beta_j^3}\sinh\beta_j e - \left(\frac{1}{\beta_j^2} + \frac{6}{\beta_j^4}\right)\cosh\beta_j e\right) ;$$

and $\beta_j = \frac{\varepsilon_{jn} L_e}{R}$ $\qquad (j = 1,2,\ldots)$

If one defines the vectors $\{\bar{F}_j\}$ by $\{\bar{F}_j\} = \sum_{e=1}^{NEH} \{\bar{f}_j\}_e$, then Eq. II-b-18 can be expressed as

$$\int_0^H \delta w(z)\cosh\left(\frac{\varepsilon_{jn} z}{R}\right) dz = \{\delta q\}^T\{\bar{F}_j\} \qquad \text{(II-b-20)}$$

Inserting Eqs. II-b-17 and II-b-20 into the fifth term of Eq. 2.36 to obtain

$$\sum_{j=1}^{\infty} b_j\left(\int_0^H \delta w(z)\cosh\left(\frac{\varepsilon_{jn} z}{R}\right) dz\right)\left(\int_0^R r\,\ddot{\xi}(r,t)\,J_n\left(\frac{\varepsilon_{jn} r}{R}\right) dr\right)$$

$$= \sum_{j=1}^{\infty} b_j\{\delta q\}^T\{\bar{F}_j\}\{F_j\}^T\{\ddot{\tilde{q}}(t)\} = \{\delta q\}^T\left(\sum_{j=1}^{\infty} b_j\{\bar{F}_j\}\{F_j\}^T\right)\{\ddot{\tilde{q}}(t)\}$$

(II-b-21)

Eq. II-b-21 leads to the definition of the mass matrix $[M_{12}]$ as

$$[M_{12}] = \sum_{j=1}^{\infty} b_j \{\bar{F}_j\}\{F_j\}^T \qquad \text{(II-b-22)}$$

II-b-5. The Coupling Mass Matrix $[M_{21}]$

The sixth and seventh terms in Eq. 2.36 lead to the definition of the mass matrix $[M_{21}]$. With the aid of Eqs. II-b-7 and 2.37, these terms can be expressed as

$$\hat{a}_0\left(\int_0^R r^{n+1}\,\delta\xi(r)dr\right)\left(\int_0^H \ddot{w}(z,t)\,dz\right) + \sum_{i=1}^{\infty} \hat{a}_i\left(\int_0^R r\,\delta\xi(r) I_n\left(\frac{\lambda_i r}{H}\right)dr\right).$$

$$\left(\int_0^H \ddot{w}(z,t)\cos\left(\frac{\lambda_i z}{H}\right)dz\right) = \hat{a}_0\left(\sum_{e=1}^{NER}\int_0^{R_e}\left(\bar{r} + (e-1)R_e\right)^{n+1}\{\delta\bar{\xi}\}_e^T\{S(\bar{r})\}d\bar{r}\right).$$

$$\left(\{F_0\}^T\{\ddot{q}(t)\}\right) + \sum_{i=1}^{\infty}\hat{a}_i\left(\sum_{e=1}^{NER}\int_0^{R_e}\left(\bar{r} + (e-1)R_e\right)\{\delta\bar{\xi}\}_e^T\{S(\bar{r})\} I_n\left[\frac{\lambda_i\left(\bar{r} + (e-1)R_e\right)}{H}\right]d\bar{r}\right).$$

$$\left(\{F_i\}^T\{\ddot{q}(t)\}\right) \qquad \text{(II-b-23)}$$

Now, define the vectors $\{\bar{f}_0\}_e$, $\{\bar{f}_i\}_e$, $\{\bar{F}_0\}$, and $\{\bar{F}_i\}$ as follows:

$$\{\bar{f}_0\}_e = \int_0^{R_e}\left(\bar{r} + (e-1)R_e\right)^{n+1}\{S(\bar{r})\}d\bar{r} = \begin{Bmatrix}\bar{f}_{01}\\ \bar{f}_{02}\end{Bmatrix}_e ;$$

$$\{\bar{f}_i\}_e = \int_0^{R_e}\left(\bar{r} + (e-1)R_e\right) I_n\left[\frac{\lambda_i\left(\bar{r} + (e-1)\,R_e\right)}{H}\right]\{S(\bar{r})\}\,d\bar{r} = \begin{Bmatrix}\bar{f}_{i1}\\ \bar{f}_{i2}\end{Bmatrix}_e ;$$

$$\{\bar{F}_0\} = \sum_{e=1}^{NER}\{\bar{f}_0\}_e \quad ; \quad \text{and} \quad \{\bar{F}_i\} = \sum_{e=1}^{NER}\{\bar{f}_i\}_e \qquad \text{(II-b-24)}$$

where

$$\bar{f}_{01} = \frac{R_e^{n+2}}{(n+2)(n+3)}\left(e^{n+3} - (n+2+e)(e-1)^{n+2}\right) ;$$

$$\bar{f}_{02} = \frac{R_e^{n+2}}{(n+2)(n+3)}\left(e^{n+3}(n+3-e) + (e-1)^{n+3}\right) ;$$

$$\bar{f}_{i1} = R_e^2 \int_0^1 \left((e-1) + (2-e)y - y^2\right) I_n\left(\beta_i(e-1+y)\right) dy ;$$

$$\bar{f}_{i2} = R_e^2 \int_0^1 \left((e-1)y + y^2\right) I_n\left(\beta_i(e-1+y)\right) dy ;$$

$$\beta_i = \frac{\lambda_i R_e}{H} \quad (i = 1,2,\ldots) \quad ; \quad \text{and } y \text{ is a dummy variable.}$$

Using the definitions in Eq. II-b-24, one can write Eq. II-b-23 in the following convenient form

$$\hat{a}_0\left(\int_0^R r^{n+1}\delta\xi(r)dr\right)\left(\int_0^H \ddot{w}(z,t)dz\right) + \sum_{i=1}^{\infty} \hat{a}_i\left(\int_0^R r\,\delta\xi(r) I_n\left(\frac{\lambda_i r}{H}\right) dr\right).$$

$$\left(\int_0^H \ddot{w}(z,t)\cos\left(\frac{\lambda_i z}{H}\right) dz\right) = \hat{a}_0\{\delta\tilde{q}\}^T\{\bar{F}_0\}\{F_0\}^T\{\ddot{q}(t)\} + \sum_{i=1}^{\infty} \hat{a}_i\{\delta\tilde{q}\}^T\{\bar{F}_i\}\{F_i\}^T\{\ddot{q}(t)\}$$

$$= \{\delta\tilde{q}\}^T\left(\hat{a}_0\{\bar{F}_0\}\{F_0\}^T + \sum_{i=1}^{\infty} \hat{a}_i\{\bar{F}_i\}\{F_i\}^T\right)\{\ddot{q}(t)\} = \{\delta\tilde{q}\}^T[M_{21}]\{\ddot{q}(t)\} \qquad \text{(II-b-25)}$$

It is worthwhile to indicate that $[M_{12}]^T = [M_{21}]$, and therefore, the overall mass matrix [M] is symmetric (refer to Appendix II-c).

Appendix II-c

Symmetry of the Mass Matrix [M]

The proof of symmetry of the overall mass matrix

$$[M] = \left[\begin{array}{c|c} [M_s] + [M_{11}] & [M_{12}] \\ \hline [M_{21}] & [M_{22}] \end{array}\right] \qquad \text{(II-c-1)}$$

is given, in detail, in this appendix. It is clear from Eqs. 1.105, II-b-9, and II-b-16 that the matrices $[M_s]$, $[M_{11}]$, and $[M_{22}]$, respectively, are symmetric. Therefore, it remains to show that $[M_{12}]^T = [M_{21}]$, or equivalently, the analytical expressions used in the derivation of these two matrices are identical.

Recalling the expression that led to the definition of $[M_{12}]$ (Eq. II-b-21), and using the definition of b_j (Eq. 2.36), yield

$$I_1 = \sum_{j=1}^{\infty} b_j \left(\int_0^H \delta w(z) \cosh\left(\frac{\varepsilon_{jn} z}{R}\right) dz \right) \left(\int_0^R r \ddot{\xi}(r,t) J_n\left(\frac{\varepsilon_{jn} r}{R}\right) dr \right)$$

$$= \sum_{j=1}^{\infty} \left(\frac{2\pi\rho_\ell}{\varepsilon_{jn} \sinh\left(\frac{\varepsilon_{jn} H}{R}\right) \left(1 - \frac{n^2}{\varepsilon_{jn}^2}\right) J_n(\varepsilon_{jn})} \right) \cdot \left(\int_0^H \delta w(z) \cosh\left(\frac{\varepsilon_{jn} z}{R}\right) dz \right) \cdot$$

$$\left(\int_0^R r \ddot{\xi}(r,t) J_n\left(\frac{\varepsilon_{jn} r}{R}\right) dr \right) \qquad \text{(II-c-2)}$$

Now, expanding $\cosh\left(\frac{\varepsilon_{jn} z}{R}\right)$ in terms of $\cos\left(\frac{\lambda_i z}{H}\right)$ where $\lambda_i = i\pi$ ($i = 0,1,2, \ldots$), yields

$$\cosh\left(\frac{\varepsilon_{jn} z}{R}\right) = \alpha_0 + \sum_{i=1}^{\infty} \alpha_i \cos\left(\frac{\lambda_i z}{H}\right) \qquad \text{(II-c-3)}$$

where $\alpha_0 = \left(\frac{R}{\varepsilon_{jn} H}\right) \sinh\left(\frac{\varepsilon_{jn} H}{R}\right)$; and $\alpha_i = 2\left(\frac{R}{\varepsilon_{jn} H}\right) \sinh\left(\frac{\varepsilon_{jn} H}{R}\right) \frac{\cos\lambda_i}{\left(1 + \left(\frac{\lambda_i R}{\varepsilon_{jn} H}\right)^2\right)}$

Inserting Eq. II-c-3 into Eq. II-c-2, one can obtain

$$I_1 = \sum_{j=1}^{\infty} \left(\frac{2\pi R \rho_\ell}{\varepsilon_{jn}^2 H \left(1 - \frac{n^2}{\varepsilon_{jn}^2}\right) J_n(\varepsilon_{jn})}\right)\left(\int_0^R r\, \ddot{\xi}(r,t)\, J_n\left(\frac{\varepsilon_{jn} r}{R}\right) dr\right).$$

$$\left(\int_0^H \delta w(z)\, dz + \sum_{i=1}^{\infty} \frac{2\cos(\lambda_i)}{\left(1 + \left(\frac{\lambda_i R}{\varepsilon_{jn} H}\right)^2\right)} \int_0^H \delta w(z) \cos\left(\frac{\lambda_i z}{H}\right) dz\right) \qquad \text{(II-c-4)}$$

Similarly, using the integral of Eq. II-b-25 which defines $[M_{21}]$, and with the aid of the definitions of $\hat{a}_0$ and $\hat{a}_i$ (Eq. 2.36), one can write

$$I_2 = \hat{a}_0\left(\int_0^R r^{n+1} \delta\xi(r) dr\right)\left(\int_0^H \ddot{w}(z,t) dz\right) + \sum_{i=1}^{\infty} \hat{a}_i\left(\int_0^R r\, \delta\xi(r)\, I_n\left(\frac{\lambda_i r}{H}\right) dr\right).$$

$$\left(\int_0^H \ddot{w}(z,t) \cos\left(\frac{\lambda_i z}{H}\right) dz\right) = \left(\frac{\pi \rho_\ell}{nHR^{n-1}}\right)\left(\int_0^R r^{n+1} \delta\xi(r) dr\right)\left(\int_0^H \ddot{w}(z,t)\, dz\right)$$

$$+ \sum_{i=1}^{\infty} \left(\frac{2\pi\, \rho_\ell \cos(\lambda_i)}{\lambda_i' I_n\left(\frac{\lambda_i R}{H}\right)}\right)\left(\int_0^R r \delta\xi(r) I_n\left(\frac{\lambda_i r}{H}\right) dr\right)\left(\int_0^H \ddot{w}(z,t)\, \cos\left(\frac{\lambda_i z}{H}\right) dz\right)$$

(II-c-5)

Now, expand r^n and $I_n\left(\frac{\lambda_i r}{H}\right)$ in terms of $J_n\left(\frac{\varepsilon_{jn} r}{R}\right)$; it follows that

$$r^n = \sum_{j=1}^{\infty} \beta_j J_n\left(\frac{\varepsilon_{jn} r}{R}\right); \text{ and } I_n\left(\frac{\lambda_i r}{H}\right) = \sum_{j=1}^{\infty} \bar{\beta}_j J_n\left(\frac{\varepsilon_{jn} r}{R}\right) \qquad \text{(II-c-6)}$$

where

$$\beta_j = \left(\int_0^R r^{n+1} J_n\left(\frac{\varepsilon_{jn} r}{R}\right) dr\right) \Bigg/ \left(\int_0^R r J_n^2\left(\frac{\varepsilon_{jn} r}{R}\right) dr\right) = \frac{2 n R^n}{\varepsilon_{jn}^2 \left(1 - \frac{n^2}{\varepsilon_{jn}^2}\right) J_n(\varepsilon_{jn})};$$

and

$$\bar{\beta}_j = \left(\int_0^R r I_n\left(\frac{\lambda_i r}{H}\right) J_n\left(\frac{\varepsilon_{jn} r}{R}\right) dr\right) \Bigg/ \left(\int_0^R r J_n^2\left(\frac{\varepsilon_{jn} r}{R}\right) dr\right)$$

$$= \frac{2 R \lambda_i I_n'\left(\frac{\lambda_i R}{H}\right)}{H \varepsilon_{jn}^2 \left(1 - \frac{n^2}{\varepsilon_{jn}^2}\right) J_n(\varepsilon_{jn}) \left(1 + \left(\frac{\lambda_i R}{\varepsilon_{jn} H}\right)^2\right)}$$

In view of Eq. II-c-6, Eq. II-c-5 can be written as

$$I_2 = \sum_{j=1}^{\infty} \left(\frac{2\pi R \rho_\ell}{\varepsilon_{jn}^2 H \left(1 - \frac{n^2}{\varepsilon_{jn}^2}\right) J_n(\varepsilon_{jn})}\right) \left(\int_0^R r \, \delta\xi(r) J_n\left(\frac{\varepsilon_{jn} r}{R}\right) dr\right) \cdot$$

$$\left(\int_0^H \ddot{w}(z,t) dz + \sum_{i=1}^{\infty} \frac{2 \cos(\lambda_i)}{\left(1 + \left(\frac{\lambda_i R}{\varepsilon_{jn} H}\right)^2\right)} \int_0^H \ddot{w}(z,t) \cos\left(\frac{\lambda_i z}{H}\right) dz\right) \qquad \text{(II-c-7)}$$

Because the interpolation functions for $\delta\xi(r)$ and $\delta w(z)$ are taken to be the same as those for $\ddot{\xi}(r,t)$ and $\ddot{w}(z,t)$, respectively, the

expression given in Eq. II-c-7 is in precisely the same form as that of Eq. II-c-4, and therefore

$$[M_{12}]^T = [M_{21}] \qquad \text{(II-c-8)}$$

REFERENCES OF CHAPTER II

1. Leissa, A.W., ed., "Vibration of Shells," NASA SP-288, National Aeronautics and Space Administration, Washington, D.C., 1973.

2. Washizu, K., Variational Methods in Elasticity and Plasticity, Pergamon Press, 1975.

3. Novozhilov, V.V., Thin Shell Theory, P. Noordhoff LTD., Groningen, The Netherlands, 1964.

4. Shih, C., and Babcock, C.D., California Institute of Technology, Personal Communication.

5. Hsiung, H.H., and Weingarten, V.I., "Dynamic Analysis of Hydroelastic Systems Using the Finite Element Method," Department of Civil Engineering, University of Southern California, Report USCCE 013, November 1973.

6. Shaaban, S.H., and Nash, W.A., "Finite Element Analysis of a Seismically Excited Cylindrical Storage Tank, Ground Supported, and Partially Filled with Liquid," University of Massachusetts Report to National Science Foundation, August 1975.

7. Balendra, T., and Nash, W.A., "Earthquake Analysis of a Cylindrical Liquid Storage Tank with a Dome by Finite Element Method," Department of Civil Engineering, University of Massachusetts, Amherst, Massachusetts, May 1978.

8. Wu, C.I., Mouzakis, T., Nash, W.A., and Colonell, J.M., "Natural Frequencies of Cylindrical Liquid Storage Containers," Department of Civil Engineering, University of Massachusetts, June 1975.

9. Yang, J.Y., "Dynamic Behavior of Fluid-Tank Systems," Ph.D. Thesis, Rice University, Houston, Texas, 1976.

10. Edwards, N.W., "A Procedure for Dynamic Analysis of Thin Walled Cylindrical Liquid Storage Tanks Subjected to Lateral Ground Motions," Ph.D. Thesis, University of Michigan, Ann Arbor, Michigan, 1969.

11. U.S. Atomic Energy Commission, "Nuclear Reactors and Earthquakes," TID-7024, Washington, D.C., 1963, pp. 367-390.

CHAPTER III

EARTHQUAKE RESPONSE OF DEFORMABLE LIQUID STORAGE TANKS

A method for analyzing the earthquake response of deformable, cylindrical liquid storage tanks is presented. The method is based on superposition of the free lateral vibrational modes obtained by a finite element approach and boundary solution techniques. A procedure for computing the natural modes of vibration was given in the preceding chapters, and the accuracy of these modes is confirmed by vibration tests of full-scale tanks as shown in Chapter IV.

The first topic, presented in Sec. III-1, is concerned with the response of the $\cos\theta$-type modes for which there is a single cosine wave of deflection in the circumferential direction. The effective load history resulting from a given ground motion is evaluated, and the seismic response is obtained by superposition of the vertical modes corresponding to $n = 1$. Furthermore, the earthquake response of deformable tanks is compared with that of similar rigid tanks to assess the influence of wall flexibility on their seismic behavior. Detailed numerical examples are also presented to illustrate the variation of the seismic response of two different classes of tanks, namely, "broad" and "tall" tanks.

The second section is devoted to examining the influence of the $\cos n\theta$-type modes on the earthquake response of tanks. Until recently, it was thought that only the $\cos\theta$-type modes would be excited significantly by seismic motions; however, shaking table experiments with aluminum tank models [1,2] and vibration tests on full-scale tanks

(refer to Chapter IV) show that cosnθ-type modes do respond to base excitations. For a perfect circular tank, cosnθ-type modes cannot be excited by rigid base motion; however, fabrication tolerances permit a significant departure from the nominal circular cross section and this tends to excite these modes. The importance of the cosnθ-type modes in an earthquake response analysis is evaluated by computing the seismic response of a hypothetical irregular tank. The hydrodynamic pressure consists therefore of two components: (i) the pressure that would result in a perfectly circular tank, and (ii) a corrective pressure arising due to cross-section irregularity.

In summary, the dynamic fluid pressure p_d on the wall of the tank is given by the superposition of four pressure components:

$$p_d = p_1 + p_2 + p_3 + p_4$$

where the pressure components are:

p_1 = the long period component contributed by the convective fluid motion (sloshing) in a tank with rigid walls;

p_2 = the impulsive fluid pressure component which varies in synchronism with the horizontal ground acceleration;

p_3 = the short period component contributed by the cosθ-type vibrations of the tank walls;

and p_4 = the contributions of the cosnθ-type vibrations of the tank walls.

Each of these four pressures has a different variation with time. It can be expected that long period pressures, if sufficiently large, will be effective in producing buckling quasi-statically. The effect of the short period pressures will be important to the degree that they influence the dynamic buckling process, or to the extent that high stresses produced by them lead to possible fracture of the tank wall.

III-1. Cosθ-Type Response to Earthquake Excitation

The liquid storage tank under consideration is subjected to a ground motion G(t) in the constant direction $\theta = 0$ as shown in Fig. III-1. It is assumed that the tank has perfect circular cross sections of radius R. Under these assumptions, only the cosθ-type modes will be excited; therefore, its seismic response can be obtained by superposition of the different vertical modes corresponding to $n = 1$.

The only special feature of the earthquake-response problem, compared with any other form of dynamic loading, is that the excitation is applied in the form of support motions rather than by external loads; thus the essential subject of the present discussion is the method of defining the effective external load history resulting from a given form of support motion. The evaluation of such effective loading can be carried out by two different methods.

In the first approach, the effective earthquake load vector can be derived in a manner entirely analogous to the development of the effective force vector for a lumped multi-degree of freedom system whose equations of motion can be written as

$$[M]\{\ddot{q}^t\} + [C]\{\dot{q}\} + [K]\{q\} = \{0\} \tag{3.1}$$

where [M], [C], and [K] are the mass, damping, and stiffness matrices, respectively; and $\{q^t\}$ is the total displacement vector which can be expressed as

$$\{q^t\} = \{q\} + \{r\}G(t) \tag{3.2}$$

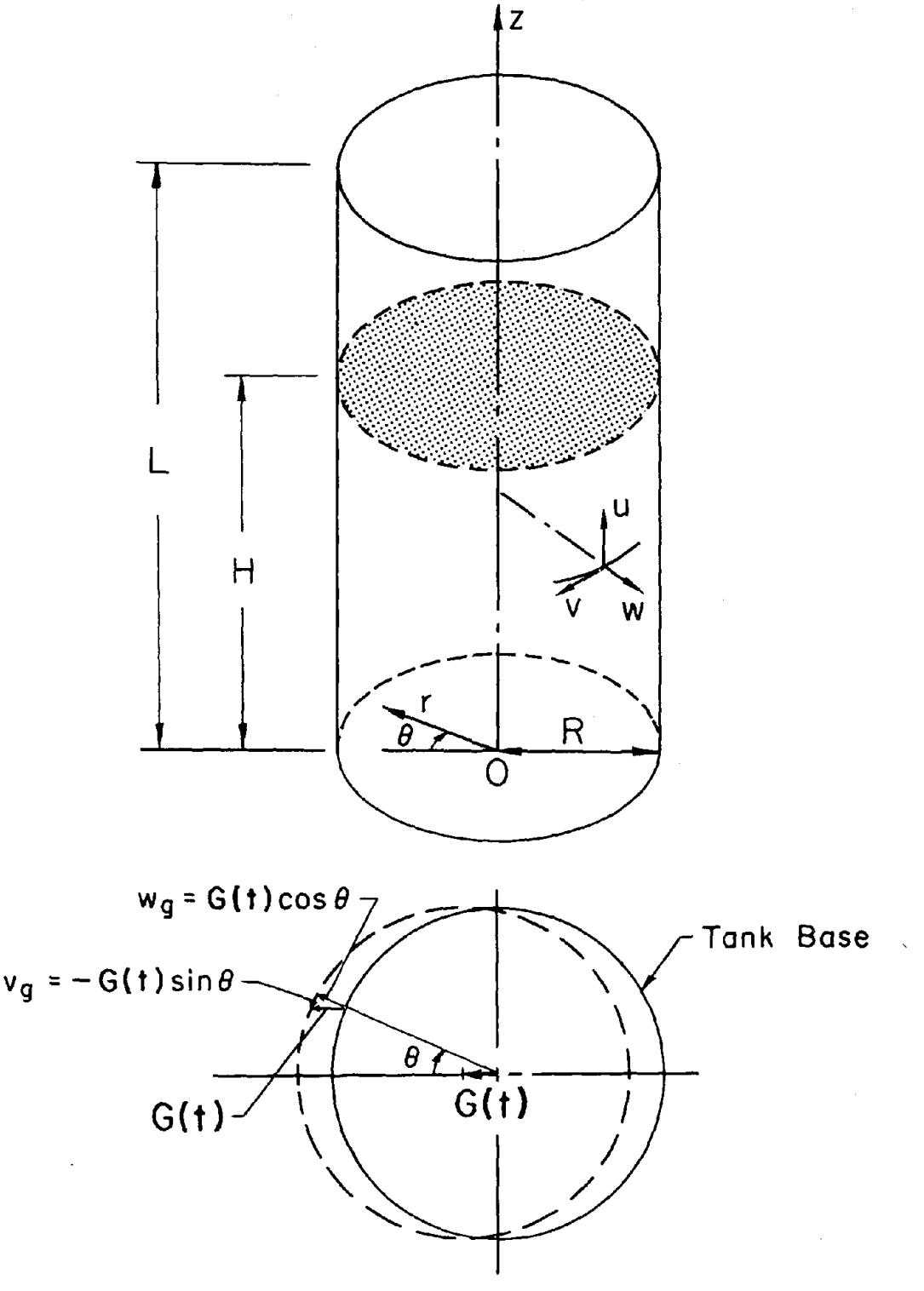

Fig. III-1. Tank Motion Due to Ground Excitation.

where $\{q\}$ is the relative displacement vector; $\{r\}$ is the influence coefficient vector which represents the displacements resulting from a unit support displacement; and $G(t)$ is the ground displacement.

Substituting Eq. 3.2 into Eq. 3.1 leads to the relative-response equations of motion

$$[M]\{\ddot{q}\} + [C]\{\dot{q}\} + [K]\{q\} = \{P_{eff}\} \tag{3.3}$$

where

$$\{P_{eff}\} = - [M]\{r\}\ddot{G}(t) \tag{3.4}$$

The matrix equations of motion which govern the earthquake response of the liquid-shell system are identical in form to the lumped-mass equations described above, except that the off-diagonal coefficients in the overall mass matrix (of the shell and its base) introduce coupling between the support displacement and the response degrees of freedom. By partitioning the overall mass matrix into matrices associated with the support degrees of freedom and into matrices associated with the response degrees of freedom (off-base nodes), the equations of motion can then be written as

$$[M]\{\ddot{q}^t\} + [M_c]\{\hat{r}\}\ddot{G}(t) + [C]\{\dot{q}\} + [K]\{q\} = \{0\} \tag{3.5},$$

and therefore, the effective force vector can be given by

$$\{P_{eff}\} = - \left([M]\{r\} + [M_c]\{\hat{r}\} \right) \ddot{G}(t) \tag{3.6}$$

where $[M_c]$ is the coupling mass matrix between the support displacement and the response degrees of freedom; and $\{\hat{r}\}G(t)$ is the generalized

displacement vector of the tank base. In most cases, the second term in the right hand side of Eq. 3.6 contributes little to the earthquake excitation load; however, it should be included in the formulation for completeness [3].

The development of the effective earthquake load vector can also be carried out by employing the expression of the work done by external loads through arbitrary virtual displacements $\{\delta d\}$. This approach is particularly effective in evaluating the force vector for an out-of-round circular tank (refer to Sec. III-2); and therefore, it is adopted throughout this investigation.

III-1-1. The Effective Force Vector

The total displacement vector of the shell can be considered as the sum of two components: the relative displacement vector $\{d\}$ defined by Eq. 1.31, and the displacement vector $\{d_g\}$ associated with the ground displacement G(t); it can be written as

$$\{d_g\} = \begin{Bmatrix} 0 \\ -\sin(\theta) \\ \cos(\theta) \end{Bmatrix} G(t) \tag{3.7}$$

The external forces acting on the shell due to ground motion G(t) include

(i) the distributed inertia force of the shell which is given by

$$\{F_g\} = -\rho_s h\{\ddot{d}_g\} = -\rho_s h\ddot{G}(t) \begin{Bmatrix} 0 \\ -\sin(\theta) \\ \cos(\theta) \end{Bmatrix} \tag{3.8};$$

and (ii) the hydrodynamic pressure on the tank wall, assumed to be rigid. This pressure can be obtained by substituting $\ddot{G}(t)$ in Eq. 1.137 instead of $\ddot{w}_n(z,t)$ and replacing the circumferential wave number n by 1; thus,

$$p_g(R,\theta,z,t) = -\frac{2\rho_\ell}{H} \sum_{i=1}^{\infty} \frac{\int_0^H \ddot{G}(t) \cos(\alpha_i \eta)\, d\eta}{\alpha_i' I_1(\alpha_i R)} I_1(\alpha_i R) \cos(\alpha_i z) \cos(\theta)$$

$$= -\frac{2\rho_\ell \ddot{G}(t)}{H} \sum_{i=1}^{\infty} \frac{(-1)^{i+1} I_1(\alpha_i R)}{\alpha_i^2 I_1(\alpha_i R)} \cos(\alpha_i z) \cos(\theta) \qquad (3.9)$$

The work done by these external loads during arbitrary virtual displacements

$$\{\delta d\} = \begin{Bmatrix} \delta u_1 \cos(\theta) \\ \delta v_1 \sin(\theta) \\ \delta w_1 \cos(\theta) \end{Bmatrix} \qquad (3.10)$$

can be expressed as

$$\delta W = \int_0^L \int_0^{2\pi} \left(\{F_g\}^T \{\delta d\} \right) R\, d\theta\, dz + \int_0^H \int_0^{2\pi} \left(p_g(R,\theta,z,t)\, \delta w_1 \cos(\theta) \right) R\, d\theta\, dz \qquad (3.11)$$

Substituting Eqs. 3.8, 3.9, and 3.10 into Eq. 3.11 yields

$$\delta W = -\rho_s \pi R \ddot{G}(t) \int_0^L h(-\delta v_1 + \delta w_1) dz$$

$$- \frac{2\pi R \rho_\ell \ddot{G}(t)}{H} \sum_{i=1}^{\infty} \left(\frac{(-1)^{i+1} I_1(\alpha_i R)}{\alpha_i^2 I_1'(\alpha_i R)} \right) \cdot \left(\int_0^H \delta w_1 \cos(\alpha_i z)\, dz \right)$$

$$= -\ddot{G}(t) \left\{ \rho_s \pi R \int_0^L h(-\delta v_1 + \delta w_1) dz + \sum_{i=1}^{\infty} b_i \int_0^H \delta w_1 \cos(\alpha_i z) dz \right\} \tag{3.12}$$

where

$$b_i = \frac{2\pi R \rho_\ell I_1(\alpha_i R)}{\alpha_i^2 H I_1'(\alpha_i R)} (-1)^{i+1} \tag{3.13}$$

With the aid of the shell displacement model (Eq. 1.74), the first term in Eq. 3.12 becomes

$$\rho_s \pi R \int_0^L h(-\delta v_1 + \delta w_1) dz = \rho_s \pi R \sum_{e=1}^{NEL} h^e \{\delta \bar{d}\}_e^T \{\bar{f}\}_e = \{\delta q\}^T \{\bar{F}\} \tag{3.14}$$

where

$$\{\bar{f}\}_e^T = \left[0 \;, -\frac{L_e}{2} \;, \frac{L_e}{2} \;, \frac{L_e^2}{12} \;, 0 \;, -\frac{L_e}{2} \;, \frac{L_e}{2} \;, -\frac{L_e^2}{12} \right] \tag{3.15}$$

and

$$\{\bar{F}\} = \sum_{e=1}^{NEL} \rho_s \pi R h^e \{\bar{f}\}_e \tag{3.16}$$

Furthermore, the second term in Eq. 3.12 can be expressed as

$$\sum_{i=1}^{\infty} b_i \int_0^H \delta w_1 \cos(\alpha_i z) dz = \sum_{i=1}^{\infty} b_i \{\delta q\}^T \{F^{(i)}\} = \{\delta q\}^T \{\bar{\bar{F}}\} \tag{3.17}$$

where $\{F^{(i)}\}$ is given by Eq. 1.143; and

$$\{\bar{\bar{F}}\} = \sum_{i=1}^{\infty} b_i \{F^{(i)}\} \tag{3.18}$$

It is important to note that the series in Eq. 3.18 converges very rapidly and only the first few terms are needed for adequate representation of the infinite series.

Substituting Eqs. 3.14, and 3.17 into Eq. 3.12, the virtual work expression can then be written as

$$\delta W = -\ddot{G}(t)\{\delta q\}^T\left(\{\bar{F}\} + \{\bar{\bar{F}}\}\right) = -\ddot{G}(t)\{\delta q\}^T\{F\} \tag{3.19};$$

and therefore, the effective earthquake load vector is given by

$$\{P_{eff}\} = -\{F\}\ddot{G}(t) \tag{3.20}$$

III-1-2. Modal Analysis

The matrix equations which govern the earthquake response of the undamped liquid-shell system are given by

$$[M]\{\ddot{q}\} + [K]\{q\} = \{P_{eff}\} \tag{3.21}$$

where $\{q\}$ is the nodal displacement vector, $[M] = [M_s] + [DM]$; $[M_s]$ and $[DM]$ are the shell mass matrix (Eq. 1.106) and the added mass matrix (Eq. 1.146), respectively, $[K] = [K_s]$; $[K_s]$ is the shell stiffness matrix (Eq. 1.98), and $\{P_{eff}\}$ is the effective earthquake load vector (Eq. 3.20). It should be noted that only the impulsive response

is being investigated, and that the added stiffness matrix has been neglected in Eq. 3.21 since its effect on the cosθ-type modes is insignificant as shown in Sec. II-1.

Eq. 3.21 can be solved directly by numerical integration; however, in analyzing the earthquake response of linear structures, it is generally more efficient to use modal superposition to evaluate the seismic response, since the support motion tends to excite strongly only the lowest modes of vibration. Thus, good approximation of the earthquake response can be obtained by carrying out the analysis for only a few natural modes.

Now, let

$$\{q\} = [\overset{*}{Q}]\{\eta(t)\} \tag{3.22}$$

where $[\overset{*}{Q}]$ is a rectangular matrix of the order N × J which contains the modal displacement vectors associated with the lowest J natural frequencies (i.e., $[\overset{*}{Q}] = [\{\overset{*}{q}\}_1 , \{\overset{*}{q}\}_2,\ldots,\{\overset{*}{q}\}_J]$); N is the number of degrees of freedom (4 × NEL); and $\{\eta(t)\}$ is the modal amplitude vector.

Substituting Eq. 3.22 into Eq. 3.21 yields

$$[M][\overset{*}{Q}]\{\ddot{\eta}\} + [K][\overset{*}{Q}]\{\eta\} = \{P_{eff}\} \tag{3.23}$$

Premultiply by $[\overset{*}{Q}]^T$ and employ the definition of the effective load vector (Eq. 3.20), one obtains

$$[\overset{*}{Q}]^T[M][\overset{*}{Q}]\{\ddot{\eta}\} + [\overset{*}{Q}]^T[K][\overset{*}{Q}]\{\eta\} = -[\overset{*}{Q}]^T\{F\}\ddot{G}(t) \tag{3.24}$$

which can be written, more conveniently, as

$$[\overset{*}{M}]\{\ddot{\eta}\} + [\overset{*}{K}]\{\eta\} = -\{\overset{*}{F}\}\ddot{G}(t) \tag{3.25}$$

where $[\overset{*}{M}]$ and $[\overset{*}{K}]$ are the generalized mass and stiffness matrices, respectively, of the order J × J; and $\{\overset{*}{F}\}\ddot{G}(t)$ is the generalized force vector of the order J × 1.

Because of the orthogonality conditions of the natural modes, namely,

$$\{\overset{*}{q}\}_i^T[M]\{\overset{*}{q}\}_j = \{\overset{*}{q}\}_i^T[K]\{\overset{*}{q}\}_j = 0 \quad (i \neq j) \tag{3.26}$$

the generalized mass and stiffness matrices are diagonal. Furthermore, the diagonal terms of the generalized stiffness matrix can be written as

$$\overset{*}{K}_{jj} = \omega_j^2 \overset{*}{M}_{jj} = \omega_j^2 \{\overset{*}{q}\}_j^T[M]\{\overset{*}{q}\}_j \quad ; \quad j = 1,2,\ldots,J \tag{3.27}$$

Therefore, Eq. 3.25 reduces to J independent differential equations for the unknowns η_j

$$\ddot{\eta}_j + \omega_j^2 \eta_j = -\frac{\overset{*}{F}_j}{\overset{*}{M}_{jj}} \ddot{G}(t) \quad ; \quad j = 1,2,\ldots,J \tag{3.28}$$

Introducing damping into Eq. 3.28, then one can rewrite such equation as follows

$$\ddot{\eta}_j + 2\zeta_j\omega_j\dot{\eta}_j + \omega_j^2\eta_j = -\beta_j\ddot{G}(t) \quad ; \quad j = 1,2,\ldots J \tag{3.29}$$

where β_j are the modal participation factors defined by

$$\beta_j = \frac{\overset{*}{F}_j}{\overset{*}{M}_{jj}} \quad ; \quad j = 1,2,\ldots J \tag{3.30}$$

The modal amplitudes $\eta_j(t)$ can be found by employing either the convolution integral or a step by step integration scheme; in this analysis, we employ the integration scheme developed in [5]. For $\ddot{G}(t)$ given by a segmentally linear function, for $t_i \leq t \leq t_{i+1}$, Eq. 3.29 becomes

$$\ddot{\eta}_j + 2\zeta_j\omega_j\dot{\eta}_j + \omega_j^2\eta_j = -\beta_j\left(\ddot{G}_i + \frac{\Delta\ddot{G}_i}{\Delta t}\left(t - t_i\right)\right) \tag{3.31}$$

where $\Delta\ddot{G}_i = \ddot{G}_{i+1} - \ddot{G}_i$; and $\Delta t = t_{i+1} - t_i$ = constant. The solution of Eq. 3.31 at time $t = t_{i+1}$ can be expressed in terms of that at $t = t_i$ by [5]

$$\begin{Bmatrix} \eta_{i+1} \\ \dot{\eta}_{i+1} \end{Bmatrix} = \left[A(\zeta,\omega,\Delta t)\right]\begin{Bmatrix} \eta_i \\ \dot{\eta}_i \end{Bmatrix} + \left[B(\zeta,\omega,\Delta t,\beta)\right]\begin{Bmatrix} \ddot{G}_i \\ \ddot{G}_{i+1} \end{Bmatrix} \tag{3.32}$$

in which the subscript j is omitted for brevity. Therefore, if the modal amplitude $\eta(t)$ and its time derivative $\dot{\eta}(t)$ are known at t_i, then the complete time history can be computed by a step by step application of Eq. 3.32. The advantage of this method lies in the fact that for a constant time interval Δt, the matrices [A] and [B] depend only on ζ, ω, and β, and are constant during the calculation of the response.

Once the η's and their time derivatives are obtained, the displacements, the force and moment resultants, and the hydrodynamic pressures can be evaluated as explained in the following subsection.

III-1-3. Computer Implementation and Numerical Examples

A digital computer program has been written to compute the earthquake response of partly filled tanks by the method outlined in the preceding subsections. The program "RESPONSE" employs first the program "FREE VIBRATION" to obtain the free vibrational modes. Then it formulates the generalized mass and load vectors, and computes shell nodal displacements and accelerations which are used to solve for the shell force and moment resultants, for the hydrodynamic pressures, and for base shear.

Example 1: A Tall Tank

The computer program is first utilized to estimate the earthquake response of an open top tall tank whose vibrational modes are obtained in Chapter I. The tank has the following dimensions: R = 24 ft, L = 72 ft, and h = 1 inch, and it is assumed to be full of water. The input ground motion is the N-S component of the 1940 El Centro earthquake; only the first ten seconds of the record are employed in the analysis and this portion is displayed in Fig. III-2-a. The modal damping ratio of the liquid-shell system is assumed to be 2%.

The time history of the relative radial component of shell acceleration at the tank top and in the $\theta = 0$ direction, $\ddot{w}(0,L,t)$, is shown in Fig. III-2-b for comparison with the ground acceleration; it is clear that the relative acceleration is much greater than that of the ground. Figures III-3-a and b show the time history of the radial and tangential components of shell displacement, respectively, at the top of the tank while Figs. III-4-a and b display the time history of the

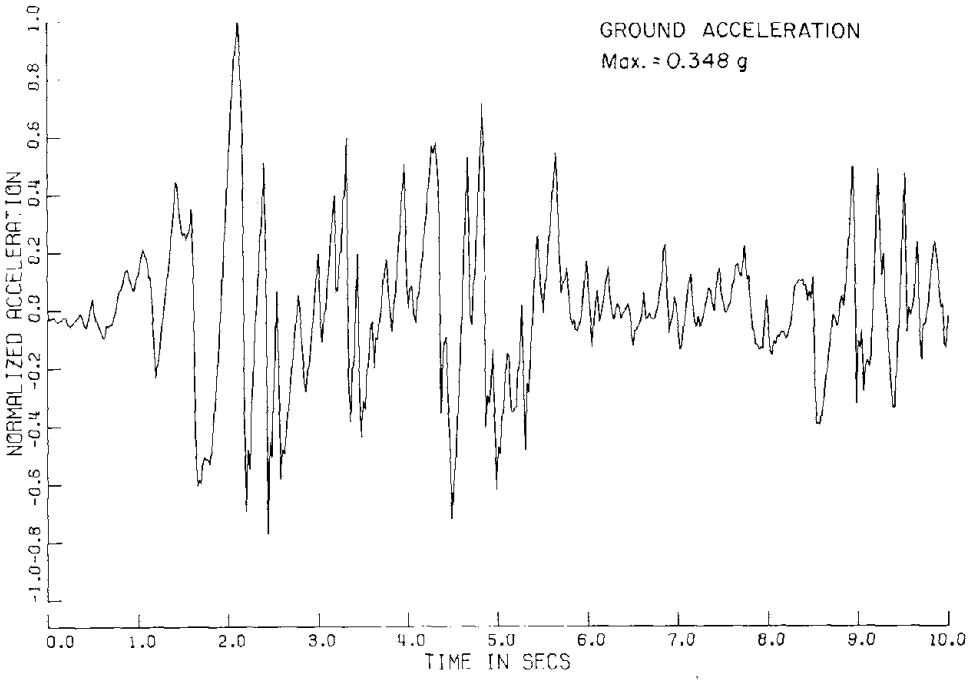

(a) N-S Component of the 1940 El Centro Earthquake.

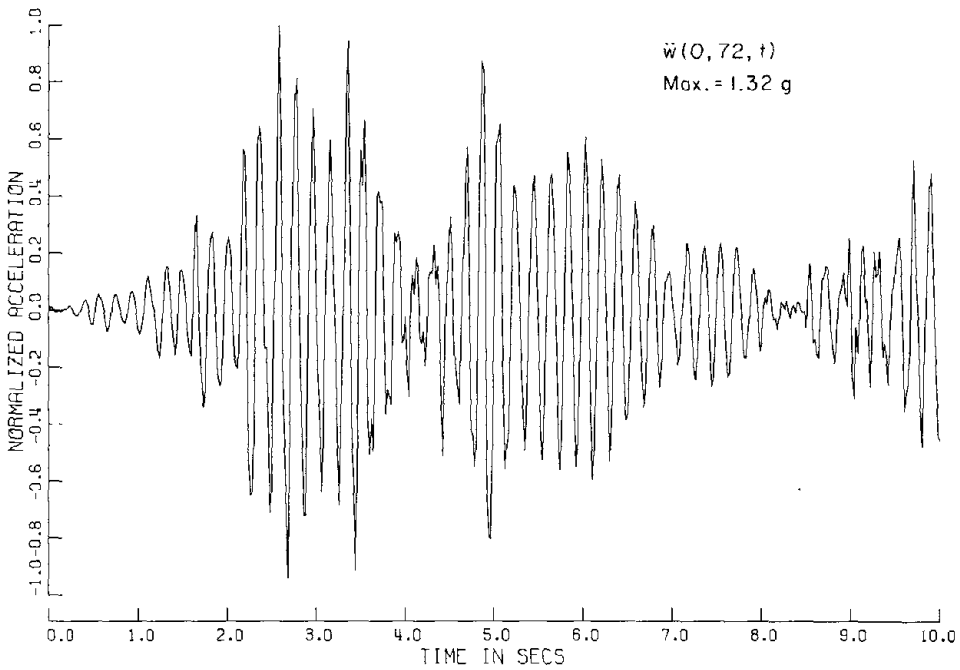

(b) Time History of the Relative Radial Component of Shell Acceleration at the Tank Top in the $\theta = 0$ Direction.

Fig. III-2

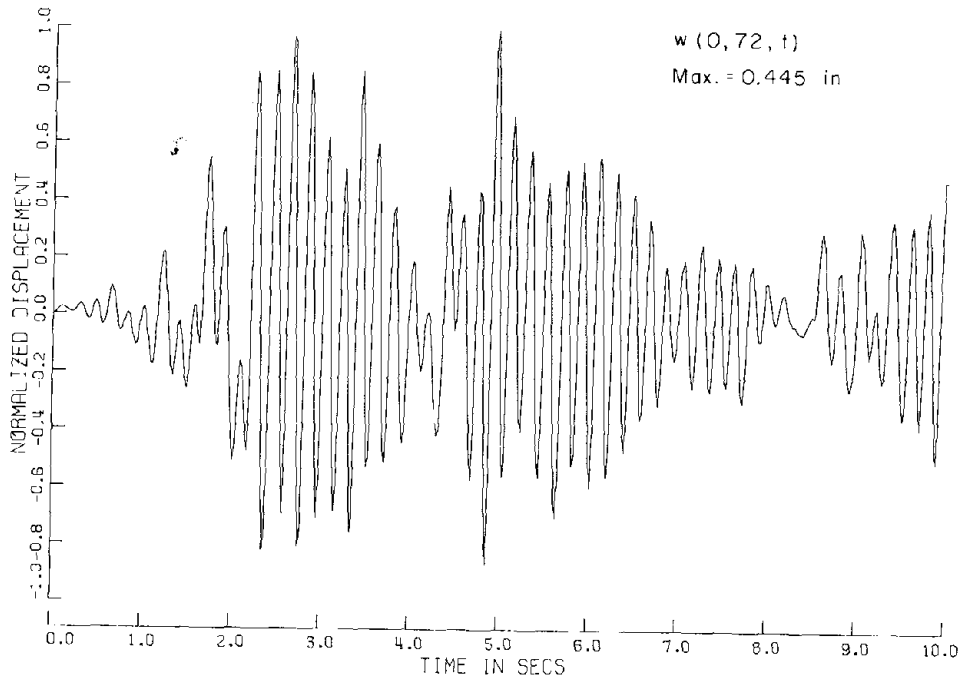

(a) Time History of the Relative Radial Component of Shell Displacement at the Tank Top in the $\theta = 0$ Direction.

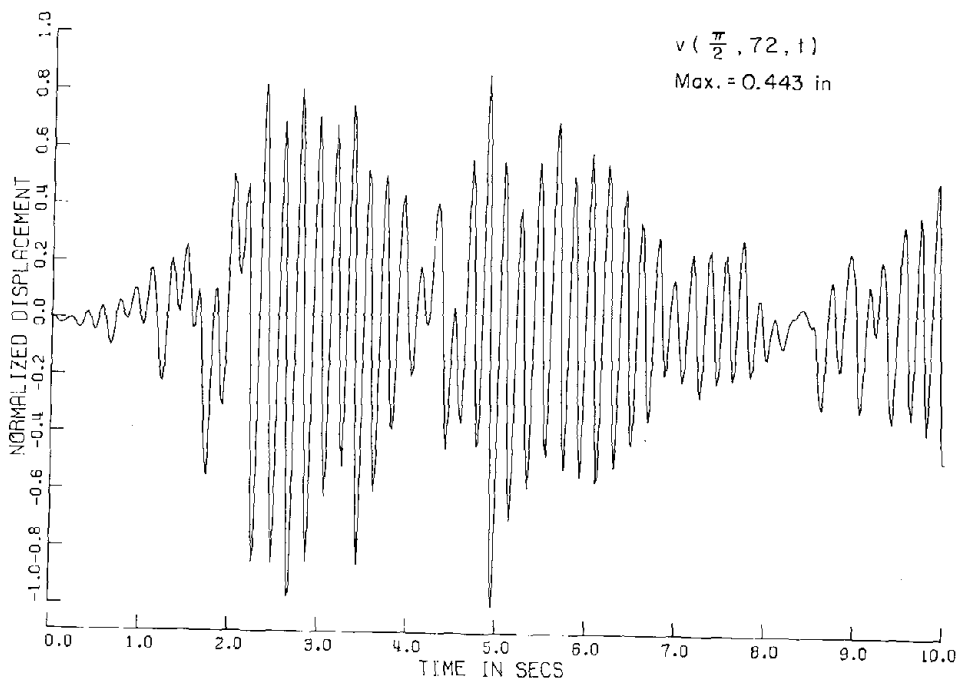

(b) Time History of the Relative Tangential Component of Shell Displacement at the Tank Top in the $\theta = \frac{\pi}{2}$ Direction.

Fig. III-3

radial components of acceleration and displacement, respectively, at mid-height.

To check the accuracy of the time integration scheme employed in Eq. 3.32, the maximum relative displacement $w_{max}(0,L,t)$ is computed using El Centro response spectrum; it can be approximately estimated by

$$w_{max}(0,L,t) = \beta S_d \overset{*}{q}_{47} \tag{3.33}$$

where β is the earthquake participation factor of the fundamental mode; S_d is the spectral displacement corresponding to the fundamental period; and $\overset{*}{q}_{47}$ is the modal amplitude of the radial mode shape at the top of the tank. Hence, $w_{max}(0,L,t) = (1.55)(0.295)(1.0) = 0.457$ inch which is in close agreement with the value of 0.445 inch obtained by time integration of Eq. 3.32 and superposition of 4 modes of vibration. This also indicates that the displacement response of the tank is due mainly to the fundamental mode.

Having obtained the relative displacements of the shell, the force and moment resultants can be computed. Figure III-5 displays the time histories of the membrane force resultant N_z computed at 3 ft and at 9 ft above the base. To compare these stresses with those induced in a similar rigid tank, one can make use of Housner mechanical model [6]. The elements of such model are given by $m_0 = 0.902$ m and $H_0 = 0.375$ H where m is the total mass of the contained liquid. The impulsive moment is therefore given by

$$M_{max} = \left(m_0 H_0 + m_s \frac{L}{2}\right) \ddot{G}_{max} = 74.78 \times 10^6 \text{ lb. ft} \tag{3.34}$$

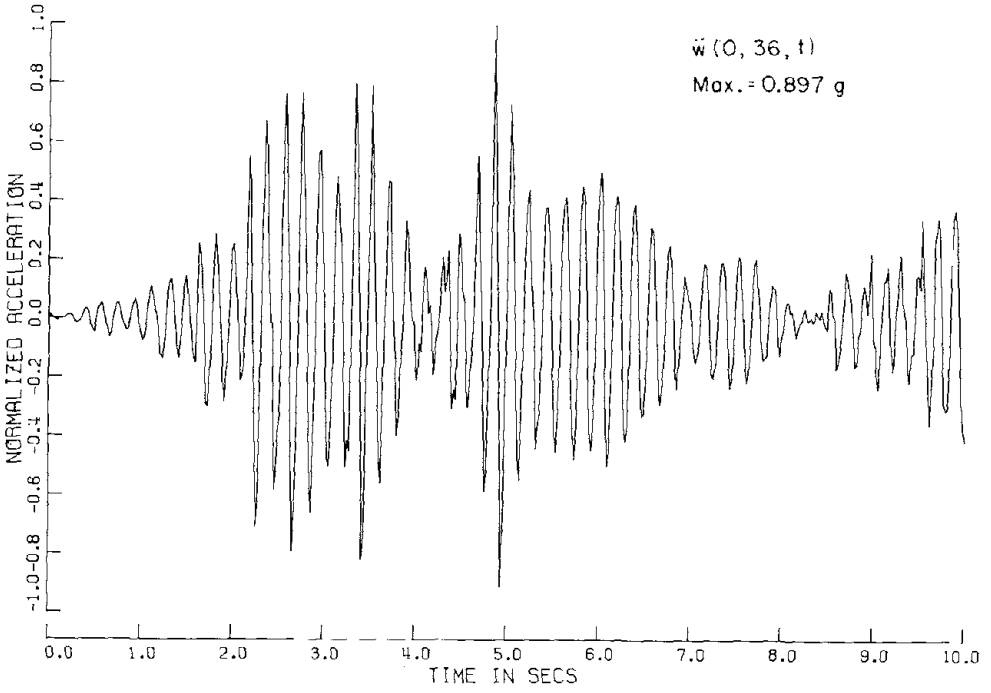

(a) Time History of the Relative Radial Component of Shell Acceleration at Mid-height in the $\theta = 0$ Direction.

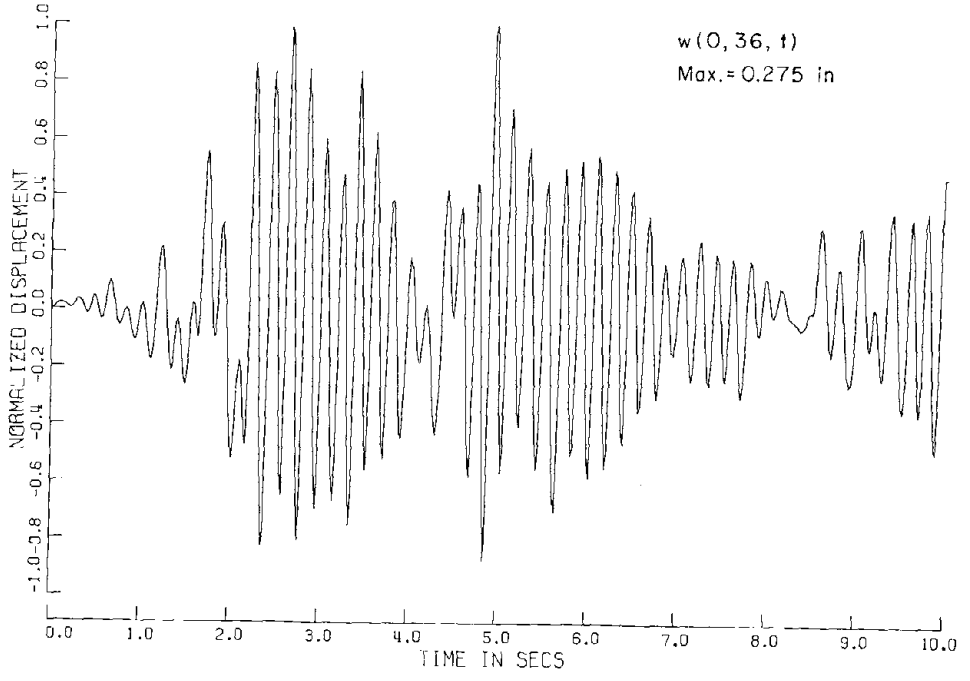

(b) Time History of the Relative Radial Component of Shell Displacement at Mid-height in the $\theta = 0$ Direction.

Fig. III-4

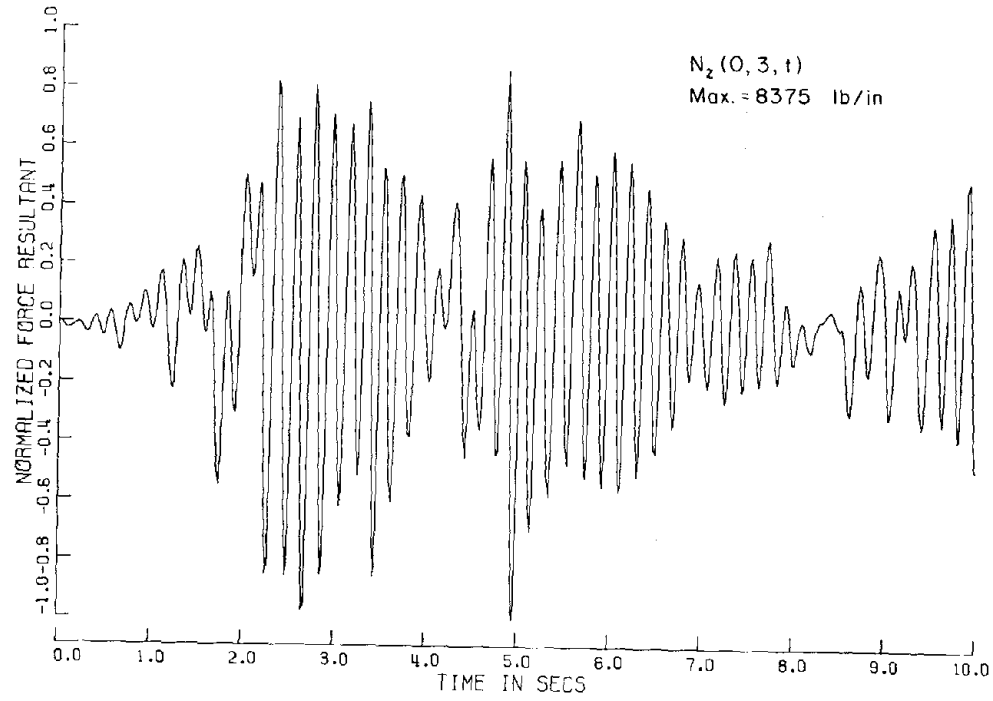

(a)

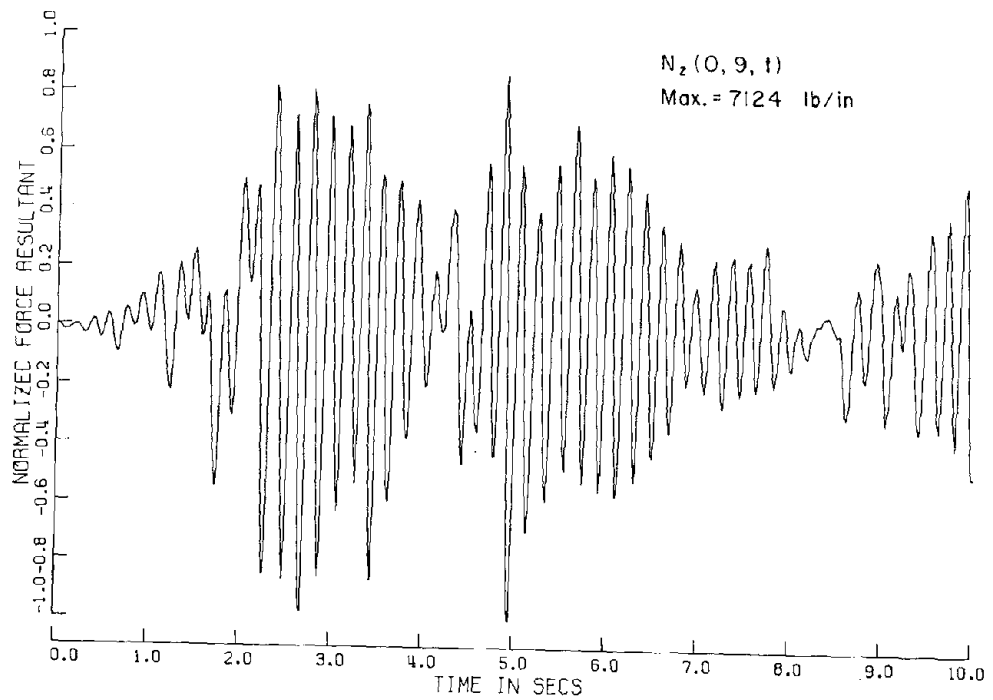

(b)

Fig. III-5. Time History of Axial Membrane Force Resultants.

which produces axial membrane force resultant

$$\left(N_z\right)_{max} = \frac{M_{max}}{\pi R^2} = 3443.8 \text{ lb/in}$$

It is clear that such force resultant is much lower than that in a flexible tank. This is due to the fact that the impulsive loads arise through acceleration of the shell. If the shell is flexible, two acceleration components must be considered: (i) the acceleration of the undeformed shell, i.e., the ground acceleration, and (ii) the relative acceleration due to shell deformations. In a rigid tank, only the acceleration of the undeformed shell is considered which introduces the noticeable difference in the magnitude of shell stresses. To further clarify this point, consider, for illustration purpose, that the masses m_0 and m_s are attached to the tank wall by springs with stiffnesses that simulate the fundamental natural period of the tank. To estimate the impulsive moment, one has to employ the spectral acceleration which is 2.46 time the ground acceleration, and therefore, the maximum axial membrane force is given by

$$\left(N_z\right)_{max} = 3443.8 \times 2.46 = 8471.8 \text{ lb/in}$$

which is in close agreement with that obtained by shell analysis.

The time history of the membrane force resultant N_θ at a distance of 6 ft above the base is shown in Fig. III-6-a; its maximum value is 2166 lb/in. To compare with that obtained in a similar rigid tank, one has to compute the hydrodynamic pressure. For a rigid tank, the maximum

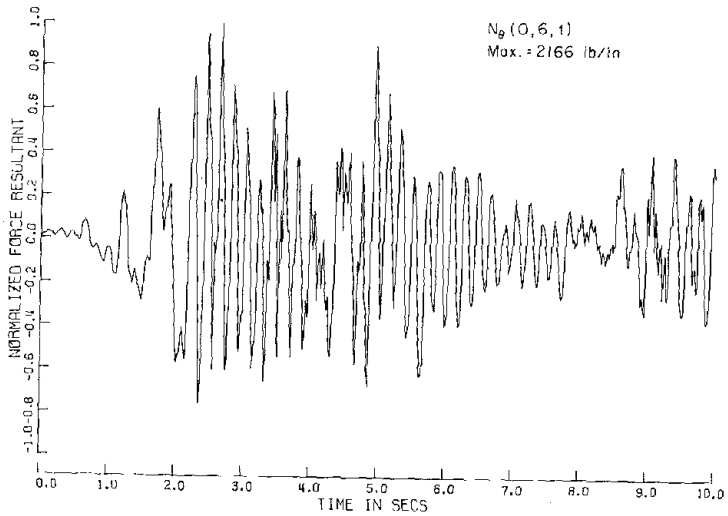

(a) Tangential Membrane Force Resultant (N_θ).

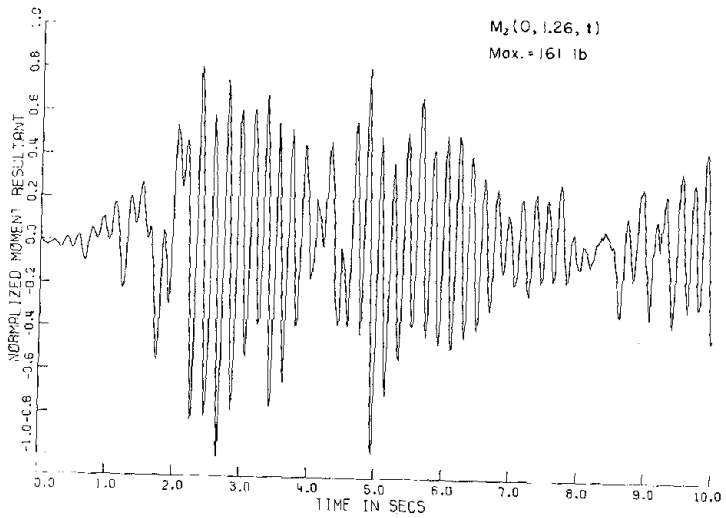

(b) Moment Resultant (M_z).

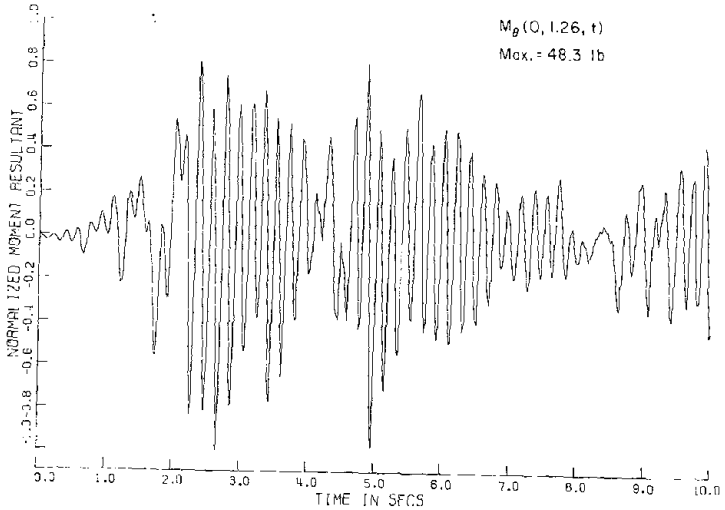

(c) Moment Resultant (M_θ).

Fig. III-6

hydrodynamic pressure occurs at the bottom of the container; its value is given by [6]

$$p_d(R,0,0,t) = \frac{\sqrt{3}\ \rho_\ell H \ddot{G}}{2} \tanh\left(\frac{\sqrt{3}\ R}{H}\right) = 4.92 \text{ psi} \qquad (3.35),$$

and consequently, the maximum dynamic membrane force resultant can be computed by

$$N_\theta(0,0,t)_{max} = \left(p_d\right)_{max} \cdot R = 1417 \text{ lb/in}$$

which is less than that of a flexible tank.

The time histories of the moment resultants M_z and M_θ are shown in Figs. III-6-b and c, respectively; these moments have negligible effect on the extreme fiber stresses of the shell.

As is known, the impulsive hydrodynamic pressure consists of two components: one due to ground acceleration and one due to the relative acceleration of the deformed shell. Figures III-7-a and b display the time histories of these pressures at a distance of 7.2 ft above the base. The maximum value of the hydrodynamic pressure due to ground acceleration only is 3.63 psi which is less than that obtained by Eq. 3.35; however, it is pointed out in [7] that the Housner model overestimates the hydrodynamic pressure for this particular H/R by about 33% which indicates close agreement between the computed pressure and the "exact" pressure in rigid tanks. The maximum additional pressure due to shell deformation at 7.2 ft above the base is 1.33 time that due to ground acceleration; however, the ratio is much larger at higher elevations as shown in Fig. III-8. It should be noted that the maximum

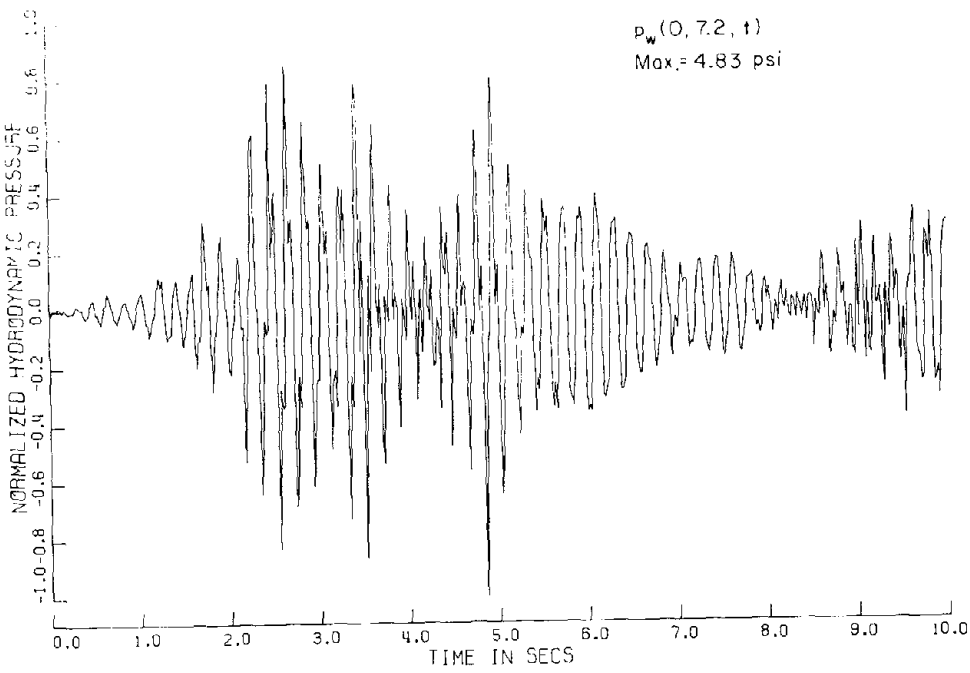

(a)

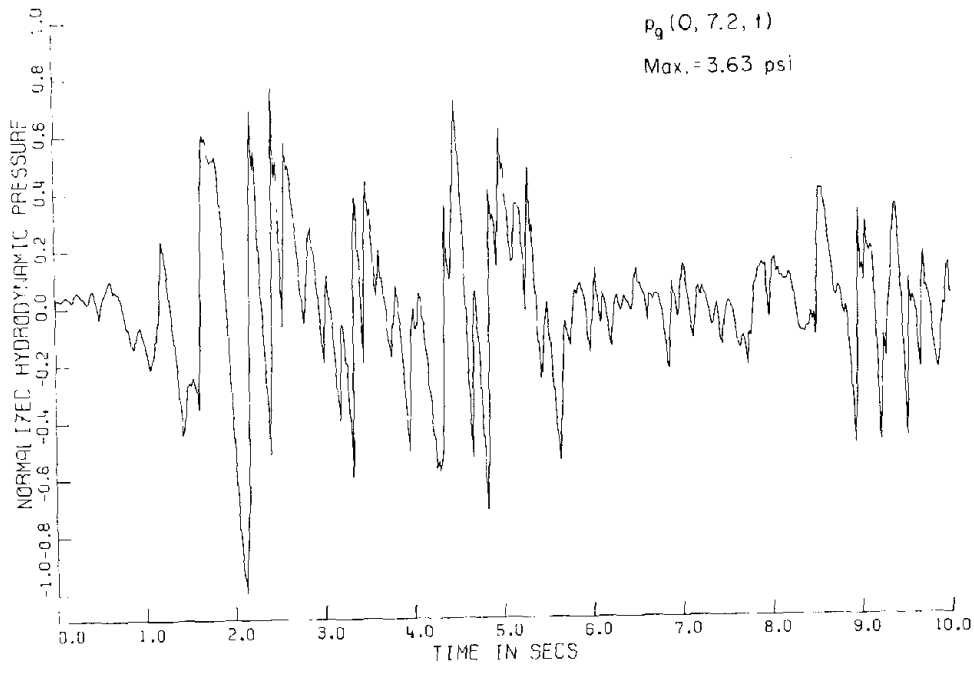

(b)

Fig. III-7. Time History of Hydrodynamic Pressures.

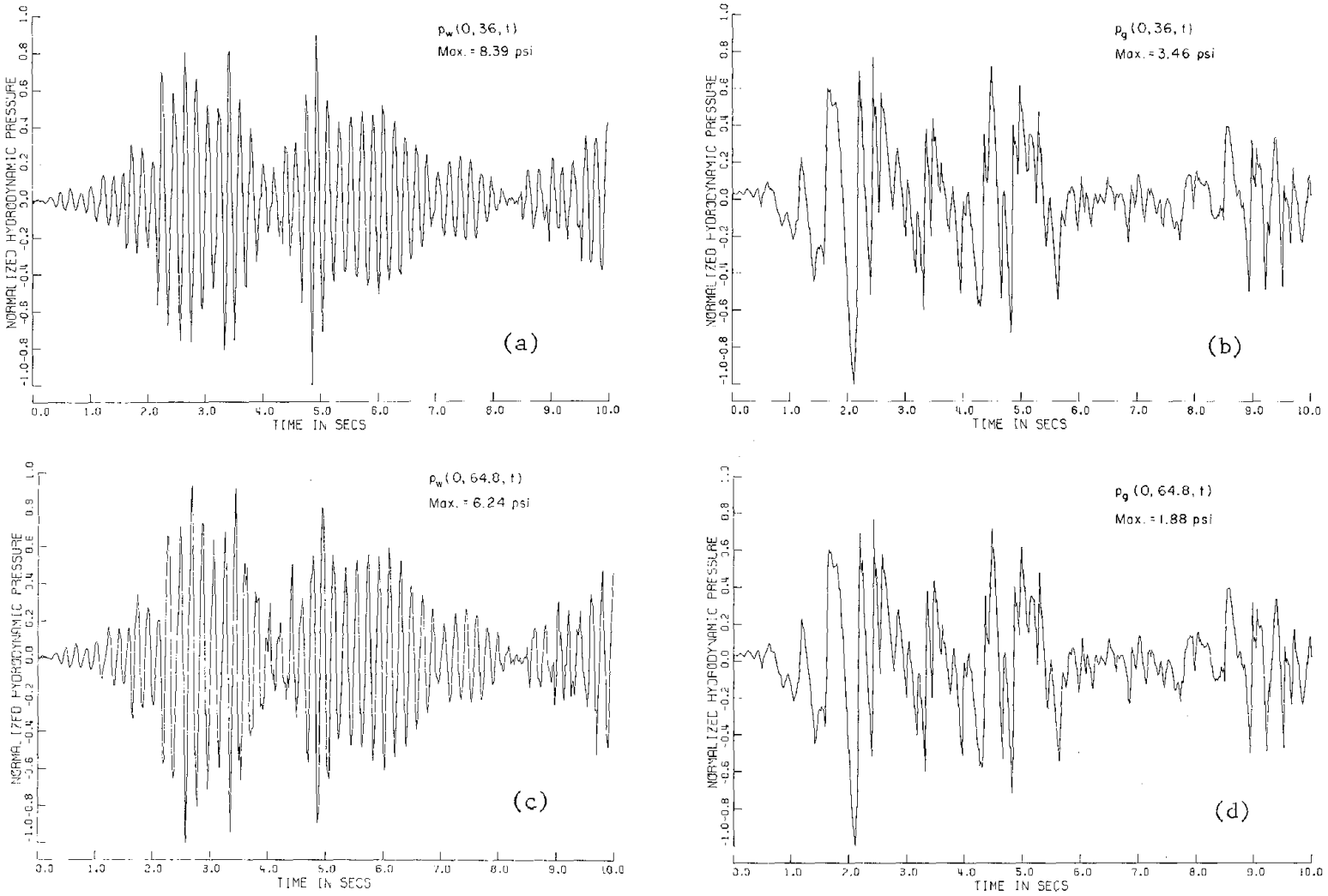

Fig. III-8. Time History of Hydrodynamic Pressures

amplitudes of these two components of the impulsive hydrodynamic pressure do not occur, in general, at the same time.

The impulsive base shear $Q_g(t)$ due to ground acceleration only and the total impulsive base shear $Q(t)$ are shown in Fig. III-9. The maximum base shear $\left(Q_g(t)\right)_{max}$ is in good agreement with that computed for rigid tanks which is given by

$$\left(Q_g\right)_{max} = (m_0 + m_s)\ddot{G}_{max} = 27.18 \times 10^5 \text{ lbs} \qquad (3.36)$$

The slight difference between this value and that of the present analysis is due to the fact that the Housner model overestimates the impulsive mass m_0 for tall tanks. The total impulsive base shear is also checked by the method presented in [7] where the liquid-shell system is analyzed using Flügge shell theory in combination with a Ritz-type procedure and the natural modes of vibration of uniform cantilever beams. The analysis gives a value of 52.47×10^5 lbs which is in close agreement with the value of 51.08×10^5 lbs obtained in the present analysis. It should be noted that the analysis in [7] is applicable only to uniform shells which are completely filled with liquid.

The troublesome aspect of analyzing the earthquake response of storage tanks is to define the appropriate value of damping. It can only be estimated from earthquake response of real tanks; unfortunately, seismic response data from tanks during past earthquakes are not available. Although a modal damping ratio of 2% seems appropriate for the liquid-shell system, the foundation soil also dissipates energy

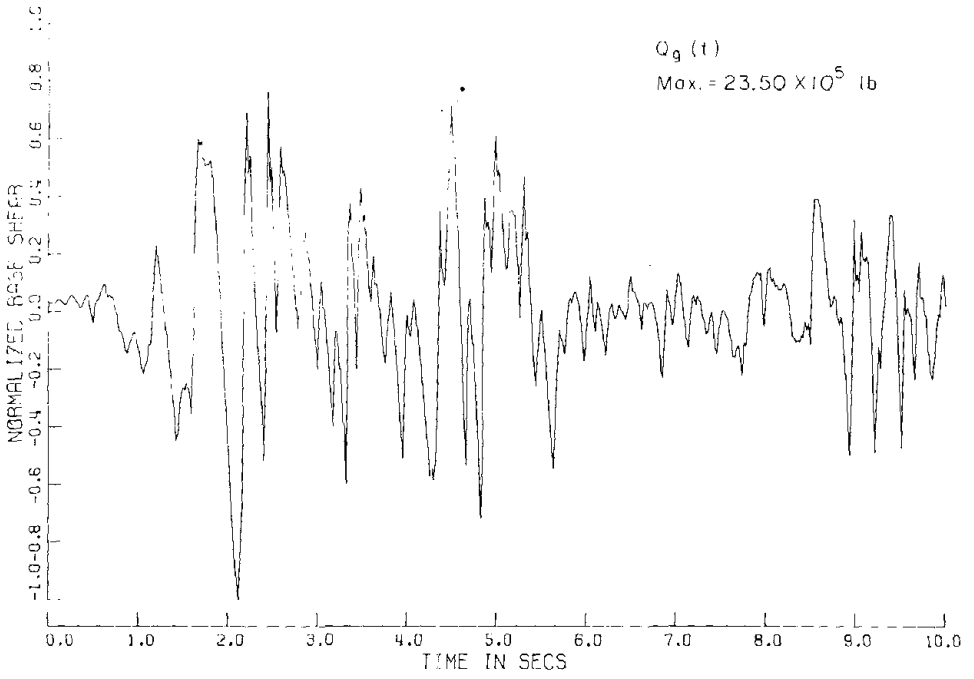

(a) Impulsive Base Shear Due to Ground Motion Only.

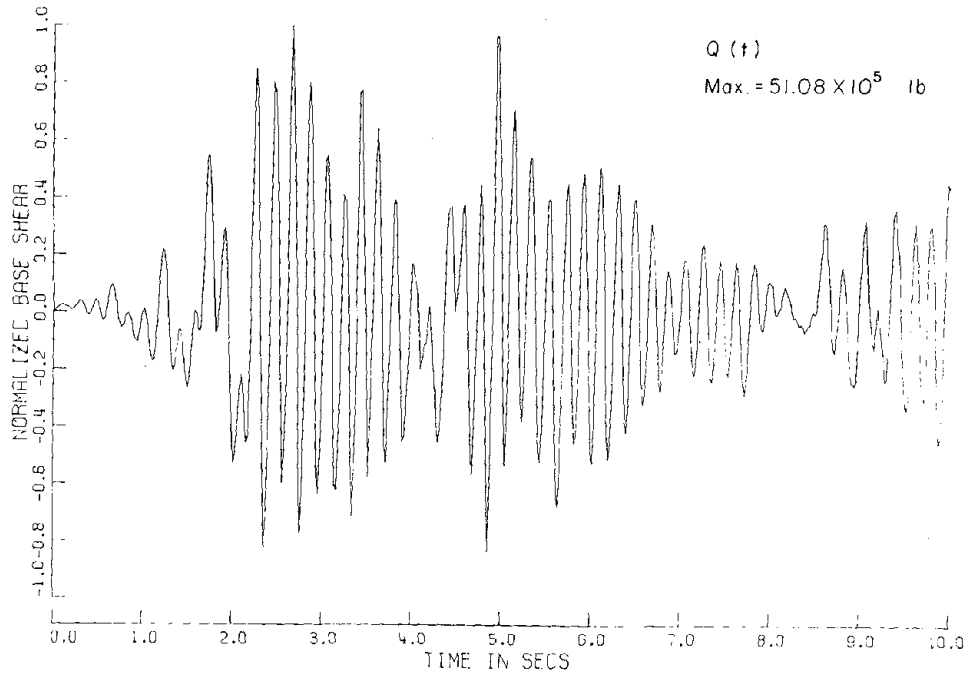

(b) Total Impulsive Base Shear.

Fig. III-9. Time History of Base Shear.

TABLE III-1

IMPULSIVE EARTHQUAKE RESPONSE OF A TALL TANK

INPUT: N-S COMPONENT OF THE 1940 EL CENTRO EARTHQUAKE

	Damping			Rigid Tank
	2%(*)	5%(**)	10%(**)	
Maximum Radial Component of Shell Displacement $w(0,72,t)$	0.445 inch	0.344 inch	0.296 inch	-
Maximum Axial Force Resultant $N_z(0,3,t)$	8375 lb/in	6473 lb/in	5564 lb/in	3444 lb/in
Maximum Tangential Force Resultant $N_\theta(0,6,t)$	2166 lb/in	1674 lb/in	1439 lb/in	1417 lb/in
Maximum Base Shear $Q(t)$	51.08×10^5 lbs	39.47×10^5 lbs	33.94×10^5 lbs	27.18×10^5 lbs

* Computed by time integration.
** Computed by response spectrum.

which cannot be exactly evaluated. For illustration purposes, Table III-1 presents the maximum radial component of shell displacement, the maximum axial and tangential force resultants and the maximum base shear computed for different values of damping ratio ζ; it also displays those in a similar rigid tank for comparison.

Example 2: A Tall Tank (Comparison with Shaking Table Results)

To illustrate the effectiveness of the analysis under consideration, the computed earthquake response of an open top tall tank is compared with that obtained by shaking table tests [2]. The tank model is made of aluminum whose modulus of elasticity is 10×10^6 psi and its density is 0.244×10^{-3} lb$\cdot$sec^2/in^4. The model has the following dimensions: R = 3.875 ft, L = 15 ft, and h = 0.09 inch in the lower 10 ft of its length and h = 0.063 inch in the upper 5 ft. The tank is partly filled with water to a depth of 13 ft. The input motion is the N-S component of the 1940 El Centro earthquake speeded by a factor of 1.73 and applied with a maximum acceleration of 0.5g as shown in Fig. III-10-a.

The time history of the computed radial component of shell acceleration at the tank top and in the $\theta = 0$ direction is displayed in Fig. III-10-b for comparison with input acceleration. Figs. III-11-a and b show the time history of the computed membrane force resultants while Figs. III-12-a and b show the time history of both the impulsive base shear due to ground motion only and of the total impulsive base shear, respectively. In addition, Table III-2 presents a comparison

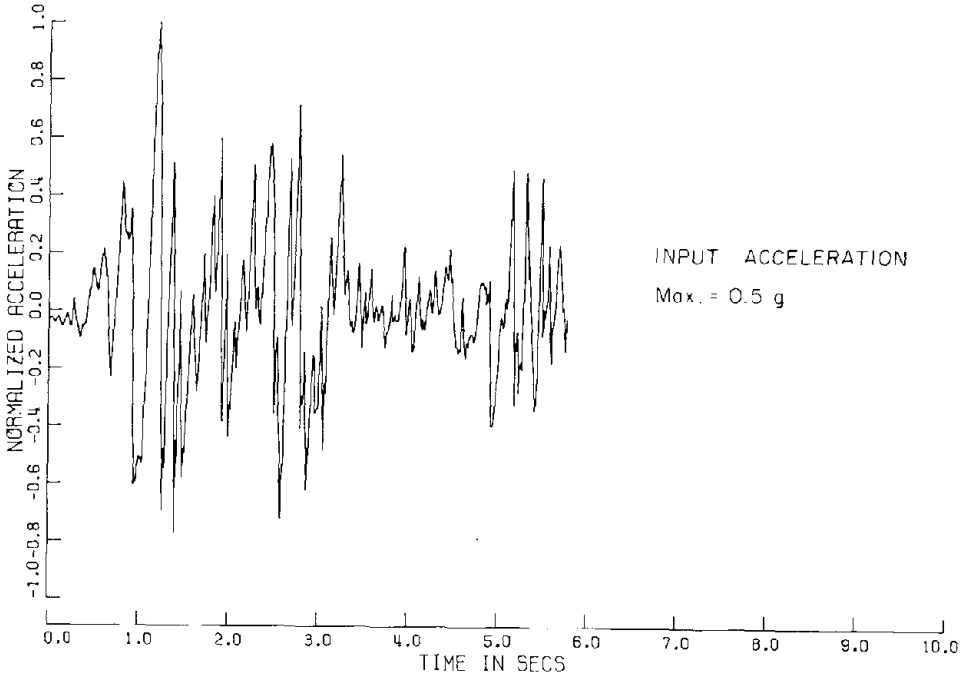

(a) Input Acceleration

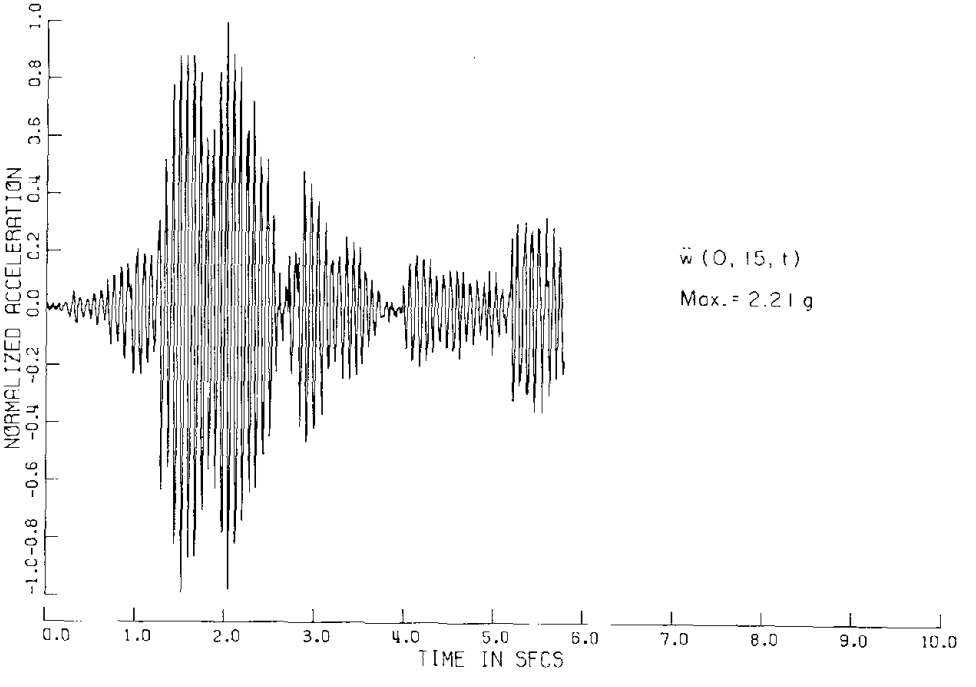

(b) Time History of the Radial Component of Shell Acceleration at the Tank Top in the $\theta = 0$ Direction

Fig. III-10.

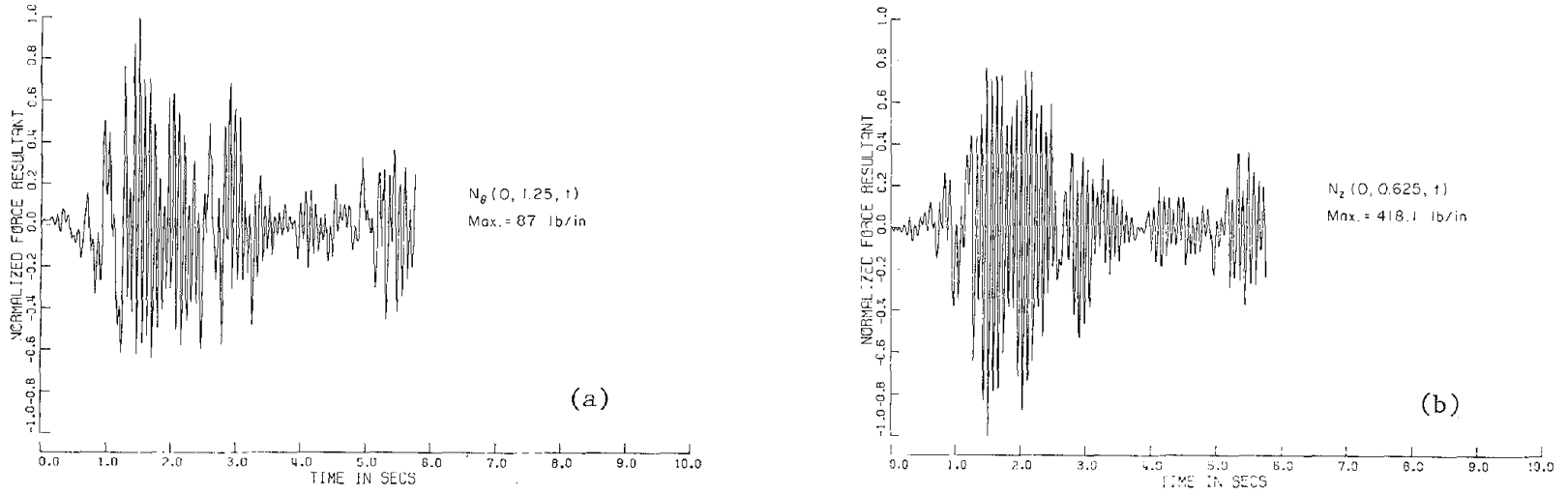

Fig. III-11. Time History of Membrane Force Resultants.

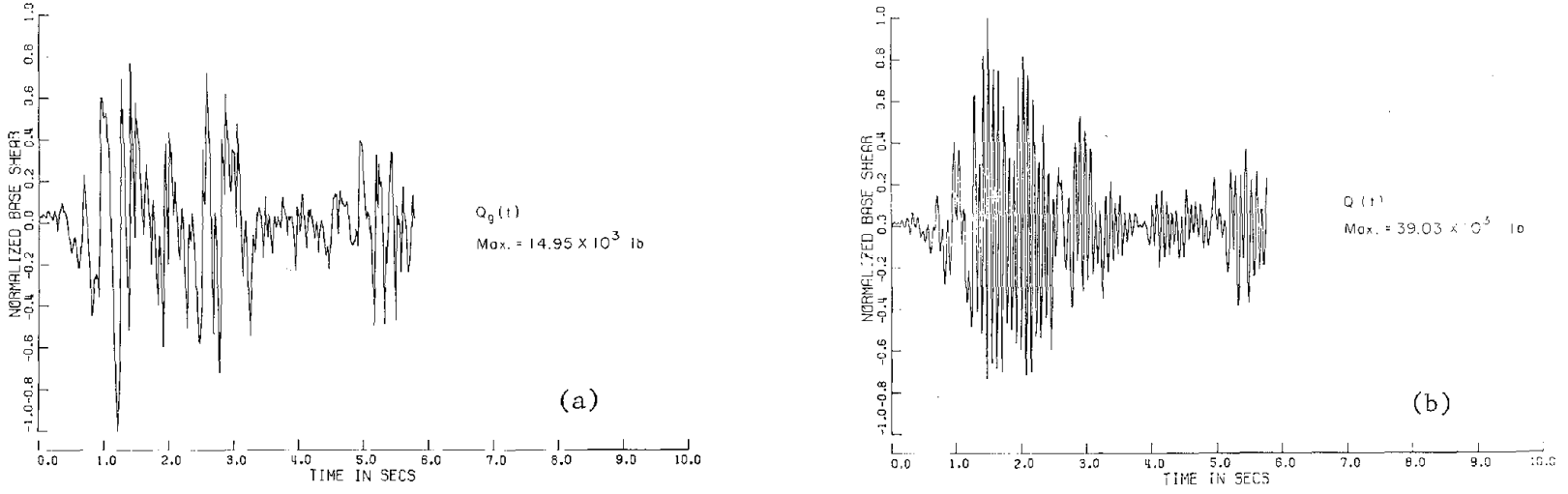

Fig. III-12. Time History of Impulsive Base Shear.

TABLE III-2

COMPARISON WITH SHAKING TABLE TESTS [2]

	Flexible (ζ = 2%)(*) (impulsive only)	Rigid (impulsive only)	Observed(*)
Max. Radial Component of Shell Displacement w (0,15,t)	0.150 inch	-	0.131 inch
Max. Axial Force Resultant N_z (0,0.625,t)	418.1 lb/in	155.3 lb/in	362.6 lb/in
Max. Base Shear Q(t)	3.90×10^4 lbs	1.79×10^4 lbs	2.75×10^4 lbs

(*) The input motion used in calculation of tank response is not identical to the actually applied shaking table acceleration.

TABLE III-3

COMPARISON OF SPECTRAL ACCELERATIONS

Periods T secs	Spectral Acceleration (g)		
	El Centro Record (Speeded Version)		Shaking Table Input
	ζ = 0%	ζ = 2%	ζ = 1%
0.077	2.80	1.45	0.95
0.100	2.45	1.43	0.88
0.200	1.92	1.18	2.08
0.400	2.57	1.28	1.56
0.800	0.60	0.35	0.49
1.200	0.46	0.32	0.38

between the computed and observed response; it also displays the response of a similar rigid tank for comparison.

Inspection of Table III-2 indicates that the computed and observed responses are much higher than those computed for a rigid tank. It can also be seen that the seismic response of a flexible tank computed by the present method is higher than the observed response in a shaking table test. However, one must keep in mind that the input acceleration used in the calculation of the response is different than the actually applied acceleration in these tests.

It is found that the input acceleration used in shaking table tests does not exactly resemble the motion of the 1940 El Centro earthquake, especially at the fundamental natural frequency of the model as shown in Table III-3. In this table, a comparison between the spectral accelerations for different natural periods is made; only the response spectrum for 1% damping ratio is available in [2], and this is compared with the spectral values obtained from [5] for 0% and 2% damping ratios and for a maximum ground acceleration of 0.5g. Because the response spectrum given in [5] is for the actual El Centro record (not the speeded up version employed in the calculations), the natural periods T are multiplied first by the 1.73 speed factor and then employed to obtain the spectral accelerations listed in Table III-3.

For the fundamental period of vibration of the model, the spectral acceleration of the actually applied motion is 0.95g for a 1% damping ratio; however, the spectral acceleration of the record employed in the calculation of the response is 1.45g for a 2% damping ratio. If

one takes into account this difference in spectral accelerations and modifies accordingly the observed response, one can achieve a good correlation between the computed and observed responses. For example, multiplication of the observed base shear of 2.75×10^4 lbs by a factor of (1.45/0.95) yields a value of 4.19×10^4 lbs which is comparable to a computed value of 3.9×10^4 lbs (note that the observed base shear includes both the impulsive and convective components; however, for the problem under consideration, the convective component is much smaller than the impulsive one). The modification suggested above yields reasonable values for all response quantities which are proportional to the acceleration; however, those quantities which are directly proportional to the spectral displacement are slightly underestimated. This indicates that the observed fundamental period is higher than the computed period by about 10%.

In view of these results, one can conclude that the flexibility of tank walls that are anchored to the base has a significant effect on the seismic response of tanks. These dynamic stresses are much greater than those computed assuming rigid walls.

Example 3: A Broad Tank

The computer program is also used to estimate the earthquake response of an open top, fixed base, broad tank whose vibrational modes were obtained in chapter I. The tank has the following dimensions: R = 60 ft, L = 40 ft, and h = 1 inch, and it is assumed to be full of water. The input ground motion is the N-S component of the 1940 El Centro earthquake shown in Fig. III-2-a and the modal damping ratios are assumed to be 2%.

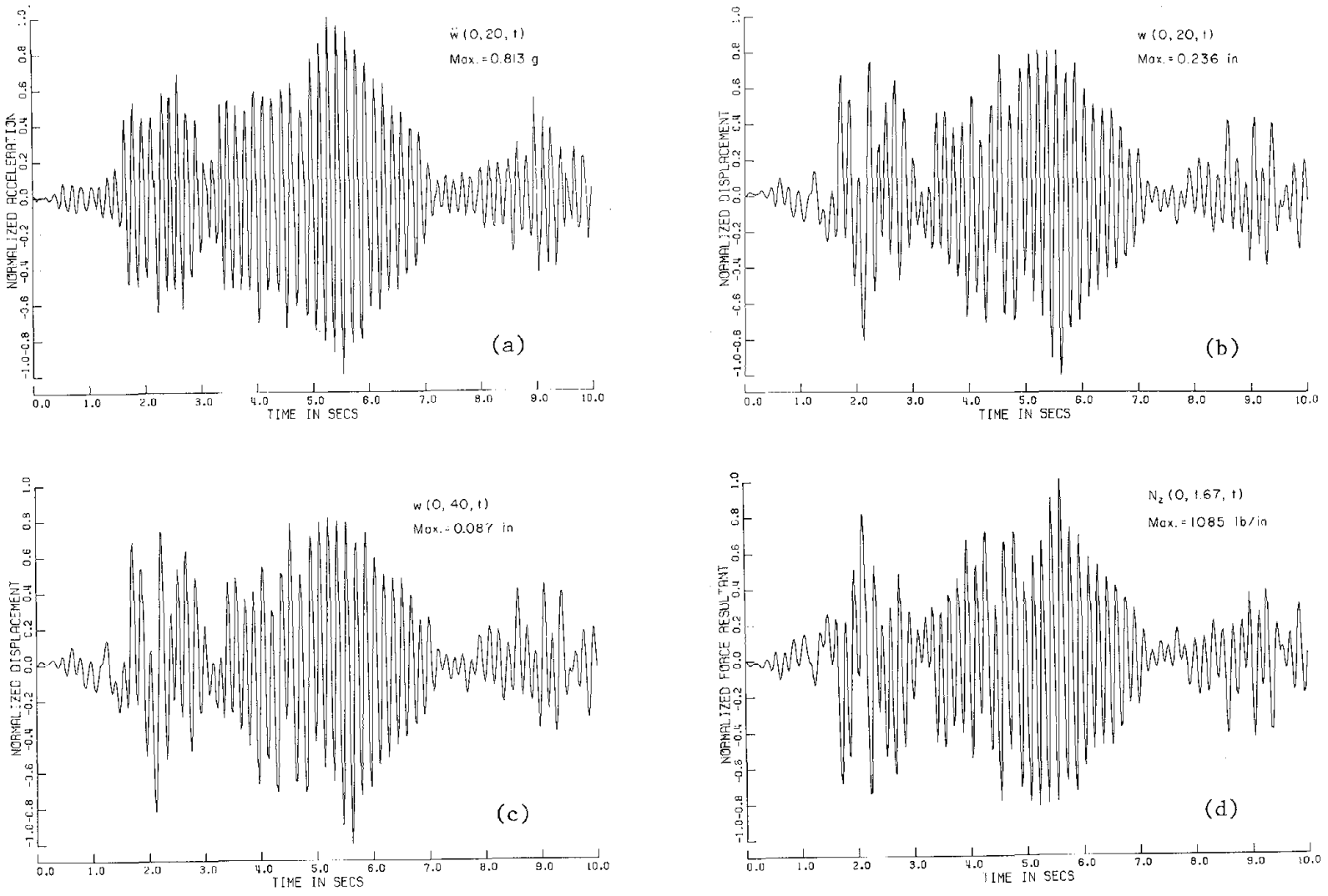

Fig. III-13. Time History of Response of a Broad Tank.

The time history of the radial component of shell acceleration at mid-height, $\ddot{w}(0,20,t)$, is shown in Fig. III-13-a; it should be noted that the maximum amplitude of the radial component of shell acceleration occurs near the bottom of the tank not at the top as in tall tanks. Figure III-13-b presents the time history of the radial component of shell displacement at mid-height which is 2.7 times greater than the radial component at the tank top shown in Fig. III-13-c. The time history of the axial membrane force resultant at 1.67 ft above the base is displayed in Fig. III-13-d. To compare this stress with that induced in a similar rigid tank, one can make use of Housner's mechanical model [6]. For the particular tank under consideration, the parameters of such a model are given by $m_0 = 0.38$ m and $H_0 = 0.375$ H. The impulsive moment is therefore given by

$$M_{max} = \left(m_0 H_0 + m_s \frac{L}{2} \right) \ddot{G}_{max} = 60.53 \times 10^6 \text{ lb. ft} ,$$

and consequently, the axial membrane force resultant can be computed by

$$(N_z)_{max} = \frac{M_{max}}{\pi R^2} = 446 \text{ lb/in}$$

which is much lower than that in a flexible tank. It should be noted that the computed dynamic moment resultants (M_z and M_θ) in fixed-base broad tanks are very high; however, in a real tank the wall is not "built in" at the base and this reduces local bending stresses significantly. Therefore, only the membrane stresses in a broad flexible tank are compared to those of a similar rigid tank.

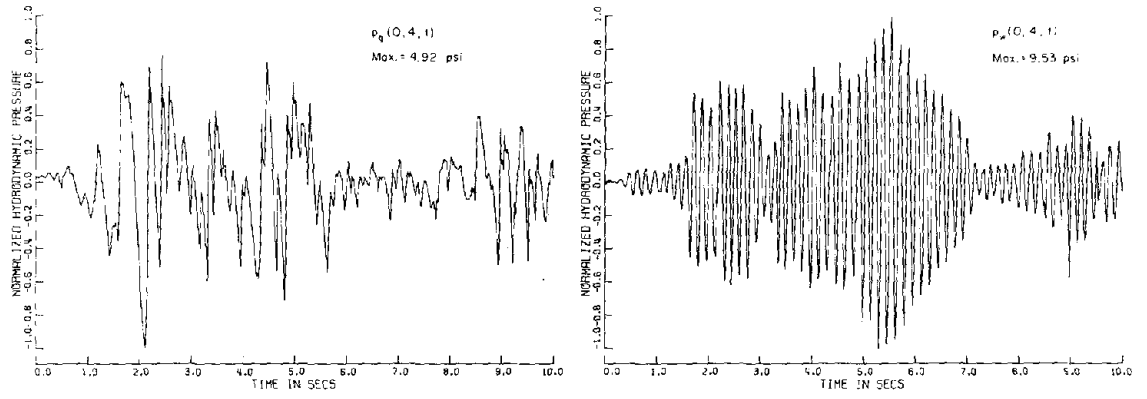

(a)

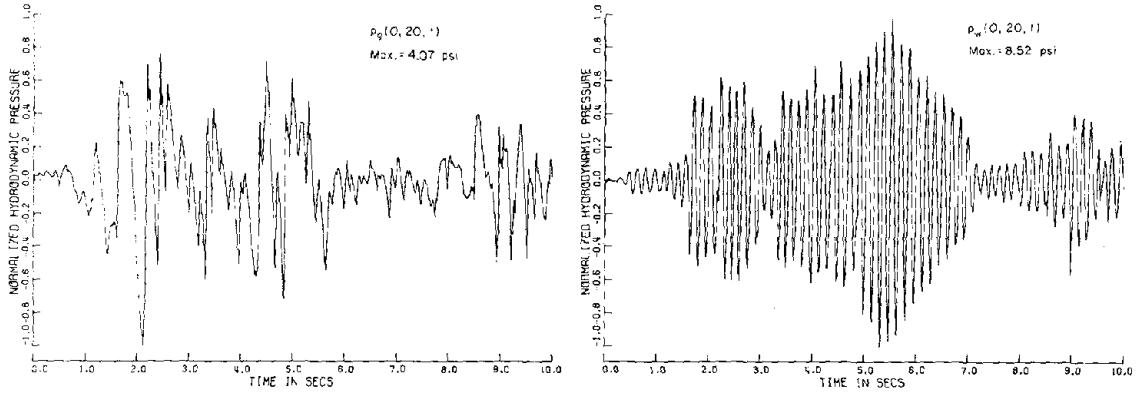

(b)

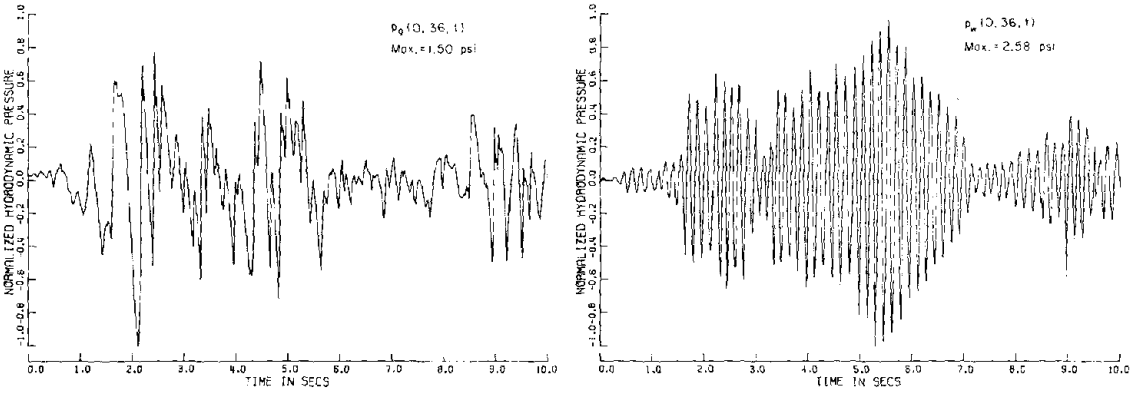

(c)

Fig. III-14. Time History of Hydrodynamic Pressures.

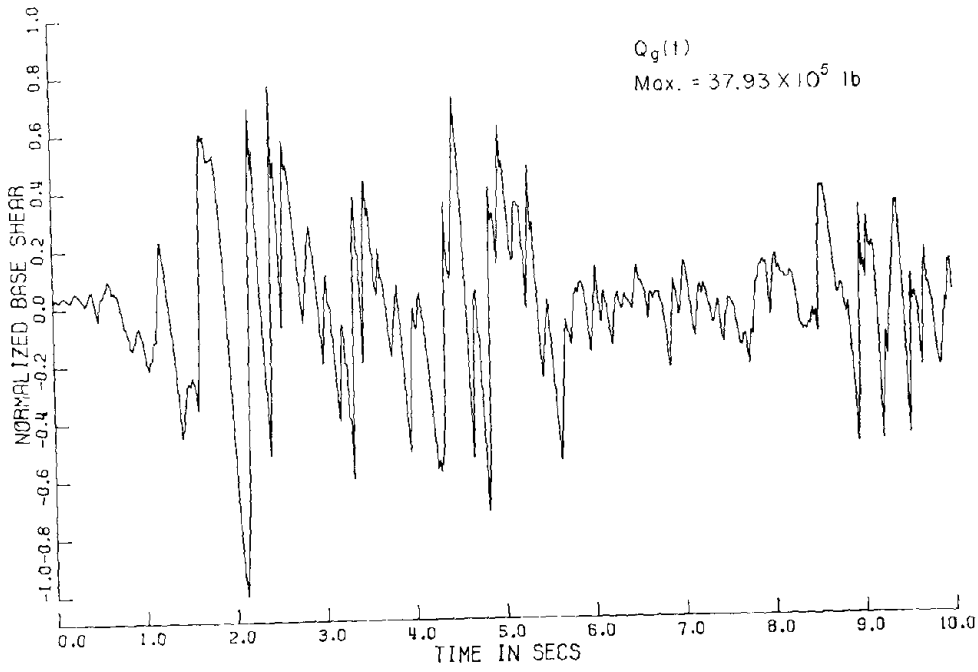

(a) Impulsive Base Shear Due to Ground Motion Only

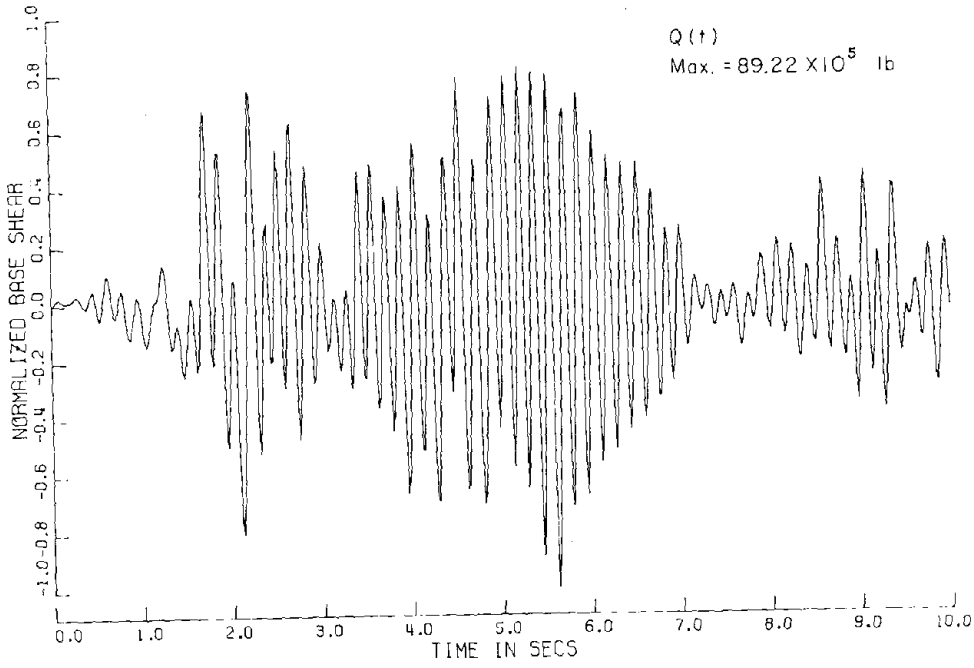

(b) Total Impulsive Base Shear

Fig. III-15. Time History of Base Shear.

Figure III-14 displays the time history of the impulsive hydrodynamic pressures at three locations along the shell height in the θ = 0 direction. The hydrodynamic pressure components p_g and p_w due to ground acceleration and due to shell deformation, respectively, are plotted separately; it can be seen that the pressure component p_w has an axial distribution similar to that of p_g which is in contrast to the pressure distribution in a tall tank.

Finally, the impulsive base shear due to ground acceleration only and the total impulsive base shear are shown in Fig. III-15.

III-2. Cosnθ-Type Response to Earthquake Excitation

In the preceding section, a method for analyzing the earthquake response of a perfectly circular cylindrical tank was presented. The seismic response is obtained by superposition of the cos θ-type modes because the effective seismic load resulting from a given base motion excites only modes having n = 1. Recently, shaking table tests with aluminum tank models [1,2] and vibration tests on full-scale tanks (refer to Chapter IV) show that cos nθ-type modes do respond to base excitations. In a perfect circular tank, cos nθ-type modes cannot be excited by rigid base motion; however, fabrication tolerances in civil engineering tanks permit a significant departure from a nominal circular cross section and this tends to excite these modes.

Little can be found in the literature about the importance of the cos nθ-type modes in an earthquake response analysis. The only investigation of the seismic response of an out-of-round tank is carried out approximately by Veletsos and Turner [10,11]. They compute the hydrodynamic pressure in an irregular rigid tank and apply it to a flexible tank. It should be noted, however, that the hydrodynamic pressures in a flexible tank may differ significantly from those of a rigid tank.

Although a complete analysis of the effect of irregularity of the circular cross sections of the tank is beyond the scope of this study, it seems logical to employ the free lateral vibrational modes obtained earlier to explore approximately such effect. Since the magnitude and distribution of fabrication error cannot be predicted, the influence

of the cos nθ-type modes can only be estimated by computing the seismic response of a hypothetical irregular tank.

III-2-1. Tank Geometry and Coordinate System

The irregular tank under consideration is shown in Fig. III-16. It is a ground-supported, circular cylindrical liquid container of nominal radius R, length L, and thickness h. The tank is partly filled with an inviscid, incompressible liquid to a height H and is subjected to ground excitation G(t).

A cylindrical coordinate system is used with the center of the base being the origin. The radial, circumferential and axial coordinates are denoted r, θ, and z, respectively. The cross sections of the tank are assumed to be irregular but symmetrical about the line of excitation, and therefore, the radius of the tank $\hat{R}(\theta,z)$ can be expressed as

$$\hat{R}(r,\theta) = R\left\{1 + \sum_{n=0}^{\infty} \varepsilon_n \psi_n(z) \cos(n\theta)\right\} \tag{3.37}$$

where $\psi_n(z)$ is an assumed distribution function of the n^{th} circumferential irregularity in the z-direction; and ε_n are small numbers in comparison to unity.

III-2-2. The Effective Force Vector

The hydrodynamic pressure in an irregular tank consists of two components:

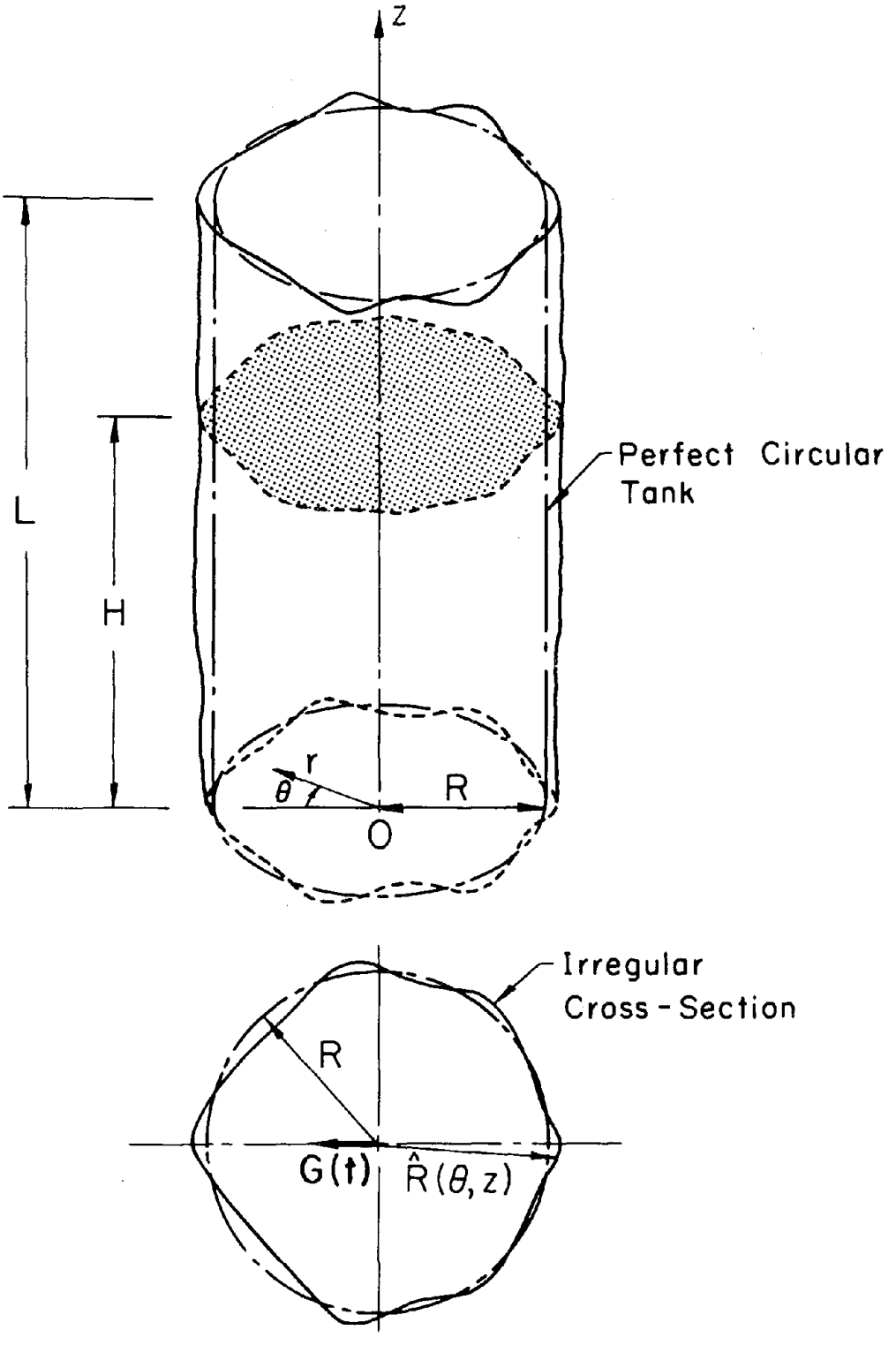

$$\hat{R}(\theta, z) = R\left\{1 + \sum_{n=0}^{\infty} \epsilon_n \psi_n(z) \cos(n\theta)\right\}$$

Fig. III-16. Irregular Cylindrical Tank.

(i) the pressure that would result in a perfectly circular tank, and

(ii) a corrective pressure arising due to cross-section irregularity.

It is the purpose of this subsection to evaluate the corrective component of the hydrodynamic pressure, and consequently, compute the effective earthquake load vector associated with irregularity of the tank.

For illustration purpose, the radius $\hat{R}(\theta,z)$ is taken to be

$$\hat{R}(\theta) = R[1 + \varepsilon \cos(n\theta)] \tag{3.38}$$

where the functions $\psi_n(z)$ of Eq. 3.37 are assumed to be 1.0 for the particular n under consideration and zero for all other n, and the subscript n of ε_n is omitted for brevity.

The velocity potential function, $\phi(r,\theta,z,t)$, must satisfy the Laplace equation (Eq. 1.1) as well as the following boundary conditions:

1. At the rigid tank bottom

$$\frac{\partial\phi}{\partial z}(r,\theta,0,t) = 0 \tag{3.39}$$

2. At the quiescent liquid free surface (impulsive case)

$$\frac{\partial\phi}{\partial t}(r,\theta,H,t) = 0 \tag{3.40}$$

3. At the irregular liquid-shell interface

$$\frac{\partial \phi}{\partial \nu}(\hat{R},\theta,z,t) = \dot{Y}_{\nu}(\theta,z,t) \tag{3.41}$$

where $\underset{\sim}{\nu}$ is the outward normal vector to the irregular shell surface; and $\dot{Y}_{\nu}(\theta,z,t)$ is the component of shell velocity in the direction of the vector $\underset{\sim}{\nu}$.

If C denotes the contour of the boundary of the cross section, then [12]

$$\frac{\partial \phi}{\partial \nu} = \frac{\partial \phi}{\partial r} \cos(\underset{\sim}{\nu},\underset{\sim}{e}_r) + \frac{1}{r}\frac{\partial \phi}{\partial \theta} \cos(\underset{\sim}{\nu},\underset{\sim}{e}_\theta) \quad \text{on} \quad C \tag{3.42}$$

$$= \frac{\partial \phi}{\partial r} r \frac{d\theta}{ds} - \frac{1}{r}\frac{\partial \phi}{\partial \theta}\frac{dr}{ds} \quad \text{on} \quad C \tag{3.43}$$

where ds is the infinitesimal distance measured along the curve C. The equation that describes the contour C is

$$r = R[1 + \varepsilon \cos(n\theta)] \quad , \tag{3.44}$$

and consequently,

$$dr = -nR\varepsilon \sin(n\theta)\, d\theta \quad \text{on} \quad C \tag{3.45}$$

Since $(ds)^2 = (r\, d\theta)^2 + (dr)^2$ and $\varepsilon << 1$, then

$$\frac{1}{r}\frac{dr}{ds} = -\frac{n\varepsilon}{R}\sin(n\theta) + O(\varepsilon^2) \quad , \tag{3.46}$$

and

$$r\frac{d\theta}{ds} = 1 + O(\varepsilon^2) \tag{3.47}$$

The derivatives $\frac{\partial \phi}{\partial r}(\hat{R},\theta,z,t)$ and $\frac{\partial \phi}{\partial \theta}(\hat{R},\theta,z,t)$ can be expressed in

terms of the derivatives at the circular contour as follows

$$\frac{\partial\phi}{\partial r}(\hat{R},\theta,z,t) = \frac{\partial\phi}{\partial r}(R,\theta,z,t) + \varepsilon R\cos(n\theta)\frac{\partial^2\phi}{\partial r^2}(R,\theta,z,t) + O(\varepsilon^2) \tag{3.48}$$

and

$$\frac{\partial\phi}{\partial\theta}(\hat{R},\theta,z,t) = \frac{\partial\phi}{\partial\theta}(R,\theta,z,t) + O(\varepsilon) \tag{3.49}$$

Now, it is assumed that the velocity potential function, $\phi(r,\theta,z,t)$, can be expanded in a power series of ε as follows:

$$\phi(r,\theta,z,t) = \phi_0(r,\theta,z,t) + \varepsilon\phi_1(r,\theta,z,t) + O(\varepsilon^2) \tag{3.50}$$

With the aid of Eq. 3.50, Eqs. 3.48 and 3.49 can be rewritten as

$$\frac{\partial\phi}{\partial r}(\hat{R},\theta,z,t) = \frac{\partial\phi_0}{\partial r}(R,\theta,z,t) + \varepsilon\frac{\partial\phi_1}{\partial r}(R,\theta,z,t) + \varepsilon R\cos(n\theta)\cdot \frac{\partial^2\phi_0}{\partial r^2}(R,\theta,z,t) + O(\varepsilon^2) \tag{3.51}$$

and

$$\frac{\partial\phi}{\partial\theta}(\hat{R},\theta,z,t) = \frac{\partial\phi_0}{\partial\theta}(R,\theta,z,t) + O(\varepsilon) \tag{3.52}$$

Substituting Eqs. 3.46, 3.47, 3.51 and 3.52 into Eq. 3.43, one can rewrite the left hand side of Eq. 3.41 as follows

$$\frac{\partial\phi}{\partial\nu}(\hat{R},\theta,z,t) = \frac{\partial\phi_0}{\partial r}(R,\theta,z,t) + \varepsilon\left\{\frac{\partial\phi_1}{\partial r}(R,\theta,z,t) + R\cos(n\theta)\cdot\right.$$

$$\left.\frac{\partial^2\phi_0}{\partial r^2}(R,\theta,z,t) + \frac{n}{R}\sin(n\theta)\frac{\partial\phi_0}{\partial\theta}(R,\theta,z,t)\right\} + O(\varepsilon^2) \qquad (3.53)$$

The right hand side of Eq. 3.41 involves the velocity of the tank normal to shell surface. This velocity consists of two components: (i) a component directly proportional to ground velocity and this contributes to the effective earthquake load vectors on the RHS of the earthquake response equations

$$[M]\{\ddot{q}\} + [C]\{\dot{q}\} + [K]\{q\} = \{P_{eff}\} \qquad (3.54);$$

and (ii) a component directly proportional to shell deformations and this contributes to both the added mass matrices and the effective earthquake load vectors of Eq. 3.54. To clarify this point, consider, for example, the radial component of shell velocity $\dot{w}_1(z,t)\cos(\theta)$. This component contributes to the added mass matrix of the tank when it vibrates in the $\cos(\theta)$-mode. In addition, it contributes to the effective earthquake load vectors when an out-of-round tank, with an irregularity proportional to $\cos(n\theta)$, vibrates in the $\cos(n-1)\theta$-mode and in the $\cos(n+1)\theta$-mode.

The tank velocity due to ground motion only in the direction of the outward normal vector $\underset{\sim}{\nu}$ can be expressed as

$$\dot{Y}_{\nu_g} = [\dot{G}(t) \cos(\theta)] \cdot 1 + [-\dot{G}(t) \sin(\theta)] \cdot [n \varepsilon \sin(n\theta)] + O(\varepsilon^2)$$

$$= \dot{G}(t)\{\cos(\theta) - n \varepsilon \sin(\theta) \sin(n\theta)\} + O(\varepsilon^2) \quad (3.55)$$

Now, it remains to define the velocity component due to shell deformations. In the following analysis, we shall be concerned with the vibration of the tank in the (n-1)θ-mode. The only component of shell deformations that contributes to the effective load vector of the (n-1)θ-mode is the one proportional to cos (θ). Therefore, the velocity $\dot{Y}_{\nu_s}$ due to shell deformation that contributes to the load vector of cos (n-1)θ-mode is

$$\dot{Y}_{\nu_s} = \dot{w}_1(z,t) \cos(\theta) + \dot{v}_1(z,t)\, n \varepsilon \sin(\theta) \sin(n\theta) + O(\varepsilon^2) \quad (3.56)$$

Substituting Eqs. 3.53, 3.55, and 3.56 into Eq. 3.41 and equating the terms on the LHS to those of equal order of ε on the RHS, then Eq. 3.41 reduces to the following simultaneous equations:

$$\frac{\partial \phi_0}{\partial r}(R,\theta,z,t) = \{\dot{G}(t) + \dot{w}_1(z,t)\} \cos(\theta) \quad (3.57);$$

and

$$\frac{\partial \phi_1}{\partial r}(R,\theta,z,t) + R \cos(n\theta) \frac{\partial^2 \phi_0}{\partial r^2}(R,\theta,z,t) + \frac{n}{R} \sin(n\theta) \frac{\partial \phi_0}{\partial \theta}(R,\theta,z,t)$$

$$= \{\dot{v}_1(z,t) - \dot{G}(t)\}\, n \sin(\theta) \sin(n\theta) \quad (3.58)$$

The solution ϕ_1 of Eq. 3.58 provides the hydrodynamic pressure component that contributes to the effective load vector of the

(n-1)θ-mode. It is assumed that the irregularity of the tank does not affect the LHS of Eq. 3.54; this is substantiated by the close agreement between the computed and measured natural frequencies of full scale tanks which are undoubtedly irregular.

The solution $\phi_0(r,\theta,z,t)$ of Eq. 3.57 which satisfies the Laplace equation and Eqs. 3.39 and 3.40 can be written as

$$\phi_0(r,\theta,z,t) = \sum_{i=1}^{\infty} A_i(t)\, I_1(\alpha_i r)\, \cos(\alpha_i z)\, \cos(\theta) \qquad (3.59)$$

where

$$\alpha_i = \frac{(2i-1)\pi}{2H} \quad ; \qquad i = 1,2,\ldots \qquad (3.60)$$

The unknowns $A_i(t)$ can be determined from Eq. 3.57 since

$$\sum_{i=1}^{\infty} \alpha_i\, A_i(t)\, \acute{I}_1(\alpha_i R)\, \cos(\alpha_i z) = \dot{G}(t) + \dot{w}_1(z,t)$$

and, consequently,

$$A_i(t) = \frac{2\int_0^H [\dot{w}_1(z,t) + \dot{G}(t)]\, \cos(\alpha_i z)\, dz}{H\, \alpha_i\, \acute{I}_1(\alpha_i R)} \qquad (3.61)$$

Substituting Eq. 3.59 into Eq. 3.58, one obtains

$$\frac{\partial \phi_1}{\partial r}(R,\theta,z,t) = -R\cos(n\theta)\left(\sum_{i=1}^{\infty} \alpha_i^2 A_i(t) I_1(\alpha_i R)\cos(\alpha_i z)\cos(\theta)\right)$$

$$-\frac{n}{R}\sin(n\theta)\left(-\sum_{i=1}^{\infty} A_i(t) I_1(\alpha_i R)\cos(\alpha_i z)\sin(\theta)\right)$$

$$+\{\dot{v}_1(z,t) - \dot{G}(t)\} n \sin(\theta)\sin(n\theta) \qquad (3.62)$$

Using the following trigonometric identities

$$\cos(\theta)\cos(n\theta) = \frac{\cos[(n-1)\theta] + \cos[(n+1)\theta]}{2}$$

and (3.63)

$$\sin(\theta)\sin(n\theta) = \frac{\cos[(n-1)\theta] - \cos[(n+1)\theta]}{2}$$

and retaining only those terms in Eq. 3.62 proportional to $\cos[(n-1)\theta]$, one can write

$$\frac{\partial \phi_1^*}{\partial r}(R,\theta,z,t) = \cos[(n-1)\theta]\left\{\sum_{i=1}^{\infty}\left[A_i(t)\left(-\frac{R}{2}\alpha_i^2 I_1(\alpha_i R) + \frac{n}{2R} I_1(\alpha_i R)\right)\cos(\alpha_i z)\right] + \frac{n}{2}[\dot{v}_1(z,t) - \dot{G}(t)]\right\} \qquad (3.64)$$

where ϕ_1^* indicates the part of the potential function ϕ_1 which is proportional to $\cos[(n-1)\theta]$.

The velocity potential function ϕ_1^* must satisfy the Laplace equation and the boundary conditions (Eqs. 3.39 and 3.40); therefore, it takes the following form:

$$\phi_1^*(r,\theta,z,t) = \sum_{i=1}^{\infty} B_i(t)\, I_{n-1}(\alpha_i r)\, \cos(\alpha_i z)\, \cos[(n-1)\theta] \tag{3.65}$$

Substituting Eq. 3.65 into Eq. 3.64, one obtains

$$\sum_{i=1}^{\infty} \alpha_i B_i(t)\, \acute{I}_{n-1}(\alpha_i R)\, \cos(\alpha_i z) = \sum_{i=1}^{\infty} \left[A_i(t) \left(-\frac{R}{2}\alpha_i^2\, \acute{I}_1(\alpha_i R) + \frac{n}{2R} I_1(\alpha_i R) \right) \cos(\alpha_i z) \right] + \frac{n}{2}\left[\dot{v}_1(z,t) - \dot{G}(t)\right] \tag{3.66}$$

Therefore, the unknown functions $B_i(t)$ can be expressed as follows:

$$B_i(t) = \frac{1}{\alpha_i\, \acute{I}_{n-1}(\alpha_i R)} \left\{ A_i(t) \left(-\frac{R}{2}\alpha_i^2\, \acute{I}_1(\alpha_i R) + \frac{n}{2R} I_1(\alpha_i R) \right) + \frac{n}{H} \int_0^H \left[\dot{v}_1(z,t) - \dot{G}(t)\right] \cos(\alpha_i z)\, dz \right\} \tag{3.67}$$

The hydrodynamic pressure p_d^* which is proportional to $\cos[(n-1)\theta]$ can be expressed as

$$p_d^*(R,\theta,z,t) = -\varepsilon \rho_\ell \frac{\partial \phi_1^*}{\partial t}(R,\theta,z,t) \tag{3.68}$$

$$= -\varepsilon \rho_\ell \sum_{i=1}^{\infty} \dot{B}_i(t)\, I_{n-1}(\alpha_i R)\, \cos(\alpha_i z)\, \cos[(n-1)\theta] \tag{3.69}$$

The work done by such hydrodynamic load during an arbitrary virtual displacement $\delta w_{n-1} \cos[(n-1)\theta]$ is given by

$$\delta W = \int_0^H \int_0^{2\pi} \left(p_d^* (R,\theta,z,t)\ \delta w_{n-1} \cos [(n-1)\theta] \right) R\, d\theta\, dz$$

$$= -\varepsilon \pi R \rho_\ell \sum_{i=1}^{\infty} \left[\dot{B}_i(t)\ I_{n-1}(\alpha_i R) \int_0^H \delta w_{n-1} \cos(\alpha_i z)\, dz \right] \quad (3.70)$$

The integral in Eq. 3.70 can be expressed as

$$\int_0^H \delta w_{n-1} \cos (\alpha_i z)\, dz = \{\delta q\}^T_{(n-1)}\ \{F^{(i)}\} \quad (3.71)$$

where $\{F^{(i)}\}$ is given by Eq. 1.143. If one writes

$$b_i(t) = \varepsilon\pi R\rho_\ell\ I_{n-1}(\alpha_i R)\ \dot{B}_i(t) \quad ; \quad \text{and} \quad \{F\} = \sum_{i=1}^{\infty} b_i\ \{F^{(i)}\} \quad (3.72)$$

then the virtual work expression can be written as

$$\delta W = -\{\delta q\}^T_{(n-1)}\ \{F\} \quad (3.73),$$

and therefore, the effective earthquake load vector for the $(n-1)\theta$-mode is given by

$$\{P_{eff}\}_{(n-1)} = -\{F\} \quad (3.74)$$

It should be noted that the load vector defined by Eq. 3.74 can only be evaluated if the response of the cos θ-type modes is known.

III-2-3. Computer Implementation and Numerical Examples

A digital computer program has been written to compute the earthquake response of partly filled irregular tanks by the method outlined in the preceding subsections. The program "IRREGULAR" employs first the program "RESPONSE" to obtain the earthquake response of the cosθ-type modes. Then it formulates the load vectors and computes shell nodal displacements and accelerations.

Examples

The computer program is utilized to estimate the earthquake response of the cos5θ-type modes of two open top, broad and tall tanks with non-circular irregularity described by

$$\hat{R}(\theta) = R(1 + \varepsilon \cos 6\theta) \tag{3.75}$$

The first tank has the following dimensions: R = 60 ft, L = 40 ft, and h = 1 inch while the second one is 24 feet in radius, 72 feet in height, and has a wall thickness of 1 inch. The tanks are assumed to be full of water and to be subjected to the N-S component of the 1940 El Centro earthquake. The modal damping ratios are assumed to be 2%.

The inclusion of the deformation of the cosθ-type modes in computing the load vector of the cosnθ-type modes can be important. To clarify this, define an "equivalent acceleration" as the sum of the ground acceleration plus the acceleration contributed by the cosθ-type modes which excite the cosnθ-type vibrations of the tank wall. This acceleration differs from the ground acceleration in two respects:

1. The amplitudes of the "equivalent acceleration", and consequently the amplitudes of the exciting force, are larger than the amplitudes of the ground motion and the corresponding exciting force (Refs [10,11]), respectively.

2. The frequency content of the "equivalent acceleration" is different from that of the ground; it is affected by the natural frequencies of the cosθ-type modes.

The amplitude of the response of the cosnθ-type modes of the tank wall is dependent on the value of ε. For the broad tank and for a practical value of $\varepsilon = 0.01$, the maximum amplitude of the radial component of the cos5θ-type displacement at the top of the wall is about 40% of that of the cosθ-type displacement. However, for the same value of ε, the amplitude of the cos5θ-type mode of the tall tank is negligibly small as compared to the displacement of the cosθ-type modes. Therefore, one can conclude that the effect of irregularity is more pronounced for broad tanks than for tall tanks. It should be noted that a recent experimental study on plastic models of tall tanks (refer to Sec. IV-5) showed that buckling of these tanks is largely dependent upon the response of the cosθ-type modes and that the higher circumferential shell modes seem to have only a secondary role.

The foregoing results concerning the response of the cosnθ-type modes are based on a very limited study aimed to providing a basis for which later work can be developed; therefore, one must guard against drawing broad conclusions on the basis of such a limited study.

III-3. Appendices

Appendix III-a

List of Symbols

The letter symbols are defined where they are first introduced in the text, and they are also summarized herein in alphabetical order:

$A_i(t)$	Time dependent coefficients of the velocity potential function ϕ_0, Eq. 3.59.
[A]	2 x 2 matrix defined by Eq. 3.32.
$B_i(t)$	Time dependent coefficients of the velocity potential function ϕ_1^*, Eq. 3.65.
[B]	2 x 2 matrix defined by Eq. 3.32.
b_i	Coefficients defined by Eq. 3.13.
$b_i(t)$	Time dependent coefficients defined by Eq. 3.72.
[C]	Damping matrix, Eq. 3.1.
[DM]	Added mass matrix defined by Eq. 1.130.
{d}	Shell displacement vector, Eq. 1.31.
$\{d_g\}$	Shell displacement vector associated with ground motion, Eq. 3.7.
{δd}	Virtual displacement vector, Eq. 3.10.
$\{\bar{d}\}_e$	Generalized displacement vector of the element "e", of order 8 x 1, Eq. 1.78.
ds	Infinitesimal distance measured along the contour of tank cross section.

e	Indicate element, and occasionally used as the number of the element "e"
$\underset{\sim}{e}_r$ and $\underset{\sim}{e}_\theta$	Unit base vectors in the r and θ directions, respectively.
$\{F\}$	Vector defined by Eq. 3.19 and by Eq. 3.72.
$\{F^{(i)}\}$	Vector defined by Eq. 1.143.
$\{\bar{F}\}$ and $\{\bar{\bar{F}}\}$	Vectors defined by Eqs. 3.16 and 3.18, respectively.
$\{F_g\}$	Inertia force vector, Eq. 3.8.
$\{\overset{*}{F}\}$	Vector defined by Eq. 3.25.
$\{\bar{f}\}_e$	Vector defined by Eq. 3.15.
$G(t)$, $\dot{G}(t)$, & $\ddot{G}(t)$	Ground displacement and its time derivatives.
$\ddot{G}_{i+1}$ and $\ddot{G}_i$	Ground accelerations at time $t = t_{i+1}$ and $t = t_i$, respectively, Eq. 3.31.
g	Acceleration of gravity
H	Liquid depth.
H_0 and H_1	Equivalent heights of Housner model for rigid tanks.
h	Shell thickness.
h^e	Thickness of the element "e".
$I_n(\ )$	Modified Bessel functions of the first kind of order n.
$'I_n(\ )$ and $''I_n(\ )$	Derivatives of $I_n(\ )$ with respect to the radial coordinate.
J	Number of vertical modes used in superposition, Eq. 3.22.

$[K]$	Stiffness matrix, Eq. 3.1.
$[K_s]$	Shell stiffness matrix.
$[\tilde{K}^*]$	Generalized stiffness matrix, Eq. 3.25.
L	Shell length.
L_e	Element length.
$[M]$	Mass matrix, Eq. 3.1.
$[M_s]$	Shell consistent mass matrix, Eq. 1.106.
$[M_c]$	Coupling mass matrix, Eq. 3.5.
$[\tilde{M}^*]$	Generalized mass matrix, Eq. 3.25.
M_z and M_θ	Bending moment resultants.
M_{max}	Maximum impulsive wall moment, Eq. 3.34.
m_0 and m_1	Impulsive and convective masses of Housner model for rigid tanks.
m_s	Shell mass per unit length.
N	Constant = 4 x NEL.
NEL	Number of shell elements.
N_z and N_θ	Membrane force resultants.
n	Number of circumferential waves.
$\{P_{eff}\}$	Effective earthquake load vector, Eq. 3.3.
$\{P_{eff}\}_{(n-1)}$	Effective earthquake load vector for the cos $(n-1)\theta$-modes, Eq. 3.74.
p_w and p_g	Hydrodynamic pressures associated with shell deformation and ground motion, respectively.
p_d^*	Hydrodynamic pressure component that contributes to the load vector of the cos $(n-1)\theta$-modes, Eq. 3.68.

$[\overset{*}{Q}]$	Rectangular matrix of the order N x J, Eq. 3.22.
$Q_g(t)$	Impulsive base shear associated with ground motion only.
$Q(t)$	Total impulsive base shear.
$\{\ddot{q}^t\}$	Absolute acceleration vector, Eq. 3.1.
$\{q\}$, $\{\dot{q}\}$, & $\{\ddot{q}\}$	Nodal displacement vector and its time derivatives, Eq. 3.1.
$\{\delta q\}_{(n-1)}$	Virtual nodal displacement vector of the cos $(n-1)\theta$-mode, Eq. 3.71.
$\{\overset{*}{q}\}$	Time independent nodal displacement vector.
$\hat{R}(\theta,z)$ and $\hat{R}(\theta)$	Radius of irregular tank, Eqs. 3.37 and 3.38, respectively.
R	Nominal radius of tank.
$\{r\}$	Influence coefficient vector, Eq. 3.2.
$\{\hat{r}\}$	Vector defined in Eq. 3.5.
r	Radial coordinate of the cylindrical coordinate system.
S_d	Spectral displacement, Eq. 3.33.
T	Period of vibration.
t	Time.
t_{i+1} and t_i	Limits of the time interval under consideration, Eq. 3.31.
δW	Virtual work.
u, v, and w	Shell displacements in the axial, tangential, and radial directions, respectively.

$u_n(z,t)$, $v_n(z,t)$, & $w_n(z,t)$	Displacement functions for the n^{th} circumferential wave.
u_g, v_g, and w_g	Shell displacements associated with ground motion.
$\dot{Y}_\nu$, $\dot{Y}_{\nu_g}$ and $\dot{Y}_{\nu_s}$	Shell velocity in the direction of the normal vector $\underset{\sim}{\nu}$ and its components due to ground motion and due to shell deformation, respectively (Eqs. 3.41, 3.55, and 3.56).
z	Axial coordinate of the cylindrical coordinate system.
α_i	Coefficients defined by Eq. 3.60.
β_j	Modal participation factors, Eq. 3.30.
$\Delta\ddot{G}_i$	Increment in ground acceleration = $\ddot{G}_{i+1} - \ddot{G}_i$, Eq. 3.31.
Δt	Time interval = $t_{i+1} - t_i$, Eq. 3.31.
δ	Variational operator.
ε_n and ε	Small numbers in comparison to unity, Eqs. 3.37 and 3.38, respectively.
ζ_j	Damping ratios, Eq. 3.29.
$\{\eta(t)\}$	Modal amplitude vector, Eq. 3.22.
η_j, $\dot{\eta}_j$, and $\ddot{\eta}_j$	Modal amplitudes and their time derivatives, Eq. 3.29.
θ	Circumferential coordinate of the cylindrical coordinate system.
$\underset{\sim}{\nu}$	Outward normal vector.
ρ_ℓ and ρ_s	Mass density of the liquid and the shell material, respectively.

ϕ	Liquid velocity potential function.
ϕ_0 and $\varepsilon\phi_1$	Leading terms in the perturbation series of the velocity potential function ϕ, Eq. 3.50.
ϕ_1^*	First perturbation term of the velocity potential function ϕ which contributes to the load vector of the cos $(n-1)\theta$-modes, Eq. 3.64.
$\psi_n(z)$	Distribution function of the n^{th} circumferential irregularity in the z-direction, Eq. 3.37.
ω_j	Circular natural frequencies.
$\dot{(\ )}$	Differentiation with respect to time.

REFERENCES OF CHAPTER III

1. Clough, D.P., "Experimental Evaluation of Seismic Design Methods for Broad Cylindrical Tanks," University of California Earthquake Engineering Research Center, Report No. UC/EERC 77-10, May 1977.

2. Niwa, A., "Seismic Behavior of Tall Liquid Storage Tanks," University of California Earthquake Engineering Research Center, Report No. UC/EERC 78-04, February 1978.

3. Clough, R.W., and Penzien, J., Dynamics of Structures, McGraw-Hill Book Company, 1975.

4. Shaaban, S.H., and Nash, W.A., "Finite Element Analysis of a Seismically Excited Cylindrical Storage Tank, Ground Supported, and Partially Filled with Liquid," University of Massachusetts Report to National Science Foundation, August 1975.

5. Analyses of Strong Motion Earthquake Accelerograms, Response Spectra, Volume III, Part A, EERL 72-80, California Institute of Technology, August 1972.

6. U.S. Atomic Energy Commission, "Nuclear Reactors and Earthquakes," TID-7024, Washington, D.C., 1963, pp. 367-390.

7. Veletsos, A.S., and Yang, J.Y., "Earthquake Response of Liquid Storage Tanks," Advances in Civil Engineering through Engineering Mechanics, Proceedings of the Annual EMD Specialty Conference, Raleigh, N.C., ASCE, 1977, pp. 1-24.

8. Balendra, T., and Nash, W.A., "Earthquake Analysis of a Cylindrical Liquid Storage Tank with a Dome by Finite Element Method," Department of Civil Engineering, University of Massachusetts, Amherst, Massachusetts, May 1978.

9. Sakai, F., and Sakoda, H., "A Study on Earthquake Response of Large-Sized Liquid-Filled Tanks," Proceedings of the Fourth Japan Earthquake Engineering Symposium, 1975.

10. Turner, J.W., "Effect of Out-of-Roundness on the Dynamic Response of Liquid Storage Tanks," M.S. Thesis, Rice University, Houston, Texas, May 1978.

11. Veletsos, A.S., and Turner, J.W., "Dynamics of Out-of-Round Liquid-Storage Tanks, Proceedings of the Third EMD Specialty Conference, Austin, Texas, ASCE, 1979.

12. Fung, Y.C., Foundations of Solid Mechanics, Prentice-Hall, Inc., Englewood Cliffs, N.J., 1965.

PART (B)

CHAPTER IV

VIBRATION TESTS OF FULL-SCALE LIQUID STORAGE TANKS

IV-1. Introduction

Adequate understanding of the behavior of complex systems is enhanced by, and generally dependent upon, the combined use of theoretical and experimental techniques in support of each other. In the first phase of this study, the dynamic analysis of liquid storage tanks was accomplished by constructing a theoretical model that governs the interaction between the liquid, the shell and the foundation. The reliability of such analysis is largely dependent on the various assumptions employed in formulating this analytical model. Experimental investigations are therefore essential to confirm the theoretical concepts and to provide the quantitative data needed for design.

Natural earthquakes can be viewed as full-scale, large amplitude experiments on structures. If the structural motion is recorded, it offers an opportunity to study the behavior at dynamic force and deformation levels directly relevant to earthquake-resistant design. Unfortunately, seismic response data from liquid storage tanks are not available and only the qualitative behavior during past earthquakes is known. The limited information available from field observations of earthquake damage demonstrates the need for experimental studies on physical models as well as on full-scale tanks.

Although the only certain way to determine the parameters of major interest in structural dynamic problems is by testing actual structures, none of these tests has been performed on full-scale tanks. In the

past, experimental data were obtained by testing reduced-scale models; however, most of these studies were concerned with dynamic problems associated with aerospace applications [1]. It was not until recently that an extensive experimental investigation of the seismic response of $\frac{1}{3}$-scale aluminum tank models was carried out at the University of California, Berkeley [2,3]. The scaled models were attached to a 20-ft square shaking table, and a hydraulic actuator system was controlled to introduce the desired seismic input. These tests provided valuable information about the seismic behavior of both broad and tall tanks and showed that earthquake loading can also excite significantly the $\cos n\theta$-type modes ($n > 1$).

In recent years, ambient vibrations of real structures, due to wind and microtremors, have been measured to estimate the natural frequencies of vibration and the associated mode shapes. The method of analysis utilizes the Fourier technique which enables the investigators to understand and interpret the frequency content of the time signals. However, the scope of ambient tests is limited because the investigator has no control of the magnitude, duration, or the frequency content of the exciting forces. The development of a vibration generation system with adequate speed control in the early 1960's enabled investigators to conduct detailed studies of the dynamic characteristics of many types of structures.

The present chapter is concerned primarily with experimental dynamic studies which were performed on three full-scale water storage tanks. A series of ambient and forced vibration tests was conducted to determine the natural frequencies and, if possible, the mode shapes

of vibration, to illustrate the effectiveness of the theoretical analysis under consideration, and to select two tanks on which permanent instruments would be installed to record future earthquakes.

IV-2. Description of the Tanks

Tests were performed on three ground supported, welded steel, water storage tanks owned by the Metropolitan Water District of Southern California. These tanks are employed to store "finished" water for use in backwashing the rapid sand filters at the Weymouth filtration plant in La Verne and at the Diemer filtration plant in Yorba Linda. The backwash operation requires a large volume of water in a short period of time; therefore, these "tall" tanks are effective in providing the necessary pressure head and in reducing the size of pumps that are required to supply the backwash water.

Each of these tanks consists of a circular cylindrical thin shell having a height to diameter ratio greater than one. Each tank has a different type of foundation, and this helps in assessing the influence of support conditions on the dynamic characteristics. Figure IV-1 shows schematic sections of the tanks and their foundations, and Fig. IV-2 shows an overall view of the two tanks, no. (1) and no. (2), located at the Weymouth filtration plant.

The wash water tank no. (1) is 48 ft in diameter, 71 ft in height, and has a storage capacity of 1,000,000 gallons. The tank consists of a thin steel shell of varying thickness; the maximum thickness at the bottom is $\frac{11}{16}$ inch and the minimum thickness at the top is $\frac{1}{4}$ inch. The tank floor consists of a thin steel plate of $\frac{1}{4}$ inch in thickness and a $\frac{5}{16}$ inch sketch plate. The roof consists of a $\frac{3}{16}$ inch steel plate,

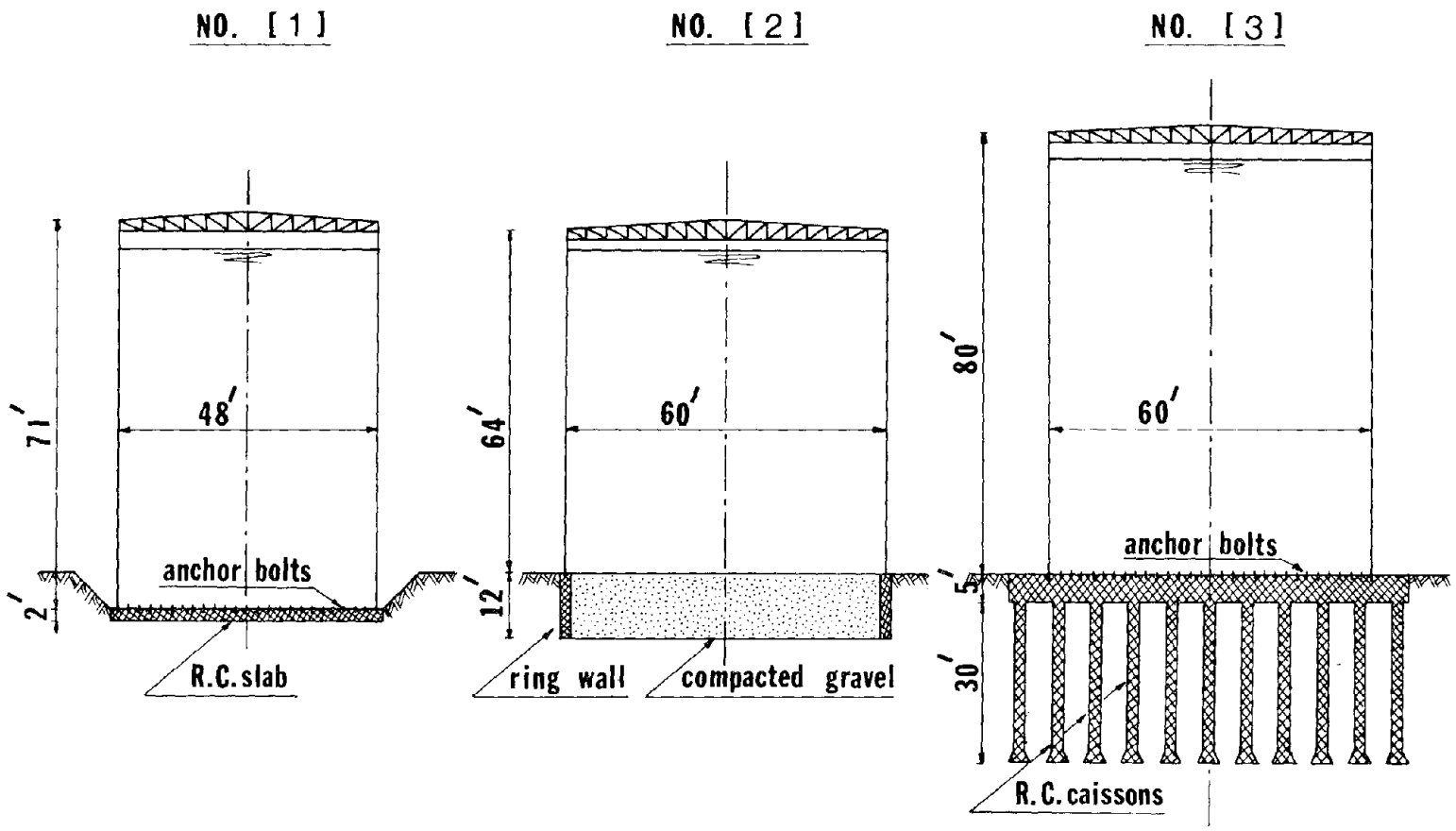

Fig. IV-1. Schematic Sections of the Tanks and Their Foundations.

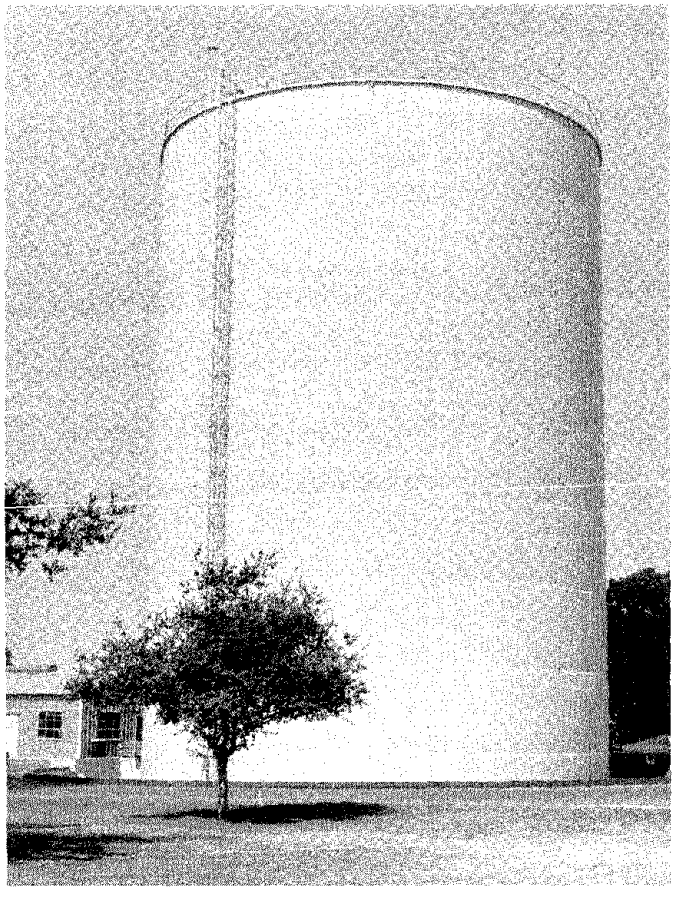

Tank No. (1)

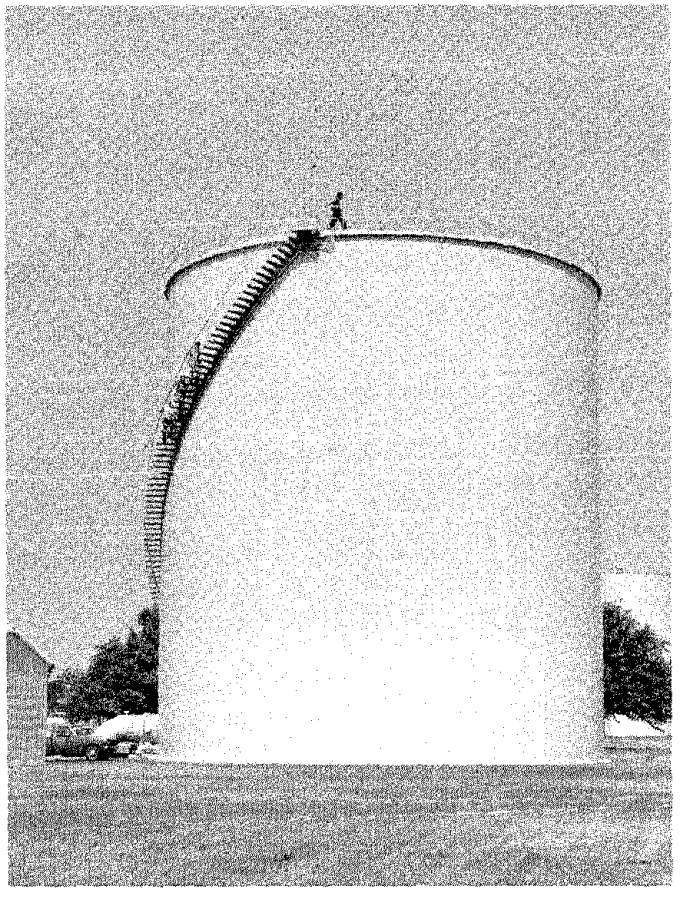

Tank No. (2)

Fig. IV-2. Overall View of Tanks Tested at the Weymouth Filtration Plant.

channel rafters, and four trusses. The tank is anchored to a 2 ft thick R.C. slab on deep alluvium with 100 anchor bolts, each $1\frac{3}{8}$ inch in diameter. More structural details can be seen in Fig. IV-3.

Tank no. (2), located also at the Weymouth filtration plant, is 60 ft in diameter, 64 ft in height, and has a storage capacity of 1,400,000 gallons of water. Tank thickness varies from $\frac{3}{4}$ inch at the bottom to $\frac{1}{4}$ inch at the top. The tank rests on a 2 ft wide, 12 ft deep concrete ring wall without anchor bolts. After the test program was completed, the Metropolitan Water District of Southern California installed a strong-motion accelerograph on the roof, as shown in Fig. IV-4, to record tank response during future earthquakes (for more details, refer to Sec. IV-5).

The third tank, located at the Diemer filtration plant, has the following dimensions: R = 30 ft and L = 80 ft. Its wall consists of thin steel plates, each 8 ft high; their thicknesses are: $1\frac{1}{4}$, $\frac{7}{8}$, $\frac{3}{4}$, $\frac{11}{16}$, $\frac{9}{16}$, $\frac{1}{2}$, $\frac{3}{8}$, $\frac{5}{16}$, $\frac{1}{4}$ and $\frac{1}{4}$ inch. The tank is anchored to a 5 ft thick R.C. foundation slab supported by 97 R.C. caissons. Each caisson is 2.5 ft in diameter and approximately 30 ft deep. Figure IV-5 shows schematic views of the tank and its foundation.

IV-3. Experimental Arrangements and Procedures

The purpose of this section is to present a brief description of the instrumentation used in both ambient and forced vibration tests. This section is also intended to outline the measuring procedures, and it contains a discussion of the data reduction procedures.

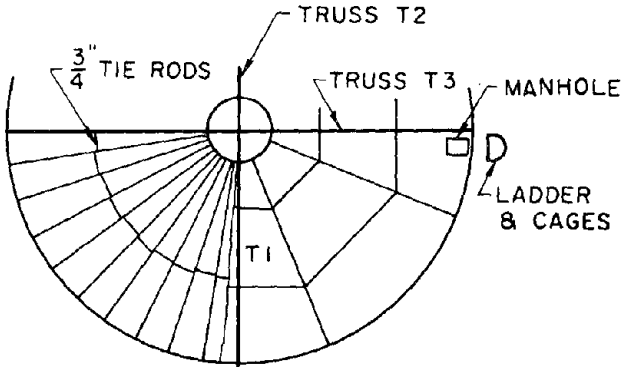

(b) ROOF PLAN

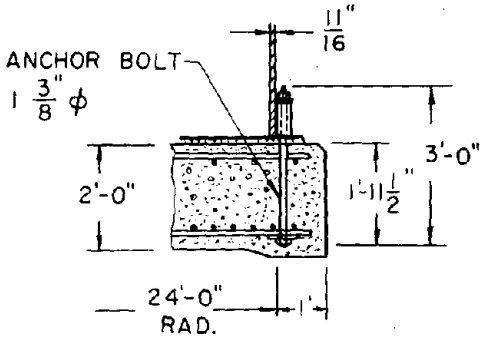

(c) SHELL CONNECTION TO FOUNDATION

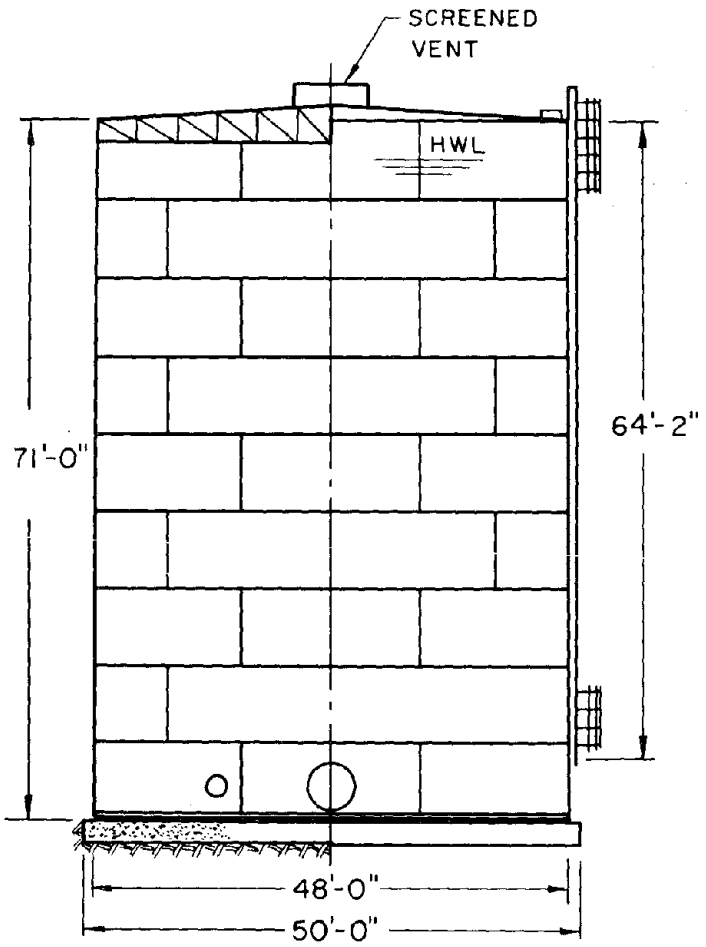

(a) ELEVATION

TANK NO. 1

Fig. IV-3.

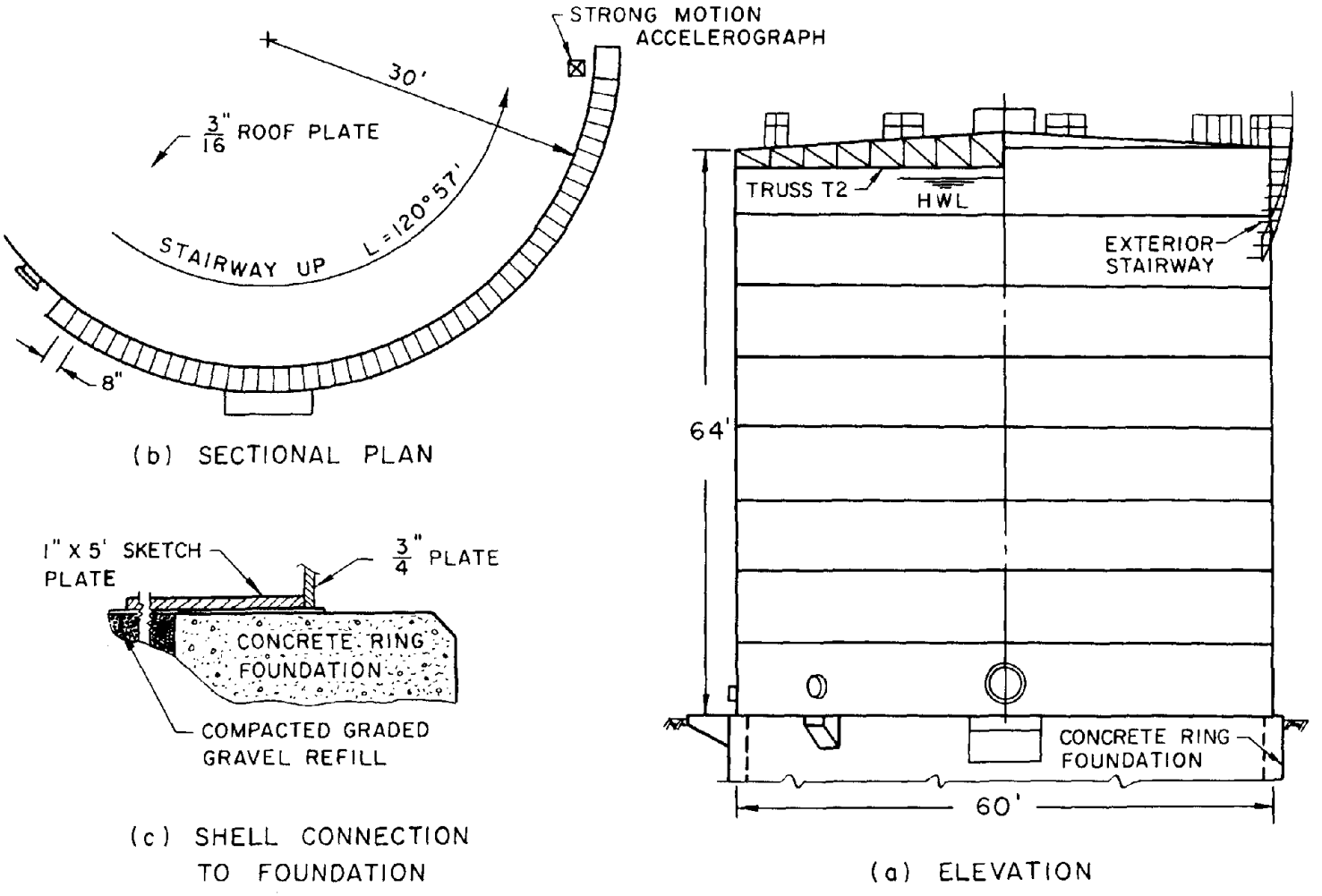

TANK NO. 2

Fig. IV-4.

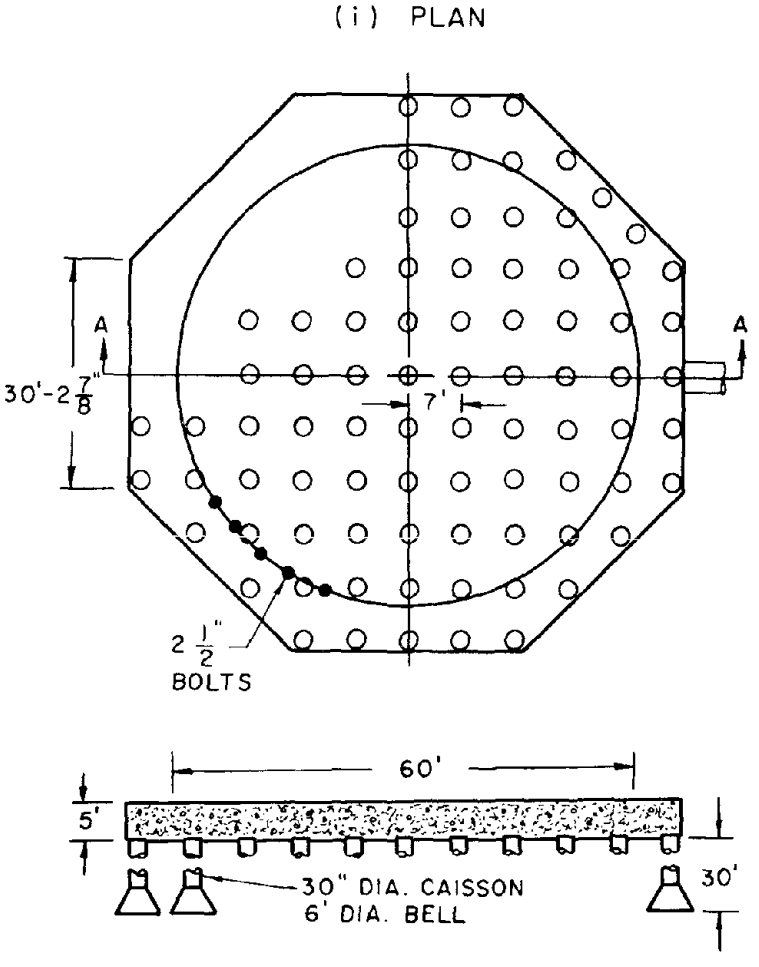

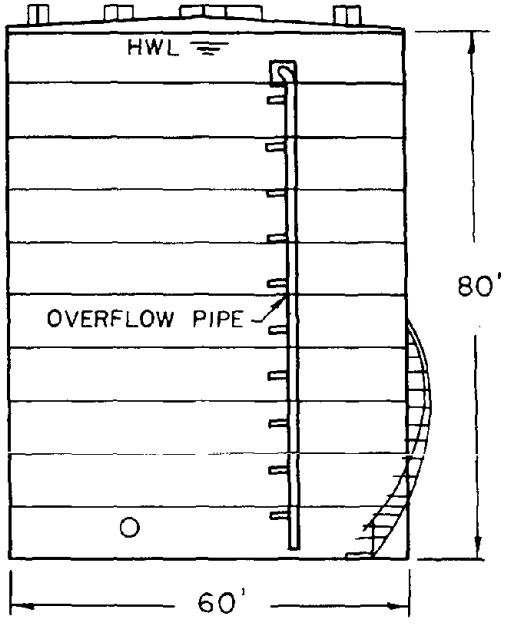

TANK NO. 3

Fig. IV-5.

IV-3-1. Description of the Instruments

One can categorize the instrumentation used in the test program in three groups: motion sensing instruments, signal conditioning and recording instruments, and vibration generation instruments; the latter were used only in the sinusoidal forced vibration tests. A brief description of these instruments is presented herein; however, for a complete description of the instruments one can refer to Refs. [4,5,6].

Vibration measurements were made using up to eight SS-1 Ranger seismometers as the motion sensing instruments. The Ranger is a velocity-type transducer with a nominal period of 1 sec. Its high sensitivity and its small size make it suitable for vibration measurements of many types of structures. Since the natural frequencies of the seismometers are in the same range of the measured frequencies and since the natural period and damping are not identical for each instrument, relative calibration must be made at all the frequencies of interest. It should also be noted that absolute calibration of the Rangers in the field is very difficult; however, it is not necessary to know the absolute values of the amplitudes of vibration since the main objective is to identify the mode shapes and this requires only the relative amplitudes of the recorded motions.

Two four-channel signal conditioners were used during the tests to amplify and to filter the outputs from the Rangers. During the ambient tests, it was decided to filter out all frequencies higher than 20 cps; however, during forced vibration tests the low-pass filter was set to a cut-off frequency of 5 cps. An HP oscillograph recorder having eight channels was used to monitor the ambient vibrations which

were also recorded on two four-channel HP tape recorders. During the forced vibration tests, the oscillograph recorder was the main recording instrument and only few samples were recorded on the tape recorders.

One or two vibration generators were used in the sinusoidal steady-state resonant tests. Briefly, a shaker consists of two counter-rotating baskets which may be loaded with a variable number of lead weights. The resulting sinusoidal force can be aligned in any fixed direction. Each shaker has a control console; however, in a master-slave set up, one uses only the master console to run the two shakers simultaneously at the same frequency.

IV-3-2. Orientation of the Instruments

Measurements of ambient and forced vibrations were made at selected points along the shell height, at the roof circumference, and around the tank bottom.

The first series of tests was conducted to measure the axial pattern of vibrational modes of tank no. (1). Six Ranger seismometers were mounted along the tank height to measure the radial motion of the shell as shown in Fig. IV-6. In addition, two seismometers were placed on the foundation slab oriented to detect vertical motion and thus to obtain a measurement of the amount of rocking of the base of the tank.

The objective of the second series of tests was to monitor the motion around the circumference. However, it was impractical in this preliminary investigation to mount the transducers around the tank at arbitrarily selected elevations and, therefore, it was decided to

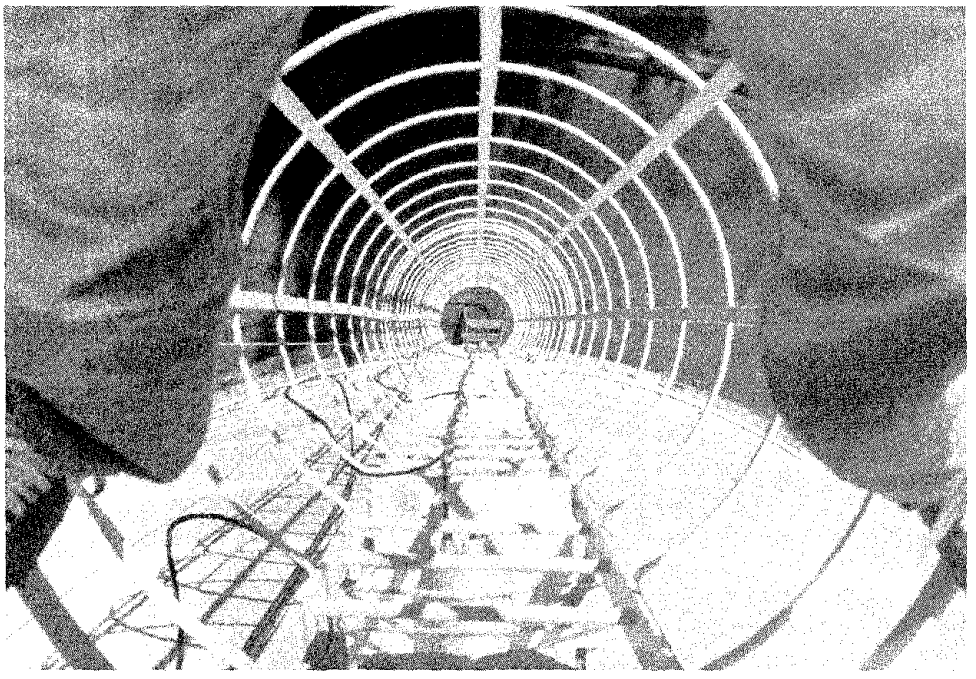

Fig. IV-6. Plan View Showing the Seismometers Used to Record the Radial Component of Shell Velocity Along the Height of Tank No. (1).

depend on measurements made along the circumference of the roof to identify the number of circumferential waves, n. Three Rangers were placed on an aluminum plate in such a way that three orthogonal components of the motion at a point could be measured. This package of transducers was moved from point to point and the motion was recorded at ten different locations around the perimeter.

One vibration generator, shown in Fig. IV-7, was used in the forced vibration test. It was anchored to a concrete slab resting on the ground adjacent to the tank. The horizontal sinusoidal force exerted by the vibration generator was transmitted through the ground and produced small amplitude vibrations of the tank.

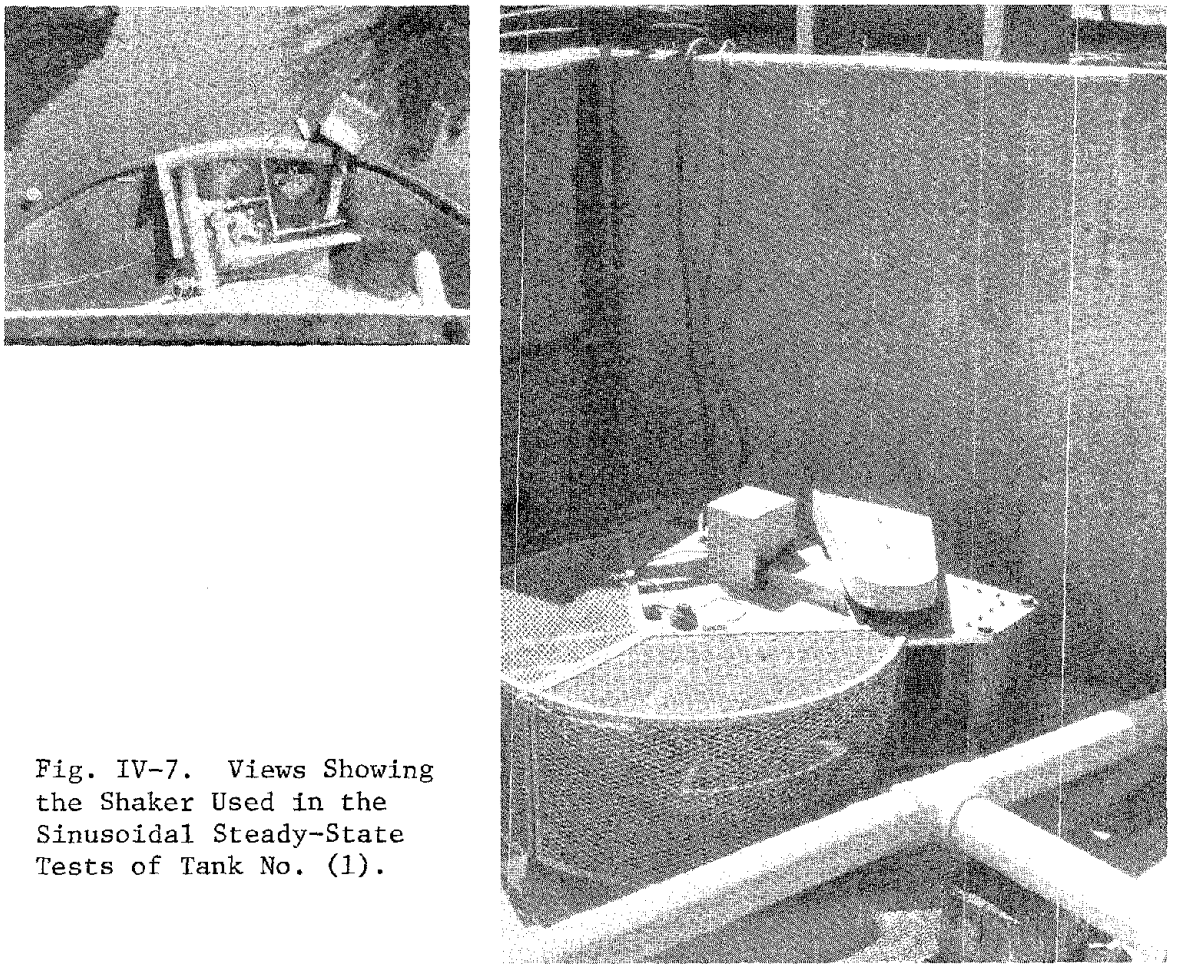

Fig. IV-7. Views Showing the Shaker Used in the Sinusoidal Steady-State Tests of Tank No. (1).

Figure IV-8 is a schematical diagram showing the experimental set-up and the instrumentation used in testing tank no. (1). Slight variations in the orientation of the instruments and in the measuring procedures were made for the other two tanks. These will be discussed, as they occur, in the following sections.

IV-3-3. Ambient Vibration Tests

The first stage of the testing program involved the measurements of the response of the tanks to ambient excitation. The ambient forces which excite these tanks are the result of wind currents and

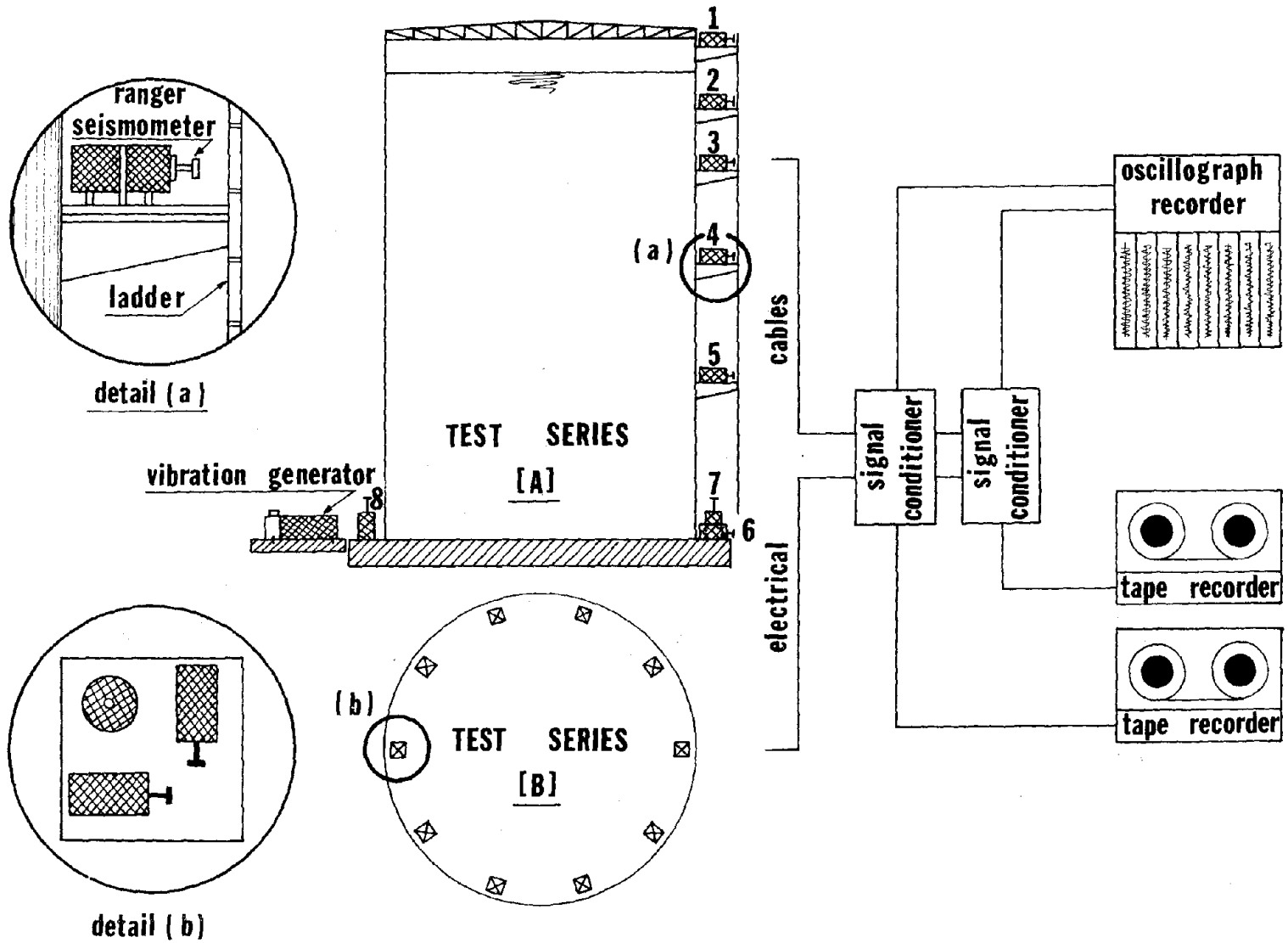

Fig. IV-8. Schematical Diagram Showing the Experimental Set-Up for Tank No. (1).

microseismic waves. These tests provide a quick means for identifying the natural frequencies of vibration. In addition, ambient tests were performed in such a way that the mode shapes can also be obtained, and these were compared with those obtained by forced vibration tests. Since the installation of a vibration generating system requires a great deal of work, ambient tests were conducted as a replacement for forced vibration testing of tank no. (3).

During the tests, the tanks were maintained full whenever possible. The water level was continuously monitored at the main operating panel-board, and if the water level meter indicated a drop of more than 3 to 4 ft during any run, the test would be repeated.

As mentioned previously, ambient vibrations were recorded on both tape and oscillograph recorders. The recording instruments were first adjusted to make sure that the signals were within their limits of operation; then, the motion was recorded for about five minutes for each run. Figure IV-9 shows sample traces from the oscillograph recorder made simultaneously during ambient vibration tests of tank no. (1).

The tape-recorded data were converted in the laboratory to a digital format on magnetic tape compatible with the Caltech IBM 370/158 digital computer. The digitization was at a rate of 40 equally-spaced points per second which resulted in a Nyquist frequency of 20 Hz. The computer program "FOURIER" was employed to compute a Fast Fourier Transform for each seismometer record; it utilizes the subroutine "RHARM" which is available from the Caltech computer program library. The resulting Fourier Amplitude Spectra are used to identify the

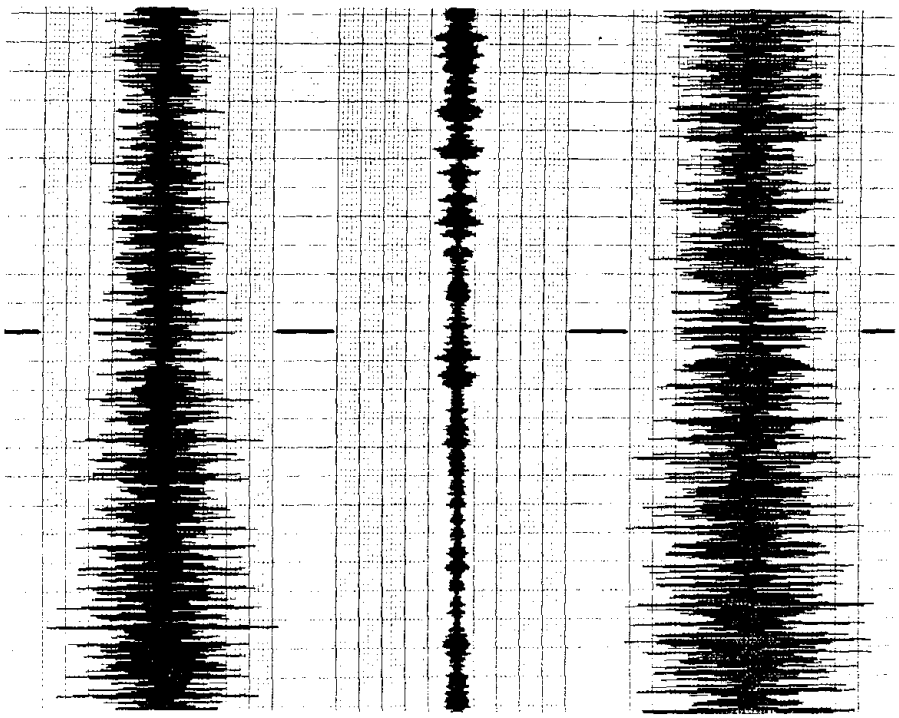

Fig. IV-9. Sample Traces from the Oscillograph Recorder Made Simultaneously During Ambient Vibration Tests of Tank no. (1).

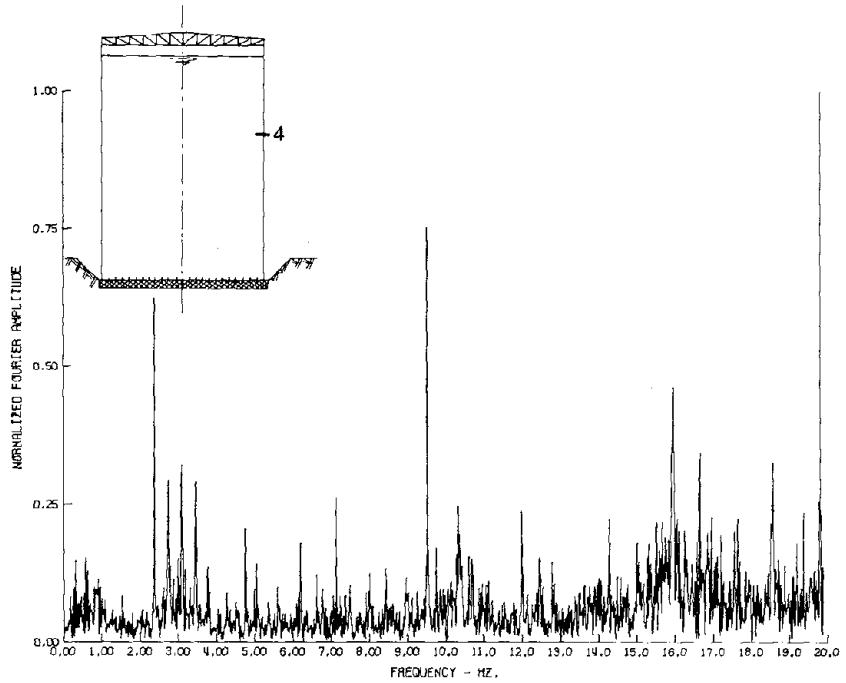

Fig. IV-10. Fourier Amplitude Spectrum of the Velocity Proportional Response of the Radial Motion Recorded at Station no. (4).

natural frequencies of vibration. Figure IV-10 displays the Fourier amplitude spectrum of the radial velocity recorded at station no. (4) of tank no. (1).

Ambient vibration tests have their advantages and limitations. One of these limitations is the inability to distinguish between those peaks in the spectrum which are due to structural vibrations and those which are due to mechanical and electrical noise. However, as a result of the relatively large wind forces acting on such tall tanks, the spectral peaks due to structural response were much higher, in most cases, than the noise level; and this facilitated the identification of the natural frequencies and the associated mode shapes.

The procedure for determining the mode shapes was to divide the spectral amplitude of the response at a given station by the spectral amplitude of the simultaneously recorded response at the reference station. This ratio was multiplied by the calibration factor which was previously obtained by a calibration test (in a calibration test, the seismometers were aligned side by side and the relative magnitudes of their output for the particular frequency under consideration were computed). The phase of the response was compared to that of the reference instrument to determine the signs of the modal amplitudes. A comparison between the measured and computed frequencies and mode shapes is presented in Sec. IV-4.

IV-3-4. Forced Vibration Tests

Steady-state forced vibration tests were conducted on both wash water tanks at the Weymouth filtration plant. Only one vibration

generator was used in testing tank no. (1) while both shakers were used for tank no. (2). The response of the tanks was recorded on the oscillograph recorder and the frequency of the vibrators was varied in increments over the desired frequency range. At each incremental frequency, the vibrators are held at a constant frequency long enough for all transient effects to decay, so only the steady-state response of the tank is recorded. The accuracy of visually measuring the response amplitudes from the oscillograph charts was checked by recording the time signals on a tape recorder, obtaining a Fourier amplitude spectrum for the recorded motion, and comparing its maximum amplitude with that obtained by the oscillograph recorder.

The force produced by the shakers is proportional to the square of the exciting frequency. Their maximum frequency is about 9.5 Hz; however, measurements of tank vibrations were made in the frequency range of 2 to 4 cps partly due to the thinness of the slab to which the shakers were anchored, and partly because the fundamental frequencies of the circumferential waves of interest lie in this range.

Data reduction procedures were similar to those made for ambient tests. However, the determination of the response curves was more involved and time consuming because several factors had to be employed: 1) the calibration factor, 2) the scale factor which accounts for the scale set by the oscillograph recorder, 3) the attenuation factor which takes into consideration the reduction of signal amplitudes set by the signal conditioner, and 4) the normalization factor to normalize the response for unit input force.

IV-4. Presentation and Discussion of Test Results

The vast amount of data recorded in the test program is far too much for detailed presentation in this report. Only selected data which provide a qualitative indication of the general nature of the dynamic behavior as well as the quantitative evidence for verification of the theoretical analysis are presented.

One phonomenon that was clearly observed in the recorded motion was that significant cos $n\theta$-type vibrations of the tank wall were developed. This can be seen in Figs. IV-11, IV-12, and IV-13 in which samples of the Fourier spectra of radial velocities are displayed. These modes were anticipated in the ambient tests because of the nature of the excitation which tends to excite many modes. However, in a forced vibration test, a perfect circular cylindrical shell should exhibit only cos θ-type modes with no cos $n\theta$-type deformations of the walls. Figure IV-14 shows the steady-state response of tank no. (1) in the frequency range 2.40 to 2.45 cps. The response of the tank attains its maximum value in this range at a frequency of 2.42 cps which corresponds to the fundamental frequency of a shell mode having a circumferential wave number $n = 5$. This can also be seen in Fig. IV-15 in which the response curve is plotted. This indicates that cos$n\theta$-type modes can be excited by rigid base motion presumably because of the initial irregularity of the shell. Similar behavior was observed for other values of n. These cos$n\theta$-type deformations were previously observed experimentally in shaking table tests [2,3]. It is thought that shell modes having n greater than 4 were observed in those tests

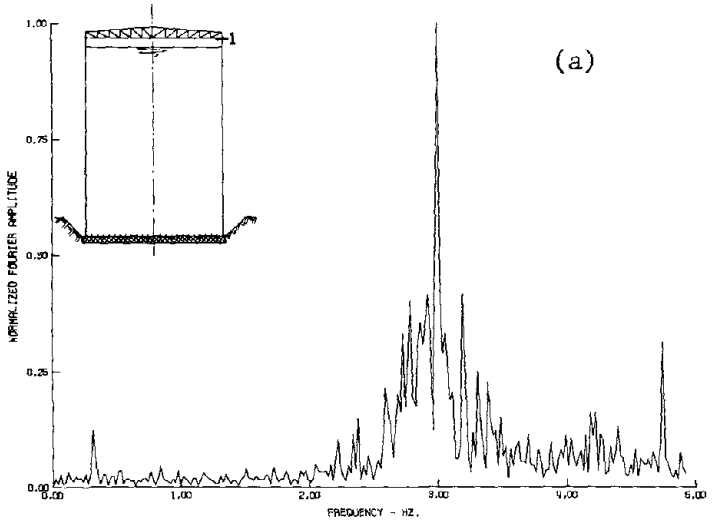

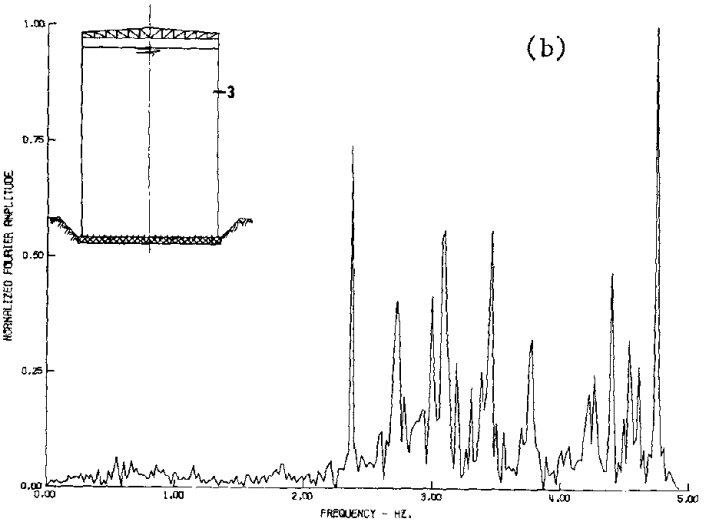

Fig. IV-11.

Fourier Amplitude Spectra of the Velocity Proportional Response of the Radial Motion Recorded at Stations no. 1, 3 and 4.

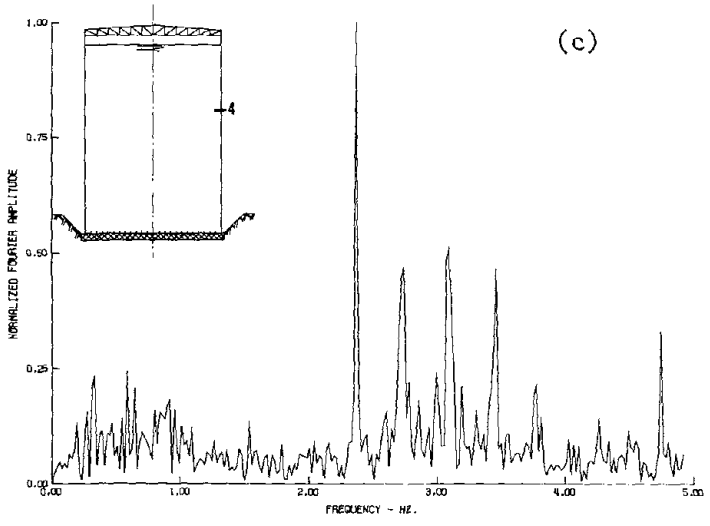

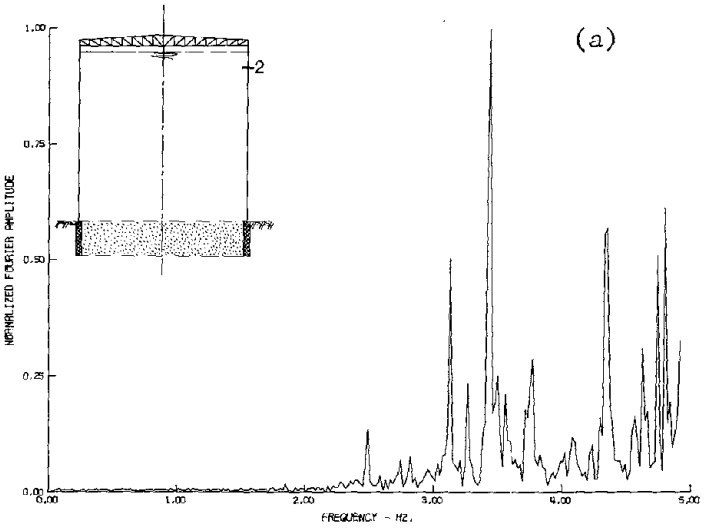

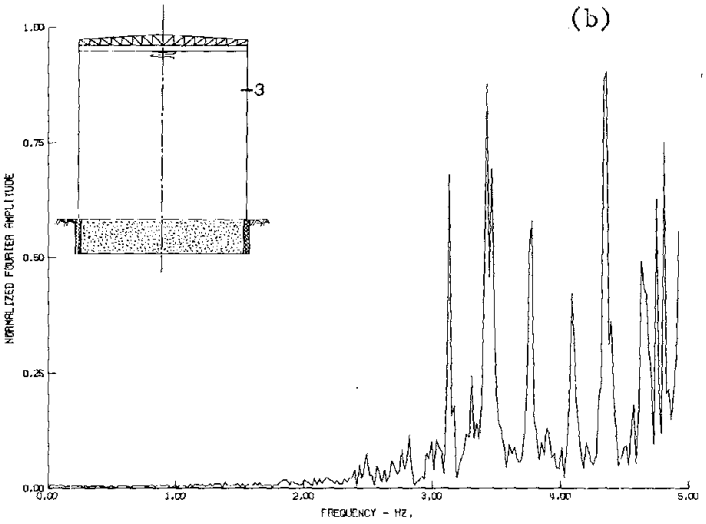

Fig. IV-12.

Fourier Amplitude Spectra of the Velocity Proportional Response of the Radial Motion Recorded at Stations no. 2, 3, and 4.

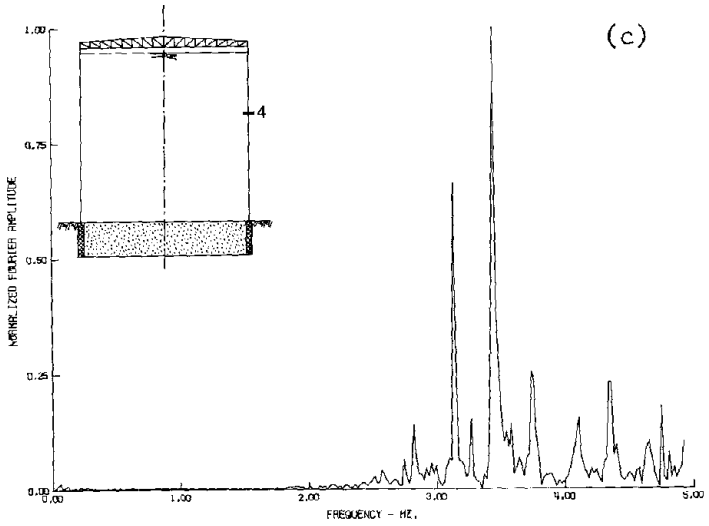

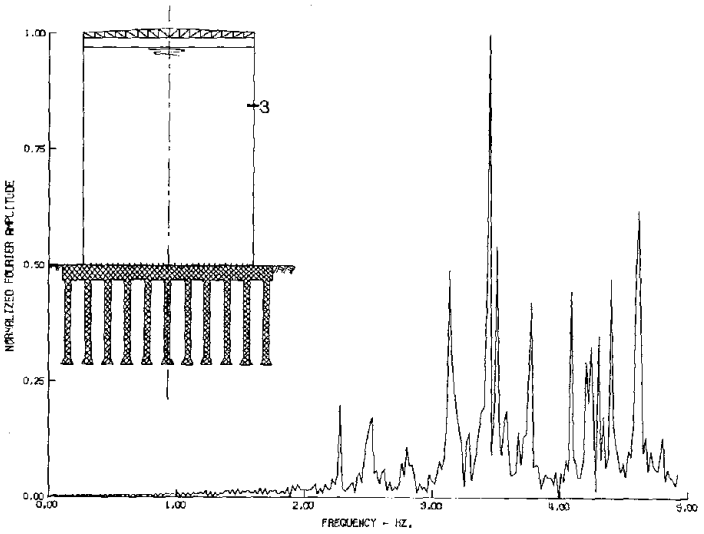

Fig. IV-13. Fourier Amplitude Spectrum of the Velocity Proportional Response of the Radial Motion Recorded at Station no. 3.

but had been identified as being of lower order because only eight displacement transducers per section had been employed. Figures IV-16-a and b show the axial and circumferential patterns of the cos5θ-mode based on ambient and forced vibration measurements; and it is clear that the roof does restrain the tank top against radial deformations. The computed natural frequency is 2.46 cps which is in close agreement with the measured one of 2.42 cps. The computed mode shape is also presented in the same figure for comparison.

The fundamental frequency of the cosθ-modes is clearly identified from Fig. IV-11-a in which the Fourier amplitude spectrum of the radial component of shell velocity of the tank top is displayed. The roof restrains the tank top against cosnθ-type deformations and only the cosθ-type modes are observed. The natural frequency is 3.01 cps which is less than that computed assuming rigid foundation. The computed

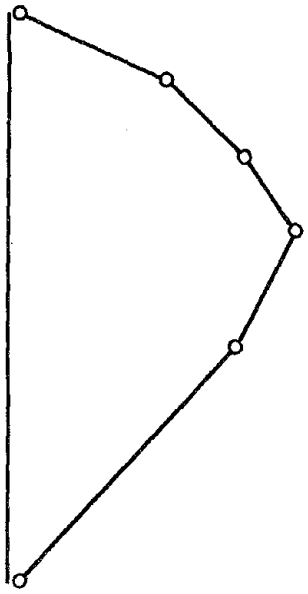

ω = 2.40 cps
Max. = 1.121

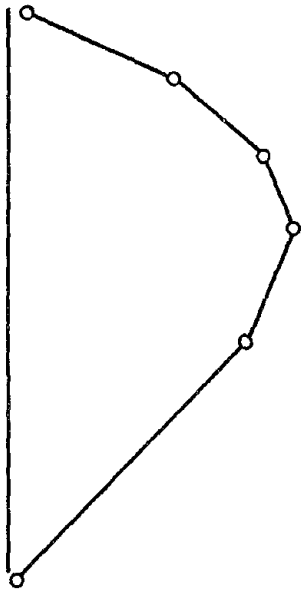

ω = 2.42 cps
Max. = 1.588

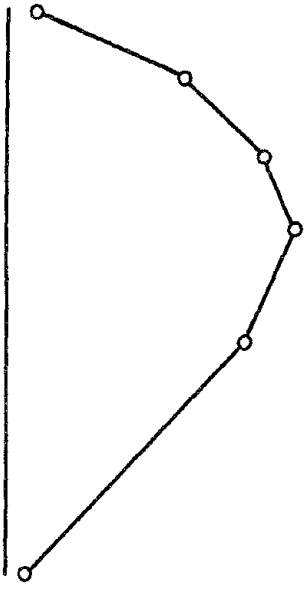

ω = 2.43 cps
Max. = 1.569

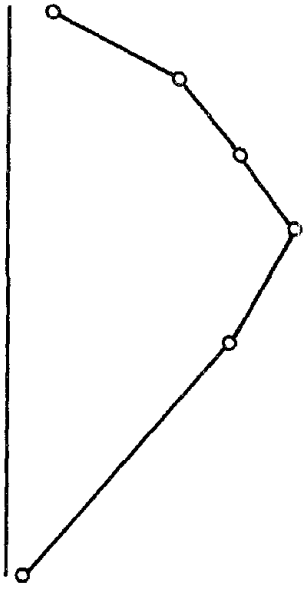

ω = 2.45 cps
Max. = 0.952

Fig. IV-14. Steady-State Response of Tank no. (1) (Frequency Range 2.40 to 2.45 cps).

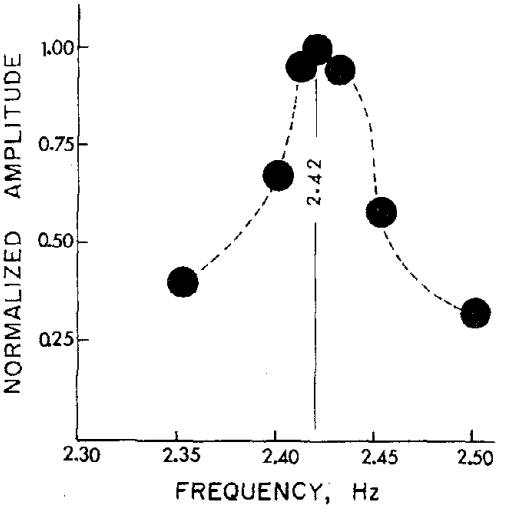

Fig. IV-15.

Response Curve of the Cos5θ-Mode.

frequencies of the second and third axial modes of the cosθ-type deformation are 10.38 and 15.11 cps, respectively; these are in reasonable agreement with those measured (9.6 and 14.3 cps, respectively). It should be noted that modes with frequencies higher than 4 cps were measured only during ambient vibrations. Figure IV-10 illustrates one of the Fourier amplitude spectra with frequency range up to 20 cps.

No attempt was made in the test program to measure sloshing frequencies of the liquid; these can be reasonably estimated by testing small-scale rigid tanks. However, Fig. IV-11-a indicates a peak at a frequency corresponding to the computed sloshing frequency of the liquid, and this was attributed to the low-frequency sloshing waves.

The foundation conditions had a noticeable influence on the response of the cosθ-type modes. Figure IV-17 shows sample traces from the Brush recorder (similar to the oscillograph recorder but with two channels only) made simultaneously during forced vibration test of tank no. (1) at the foundation level. These records show that the two

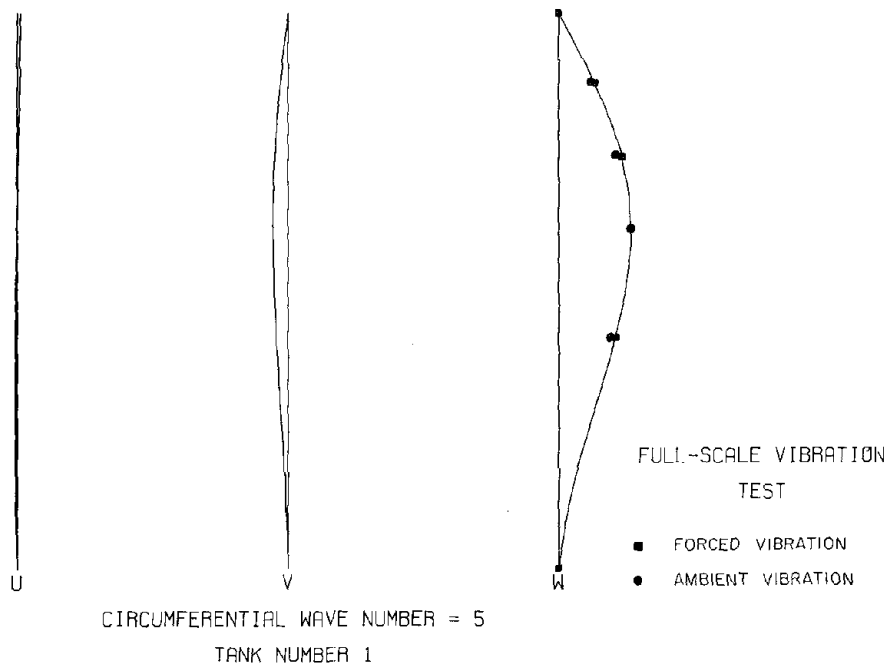

(a) Axial pattern

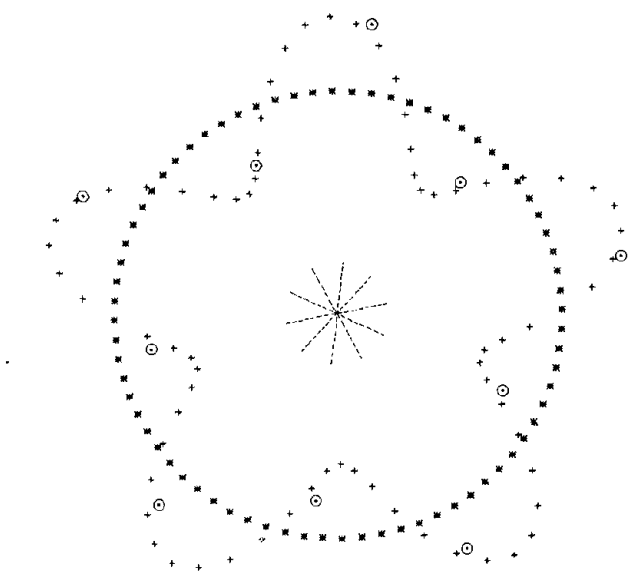

(b) Circumferential Pattern

Fig. IV-16. Comparison Between Computed and Measured Mode Shapes.

vertical seismometers (7) and (8) have the same amplitude and are 180° out of phase. This rocking motion occurs at 3.01 cps and is clearly seen in the Fourier amplitude spectrum shown also in Fig. IV-17. The interaction of the cosnθ-type deformation with the foundation was found to be insignificant. This was expected because a distributed radial force varying as cosnθ with $n \geq 2$ has no lateral resultant force. Rocking motion was not observed in tank no. (3) which had a very rigid foundation. Tank no. (2), which is not anchored to the foundation, exhibited behavior slightly different from the other two tanks. However, it is believed that it would behave much differently with a high level of excitation.

No axial mode shapes were obtained for tank no. (2) and tank no. (3) because it was impractical to place the seismometers along a generator of the shell (in testing tank no. (1), the seismometers were mounted on the vertical ladder which is firmly connected to the shell). However, the circumferential pattern of these modes was identified from measurements made around the perimeter of the roof. Figures IV-18-a and b display the computed and measured circumferential patterns of modes having $n = 3$ and $n = 4$, respectively. Figure IV-19 displays Fourier amplitude spectrum of the radial component of shell velocity recorded at station no. (4) on tank no. (3). The circumferential modes with n up to 5 were identified from the ambient measurements. The availability of the computed frequencies and the good correlation between the measured and the computed frequencies helped in identifying the mode number with $n \geq 6$. It should be mentioned that the low-pass filter of the signal conditioner was set, by mistake, to 4 cps in

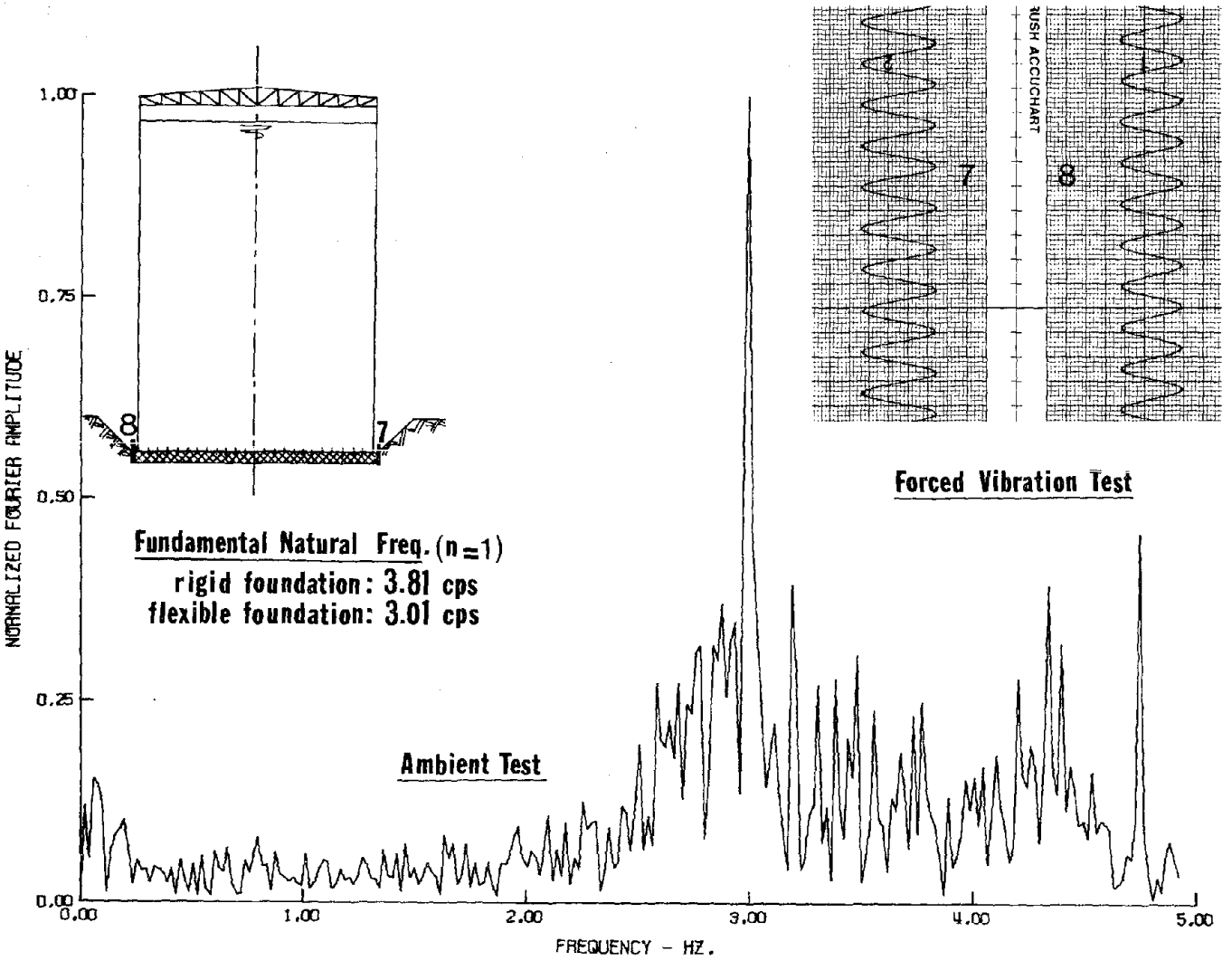

Fig. IV-17. Soil-Tank Interaction.

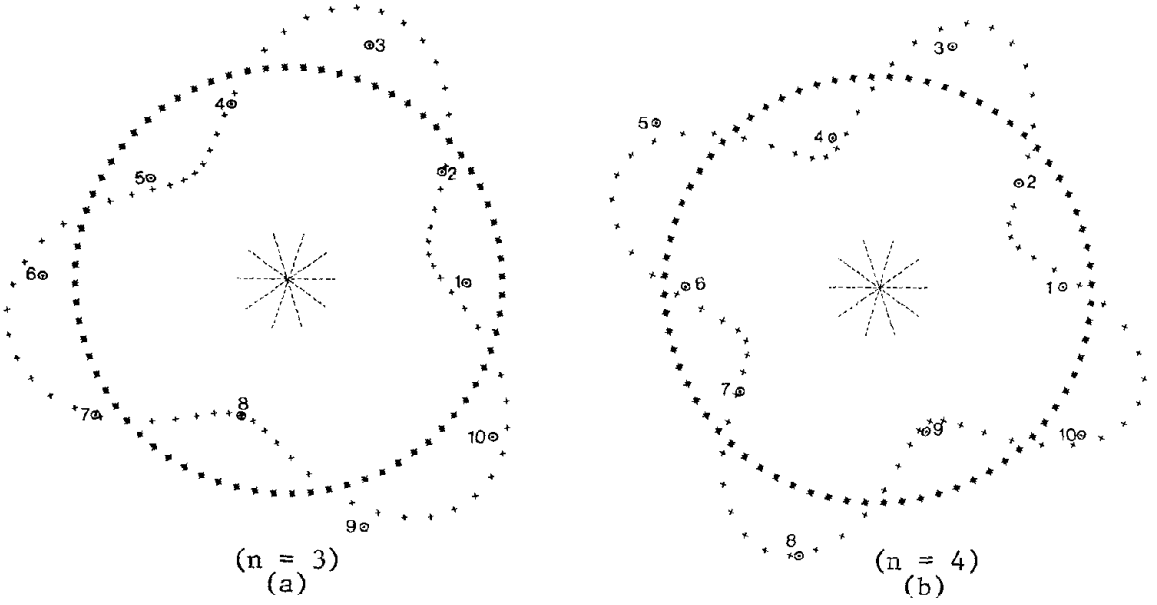

Fig. IV-18. Comparison Between Computed and Measured Circumferential Pattern of the Radial Component of Shell Velocity of Tank no. (3).

testing the third tank and therefore the peaks in the range 4 to 5 cps do not appear in their respective magnitude. Also, the high peak at 3.45 cps is attributed to environmental noise which was also observed in the calibration test. Figure IV-20 shows a comparison between the computed and measured frequencies of tank no. (3).

CONCLUSIONS

The following conclusions were drawn from the results of the tests reported here:

(1) Significant $\cos n\theta$-type deformations were developed in the tanks in response to ambient and forced excitations.

(2) The roof and the foundation do have a noticeable influence on the dynamic characteristics of liquid storage tanks.

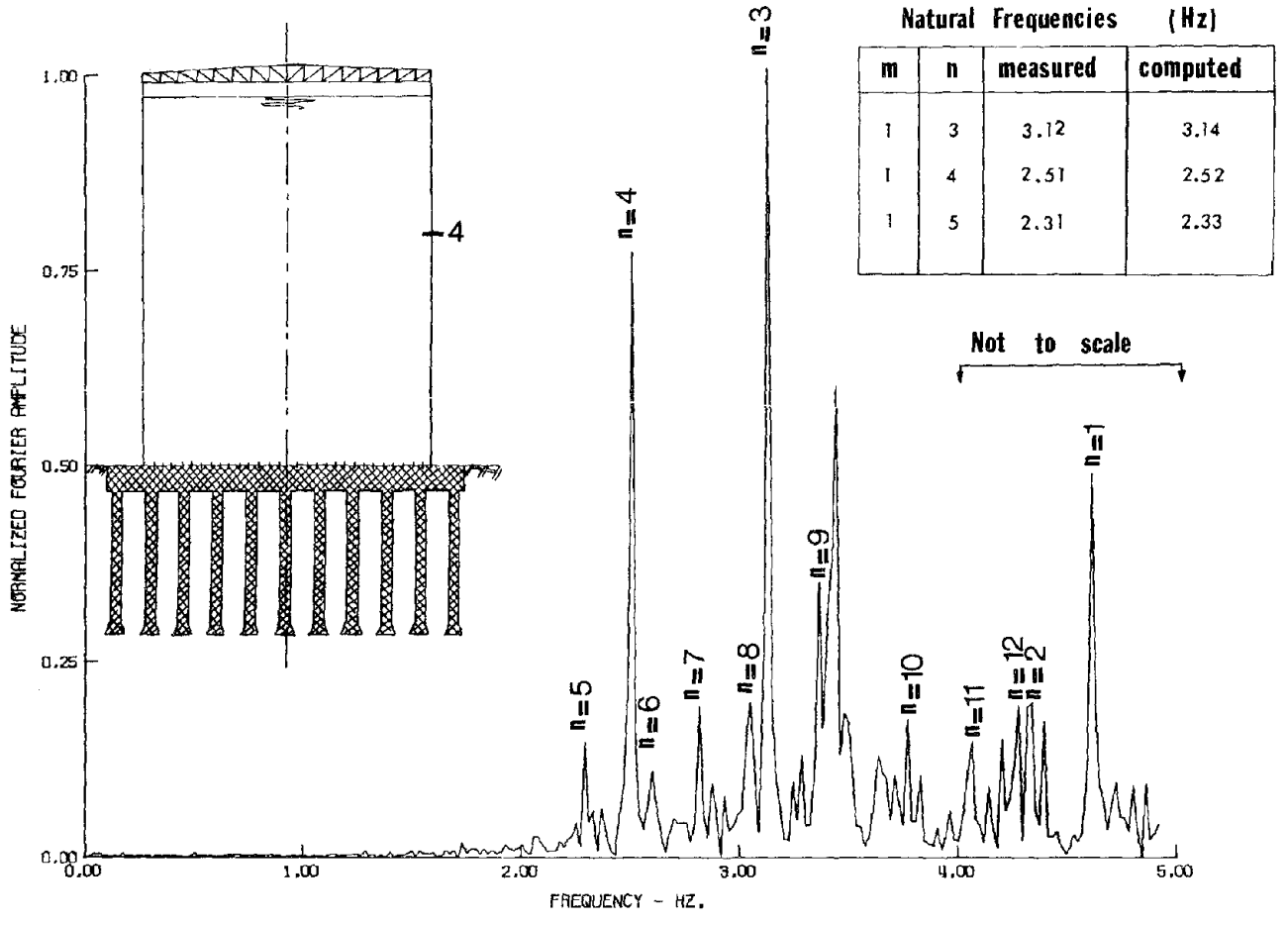

Fig. IV-19. Fourier Amplitude Spectrum of the Velocity Proportional Response of the Radial Motion Recorded at Station no. 4. (Comparison with Computed Frequencies).

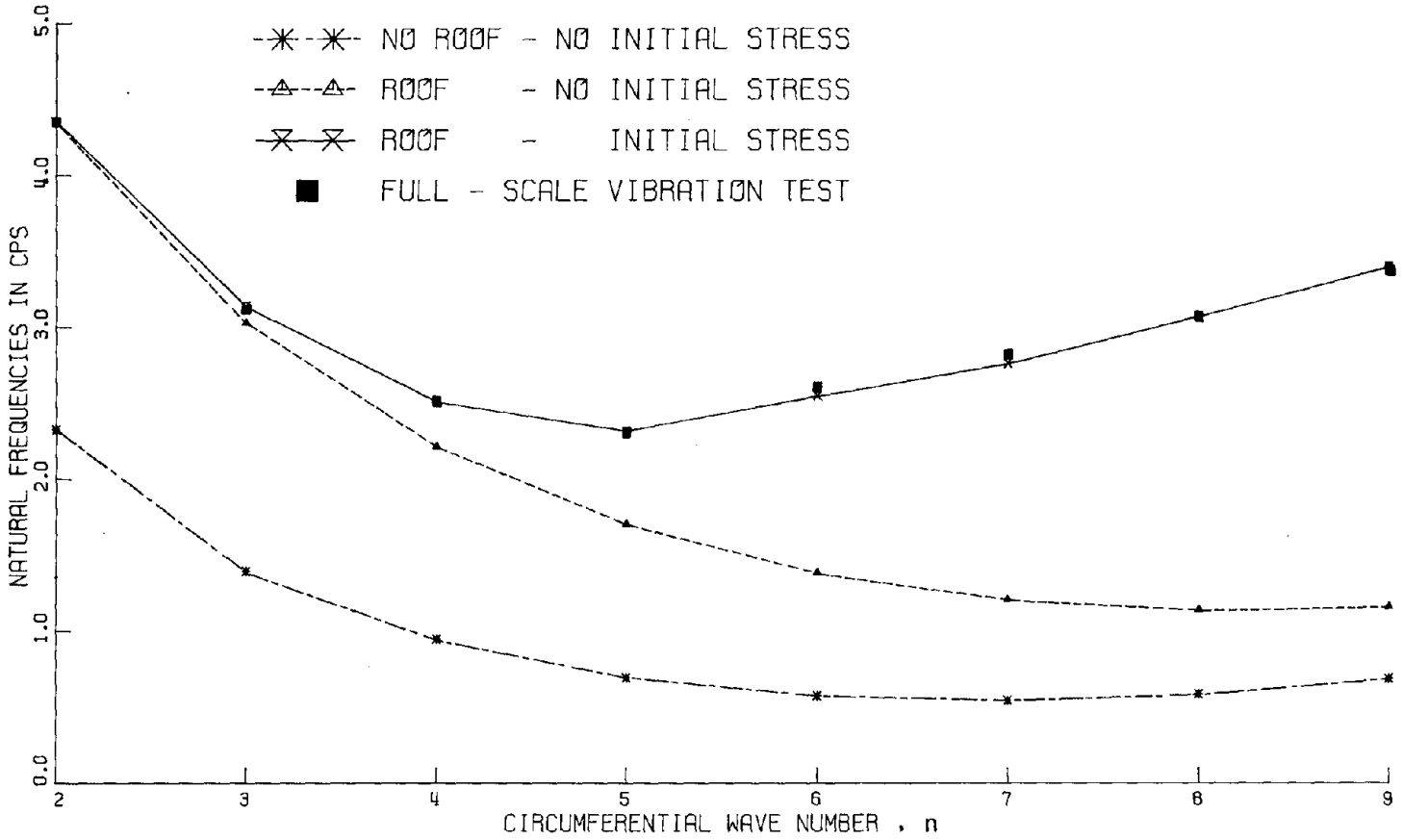

Fig. IV-20. Comparison Between Computed and Measured Frequencies of Tank No. (3).

(3) Field measurements of the natural frequencies and mode shapes showed good agreement with the computed values.

(4) The behavior of unanchored tanks cannot be well observed with such a low level of excitation.

IV-5 Experimental Investigation of the Dynamic Buckling of Liquid-Filled Model Tank

In a vibration test of full-scale tank, one can only measure the structural response under a low level of excitation, partly due to the difficulty of generating large dynamic forces, and partly due to the concern about the safety of the structure. Therefore, the dynamic buckling failure of liquid-filled tanks can only be studied by conducting vibration tests on scaled models. A separate experimental investigation of the buckling phenomenon of plastic models was conducted at Caltech [8]. The plastic models were mounted on a small shaking table and were subjected to a harmonic base excitation. The study provided results of practical interest; a brief summary of these results is presented herein.

Before carrying out the buckling tests, the natural frequencies of vibration and the associated mode shapes were determined. A comparison between the measured and the computed frequencies showed a very good agreement for all values of n except for $n = 1$. For this particular n, the measured frequency was less than the computed one by about 15%. It is believed that this disagreement is most likely due to the flexibility of the shaking table in the rocking mode [8].

Buckling tests were then carried out by fixing the frequency of excitation and increasing the amplitude of the shaking table motion until buckling occurs. Theoretically, the buckling was assumed to occur when the axial membrane stress at the bottom of the tank reaches the classical value

$$\sigma_x = Eh / (R\sqrt{3(1-\nu^2)})$$

Test results, when correlated with the theoretical level of excitation required to cause buckling (computed from the analysis of Chapter III modified for harmonic excitation), indicated that buckling of tanks is largely dependent upon the n = 1 response as shown in Fig. IV-21. No "knockdown" factor was used to account for the imperfection of the tank cross-section. It is of interest to note that the higher circumferential shell modes ($n \geq 2$) seem to have only a secondary role as seen in Fig. IV-21. For more details, refer to reference [8].

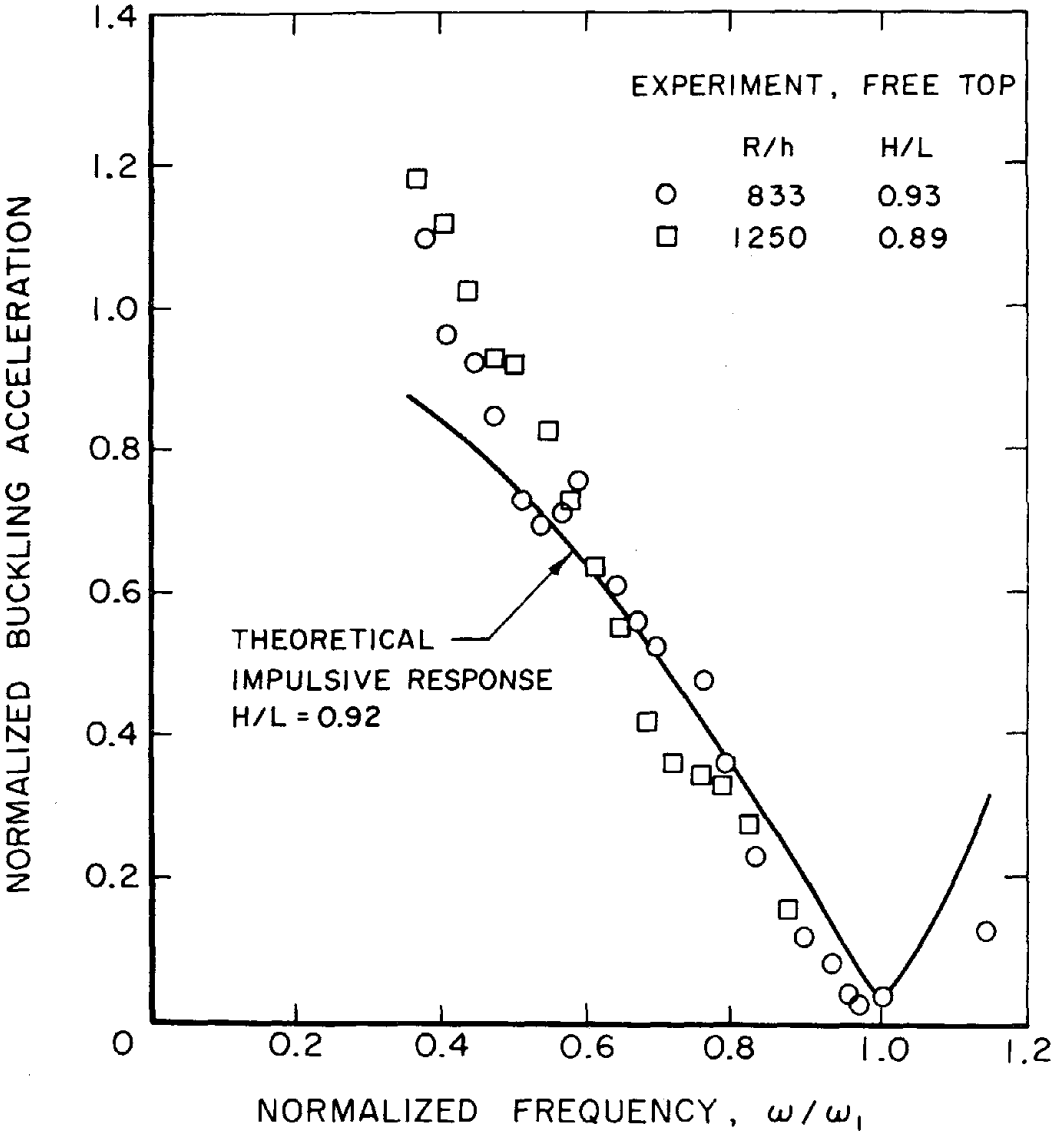

Fig. IV-21

IV-6. Seismic Instrumentation of Liquid Storage Tanks

It is becoming increasingly customary to provide important structures with permanently installed instrumentation systems to record future earthquake motions. Proper placement of such instruments can yield valuable information about the response of the structure at dynamic force and deformation levels directly relevant to earthquake-resistant design.

As far as the earthquake response of anchored tanks is concerned, those records can throw light on the actual dynamic properties of the liquid-shell system and offer an opportunity to compare these values with those obtained by vibration tests. Furthermore, conventional vibration tests are not suitable for unanchored tanks and many questions about their behavior cannot be answered with such a low level of excitation.

The purpose herein is to recommend minimum instrument requirements to cover these two distinct types of ground-supported, liquid storage tanks. It is suggested that the two wash water tanks located at the Weymouth filtration plant be instrumented.

Adequate definition of the input ground motion is necessary to get any valuable information about the behavior of these tanks. For this purpose, it is recommended that one instrument be located at the foundation level in the immediate vicinity of each tank; one in the grounds maintenance building and one in the polymer storage building as shown in Fig. IV-22. These accelerographs must be firmly bolted down to the concrete foundation slabs. In the event of instrument malfunction, the ground motion measured by the other instrument can

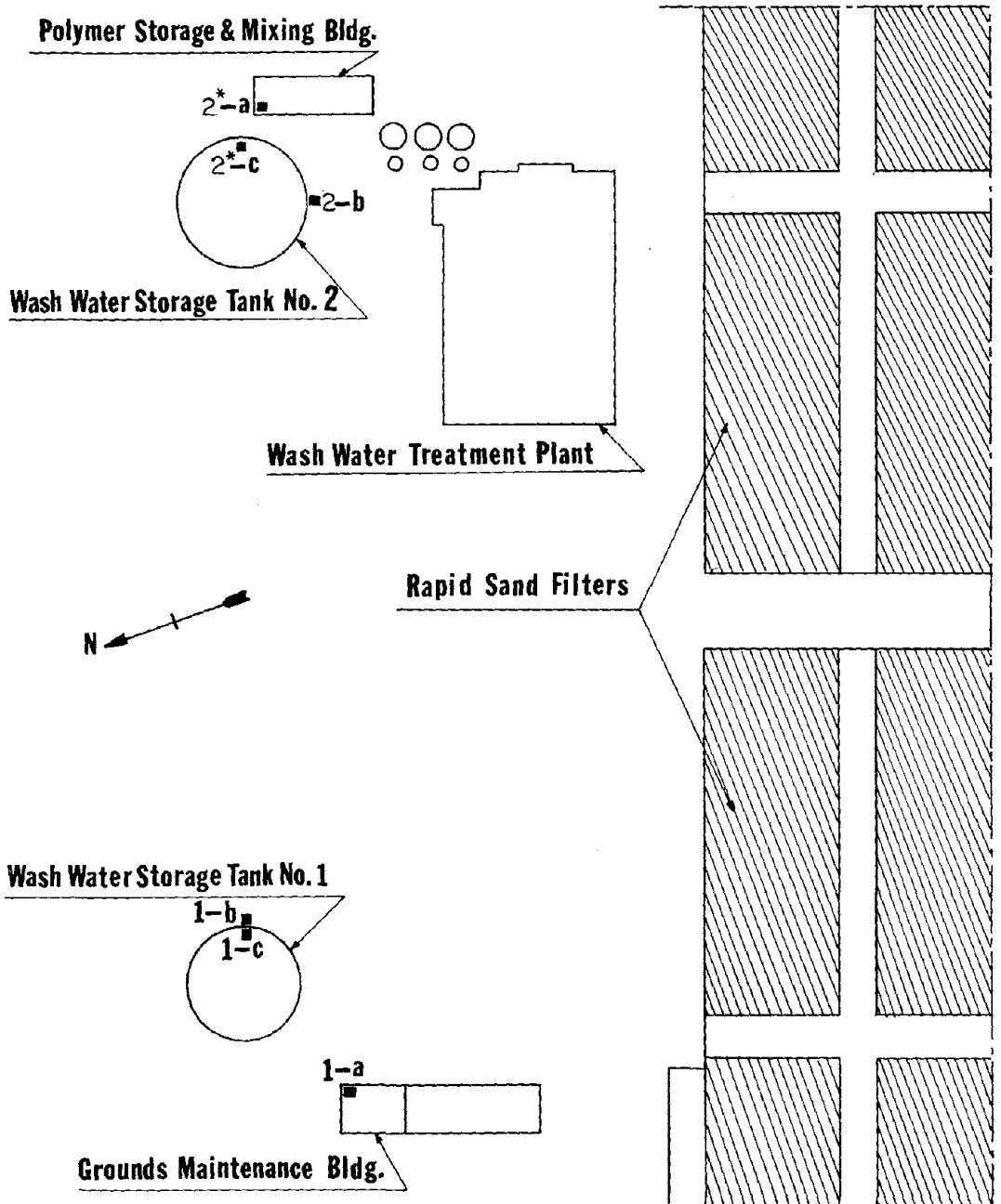

*has been installed.

Fig. IV-22. Part Plan of the Weymouth Filtration Plant Showing the Proposed Strong Motion Instrumentation System.

be used as the input for both tanks, thus ensuring some useful information. To investigate the effect of the soil-tank interaction (mainly a rocking motion), the accelerograph at station 1-a can be replaced by two instruments mounted on the foundation slab of tank no. (1) at the two ends of the principal diameter.

One instrument should be located at the top of each tank to record its response. The instruments should be situated to record the two horizontal components of motion in the radial and tangential directions of the tank as well as the vertical component of acceleration. It is believed that these instruments will provide adequate information about the cos θ-type response (basic response) of the tanks. However, vibration tests showed that cos $n\theta$-type deformations of the tank walls were developed in response to ground motion induced by the vibration generator. Since the magnitude of such deformations is dependent on the irregularity of the tank which is unknown, and since the number of instruments required to measure and interpret these modes is economically not feasible, no attempt will be made to sense these motions; however, the relative importance of the cos $n\theta$-type modes as compared to the cos θ-type modes can be crudely estimated by placing one instrument at the mid-height of each tank.

In view of test results, the Metropolitan Water District of Southern California has installed two strong-motion accelerographs at the locations 2-a and 2-c to record ground motion and tank response, respectively, during future earthquakes. An effort is underway to provide other instruments for tank no. (1). It is hoped that this

instrumentation program will yield valuable information about the basic seismic response of liquid storage tanks which eventually will lead to an improvement in the design of such structures to resist earthquakes. It should also be noted that the proposed instrumentation system represents the minimum requirements to obtain the essential data needed for refinement of the theoretical analysis. Therefore, if one wants to obtain a full understanding of the seismic behavior of tanks, various types of transducers must be installed to measure strains in the cylindrical shell, to measure the dynamic change in pressures at the liquid-shell interface, and to measure the free surface displacements (wave-height).

REFERENCES OF CHAPTER IV

1. Abramson, H.N., ed., "The Dynamic Behavior of Liquids in Moving Containers," NASA SP-106, National Aeronautics and Space Administration, Washington, D.C., 1966.

2. Clough, D.P., "Experimental Evaluation of Seismic Design Methods for Broad Cylindrical Tanks," University of California Earthquake Engineering Research Center, Report No. UC/EERC 77-10, May 1977.

3. Niwa, A., "Seismic Behavior of Tall Liquid Storage Tanks," University of California Earthquake Engineering Research Center, Report No. UC/EERC 78-04, February 1978.

4. Foutch, D.A., "A Study of the Vibrational Characteristics of Two Multistory Buildings," Earthquake Engineering Research Laboratory, EERL 76-03, California Institute of Technology, Pasadena, California, September 1976.

5. Abdel-Ghaffar, A.M., and Housner, G.W., "An Analysis of the Dynamic Characteristics of a Suspension Bridge by Ambient Vibration Measurements," Earthquake Engineering Research Laboratory, EERL 77-01, California Institute of Technology, Pasadena, California, January 1977.

6. Hudson, D.E., "Synchronized Vibration Generators for Dynamic Tests of Full-Scale Structures," EERL, California Institute of Technology, Pasadena, California, 1962.

7. Hudson, D.E., "Dynamic Tests of Full-Scale Structures," Journal of the Engineering Mechanics Division, ASCE, Vol. 103, December 1977, pp. 1141-1157.

8. Shih, C., and Babcock, C.D., "Scale Model Buckling Tests of a Fluid Filled Tank Under Harmonic Excitation," submitted for presentation at the 1980 Pressure Vessels and Piping Conference, ASME, San Francisco.

PART (C)

SIMPLIFIED STUDIES OF THE SEISMIC RESPONSE OF LIQUID STORAGE TANKS

With few exceptions, current seismic design procedures for liquid storage tanks are based on the mechanical model derived by Housner for rigid tanks (Fig. C-1). However, the results of the first two phases of the study indicate that wall flexibility has a significant effect on the hydrodynamic pressures. The principal aim of this part of the study is to provide practicing engineers with simple, fast, and sufficiently accurate tools for estimating the seismic response of liquid storage tanks.

A similar mechanical analog, which takes into account the deformability of the tank wall, is developed. The model, shown in Fig. C-2, is based on the results of the finite element analysis of the liquid-shell system presented in Part A of this report. The parameters of such a model are displayed in charts which facilitate the calculations of the equivalent masses, their centers of gravity, and the periods of vibration. The equivalent masses m_r, m_f, and m_s correspond to the forces associated with ground motion, wall deformation, and liquid sloshing, respectively. Once the parameters of the mechanical model of the particular tank under consideration are found, the maximum seismic loading can be predicted by means of a response spectrum characterizing the design earthquake. This procedure can be easily used by practicing engineers to compute the earthquake response of deformable tanks.

HOUSNER MODEL

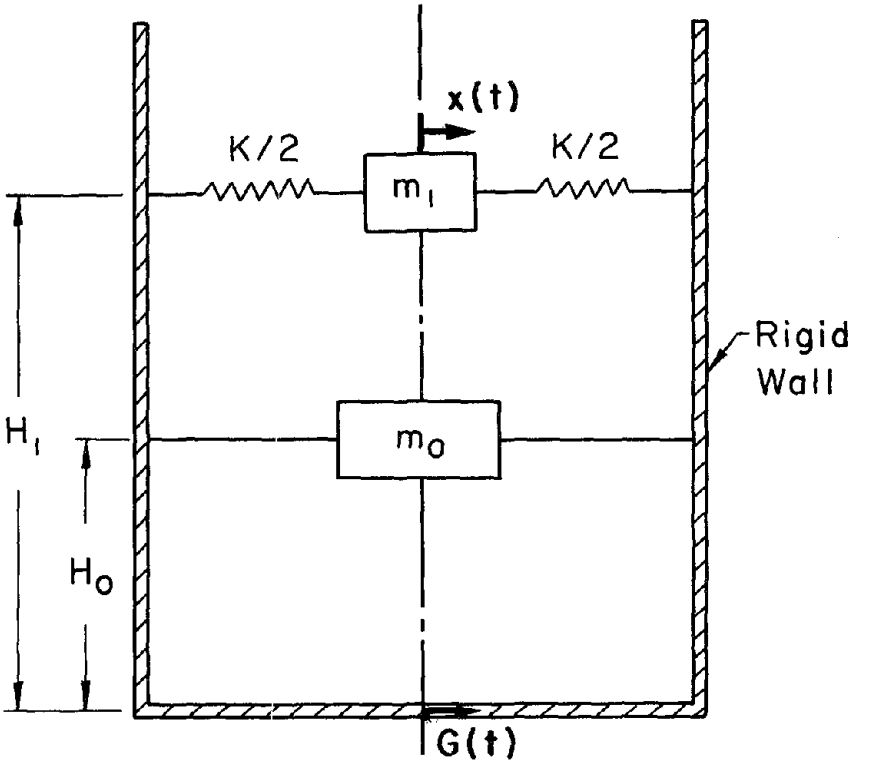

$$\text{Base Shear} = \sqrt{(m_o \ddot{G}_{max})^2 + (m_1 S_a)^2}$$

$$\text{Base Moment} = \sqrt{(m_o H_o \ddot{G}_{max})^2 + (m_1 H_1 S_a)^2}$$

Fig. C-1.

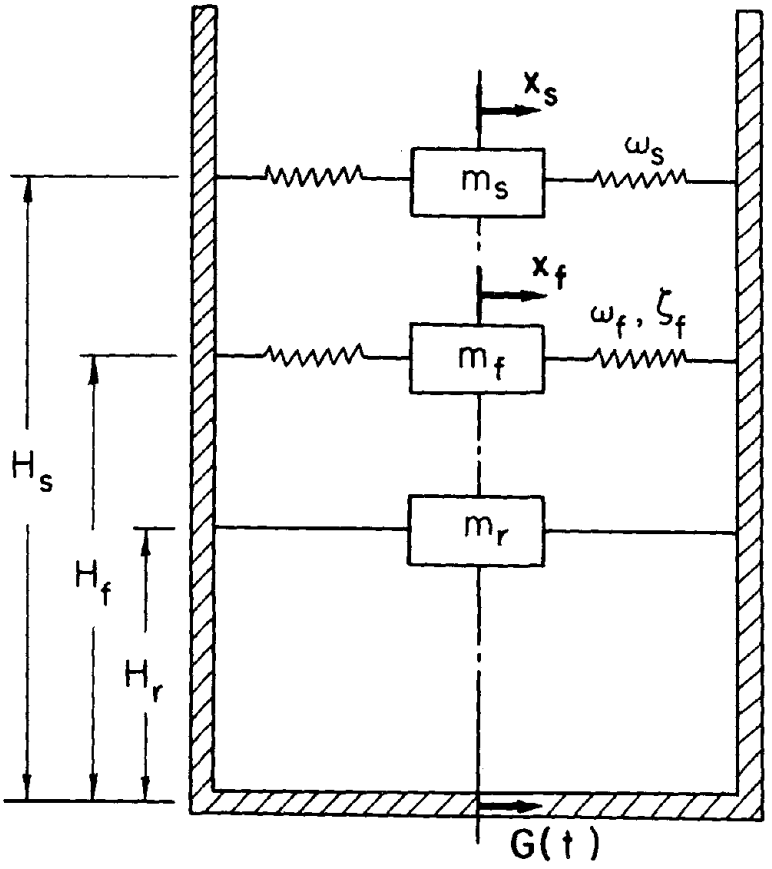

FLEXIBLE TANK

$$\text{Base Shear} = \sqrt{\left[(m_r - m_f)\,\ddot{G}_{max}\right]^2 + (m_f\,S_{af})^2 + (m_s\,S_{as})^2}$$

$$\text{Base Moment} = \sqrt{\left[(m_r H_r - m_f H_f)\,\ddot{G}_{max}\right]^2 + (m_f H_f\,S_{af})^2 + (m_s H_s\,S_{as})^2}$$

Fig. C-2

A simplified analysis is also developed to investigate the interaction between the foundation soil and liquid storage tanks. The significance of such interaction for the response of rigid tanks is first evaluated. The combined effect of wall flexibility and soil deformability is then investigated using the simplified model shown in Fig. C-3. In this approach, the tank is assumed to behave as a vertical cantilever beam with bending and shear stiffness, and the foundation soil is represented by a discrete system of springs and dampers. Such analysis is applicable only to "tall" tanks.

The research that was carried out in the final phase of the study provided results that should be of interest to practicing engineers. Therefore, it was decided to present these results in a separate Earthquake Engineering Research Laboratory report which also includes recommended design provisions for the seismic design of cylindrical liquid storage tanks.

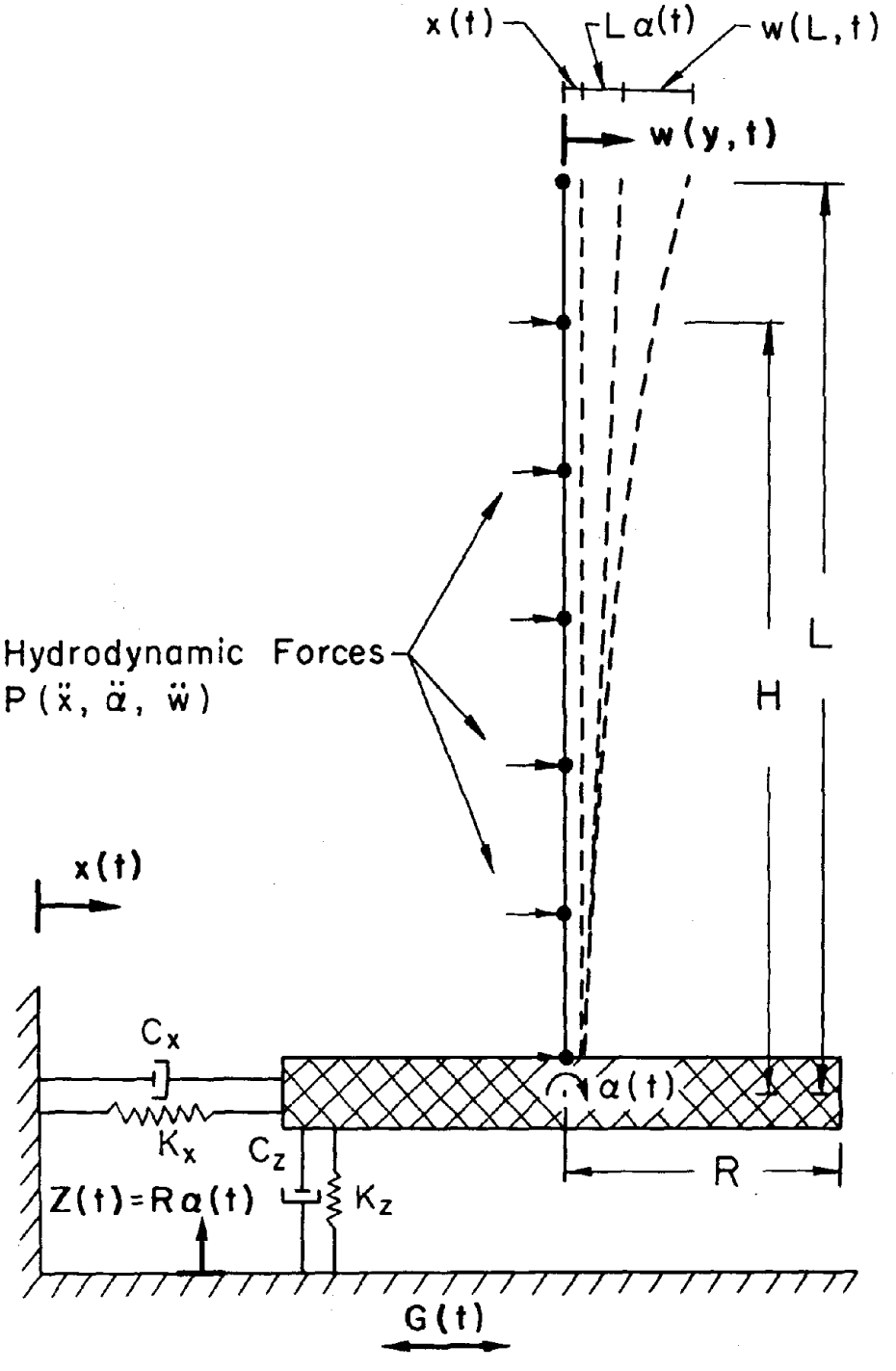
x(t)
Lα(t)
w(L,t)
w(y,t)
Hydrodynamic Forces
P(ẍ, α̈, ẅ)
L
H
x(t)
Cx
Kx
Cz
Kz
α(t)
R
Z(t)=Rα(t)
G(t)

Fig. C-3.

SUMMARY AND CONCLUSIONS

The study develops a method of dynamic analysis for the free lateral vibrations of ground-supported, cylindrical liquid storage tanks. A method is also presented to compute the earthquake response of both perfect circular and irregular tanks; it is based on superposition of the free lateral vibrational modes.

Natural frequencies of vibration and the associated mode shapes are found through the use of a discretization scheme in which the elastic shell is modeled by finite elements and the fluid region is treated as a continuum by boundary solution techniques. In this approach, the number of unknowns is substantially less than in those analyses where both tank wall and fluid are subdivided into finite elements.

Detailed numerical examples are presented to illustrate the applicability and the effectiveness of the analysis and to investigate the dynamic characteristics of tanks with widely different properties. Furthermore, a rigorous comparison with previous results obtained by other investigators is made.

Ambient and forced vibration tests are conducted on three full-scale water storage tanks to determine their dynamic characteristics. These frequencies and mode shapes are determined for small amplitude vibrations and, hence, indicate the structural behavior in the range of linear response. Comparison with previously computed mode shapes and frequencies shows good agreement with the experimental results, thus confirming both the accuracy of the experimental determination and the reliability of the method of computation.

The study also develops a method which allows, from the engineering point of view, a simple, fast and sufficiently accurate estimate of the dynamic response of liquid storage tanks to earthquakes.

It is believed that the research presented in this report advances the understanding of the dynamic behavior of liquid storage tanks, and provides results that should be of practical value.